The study of RAS-induced metabolic reprogramming and the role of the pentose phosphate pathway in tumor metabolism

Adrián Benito Mauricio

The study of RAS-induced metabolic reprogramming and the role of the pentose phosphate pathway in tumor metabolism

Adrián Benito Mauricio

PhD Thesis

2013

The image used in the cover as background was obtained and modified from KEGG database (Kanehisa Laboratories) and corresponds to Reference Pathway for metabolism.

PROGRAMA DE DOCTORADO EN BIOTECNOLOGÍA

Departament de Bioquímica i Biologia Molecular

Facultat de Biologia

The study of RAS-induced metabolic reprogramming and the role of the pentose phosphate pathway in tumor metabolism

Memoria presentada por Adrián Benito Mauricio para optar al grado de Doctor por la Universitat de Barcelona

Marta Cascante Serratosa

Codirectora

Silvia Marín Martínez

Codirectora i tutora

Adrián Benito Mauricio

Doctorando

A mi familia y a Ana, por estar siempre ahí.

"Lo importante en ciencia no es tanto obtener nuevos hechos como descubrir nuevas formas de pensar sobre ellos"

Sir WILLIAM LAWRENCE BRAGG
(1890-1971)
Premio Nobel de Física 1915

INDEX

1. ABBREVIATIONS

1. ABBREVIATIONS

αKG	α-Ketoglutarate
6PGL	6-Phosphogluconate Dehydrogenase
6PG	6-Phosphogluconolactone
ACC	Acetyl-CoA Carboxylase
ACLY	ATP Citrate Lyase
ACoA	Acetyl-CoA
Cit	Citrate
DCA	Dichloroacetate
DHAP	Dihydroxyacetone phosphate
E4P	Erytrose-4-phosphate
ELOLV	Very Long Chain Fatty Acid
F16BP	Fructose-1,6-biphosphate
F26BP	Fructose -2,6-biphosphate
F6P	Fructose-6-phosphate
FASN	Fatty Acid Synthase
G6P	Glucose-6-phosphate
G6PD	Glucose-6-phosphate Dehydrogenase
GAP	Glyceraldehyde-3-phosphate Dehydrogenase
GAPDH	Glyceraldehyde-3-phosphate Dehydrogenase
GLDH	Glutamate dehydrogenase
GLS	Glutaminase
HexP	Hexose phosphate pool
HIF1	Hypoxia-Inducible Factor 1
HK	Hexokinase
IDH	Isocitrate Dehydrogenase
IDH1	Isocitrate Dehydrogenase isoform 1
KEAP1	Kelch-like ECH-associated protein 1
LDH	Lactate Dehydrogenase
Mal	Malate
MDH	Malate Dehydrogenase
ME	Malic Enzyme
ME1	Malic Enzyme isoform 1
NRF2	Nuclear factor erythroid 2-Related Factor 2
Oaa	Oxaloacetate
PC	Pyruvate Carboxylase
PDH	Pyruvate Dehydrogenase
PDK	Pyruvate Dehydrogenase
PenP	Pentose phosphate pool
PEP	Phosphoenolpyruvate
PFK1	Phosphofructokinase 1
PFK2	Phosphofructokinase 2
PK	Pyruvate Kinase
PGLS	6-phosphoglucolactonase
PPP	Pentose Phosphate Pathway
Pyr	Pyruvate
R5P	Ribose-5-phosphate

RPE	Ribose phosphate 3-epimerase
RPIA	Ribose-5-phosphate isomerase
ROS	Reactive Oxygen Species
S7P	Sedoheptulose-7-phosphate
SCDs	Stearoyl-CoA Desaturase
SRBPs	Sterol Regulatory Binding Proteins
SucCoA	Succinil-CoA
TALDO	Transaldolase
TALDO1	Transaldolase 1
TCA	Tricarboxylic Acid
TKT	Transketolase
TKTL1	Transketolase-like 1
TrisP	Triose phosphate pool
X5P	Xilulose-5-phosphate

2. INTRODUCTION

2. INTRODUCTION

2.1 A GENERAL OVERVIEW OF CANCER FUNDAMENTALS

Cancer is a generic term that includes a large group of diseases in which abnormal cells divide without control and are able to invade other tissues resulting in metastasis formation (www.cancer.gov). In 2008, more than 12.6 millions of new cases of cancer were diagnosed and around 7.5 millions of cancer deaths were registered worldwide, being lung and breast cancer the most frequent among men and women respectively (Ferlay et al., 2010).

The development and progression of cancer requires that malignant cells acquire certain capabilities along the carcinogenic process. Since there are more than 100 types of cancer, a high degree of both inter- and intratumor heterogeneity exists. However, some similarities common to the majority of cancers have been outlined (Hanahan and Weinberg, 2011). Figure 2.1 highlights these capabilities, also commonly known as the hallmarks of cancer.

Healthy tissues carefully regulate proliferative stimuli, which are transmitted by signaling pathways and govern cell growth and division signals. On the contrary, in cancer cells these signaling pathways are often altered, rendering cancer cells to proliferate autonomously (Davies and Samuels, 2010; Hynes and MacDonald, 2009). As an example, activating mutations in the RAS signaling pathway controlling proliferative signals are frequently found in a variety of cancers (Malumbres and Barbacid, 2003). However, uncontrolled proliferation requires not only the existence of enhanced proliferative signals but also inactivation of the mechanisms that restrict cell proliferation. In this regard, cancer cells must also bypass powerful programs aimed to negatively control cell proliferation, which are mainly regulated through the action of tumor suppressor genes, such as *TP53* or *RB* (Burkhart and Sage, 2008; Sherr and

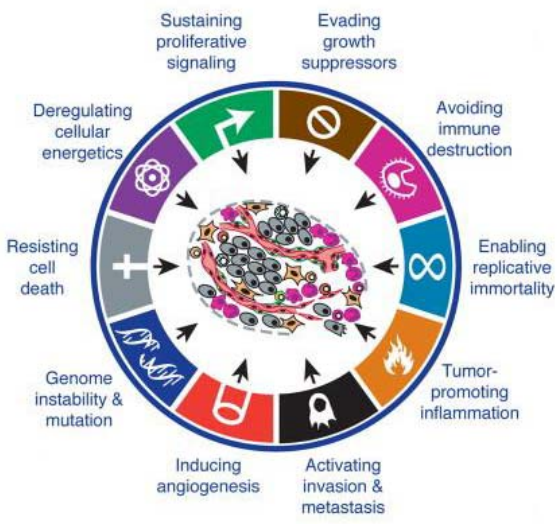

Figure 2.1 The hallmarks of cancer

The required capabilities for tumor growth and progression are shown.
Reprinted from Cell, 144(5), Hallmarks of cancer: the next generation, 646-674, Copyright © 2011, with permission from Elsevier.

McCormick, 2002). In the same sense, cancer cells must also circumvent the inherent cell death program of apoptosis, which serves as a natural barrier to cancer development. Thus, tumor cells adopt a variety of strategies to evade this process, such as loss of *TP53* tumor suppressor function, induction of antiapoptotic regulators (BCL-2, BCL-x_L) or downregulation of proapoptotic factors (BAX, BIM, PUMA) (Adams and Cory, 2007; Junttila and Evan, 2009; Lowe et al., 2004).

The above-mentioned traits do not suffice to guarantee the progression of the tumor. It is generally accepted that cancer cells require unlimited replicative potential in order to generate macroscopic tumors. In healthy tissues, the replicative capacity is limited by two main mechanisms: senescence, which maintains cells in a resting but viable state, and crisis, which involves cell death. The ability of cancer cells to overcome these limitative processes has been called immortalization and is considered a pivotal hallmark in cancer progression. The enzyme telomerase plays an essential role in this process and is correlated with a resistance to induction of both senescence and crisis, conferring cancer cells the capability for unlimited replicative capacity (Blasco, 2005).

Despite of the capability to proliferate uncontrollably and limitlessly, no proliferation is feasible without a properly sustenance in the form of nutrients and oxygen as well as an ability to evacuate metabolic wastes and carbon dioxide efficiently. As tumor grows, a new and more extensive local vasculature must be created to fulfill these requirements in a process called angiogenesis. Then, an angiogenic switch takes place during tumorigenesis and remains almost always activated, causing normally quiescent vasculature to continually sprout new vessels that help sustain expanding neoplasic growth (Hanahan and Folkman, 1996). This angiogenic process is the result of a balance between pro- and anti-angiogenic signals. In this sense, tumor cells display a variety of strategies to enhance neovasculature formation, such as upregulation of *VEGF*, the gene encoding the main ligand involved in orchestrating new blood vessel formation (Ferrara, 2009).

Although the described hallmarks are essential to cancer progression, the mortality of cancer lies in the capability of cancer cells for spreading to other parts of the body in a multistep process of invasion and metastasis. This process consist of a succession of cell changes, beginning with local invasion, then intravasation into nearby blood and lymphatic vessels, transit of cancer cells through the lymphatic and hematogenous system, followed by extravasation, the formation of micrometastasis and finally the growth of micrometastasis lesions into macroscopic tumors in a process called colonization (Talmadge and Fidler, 2010). Over this process, cancer cells develop alterations in their shape as well as in their attachment to other cells and to the extracellular matrix. A pivotal role in this process is played by E-cadherin, a protein involved in adherent junctions with adjacent epithelial cells that has been documented to be frequently downregulated and mutated in human carcinomas (Berx and van Roy, 2009).

Over the last years, the intensive research in cancer has prompted the appearance of two emergent new hallmarks of cancer (Hanahan and Weinberg, 2011). First, the capacity of cancer cells to evade the immune system, which is responsible for detecting and eliminating the vast majority of incipient cancer cells and nascent tumors. It is still unclear how cancer cells evade the immune system, but some studies indicate they can

do so by secreting TGF-β or other immunosuppressive factors (Yang et al., 2010b). The second emergent hallmark corresponds to the reprogramming of cancer metabolism. In order to achieve all the above-mentioned hallmarks, cancer cells must reorganize the metabolic network at the service of an increased demand of energy and macromolecules to sustain cell proliferation and tumorigenesis (Ward and Thompson, 2012). The study of the cited tumor metabolic reprogramming that takes place in cancer, mainly focused on oncogene-induced metabolic reprogramming, and the identification of key players in the metabolic network constitutes the main topic of this thesis. Aiming to provide a general knowledge of this emergent hallmark, the essential traits of cancer cell metabolic reprogramming are presented throughout the next pages.

2.2 TUMOR METABOLIC REPROGRAMMING

Metabolism is the set of life-sustaining chemical transformations within the cells of living organisms. These enzyme-catalyzed reactions allow organisms to grow and reproduce, maintain their structures, and respond to their environments. All the cells in our body require certain amounts of nutrients and oxygen to perform their cellular functions. Nutrients can either be burned to produce energy (catabolism) or used to produce building blocks to sustain proliferation (anabolism). Accordingly, the requirements of nutrients are particularly high in proliferating cells, since they need not only to preserve their integrity and perform their physiological functions but also to generate a new daughter cell. Then, as cancer is a tissue-proliferation disorder, it is expected that cancer cells rewire metabolism at the service of proliferation. Furthermore, all the above-mentioned hallmarks of cancer are also intimately related to certain aspects of cellular metabolism, extending the role of metabolism beyond growth and proliferation (Kroemer and Pouyssegur, 2008).

In the 1920s, Otto Warburg showed that tumor slices displayed increased rates of glucose uptake compared with normal tissues and that, even in the presence of oxygen, tumors metabolized glucose via oxygen-independent aerobic glycolysis rather than via oxidative phosphorylation (Jones and Schulze, 2011; Warburg et al., 1927). Today, this

phenomenon is widely called the "Warburg effect". It has been long stated that altered metabolism in cancer cells is merely an indirect phenomenon in cancer, a secondary effect that pales into insignificance beside the activation of primary proliferative and survival signals. The majority of oncogenes and tumor suppressor genes encode proteins involved in signal transduction pathways, whose roles in carcinogenesis have been attributed to their ability to trigger proliferative, survival and anti-apoptotic processes. However, over the last years, a new paradigm has emerged (Ward and Thompson, 2012). The pivotal role of activated oncogenes and deactivated tumor suppressor genes well might be to reprogram cellular metabolism. Classical view of metabolism supports the idea that metabolic fluxes are governed by allosteric effects of metabolites on rate-limiting steps of the metabolic pathways, giving them self-regulatory capacity. Nevertheless, although these mechanisms exist in proliferating cells, the efforts to elucidate the consequences of signal transduction on cell proliferation have revealed a variety of signaling effects directed at metabolic fluxes. For instance, during proliferation of tumor cells and lymphocytes, growth-factor signaling suppresses β-oxidation of fatty acids, minimizing futile cycling and promoting lipid synthesis (Deberardinis et al., 2006). Therefore, growth-factor signaling can reorganize metabolic fluxes independently of traditional allosteric mechanisms of pathway regulation.

Proliferating and non-proliferating cells display an opposite metabolic behavior. Non-proliferating differentiated cells are surrounded by an abundance of nutrients, but they are not autonomous for nutrient uptake. Instead, they compete for limiting levels of growth factors that direct this process. To survive in such conditions, they adopt a catabolic metabolism focused on maximizing the efficiency of ATP production. In contrast, when growth factors are abundant and proliferation and signaling pathways are activated, cells increase their nutrient uptake and adopt an anabolic status.

The components of signaling pathways controlling both proliferation and survival and metabolic network are largely conserved between tumor and normal cells. The main differences arise from the fact that in normal cells initiation of signaling requires extracellular stimulation, whereas cancer cells often harbor mutations that trigger a sustained activation of the signaling processes (Kan et al., 2010). These signaling

pathways activate proliferative and survival programs in which metabolism must be reorganized to fulfill the energetic and biosynthetic requirements. As an example, mutations in PI3K, a key player in PI3K/AKT/mTOR signaling pathway involved in cell proliferation and survival, is mutated in approximately 20-30% of breast, brain and gastric tumor analyzed by Samuels and collaborators (Samuels et al., 2004). PI3K stimulates a plethora of downstream effects regulating the metabolic network, from enhancing glucose uptake and glycolysis to fatty acids synthesis, which are required for the tumorigenic process (Bauer et al., 2005) Thus, increasing evidence support that metabolic reprogramming is not a merely bystander in tumorigenesis, but an essential requirement.

2.2.1 Obtaining ATP: cancer cell bioenergetics and the Warburg effect.

2.2.1.1 Glucose catabolism, ATP production and the Warburg effect

As it has been mentioned before, cancer cells display an enhanced glycolysis even in the presence of oxygen. The so-called Warburg effect has been demonstrated in different cancer types and has turned into a very valuable clinical tool for detection of tumors by ^{18}F-deoxyglucose positron emission tomography (FDG-PET)(Som et al., 1980). Metabolizing glucose by glycolysis to produce lactate is energetically inefficient, since most of the ATP generated by glucose catabolism (34 out of 36 ATP molecules per molecule of glucose) occurs not in glycolysis but during the TCA (Tricarboxilic Acid) cycle. Then, this increased glycolysis displayed in tumors presented a paradox that today still remains unclear. In order to understand the potential benefits of this phenotype, a number of explanations have been proposed.

One of these explanations postulates that an increased glycolysis allows cells to use glucose (the most abundant extracellular nutrient) to produce ATP, and although the yield of ATP per molecule of glucose is low, the percentage of cellular ATP produced from glycolysis can exceed that produced from oxidative phosphorylation (Guppy et al., 1993). Nonetheless, Kilburn and collaborators documented that the amount of

additional energy (assuming that glucose is the main substrate) to produce a new cell is 50% above the baseline required to maintain cellular homeostasis. Hence, it is surmised that the amount of ATP in a proliferating cell is not dramatically different from a resting cell, but the proliferative cell must accumulate biomass, replicate DNA and divide (Kilburn et al., 1969). A second explanation proposes that the Warburg effect can provide cells with an adaptive advantage under circumstances of low glucose availability, since it confers the capability of synthesizing ATP at high rate, what is particularly important when a competition for glucose exists (Pfeiffer et al., 2001). A third is that a heightened glycolysis provides proliferating cells with metabolic intermediates needed for biosynthetic pathways including ribose for nucleotides, glycerol and citrate for lipids, and aminoacids. Thus, it seems fairly clear that the Warburg effect might contribute to meet both energetic and biosynthetic needs. A fourth idea to explain the observed Warburg effect is that a decreased dependence on aerobic respiration becomes advantageous within the unique tumor microenvironment. As early tumor expands it outgrows the diffusion limits of its local blood supply and oxygen becomes scarce. Low and fluctuating levels of oxygen led to the stabilization of HIF1α, thus contributing to the Warburg effect (Denko, 2008; Stubbs and Griffiths, 2009). Additionally, glycolytic cancer cells generate high amounts of lactate with the subsequent acidification of the extracellular milieu, which favors tumor invasion due to the pH-dependent activation of cathepsines and metalloproteinases that degrade extracellular matrixes and basements membranes (Kroemer and Pouyssegur, 2008; Swietach et al., 2007). Finally, the Warburg effect could positively influence the evasion of apoptosis, one of the hallmarks of cancer, since highly glycolytic cells under-use the mitochondria, which is the main source of apoptotic stimuli. This idea is fully supported by the fact that activation of PDH complex by pyruvate dehydrogenase kinase (PDK) inhibitor dichloroacetate (DCA) in highly glycolytic cancer cells activates oxidative phosphorylation and promotes apoptosis (Bonnet et al., 2007).

2.2.1.2 The Warburg effect, oncogenes and tumor suppressor genes

Accumulating evidence indicate that oncogenes and tumor suppressor genes affect metabolic regulation. Then it is not surprising that the Warburg effect is regulated by many signaling pathways at different levels (Bensinger and Christofk, 2012; Soga, 2013). Elevated expression of glucose transporters and glycolytic enzymes are found in numerous cancers and may contribute to tumor progression (Adekola et al., 2012; Palaskas et al., 2011). This metabolic phenotype can be due to the action of HIF1α (Hypoxia-Inducible Factor 1α), which is activated in many tumors by a variety of mechanisms, some of them triggered by the action of oncogenes (Stubbs and Griffiths, 2009). MYC is an important regulator of the metabolic phenotype in cancers. Among the thousands of genes upregulated by MYC are several glucose transporters and glycolytic enzymes`, as well as PDK1 and LDH-A (Dang et al.; Shim et al., 1997). Moreover, MYC can collaborate with hypoxia-inducible transcription factor (HIF), considered one of the main regulators of glycolysis, to activate many target genes involved in this metabolic pathway (Gordan et al., 2007). The tumor suppressor *TP53* is another important transcription factor that regulates metabolism by decreasing the glycolytic flux through inhibiting glucose transporters, decreasing expression of glycolytic enzymes and increasing the expression of TIGAR, a negative regulator of glycolysis (Kondoh et al., 2005; Pilkis et al., 1981; Schwartzenberg-Bar-Yoseph et al., 2004; Vousden and Ryan, 2009).

2.2.1.2.1 RAS oncogene

A very illustrative example of oncogene-induced metabolic reprogramming is the case of *RAS*. In humans, *RAS* gene encodes four distinct but highly homologous 21 kDa RAS proteins: HRAS, NRAS, KRAS4A and KRAS4B (these last two proteins are alternative splice variants of the *KRAS* gene). *RAS* gene is mutated in approximately 30% of human tumors (Fernandez-Medarde and Santos, 2011; Takashima and Faller, 2013) and K-RAS isoform is the most frequently mutated among the three isoforms in malignancies; with a mutation rate in all tumors estimated to be 25-30%. In contrast, mutations in *NRAS* and *HRAS* are less common (8 and 3% mutation rate, respectively) (Fernandez-Medarde

and Santos, 2011; Takashima and Faller, 2013). RAS proteins act as transducer that couple cell surface receptors to intracellular effectors and alternate between on and off conformation that are conferred by binding of GTP or GDP respectively (Figure 2.2).

Under physiological conditions, the transitions between these two states is regulated by guanine nucleotide exchange factors (GEFs), which promote the activation of RAS by stimulating GDP for GTP exchange, and by GTPase activating proteins (GAPs), which

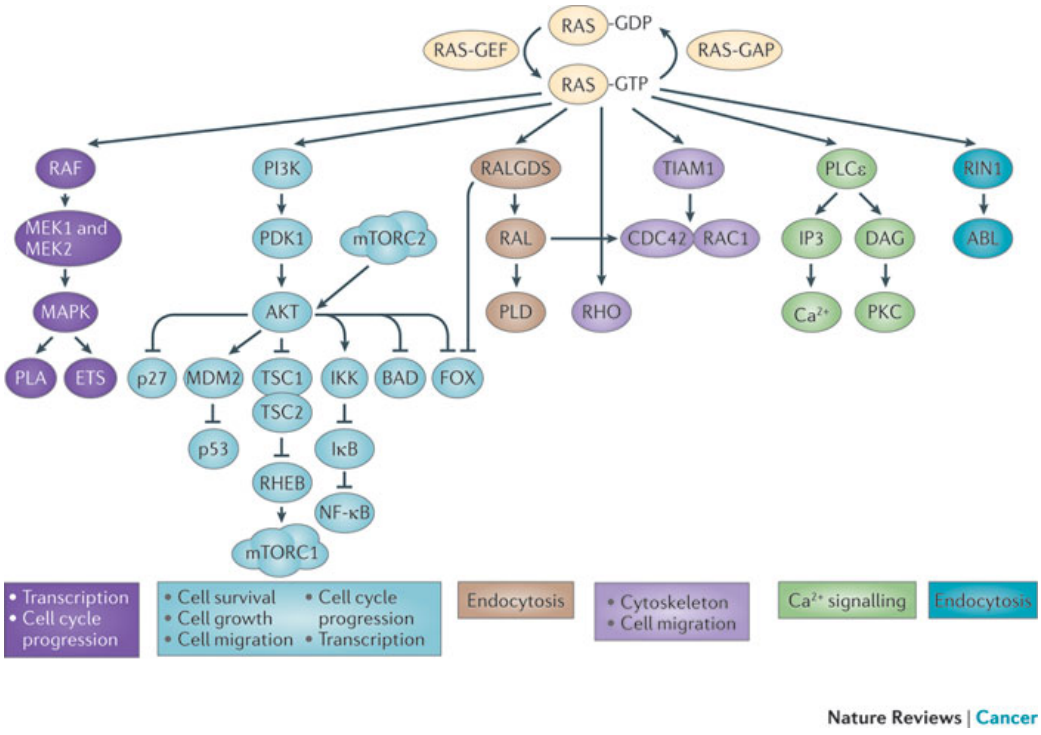

Figure 2.2 RAS signaling pathway

RAS protein activates several major signaling pathway involved in a wide range of cellular functions. Two of the main pathways activated by RAS are RAF-MEK-MAPK pathway and PI3K/AKT pathway, which in addition to the processes shown in the figure, also regulate cellular metabolism. BAD, BCL-2 antagonist of cell death; CDC42, cell division cycle 42; DAG, diacylglycerol; FOX, forkhead transcription factor; GAP, GTPase-activating protein; GEF, guanine nucleotide exchange factor; IKK, IκB kinase; IP3, inositol-1,4,5-trisphosphate; mTORC, mTOR complex; NF-κB, nuclear factor-κB; PDK1, phosphoinositide-dependent kinase 1; PKC, protein kinase C; PLA, phospholipase A; PLCε, phospholipase Cε; PLD, phospholipase D; RALGDS, RAL guanine nucleotide dissociation stimulator; RHEB, RAS homologue enriched in brain; RIN1, RAS and RAB interactor 1; TSC1/2, tuberous sclerosis 1/2; TIAM1, T cell lymphoma invasion and metastasis 1. Reprinted by permission from Macmillan Publishers Ltd: Nature Reviews Cancer. Berndt, N., A. D. Hamilton, et al. (2011). Targeting protein prenylation for cancer therapy. Nat Rev Cancer 11(11): 775-791, Copyright © 2011.

accelerate RAS-mediated GTP hydrolysis (Pylayeva-Gupta et al., 2011). This inactivation of RAS activity by GAPs is the predominant target of the most common somatic mutations that are found in the oncogenic variants of RAS alleles. Oncogenic substitutions in residues G12 and G13 of RAS prevent the formation of Van der Waals bonds between RAS and the GAP through esteric hindrance, perturbing the proper orientation of the catalytic glutamine Q61 in RAS, which results in the pronounced attenuation of GTP hydrolysis (Scheffzek et al., 1997). The outcome of these substitutions is the persistence of the GTP-bound state of RAS and, as a consequence, the permanent activation of a multitude of RAS dependent downstream effectors pathways, involved in many aspects of the tumor phenotype such as promotion of proliferation, suppression of apoptosis, metabolic reprogramming, remodeling of the microenvironment, evasion of the immune response and metastasis (Pylayeva-Gupta et al., 2011). As it is the case for PI3K, RAS also promotes a remodeling of the metabolic network.

Although RAS modulates different metabolic processes in the cell, regulation of glycolysis is one of the most important metabolic effects (Figure 2.3). Its main effect on metabolism is targeted to glycolysis by upregulating HIF1α, considered one of the main regulators of glycolysis, and glucose transporter expression (Blum et al., 2005; Chen et al., 2001; Chun et al., 2010; Kikuchi et al., 2009). Additionally, RAS family proteins act upstream PI3K/AKT/mTOR pathway, which is a regulatory axis with deep effects on aerobic glycolysis and cellular biosynthesis. This pathway has been shown to stimulate cell growth and ATP production by regulating the activity and expression of key glycolytic enzymes and nutrient transporters, enabling increased uptake of glucose, aminoacids and other nutrients (Barata et al., 2004; Edinger and Thompson, 2002; Roos et al., 2007; Wieman et al., 2007). In addition, AKT activation is sufficient to increase glycolysis and lactate production to induce a Warburg effect in either transformed cells or cancer cells (Elstrom et al., 2004; Plas et al., 2001; Rathmell et al., 2003). RAS also induces the Warburg effect partly through increasing the activity of MYC in an example of a cooperative mechanism between oncogenes to regulate metabolism (Sears et al., 1999).

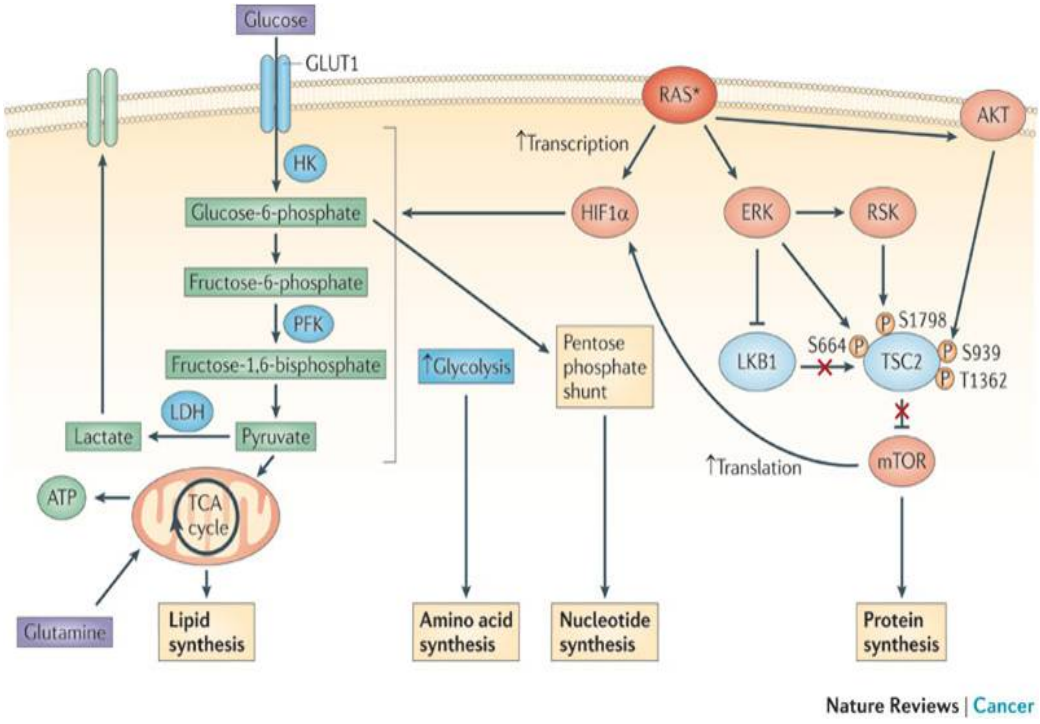

Figure 2.3 RAS effects on metabolism

RAS exerts most of its metabolic effects by activating hypoxia inducible factor 1α (HIF1α), either directly or via activation of PI3K/AKT or ERK, both converging in the activation of mTOR (mammalian target of rapamycin), which subsequently activates HIF1α. The activation of HIF1α leads to an overexpression of some glycolytic enzymes such as hexokinase (HK), phosphofructokinase (PFK) or lactate dehydrogenase (LDH). The activation of glycolysis promotes an increase of metabolic precursors available for synthesis of macromolecules such as lipids, aminoacids and proteins, and nucleotides. Also, part of the RAS-induced metabolic effects can be carried out by AKT or mTOR activation through a HIF1α-independent process. TSC2, tuberin or tuberous sclerosis 2; LKB1, liver kinase B1; RSK, ribosomal protein S6 kinase. Reprinted by permission from Macmillan Publishers Ltd: Nature Reviews Cancer. Pylayeva-Gupta, Y., E. Grabocka, et al. (2011). RAS oncogenes: weaving a tumorigenic web. Nat Rev Cancer 11(11): 761-774, Copyright © 2011.

2.2.1.3 Glutamine catabolism and ATP production

Although glucose is the major energetic substrate, other nutrients can be processed with energetic purposes. One of the nutrients most largely available to tumors is glutamine, the most abundant aminoacid in the plasma. Tumor cells consume glutamine in a larger amount than normal cells both *in vitro* and *in vivo*. (Eagle, 1955; Sauer and Dauchy, 1983; Sauer et al., 1982). These observations led to the notion that

glutamine metabolism stood with the Warburg effect as a major component of the general metabolic phenotype of tumor cells.

Glutamine takes part in many different physiological processes in the cells, being involved in both ATP and NADPH production as well as in biosynthetic and anaplerotic reactions. These processes can roughly be divided into reactions that use glutamine for its γ-nitrogen (nucleotide and hexosamine synthesis) and those that use either the α-nitrogen or the carbon skeleton directly from glutamine or from glutamine-derived glutamate or α-ketoglutarate (transamination, synthesis of aminoacids, lipids, or glutathione, ATP and NADPH production) (DeBerardinis and Cheng, 2010). Oxidation of glutamine carbon skeleton in the mitochondria with energetic purposes is an important metabolic fate of glutamine. The complete oxidation of glutamine requires α-ketoglutarate to progress along the TCA cycle and the exit as malate, its conversion first to pyruvate by malic enzyme and next to acetyl-CoA (ACoA) to finally reentry into TCA cycle with the subsequent ATP production. Alternatively, cells can partially oxidize glutamine and the formed pyruvate can be converted to lactate in a process known as glutaminolysis (DeBerardinis et al., 2007). In both complete and partial oxidation of glutamine, this aminoacid contributes to the synthesis of not only ATP through oxidative phosphorylation (OXPHOS) but also NADPH.

2.2.2 Building a new cell: biosynthetic processes in cancer cell metabolism

The Warburg effect provides proliferating cells with a rapid and oxygen-independent source of ATP, as well as metabolic intermediates for biosynthesis of macromolecules. The latter aspect is critical to provide cells with enough nucleotides, proteins, and lipids for a cell to double their total biomass and then divide to produce two daughter cells. This process requires a profound remodeling of metabolism, which involves the major metabolic pathways shown in Figure 2.4.

In contrast to the catabolic metabolism of differentiated cells, the anabolic metabolism, essential to cell growth and proliferation, is not focused on maximizing ATP yield.

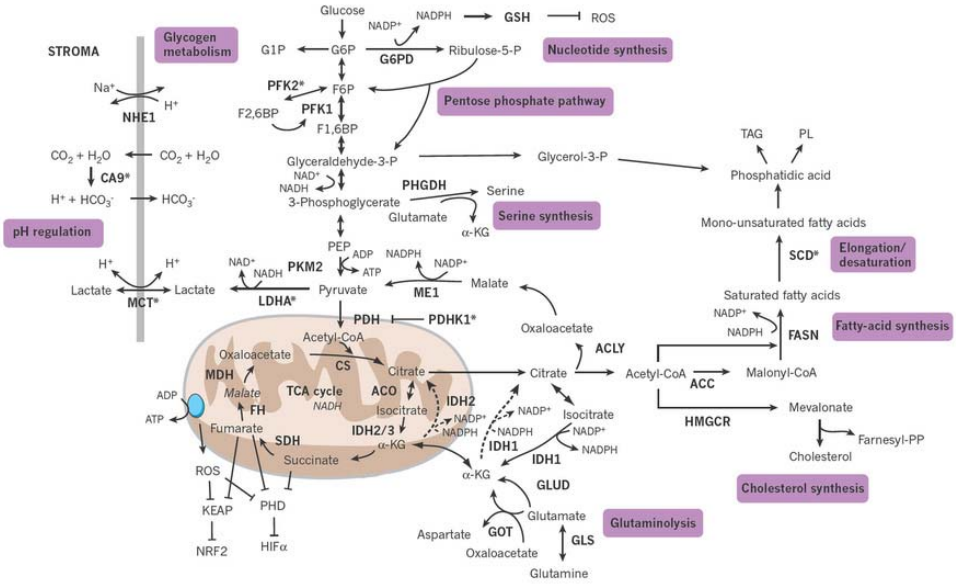

Figure 2.4 Main metabolic pathways involved in tumor metabolic reprogramming

The picture shows an overview of the major metabolic pathways involved in the synthesis of macromolecules: nucleotide synthesis, the pentose phosphate pathway, serine synthesis, glutaminolysis, cholesterol synthesis, fatty-acid synthesis and elongation desaturation. The enzymes involved in these pathways are shown in bold and those induced in response to hypoxia are marked with an asterisk. Reductive carboxylation of α-KG by IDH1 and IDH2 produces citrate for lipid synthesis in hypoxic cells (black dashed arrow). ACC, acetyl-CoA carboxylase; ACLY, ATP citrate lyase; ACO, aconitase; CA9, carbonic anhydrase 9; CoA, coenzyme A; CS, citrate synthase; FASN, fatty-acid synthase; F1,6BP, fructose-1,6-bisphosphate; F2,6BP, fructose-2,6-bisphosphate; F6P, fructose-6-phosphate; FH, fumarate hydratase; GLS, glutaminase; GLUD, glutamate dehydrogenase 1; GOT, glutamic-oxaloacetic transaminase; GSH, glutathione; G1P, glucose-1-phosphate; G6P, glucose-6-phosphate; G6PD, G6P dehydrogenase; HIF, hypoxia inducible factor; HMGCR, 3-hydroxy-3-methylglutaryl-CoA reductase; KEAP, kelch-like ECH-associated protein 1; LDHA, lactate dehydrogenase A; MCT, monocarboxylate transporters; MDH, malate dehydrogenase; ME1, malic enzyme 1; NHE1, Na+/H+ exchange protein 1; NRF2, nuclear factor (erythroid-derived 2)-like 2; PDH, pyruvate dehydrogenase; PDHK1, pyruvate dehydrogenase kinase; PEP, phosphoenolpyruvate; PFK, phosphofructokinase; PHD, prolyl hydroxylases; PHGDH, phosphoglycerate dehydrogenase; PKM2, pyruvate kinase M2; PL, phospholipids; ROS, reactive oxygen species; SCD, stearoyl-CoA desaturase; SDH, succinate dehydrogenase; TAG, triacylglycerides. Modified by permission from Macmillan Publishers Ltd: Nature. Schulze, A. and A. L. Harris (2012). How cancer metabolism is tuned for proliferation and vulnerable to disruption. Nature 491(7424): 364-373, Copyright © 2012.

Rather than ATP, proliferating cells have a greater requirement of carbon and nitrogen, as well as cytosolic NADPH for reductive biosynthetic reactions. The recognition that proliferating cells do not maximize ATP production through mitochondrial oxidative phosphorylation has contributed to the misconception that proliferating cells, particularly cancer cells, do not utilize mitochondria. In fact, most cancer cells and

proliferating normal cells still derive a fraction of their ATP through OXPHOS. However, in proliferating cells, in contrast to quiescent cells, this OXPHOS-dependent production of ATP appears secondary to the use of mitochondrial enzymes in the synthesis of anabolic precursors (Ward and Thompson, 2012). Therefore, a pivotal role of the TCA cycle in proliferating cells might be to act as a hub for biosynthesis, resulting in a continuous efflux of TCA cycle intermediates, in a process named cataplerosis (Owen et al., 2002). A very illustrative example of this process is the synthesis of lipids or lipogenesis. However, a continuous efflux of TCA cycle intermediates from the mitochondria might end up in a depletion of intermediates. This process is compensated by the activation of metabolic routes that contribute to the influx of carbons into TCA cycle in a process called anaplerosis. A paradigmatic example of anaplerosis is the metabolism of glutamine.

2.2.2.1 The synthesis of lipids or lipogenesis

Although most cells in the adult body rely on lipids from the bloodstream, many cancer cells show reactivation of *de novo* fatty acid synthesis (Santos and Schulze, 2012). The high proliferation of cancer cells requires large amount of lipids as building blocks for biological membranes. This enhanced lipid demand is fulfilled through the export of mitochondrial citrate to the cytosol, where it is converted to oxaloacetate and the lipogenic precursor ACoA by the enzyme ATP-citrate lyase (ACLY). Then, oxaloacetate can be converted into pyruvate by the malic enzyme (ME), generating NADPH for lipid synthesis. Fatty acids biosynthesis requires the activation of ACoA to malonyl-CoA, catalyzed by the enzyme acetyl-CoA carboxylase (ACC). The acetyl and malonyl groups are then coupled to the enzyme fatty acid synthase (FASN). Further elongation and desaturation of newly synthesized fatty acids are obtained through the action of a family of enzymes named elongation of very long chain fatty acids (ELOVL) proteins that add two carbons to the end of the chain in each cycle of reaction. Next, desaturation is catalyzed by fatty acyl-CoA desaturases, which include stearoyl-CoA desaturases (SCDs).

In the 60s, it was noted that neoplasic tissues were able to synthesize lipids. Since then, several studies have documented that cancer cells reactivate *de novo* lipid synthesis.

Some cancers show increased expression of FASN (Swinnen et al., 2000; Yoon et al., 2007). Moreover, ACLY has been shown to be required for cell transformation *in vitro* and for tumor formation *in vivo* (Bauer et al., 2005; Hatzivassiliou et al., 2005), and chemical inhibition of ACC induces growth arrest and apoptosis in prostate cancer cells (Beckers et al., 2007). These studies demonstrate that lipogenesis is essential in tumorigenesis.

Furthermore, lipogenesis is controlled by many signaling pathways often deregulated in cancer. Expression of the enzymes involved in the synthesis of fatty acids and cholesterol is regulated by the sterol regulatory binging proteins family (SREBPs), which are in turn partially regulated by PI3K/AKT/mTOR, and have been found overexpressed in a number of cancers (Menendez and Lupu, 2007). AKT can also phosphorylate ACLY (Berwick et al., 2002) and activate the expression of several genes involved in cholesterol and fatty-acid biosynthesis (Porstmann et al., 2005). Moreover, lipogenesis is also controlled by RAS oncogene through the action of HIF1, which induces the expression of FASN in human breast cancer cell lines, (Furuta et al., 2008). In this regard, the activity of stearoyl-CoA desaturase 1 (SCD1) has been demonstrated to be essential for RAS-mediated transformation (Fritz et al.).

2.2.2.2 Mitochondrial metabolism and glutamine as biosynthetic precursor

Mitochondrial metabolism roughly consist of the metabolic reactions that make up TCA cycle, where reduced coenzymes are generated, and the process termed oxidative phosphorilation, where the coenzymes are oxidized back in a process placed in the electron transport chain that involves oxygen consumption and ATP production.

The export of citrate for lipid synthesis impacts over the function of the TCA cycle, resulting in what has been called a “truncated” cycle due to the relative decrease in the fraction of citrate that is oxidized (Hatzivassiliou et al., 2005; Parlo and Coleman, 1986). To sustain TCA cycle function and compensate for cataplerotic processes, cells must activate an influx of carbons through anaplerotic reactions to resupply mitochondrial intermediates. This essential feature of proliferating metabolism is known as anaplerosis

provides cells with the ability to use TCA cycle as a hub of macromolecules precursors. Several mechanisms exist to produce anaplerotic activity within the cell. The main of them uses pyruvate carboxylase (PC), which transforms pyruvate into OAA that replenish TCA cycle to keep on cycling.

An alternative source of anaplerosis is through metabolism of aminoacids, particularly glutamine. Proliferating cells metabolize glutamine in multiple processes for bioenergetics and biosynthesis. As mentioned earlier, these processes can roughly be divided into reactions that use glutamine for its γ-nitrogen and those that use either the α-nitrogen or the carbon skeleton (DeBerardinis and Cheng, 2010). The processes in the second group are tightly related to anaplerotic reactions, since they supply carbon atoms to TCA cycle.

The role of glutamine anabolism in cancer cell proliferation and survival has been demonstrated to be essential in certain types of cancer (Wise et al., 2008; Yuneva et al., 2007) and it has even been suggested that some tumors are glutamine addicted (Wise et al., 2008). Furthermore, this aminoacid also contributes importantly to the synthesis of lipids, not only by oxidative metabolism of its carbons but also by reductive carboxylation via its conversion to α-ketoglutarate and subsequently to isocitrate by IDH reversible reaction. This process is particularly important in hypoxia, VHL-deficient cells (cells with mutation or suppression of the von Hippel Lindau protein) and tumor cells with defective mitochondria, since it has been demonstrated to sustain cell growth and proliferation under these circumstances (Gameiro et al., 2013; Holleran et al., 1995; Metallo et al., 2012; Mullen et al., 2012; Wise et al., 2011).

Mitochondrial metabolism is the main source of metabolic precursors for anabolic reactions that allow cells to proliferate. Then, it is expected that the master signaling pathways that drive proliferation control directly or indirectly mitochondrial metabolism. In particular, the PI3K/AKT/mTOR pathway, as it has been described previously, regulates lipid metabolism and, unbreakably, mitochondrial metabolism. Also some of the most relevant oncogenes trigger important effects on mitochondrial and glutamine metabolism (Li et al., 2005). For instance, MYC oncogene promotes mitochondrial and glutamine metabolism and cells overexpressing this oncogene are glutamine addicted,

since glutamine metabolism inhibition leads to cell death in *vitro* and inhibition of the tumor growth *in vivo* (Gao et al., 2009b; Li et al., 2005; Wise et al., 2008) (Dang et al., 2009).

RAS oncogene also modulates mitochondrial metabolism, although the metabolic consequences of this modulation are not fully understood. Some studies performed using human KRasV12-transfected cells (Hu et al., 2012) and mouse HRasV12-transfected cells (Yang et al., 2010a) describe that RAS oncogenic activation leads to an impairment of mitochondrial respiration combined with a gradually acquisition of the Warburg effect. Also, an impairment of mitochondrial respiration has been reported in mouse fibroblast transfected with oncogenic H-RasQ61L (de Groof et al., 2009). On the contrary, human HRasV12-expressing cells have been reported to increase mitochondrial metabolism (Telang et al., 2007). Despite of these opposed conclusions on the regulation of mitochondrial metabolism by RAS, it is widely accepted that glutamine and mitochondrial metabolism are essential for cell cycle progression (Gaglio et al., 2009) and *in vivo* tumorigenesis in KRAS-driven tumors (Son et al., 2013; Weinberg et al., 2010). Moreover, it has been documented that K-RAS regulates a specific pathway for glutamine mitochondrial metabolization where glutamine-derived glutamate can be converted into oxaloacetate by aspartate transaminase and this oxaloacetate is subsequently converted into malate and then pyruvate by malic enzyme, increasing the NADPH/NADP ratio (Son et al., 2013).

2.2.2.3 The pentose phosphate pathway

An increased proliferation requires the fulfillment of an enhanced demand of DNA and RNA synthesis. DNA and RNA are polymers of nucleotides, which consist of a nucleobase, a five-carbon sugar (ribose or deoxyribose), and a phosphate group. The five-carbon sugar or pentose is mainly synthesized through the pentose phosphate pathway (PPP), being then this pathway essential to nucleotide production.

On the other hand, the increased biosynthetic activity of cancer cells requires not only synthesis of precursors of macromolecules, but also an increase in the production of

reduced equivalents such as NADPH (Ward and Thompson, 2012). This cofactor is involved in many essential processes in the cell, such as lipids, nucleotides and aminoacids synthesis. Moreover, NADPH is used in the maintenance of the reduced glutathione pool to counteract oxidative stress. At least five sources of NADPH exist in the cell: ME, IDH, aldehyde dehydrogenase (ALDH), NAD kinase (NADK) and the enzymes of the PPP glucose-6-phosphate dehydrogenase (G6PD) and 6-phosphogluconate dehydrogenase (6PGD). The role that each reaction plays in providing cells with NADPH remains to be examined in deeper detail and it is probable that cells do not rely on a single NADPH generating system (Pollak et al., 2007; Wamelink et al., 2008).

Then, the PPP is committed to both the production of macromolecules and to the supply of reduced equivalents. It provides an alternative pathway for glucose oxidation and the percentage of glucose metabolized through PPP may vary from 5 to 30% in a tissue dependent-manner.

PPP is classically divided into the oxidative and the nonoxidative branch (Figure 2.5). The oxidative branch is a non-reversible metabolic pathway. There, glucose-6-phosphate is transformed into 6-phosphoglucono-δ-lactone by G6PD, which is hydrolyzed to 6-phosphogluconate by 6-phosphoglucolactonase (PGLS) and subsequently transformed into ribulose-5-phosphate 6PGL with the subsequent production of NADPH and CO_2. The resulting ribulose-5-phosphate can be then converted into ribose-5-phosphate and used for the synthesis of nucleotides. Proliferating cells require high amounts of pentoses phosphate, and this demand is particularly high in cancer cells. There are two main conditions that regulate the activity of PPP. The first one is the cell proliferation rate: the greater is the proliferation, the greater is the requirement for ribose-5-phosphate and NADPH. The second condition is the requirement of NADPH. The enzyme of the oxidative branch of the PPP G6PD, can be active in human cells as a dimer or tetramer (formed by the association of two dimers), each inactive monomer being composed of 515 aminoacids (Au et al., 2000; Riganti et al., 2012). The $NADP^+$ amount is critical for the activity of this enzyme. G6PD activity is directly related to the $NADP^+$/NADPH ratio, since $NADP^+$ is necessary for stabilizing the dimer (Au et al., 2000).

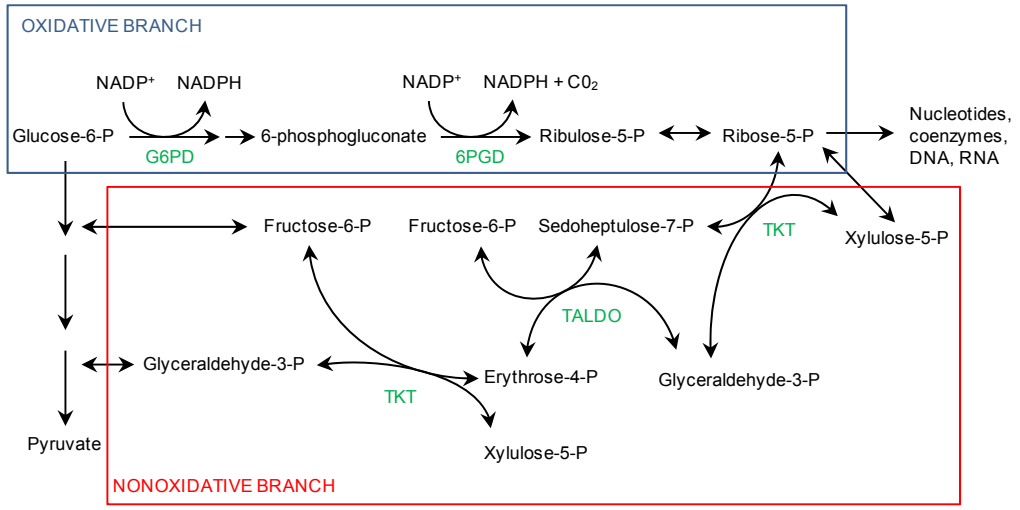

Figure 2.5 Metabolic scheme of the pentose phosphate pathway

The oxidative and nonoxidative branches of the pentose phosphate pathway are depicted. The irreversible oxidative pathway is catalyzed by G6PD (glucose-6-phosphate dehydrogenase), 6-phosphogluconolactonase (not shown) and 6PGD (6-phosphogluconate dehydrogenase). This branch produces NADPH, used to convert the oxidized form of glutathione into the reduced form and to synthesize fatty acids. The reversible nonoxidative pathway carries out a carbon exchange between PPP and glycolysis, either recycling the excess of pentoses or synthesizing ribose from glycolytic intermediates. The main enzymes involved in this branch are TKT (transketolase) and TALDO (transaldolase).

When NADPH raises, some NADPH molecules might bind G6PD instead of $NADP^+$, but NADPH lacks stabilizing effects (Kotaka et al., 2005) and reduces G6PD activity. It is worth noting that G6PD usually works at 1-2% of its maximal potential in healthy subjects, because of the high concentration of NADPH in resting conditions. Upon NADPH oxidation, $NADP^+$/NADPH ratio increases and G6PD shifts to the most active state, increasing oxidative PPP flux (Eggleston and Krebs, 1974). Consistent with the role of G6PD in the synthesis of NADPH for lipogenesis, a negative regulation of this enzyme by the lipid intermediate palmitoyl-CoA has also been described (Asensio et al., 2007).

The nonoxidative branch of the PPP, on the contrary to the oxidative one, consists of a set of reversible reactions. In this branch, ribose-5-phosphate and xilulose-5-phosphate generated from glucose-6-phosphate undergo the exchange of two carbon units operated by tranketolase enzyme (TKT), to yield glyceraldehyde-3-phosphate and sedoheptulose-7-phosphate. These two products generate fructose-6-phosphate and

erytrose-4-phosphate via a three carbon exchange reaction catalyzed by transaldolase (TALDO). Next, TKT catalyzes again the exchange of two carbon units between a second xylulose-5-phosphate and erytrose-4-phosphate, finally producing fructose-6-phosphate and glyceraldehyde-3-phosphate, which can be either metabolized in the glycolytic pathway or reintroduced in the PPP.

Since PPP provides essential substrates required for proliferation and also regulates oxidative through the synthesis of NADPH, changes in the PPP activity usually occur during cancer development and progression. PPP plays a role in many aspects of tumor biology, such as proliferation and survival, tumor invasion, angiogenesis, and response to chemo- and radiotherapy, and it has been proposed that the regulated activation of the entire PPP could be regarded as a hallmark of cell transformation (Riganti et al., 2012). Because intracellular nucleotides reservoir is unable to meet the requirements for cell duplication, the metabolic routes that provide the cell with precursors of these nucleotides are needed to be upregulated in proliferating tissues. Accordingly, an overexpression of the main PPP genes has been shown in certain tumor types including gastric, colorectal and kidney (Kekec et al., 2009; Langbein et al., 2008). Furthermore, G6PD and TKT are both increased in human colon cancer cells and their maximal activity is found during late G1 and S phases, suggesting that changes in PPP mediate in cell cycle progression (Vizan et al., 2009).

In particular, the role of the oxidative PPP branch in tumor biology has been studied in the context of cell proliferation and transformation. Although G6PD works at a low basal rate in nontransformed cells, it can exert a strong proliferative role when it becomes deregulated. The key role of G6PD in tumorigenesis is also supported by the fact that G6PD gene overexpression transforms NIH3T3 cells and induces tumors in nude mice (Kuo et al., 2000). In accordance, cells overexpressing G6PD proliferate more than wild-type cells (Leopold et al., 2003; Tian et al., 1998).

On the other hand, also the nonoxidative branch has been described to contribute importantly to ribose-5-phosphate synthesis in tumors (Boros et al., 1998; Cascante et al., 2000). Given the reversibility of the reactions involved in the nonoxidative branch, an increased glycolysis (Warburg effect) can enhance the use of this branch (Pelicano et al.,

2006). In experiments *in vitro* using pancreatic adenocarcinoma cells, around 85% of the ribose has been reported to be synthesized through the nonoxidative pathway and the inhibition of TKT by oxythiamine led to a decrease of 90% in final tumor mass in mice hosting Ehrlich's ascitic tumor (Boros et al., 1997). Furthermore, in pancreatic ductal adenocarcinoma mouse model ribose biogenesis is mainly carried out through the nonoxidative PPP branch and it is essential for tumor progression *in vivo* (Ying et al., 2012).

The enzyme TKT belongs to a family that includes genes encoding TKT and two other TKT-like proteins (TKTL1 and TKTL2)(Coy et al., 2005). Given the important role of TKT described in some tumors , the presence and state of all three isoforms has been examined in cancer cells (Coy et al., 2005) and overexpression of TKTL1 has been found in some tumors (Krockenberger et al., 2007; Langbein et al., 2006; Staiger et al., 2006). Moreover, TKTL1 contributes significantly to the total TKT activity in human hepatoma and colon cancer cells (Hu et al., 2007; Xu et al., 2009; Zhang et al., 2007). It has also been demonstrated that the specific inhibition of TKTL1 expression by shRNA triggers apoptosis and suppresses tumor growth in HCT116 colon cancer cells (Xu et al., 2009). Finally, although more efforts are required to elucidate the role of TKTL1 in cancer, it has been hypothesized that this isoform could generate ACoA, which would link glycolysis and lipogenesis through the non-oxidative PPP (Coy et al., 2005).

In the context of anabolic tumor metabolism, PPP is regulated by some of the most important oncogenes and tumor suppressor genes. It has been described that oncogenic transformation by K-RAS is accompanied by an increase in PPP and glycolysis because of the simultaneous upregulation of G6PD, pyruvate kinase (PK) and lactate dehydrogenase (LDH) (de Atauri et al., 2011). Moreover, it has been demonstrated that K-RAS drives glycolysis intermediates into the nonoxidative PPP for ribose biogenesis in pancreatic ductal adenocarcinoma cells (Ying et al., 2012). Also, PI3K/AKT signaling promotes anabolic metabolism through PPP by activating NRF2, a transcription factor involved in response to cellular stress that activates G6PD among other enzymes. Under activation of PI3K signaling, TKT and G6PD are essential to NRF2-driven tumor proliferation and their simultaneous inhibition impaired tumor growth *in*

vivo (Mitsuishi et al., 2012b). On the other hand, tumor suppressor genes also regulate PPP. A very illustrative example is the case of p53, which modulates PPP activity by regulating G6PD dimer formation (Jiang et al., 2011).

2.2.3 Maintenance of redox homeostasis: ROS detoxification

As a result of the oxidative metabolism carried out mainly in the mitochondria, not only many essential compounds are produced, but also waste by-products that must be either excreted or neutralized. Part of these compounds are known collectively as reactive species and can be toxic if the concentration increases, producing what is commonly known as oxidative stress. Reactive species can be classified into four groups based on the main atom involved: reactive oxygen species (ROS), reactive nitrogen species (RNS), reactive sulfur species (RSS) and reactive chloride species (RCS). Among all the compounds derived from oxidative metabolism, ROS are the most abundantly produced. ROS are essential for many biological functions such as cell growth and differentiation, enzyme regulation or inflammation, and they regulate many signal transduction pathways involved in these processes. They can be produced either inside the cells (internal sources) or by environmental agents (external sources). Sources of internal oxidative stress include peroxisomes and enzymes, particularly the detoxifying enzymes from the p450 complex, xanthine oxidase complexes, and the NADPH oxidase complexes. Most of these enzymes operate in the mitochondria, which is the main source of oxidative stress. With regard to the external sources of oxidative stress, they include UV radiation, chemical compounds and exercise (Sosa et al., 2013).

2.2.3.1 ROS, cancer and oncogenes

Oxidative stress is important from the biomedical point of view because it is related to a wide variety of illnesses, such as cancer. A moderate increase in ROS can promote cell proliferation and differentiation, whereas excessive amount of ROS can damage many molecules, including DNA, RNA, lipids and proteins, inducing senescence and/or cell death (Figure 2.6) (Perry et al., 2000). Then, levels of ROS need to be finely regulated

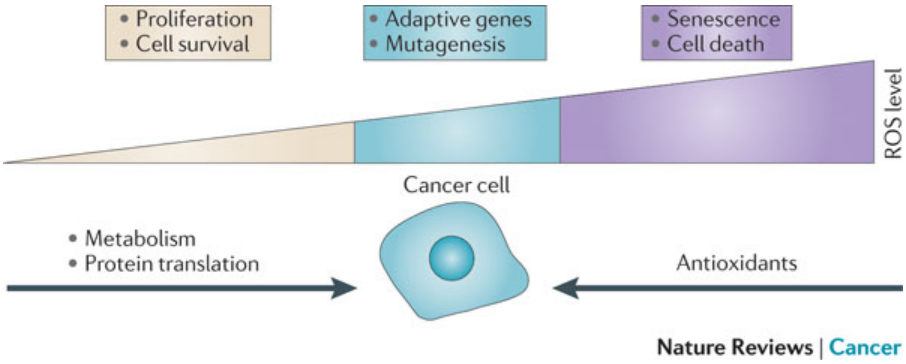

Figure 2.6 ROS levels and cancer

Cancer cells deal with increased levels of ROS as a consequence of intrinsic or extrinsic factors. A slight increase in ROS levels can promote proliferation and cell survival. However, a great increase results in cell death and senescence. Then cancer cells must keep a balance between processes producing and removing ROS. This is achieved by activating a serie of genes involved in ROS detoxification, such as NRF2-KEAP1 system, which lead to the synthesis of antioxidants that allow cells to counter the excess of ROS, but also increases the chance that the cell experience additional ROS-mediated mutagenic events and stress responses that promote tumorigenesis. Reprinted by permission from Macmillan Publishers Ltd: Nature Reviews Cancer. Cairns, R. A., I. S. Harris, et al. (2011). Regulation of cancer cell metabolism. Nat Rev Cancer 11(2): 85-95, Copyright © 2011.

(Boonstra and Post, 2004) and this regulation is achieved through modulating the ROS generation and elimination by scavenging systems, such as superoxide dismutases, glutathione peroxidase, peroxiredoxins, glutaredoxins, thioredoxins or catalase.

Abnormal cancer cell growth is associated with increase in ROS and reflects a disruption of redox homeostasis, due to either an elevation of ROS production or to a decrease of ROS-scavenging capacity, resulting in a condition known as oxidative stress. Oxidative stress mediated signaling events have been reported to affect all features of cancer cell behavior, including cell cycle progression and proliferation, cell survival and apoptosis, energy metabolism, cell morphology, motility and adhesion, angiogenesis, and tumor stemness (Sosa et al., 2013). This regulation is performed by modulating several signaling pathways profoundly involved in cancer, such as MAPK pathway or PI3K/AKT pathway (Liou and Storz, 2010). In fact, the requirement of ROS in tumorigenesis is clearly demonstrated by the mechanisms developed by cancer cells to avoid ROS activation of p38α, a negative regulator in the process of transformation induced by H-RAS (Dolado et al., 2007). Because the increase in ROS may play an important role in cancer initiation and progression, such oxidative stress is often viewed as an adverse

event. Nevertheless, as excessive levels of ROS stress can be toxic, cancer cells with increased oxidative stress are likely to be more vulnerable to damage by further ROS insults induced by exogenous agents, opening new avenues for therapeutic intervention (Trachootham et al., 2009).

Compared to normal cells, malignant cells display higher levels of endogenous oxidative stress *in vitro* and *in vivo* (Kawanishi et al., 2006; Szatrowski and Nathan, 1991). Breast tumors are a paradigmatic example, since they are characterized by persistent ROS generation (Brown and Bicknell, 2001; Kang, 2002). Also, markers of constitutive oxidative stress have been detected in samples from *in vivo* breast carcinomas (Toyokuni et al., 1995; Portakal et al., 2000). In the same line, 8-hydroxy-2'-deoxyguanosine, one of the major oxidatively modified DNA base products, is almost ten-fold more prevalent in invasive ductal breast carcinoma cells than in normal control samples from the same patient (Toyokuni et al., 1995).

Despite the clear implications of ROS in tumorigenesis, the precise mechanisms leading to oxidative stress in cancer cells remain unclear. However, some intrinsic and extrinsic mechanisms are demonstrated to cause oxidative stress during cancer development and disease progression. Oncogene activation, aberrant metabolism, mitochondrial dysfunction, and loss of p53 are intrinsic factors known to cause increased ROS production in cancer cells. Moreover, the expression of genes associated with tumor transformation, such as *RAS, BCR-ABL* and *c-MYC*, were found to induce ROS production (Trachootham et al., 2006; Weinberg et al., 2010). In HRasV12-transformed NIH3T3 fibroblasts, a large amount of superoxide was generated through the activation of the membrane associated ROS-producing enzyme NADPH oxidase (NOX) (Irani et al., 1997).

In addition to the intrinsic mechanisms, extrinsic ones such as inflammatory cytokines, imbalance of nutrients, and a hypoxic environment could also affect intracellular redox homeostasis (Cook et al., 2004). As cancer cells actively produce high levels of ROS and are continuously exposed to oxidants, it is reasonable that oxidative stress may exert selective pressure to enrich the population of cells that are capable of adapting to oxidative stress. Those cells that survive under oxidative stress are likely to have

acquired adaptive mechanisms to counteract the potential toxic effects of elevated ROS and promote cell survival pathways. For instance, oncogenic HRas-transformed cells, which exhibited increased superoxide and hydrogen peroxide levels, were shown to express higher levels of antioxidant enzymes such as peroxiredoxin-3 and thioredoxin peroxidase compared with their non-tumorigenic parental cells (Young et al., 2004). Their enhanced antioxidant capability is likely to serve as a key mechanism to evade ROS-induced apoptosis as evidenced by the resistance to hydrogen peroxide-induced cell death that was observed in the HRas-transformed cells (Young et al., 2004). In the same line, RAS-transformed cells were also found to be more sensitive to depletion of glutathione, leading to ROS accumulation and cell death (Trachootham et al., 2006). Also, an increase of the flux through the oxidative branch of PPP (Vizan et al., 2005) as well as the overexpression of the NADPH producing enzyme G6PD has been reported in KRas-transfected NIH3T3 cells (de Atauri et al., 2011; Vizan et al., 2005). Then, it is possible that along tumorigenesis, oncogenic signals stimulate both the formation of ROS to enhance proliferation and the promotion of antioxidant mechanisms to minimize oxidative damage. The mechanisms of redox regulation involve multiple signaling pathways which employs several antioxidant-sensitive transcription factors such as nuclear factor-κB (NF-κB), nuclear factor (erythroid-derived 2)-like 2 (NRF2), c-JUN, and HIF1, which led to the increased expression of antioxidant molecules such as superoxide dismutase (SOD), catalase, thioredoxin and reduced glutathione.

2.2.3.2 The NRF2 detoxification system

Of particular interest in redox homeostasis maintenance is the role of NRF2 transcription factor. It is a potent transcriptional activator that plays a pivotal role in the inducible expression of many cytoprotective genes in response to oxidative stress. The main regulator of NRF2 is the protein Kelch-like ECH-associated protein 1 (KEAP1). Under normal conditions, NRF2 is constantly ubiquitinated through KEAP1 in the cytoplasm, and degraded in the proteasome (Figure 2.7). KEAP1 is a thiol-rich protein that possesses multiple highly reactive cysteine residues. Upon exposure to ROS, these cysteine residues are modified, leading to the inactivation of KEAP1 and the stabilization

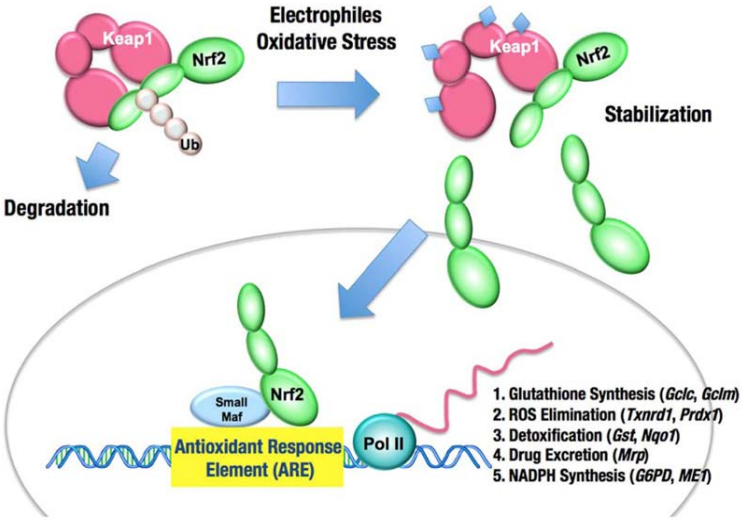

Figure 2.7 KEAP1-NRF2 system

Under normal conditions, NRF2 is constantly ubiquitinated through Keap1 and degraded in the proteasome. Following exposure to electrophiles or oxidative stress, KEAP1 is inactivated. Stabilized NRF2 accumulates in the nucleus and activates many cytoprotective genes. Ub, ubiquitin. Original work from Mitsuishi, Y., H. Motohashi, et al. (2012). The Keap1-Nrf2 system in cancers: stress response and anabolic metabolism. Front Oncol 2: 200 doi: 10.3389/fonc.2012.00200.

of NRF2. Consequently, NRF2 translocates into the nucleus and activates the transcription of many cytoprotective genes that encode detoxifying enzymes and antioxidant proteins. NRF2 target genes are mainly involved in glutathione synthesis, the elimination of ROS, xenobiotic metabolism, and drug transport (Mitsuishi et al., 2012a).

Interestingly, an increase in NRF2 levels has been frequently detected in various types of human cancers, resulting in an overactivation of its target genes that provide cells with additional capabilities of malignance (Kim et al., 2010; Singh et al., 2006; Solis et al., 2010; Tsai et al., 2008). Also, highly activated NRF2 target genes confer a great advantage to cancer cells for survival against anticancer drugs and irradiation (Singh et al., 2010; Zhang et al., 2010). Moreover, NRF2 knockdown in constitutively NRF2-activated lung cancer cells suppresses tumor growth, and results in increased sensitivity to chemotherapeutic drug–induced cell death *in vitro* and *in vivo*. (Singh et al., 2008).

Several mechanisms have been reported to explain the increased activity of NRF2-KEAP1 system in cancer cells: somatic mutation in *KEAP1* or *NRF2*, DNA hyperventilation at the promoter region, the aberrant accumulation of proteins that disrupt the KEAP1-NRF2 interaction, transcriptional upregulation of NRF2 gene through oncogene-dependent signaling, and the modification of KEAP1 protein through oncometabolites (Mitsuishi et al., 2012a). The regulation of NRF2 by oncogene-dependent signaling is particularly interesting (Ganan-Gomez et al., 2013). In a recent study, this type of regulation has been described to be determinant in NRF2 activity (DeNicola et al., 2011). Therein, it is reported that K-RAS activates *NRF2* transcription through the MEK-ERK-JUN signaling pathway and reduces ROS levels in primary fibroblasts. Furthermore, the activation of this transcription factor by oncogenic signals is demonstrated to play a pivotal role in ROS detoxification and tumorigenesis (DeNicola et al., 2011).

A significant portion of the genes regulated by NRF2 are metabolic genes involved in PPP and NADPH production, such as *G6PD, PGD* (phosphoglycerate dehydrogenase), *TKT*, *TALDO1* (transaldolase 1), *ME1* (malic enzyme 1) and *IDH1* (isocitrate dehydrogenase 1), all of them containing antioxidant response element sequences in their promoters. These genes are not only involved in maintenance of redox homeostasis but also in anabolic reactions for synthesis of macromolecules. Indeed, PPP enzymes G6PD and TKT are reported to be essential to NRF2-induced tumor growth *in vitro* (Mitsuishi et al., 2012b). NRF2 also promote glutamine consumption through enhancing glutaminolysis and glutathione synthesis. Then, these results place NRF2 as the cornerstone in the interface between redox homeostasis maintenance and anabolic metabolism, pointing out the intimate collaboration between carbon metabolism and ROS detoxification systems.

2.2.3.3 The metabolic network in the maintenance of redox homeostasis

The metabolic network plays a fundamental role in redox homeostasis. Some metabolic reactions produce reduced coenzymes, such as NADPH, which are essential to the maintenance of the reduced antioxidants pool. On the other hand, the use of some metabolic routes, such as TCA cycle, can increase the concentration of ROS. In this

regard, the Warburg effect has often been considered as an adaptive mechanism not only to produce high amounts of glycolytic intermediates required for proliferation of cells but also to avoid ROS generation proceeding from oxidative metabolism in the mitochondria (Sosa et al., 2013). Besides, this high glycolytic rate also provides substrates for PPP that contribute to ROS homeostasis via NADPH production, as described earlier. In this sense, the essential role of the enzyme G6PD in protection against oxidative stress is sturdily documented (Cheng et al., 2004; Gao et al., 2009a; Ho et al., 2000). The shunting of glycolytic intermediates towards PPP is finely regulated by the enzyme PKM2. This enzyme oscillates between an active tetrameric form and an almost inactive dimeric form. The tetrameric form displays high affinity to its substrate, phosphoenolpyruvate (PEP), then promoting conversion of glucose to lactate. The dimeric form displays low affinity by PEP, promoting the accumulation of glycolytic intermediates and its use in different biosynthetic processes (Mazurek, 2011). It has been shown that PKM2 oxidation on C358 in high ROS concentrations reduces PKM2 activity by impairing tetramer association. (Anastasiou et al., 2011). This ROS-dependent inhibition of PKM2 leads to an enhanced flux of glucose-6-phosphate into the PPP which provides NADPH required for glutathione reductase to generate reduced glutathione (GSH) for ROS detoxification. The impairment of this mechanism has been demonstrated to result in sensitization to oxidative stress and increased apoptosis (Brimacombe et al., 2010). Moreover, PKM2 activity is also regulated by growth-factor signaling pathways. In particular, PKM2 is regulated by RAS oncogene, which induces its tetramerization and subsequently the Warburg effect (Mazurek, 2011; Mazurek et al., 2001). Then, many of the oncogenes that induce both the Warburg effect and ROS generation simultaneously, such as RAS, are indeed inducing a dual metabolic program aimed to provide cancer cells with metabolic precursors and ROS protection, fulfilling two essential requirements for tumor progression.

Glycolysis is not the unique metabolic pathway involved in redox homeostasis. Also glutaminolysis participates in redox regulation by providing carbons for NAPDH-producing reactions catalyzed by ME and IDH (DeBerardinis et al., 2007). In an analogous manner to glycolysis, this pathway is regulated by oncogenes that produce ROS deregulation such as RAS (Son et al., 2013). In KRas-mutated pancreatic tumors,

glutamine supports tumor growth by fueling a KRas-regulated metabolic pathway. It leads to an increased NADP/NADPH ratio by enhancing a serie of reactions involving transaminases and malic enzyme (Son et al., 2013).

2.3 THE STUDY OF TUMOR METABOLISM

With the emergence of modern molecular biology, research on cancer metabolism has been mainly focused on the role of oncogenes and tumor suppressor genes and how some of these proteins regulate a particular metabolic pathway, reaction or enzyme (Jones and Thompson, 2009; Levine and Puzio-Kuter, 2010). Although this approach has contributed notably to the current knowledge in cancer metabolism, it often does not suffice to describe the metabolism in great detail. This approach has been traditionally focused on analyzing transcriptomic or proteomic data rather than metabolic information. For instance, transcriptomics data cannot provide information about the directionality or activity of biochemical pathways. Additionally many reactions compete for common substrates what can result in misleading conclusions on the biochemical status of a reaction if only a single reaction or a small portion of the metabolic network is considered. As a consequence, metabolism of tumor cells cannot be studied by using transcriptomics or proteomics data exclusively, and the inclusion of biochemical information will more completely characterize the metabolic phenotype of cancer cells. Therefore, the study of metabolism is commonly addressed from an integrated perspective that aims to consider the metabolic network in its entirety. To this end, experimental and computational approaches are joined in the framework of Computational Systems Biology, an emerging discipline described as the integration of experimental and computational approaches in order to explain and predict complex cellular behavior of biological systems (Borodina and Nielsen, 2005; Cascante and Marin, 2008; Hiller and Metallo, 2012).

Although transcriptomics data can provide very relevant information, metabolic data is still required to reliably study metabolic networks. Metabolomics or “metabolome analysis” addresses the identification and quantification of all the metabolites of an

organism (Fiehn, 2002). Recent advances in mass spectrometry and NMR have allowed for quantification of large amount of metabolites simultaneously (Denkert et al., 2008; Mal et al., 2012). However, while metabolomics provides invaluable information of the metabolic status of a system, it only provides a picture of the metabolic status of the cell in a particular moment. Insights into the performance of the metabolic network cannot be obtained by solely analyzing the concentration of metabolites. Metabolites form part of the metabolic processes that occur within the living cell. The complete metabolic picture is a consequence of the transformation and transport of metabolites throughout metabolic reactions and transport processes, which are finely regulated at different levels, including transcription. To overcome these limitations, the analysis of flux distributions and the changes associated to them are explored at cellular level in the emergent field called fluxomics (Cascante and Marin, 2008; Winter and Kromer, 2013). The fluxome, or the total set of fluxes in the metabolic network of a cell, represents an additional layer of information in Computational Systems Biology. Thus, metabolomics and fluxomics complement each other and allow the study of the metabolism in different contexts, such as tumor cell metabolism (Cascante and Marin, 2008).

2.3.1 Fluxomics: the study of metabolic fluxes

2.3.1.1 Flux Balance Analysis

Metabolic fluxes can be studied at various levels in biological systems, ranging from *in silico* constraint-based models that estimate what is stoichiometrically possible, to experiments that analyze individual metabolic reactions in detail.

A traditional technique employed in the study of metabolic networks is flux balance analysis (FBA). It involves the computational profiling of metabolic flux distributions across all known biochemical reactions based on their stoichiometry (Orth et al., 2010). These techniques can employ annotated genome-scale metabolic networks that are usually pared down using gene expression data. In order to constraint the flux map distribution in *in vitro* metabolic experiments, measurements of metabolite exchanges

with cell culture media are needed. However, due to the complexity of these metabolic networks and depending on the available experimental data, there is usually an important level of uncertainty affecting unmeasured exchanges and internal reactions (ramifications, cycles, etc). The range of possible flux values for each reaction can be determined using linear programming techniques where each reaction flux is maximized or minimized while leaving all other reaction fluxes free, as applied by Llaneras and Pico (Llaneras and Pico, 2007) in the flux spectrum approach. In FBA, the usually large solution space of possible metabolic flux distributions for a particular network is constrained by optimizing particular objective functions (e.g., biomass production). However, in complex biological systems such as tumor cells, a clear objective function to be optimized does not exist. (Hiller and Metallo, 2012).

2.3.1.2 ^{13}C-Metabolic Flux Analysis

2.3.1.2.1 ^{13}C-assisted metabolomics experiments

The use of stable isotope-labeled precursors of metabolic pathways, mainly ^{13}C-labeled substrates, provides a valuable additional source of constraints for reducing the space of possible flux distributions together with those used in FBA mentioned above (Boren et al., 2001; Hellerstein and Neese, 1992). The use of ^{13}C-labeled substrates for flux estimation is commonly known as ^{13}C metabolic flux analysis (^{13}C-MFA) (Antoniewicz, 2013). In these methods, cells are fed with ^{13}C-labeled substrates (also called tracers), resulting in ^{13}C-labeled metabolites downstream of the tracer. Depending on the metabolic pathway driven by the tracer, ^{13}C atoms are incorporated into the newly formed metabolites in distinct numbers and at different positions, producing metabolites with a particular mass isotopomer distribution. In the context of ^{13}C labeling, mass isotopomer (or isotopologue) refers to isomers with specific number of ^{13}C substitutions and positional isotopomer (or isotopomer) to isotopes with ^{13}C substitution in a specific carbon position (Paul Lee et al., 2010). Thus, mass isotopomer accounts for those reaction products with zero, one, two, etc. ^{13}C substitutions, which are denoted as m_0, m_1, m_2, etc. respectively. For a specific metabolite, the number of possible mass isotopomers, n+1, depends on the number, n, of carbons of each

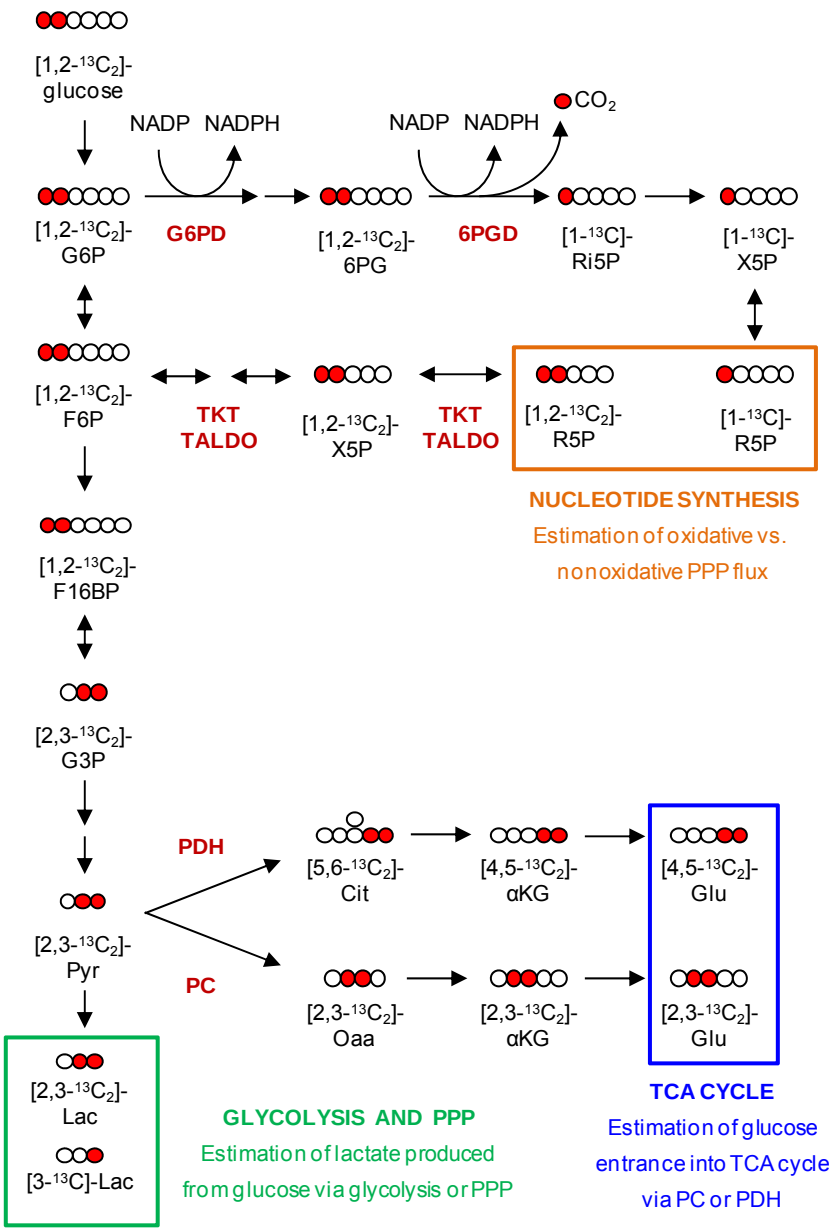

Figure 2.8 ^{13}C-assisted metabolomics experiment using [1,2-^{13}C$_2$]-glucose

The use of [1,2-^{13}C$_2$]-glucose allows estimating the performance of several major metabolic pathways such as pentose phosphate pathway (PPP), glycolysis or TCA (tricarboxylic acid) cycle. The contribution of the oxidative and the nonoxidative PPP branches to R5P (ribose-5-phosphate) production, required for the synthesis of nucleotides, can be estimated by determining the mass isotopomer distribution of RNA ribose through quantifying the percentage of R5P molecules containing one ^{13}C (m1 ribose, mainly [1-^{13}C]-R5P) or two ^{13}C (m2 ribose, mainly [1,2-^{13}C$_2$]-R5P). Also, the mass isotopomer distribution of Lac (lactate) gives information of the pathway used for glucose metabolization, since [2,3-^{13}C$_2$]-Lac (m2 lactate) is produced by glycolysis whereas [3-^{13}C]-Lac (m1 lactate) is produced by metabolization of glucose by PPP, where [1-^{13}C-R5P] is reintroduced into glycolysis through the

metabolite, whereas the positional isotopomers are 2^n. For instance, three-carbon molecules such as lactate can potentially give 3+1=4 mass isotopomers and 2^3=8 positional isotopomers. Thus, a lactate molecule denoted as m_2 can correspond to three possible positional isotopomers ($^{13}C_1$-$^{13}C_2$-$^{12}C_3$, $^{13}C_1$-$^{12}C_2$-$^{13}C_3$ and $^{12}C_1$-$^{13}C_2$-$^{13}C_3$).

When performing a ^{13}C-assisted metabolomics experiment, the selection of the appropriate tracers and labeled products to be analyzed is a major challenge that is conditioned by the intracellular fluxes to be quantified and strongly influences the quality of the estimated fluxes (Metallo et al., 2009). Depending on the fluxes under study, a wide range of tracers exists. Among them, ^{13}C-glucose and ^{13}C-glutamine are the most widely used. Traditionally, ^{13}C tracers have been employed in the study of microbial metabolism, where microorganisms are generally fed with single carbon source (Al Zaid Siddiquee et al., 2004). The issue of tracer choice is more complex in mammalian cell systems, which are cultured with multiple carbon sources and are grown in complex media containing all amino acids and often additional compounds such as nucleotides or lipids. Researchers have used a variety of tracers in order to study particular metabolic pathways, including labeled glucose, glutamine, acetate and atypical substrates such as propionate (Burgess et al., 2007; Collins et al., 2011; Gaglio et al., 2011; Rodriguez-Prados et al., 2010).

Among ^{13}C-glucose tracers, [1,2-$^{13}C_2$]-glucose is one of the most informative and widely used, because it allows the reliable metabolic assessment of glycolysis, pentose phosphate pathway, pyruvate oxidation versus carboxylation or *de novo* synthesis of lipids (Figure 2.8) (Boren et al., 2003; Marin et al., 2003; Vizan et al., 2009). However, in

nonoxidative PPP giving m1 labeled glycolytic intermediates (for simplicity, glycolytic intermediates corresponding to this process are not shown in the figure). Glucose entrance into the mitochondria can also be estimated by analyzing the mass isotopomer distribution of Glu (glutamate). According to the pathway employed to shunt pyruvate into the TCA cycle, the positional isotopomer distribution of glutamate will vary. Entrance of glucose via PDH (pyruvate dehydrogenase) yields [4,5-$^{13}C_2$]-Glu, whereas entrance via PC yields [2,3-$^{13}C_2$]-Glu. Details about the procedures used to determinate the mass isotopomer distribution of all these metabolites are described in *Section 4.10*. G6P, glucose-6-phosphate; G6PD, glucose-6-phosphate dehydrogenase; 6PG, 6-phosphogluconate; 6PGD, 6-phosphogluconate dehydrogenase; Ri5P, ribulose-5-phosphate; X5P, xilulose-5-phosphate; TKT, transketolase; TALDO, transaldolase; F6P, fructose-6-phosphate; F16BP, fructose-1-6-biphosphate; G3P, glyceraldehyde-3-phosphate; Pyr, pyruvate; Cit, citrate; αKG, α-Ketoglutarate.

cancer cells, ^{13}C-glucose does not allow for assessing the TCA cycle fluxes reliably, since, most ^{13}C atoms can be excreted in the form of lactate and alanine. In this case, ^{13}C-glutamine tracers can be used to better resolve the activity of the TCA cycle. One of the most extensively used ^{13}C-glutamine tracer is [U-^{13}C]-glutamine (Metallo et al., 2012)

According to the number of tracers employed in ^{13}C-assisted metabolomics experiments, these can be divided in single labeling experiments and parallel labeling experiments. For a single ^{13}C-assisted metabolomics experiment design, only one experiment is conducted, which can involve the use of a single labeled substrate (e.g [1,2-$^{13}C_2$]-glucose), a mixture of tracers of the same substrate (e.g a mixture of [1,2-$^{13}C_2$]-glucose and [U-^{13}C]-glucose) or multiple labeled substrates (e.g. [U-^{13}C]-glucose and [U-^{13}C]-glutamine). For a parallel labeling experiment design, two or more tracer experiments are conducted in parallel. In each experiment a different tracer set is used (e.g. [1,2-$^{13}C_2$]-glucose in one experiment and [U-^{13}C]-glutamine in the other experiment). Typically, parallel experiments are started from the same seed culture to minimize biological variability (Ahn and Antoniewicz, 2013; Antoniewicz et al., 2006; Crown and Antoniewicz, 2013). Parallel experiments offer several advantages that include tailoring to resolve specific fluxes with high precision, reducing the length of labeling experiments by introducing multiple entry points of tracers, validating biochemical network models, and improving the performance of ^{13}C-MFA in systems where the number of measurements is limited (Crown and Antoniewicz, 2013).

2.3.1.2.2 Mass Isotopomer Distribution Analysis

The mass isotopomer distribution of specific ^{13}C-labeled metabolites downstream the tracer, in combination with measurements of the extracellular fluxes involving the tracer and/or other substrates, can be used to determine either some intracellular fluxes or the ratio among some of them. This is achieved by using simple analytical formulas based on the previous knowledge of the reactions that compose the metabolic network. This ^{13}C-MFA approach is known as Mass Isotopomer Distribution Analysis (MIDA). As an example, ^{13}C tracer propagation from [1,2-$^{13}C_2$]-glucose to ribose can be analyzed to determine the approximate ratio of fluxes through the oxidative and nonoxidative

branches of PPP (Figure 2.8)(Alcarraz-Vizan et al., 2010; Ramos-Montoya et al., 2006). Glycolytic intermediate glucose-6-phosphate loses carbon 1 when metabolized through the oxidative PPP branch, yielding m1 ribose ([2-^{13}C]-ribose). On the contrary, if ribose is synthesized trough the nonoxidative PPP branch, [1,2-^{13}C]-glucose is converted into [1,2-^{13}C]-fructose, which in turn yields m2 ribose ([1,2-^{13}C]-ribose) through the nonoxidative PPP branch reactions. Likewise mass isotopomer distribution of lactate in combination with produced amount of lactate can be used to determine the approximate glucose to lactate flux via PPP and via direct glycolysis, as described in *Section 4.11.1*. In addition, ^{13}C tracer propagation from [1,2-$^{13}C_2$]-glucose to glutamate can be analyzed to estimate the approximate relative contributions of PC and PDH to TCA cycle (Marin et al., 2003). Hence, MIDA provides a simple and fast way to quantify some metabolic fluxes and the relative use of some metabolic pathways.

2.3.1.2.3 Fluxomics

^{13}C-labeled substrates can facilitate the estimation of intracellular fluxes by incorporating labeling data into detailed computational atom-transition metabolic network models. According to the mass isotopomer distribution of the downstream metabolites, this labeling data can correspond to isotopic or nonisotopic steady state. Under isotopic steady state, the isotopomer distribution of a particular metabolite remains stable over time, while it is changing under nonisotopic steady state. In the first case, mass isotopomer distributions can be predicted by analogous methods to those employed in FBA under steady state (Antoniewicz et al., 2006; Antoniewicz et al., 2007). However, isotopic steady state in extracellular metabolites can take too long to reach, thus limiting the application of isotopic analysis to long incubation times. To overcome this limitation, nonisotopic or dynamic flux analysis should be performed. This is carried out by combining the kinetic information of the enzymes involved in the metabolic network under study as well as the concentrations and isotopomer distributions of intermediary metabolites. Estimation of fluxes by this method requires alternative mathematical approaches and may offer improved resolution over isotopic steady-state methods (Baxter et al., 2007; Noh et al., 2006; Selivanov et al., 2006; Selivanov et al., 2005; Selivanov et al., 2010).

Regardless of using isotopic or nonisotopic approaches to estimate the metabolic fluxes, the computational models simulate all the rearrangements of labeled carbon isotopes in the reaction network contributing to the obtained pattern of isotopomer distribution. The computed isotopomer distribution is obtained as a result of simulation of metabolic fluxes; the best fit of all experimental data obtained from ^{13}C-assisted metabolomics experiment

2.3.2 Metabolic control analysis: the identification of controlling enzymes

When analyzing metabolic networks, questions regarding the existence of rate-limiting reactions often arise. The detection of the rate-limiting step in a particular metabolic pathway is of special relevance since variations in its activity change the flux through the metabolic pathway. However, some evidences show that in many cases there is not a unique step controlling the flux of the metabolic pathway, but the control is shared among various steps. (Fell, 1997). Metabolic Control Analysis (MCA) is a powerful approach applied to study the genetic-, enzymatic- and substrate-level regulatory mechanisms in metabolic networks (Fell, 1997; Kacser and Burns, 1973). In the framework of MCA, sensitivity coefficients are estimated to measure in what extent a perturbation of a system parameter (e.g. K_m, V_{max} or enzyme concentration) affects the steady state value of a system variable (e.g. metabolite concentration or flux through a metabolic route), when the whole system is allowed to relax to a new steady state. Among these sensitivity coefficients, the control coefficients are the most important. (Fell, 1997; Kacser and Burns, 1973). System properties of the whole metabolic network are described as a function of the local properties of individual enzymes (or blocks of enzymes). Steady state fluxes through the metabolic network, metabolite concentrations and control coefficients are system properties. Individual enzyme activities and elasticities, by contrast, are local properties, and depend on the specific mechanism and parameters governing the enzyme kinetics. In the framework of MCA, an elasticity ε_{qk} is the parameter sensitivity of the rate v_q (enzyme activity) of an isolated reaction (at the same conditions as in the whole and system at the steady state of

interest) to changes in the concentration x_k of one of its substrates, an inhibitor or any other kinetic effector of the isolated reaction (Cornish-Bowden, 2000; Fell, 1997):

$$\varepsilon_{qk} = \frac{\partial \ln v_q}{\partial \ln x_k} \tag{1}$$

Similarly, a concentration or flux control coefficient is a system property defined as the sensitivity of a steady state metabolite concentration x_g or a steady state flux J_q to changes in some parameter *p,* usually the enzyme concentration that will in principle be proportional to the individual activity of the enzyme v_k (Cornish-Bowden, 2000; Fell, 1997):

$$C_{gk} = \frac{\partial \ln x_g}{\partial \ln p} \Big/ \frac{\partial \ln v_k}{\partial \ln p} = \frac{\partial \ln x_g}{\partial \ln v_k} \tag{2}$$

$$C_{qk} = \frac{\partial \ln J_q}{\partial \ln p} \Big/ \frac{\partial \ln v_k}{\partial \ln p} = \frac{\partial \ln J_q}{\partial \ln v_k} \tag{3}$$

Therefore, the greater the control coefficient of an enzyme, the greater is its contribution to pathway control and regulation, being the flux or the metabolite concentration more sensitive to changes in the activity of this enzyme.

Different approaches have been proposed for deriving control coefficients from elasticities, including methods based on matrix equations (Cascante et al., 1989a; Cascante et al., 1989b; Fell and Sauro, 1985; Reder, 1988; Westerhoff and Kell, 1987). These methods allow the derivation of large expressions describing the control coefficients, whose sign and magnitude are a function of the pathway stoichiometry, the elasticities, and the ratios of fluxes in branched pathways. In systems with moiety conservations, concentrations are also required (Reder, 1988).

However, the sign of a control coefficient (positive or negative) is sufficient to predict whether a flux or concentration will increase or decrease when an enzyme activity is changed. From equations 2 and 3, a positive control coefficient indicates that changes

in x_g or J_q will follow the same pattern as changes in enzyme activity v_k. This means that an increase of v_k will induce an increase of x_g or J_q, while a decrease of v_k will also decrease the value of x_g or J_q. A negative control coefficient, on the contrary, indicates that changes in v_k will induce an inverse effect on x_g or J_q.

Given a particular network structure and when the magnitude of elasticities are unknown, but not their signs, some control coefficients have fixed signs, irrespective of the magnitudes of the elasticities and fluxes, and they are either always positive or always negative (Baldazzi et al., 2010; Sen, 1996). Moreover, some control coefficients are always zero, and other control coefficients are sign-indeterminate, meaning they can be positive or negative depending on the unknown magnitude of the elasticities and fluxes. The classification of control coefficients according to their signs, in general requires only the knowledge of the metabolic network structure and direction of the regulatory dependencies of the network, which basically refer to the positive or negative sign of the elasticities: i) elasticities with respect to substrates or activators are always positive; ii) elasticities with respect to inhibitors (or products in reversible reactions) are always negative. As previously defined (Eqs. 2 and 3), each control coefficient predicts changes in fluxes and concentrations resulting from the change of one enzyme activity. The predictive value of this sensitivity coefficient is defined for infinitesimal changes of the enzyme activity and decays for larger changes. The positive or negative sign of a fixed-sign control coefficient will be maintained for larger changes as long as the sign of elasticities are maintained. These control coefficients with fixed signs can be used in order to evaluate if observed increases or decreases in fluxes and concentrations can be explained by observed increases or decreases in particular enzyme activities.

MCA has had a considerable impact on the study of regulatory processes in central carbon metabolism because of the relevant information it has provided. The estimation of control coefficients has facilitated the correlation between changes at the molecular level and pathological alterations at the physiological level (Agius, 1998). Furthermore, what is of greater interest is the potential application of MCA to the rational design of drug therapies in the treatment of complexes diseases such as cancer (Cascante et al.,

2002; Hornberg et al., 2007). According to MCA, the enzymes with the highest control coefficients in a given metabolic process are the most suitable sites to target drugs at (Boren et al., 2002). Thus, although each enzyme is essential for the existence of the metabolic process, the effects on the metabolic fluxes are likely to be obtained by modulating an enzyme with high control coefficient (Salter et al., 1994).

2.4 TARGETING TUMOR METABOLISM

2.4.1 Exploiting oncogene-induced metabolic dependencies

Over the previous pages it has been described how tumor cells rewire carbon metabolism to fulfill metabolic requirements. This metabolic reprogramming renders cancer cells highly dependent on specific metabolic enzymes or pathways, thus providing a set of attractive therapeutic targets. Many cancer-causing genetic alterations converge in a single metabolic phenotype, which is characterized by cell autonomous nutrient uptake and reorganization of metabolic pathways to support biosynthesis. For instance, a vast array of mutations in PI3K and RAS induce Warburg effect, suggesting that glycolysis activation is a common adaptive metabolic strategy regardless of the genetic origin of the tumor. As it has been stated before, proliferation signaling pathways frequently altered in tumors promote metabolic reprogramming. In spite of the great progress carried out over the last decades, effective agents targeting many of the common driver mutations located in these signaling pathways are not available. Mutations in RAS or deregulated expression of MYC are frequent events in human cancer, but no specific therapies exist to treat cancers based on either genetic event, and many RAS-driven cancers are refractory to existing therapies (Linardou et al., 2009). The presence of mutations in oncogenes and tumor suppressor genes rewire metabolism in such a profound way that renders cells dependent on particular metabolic pathways. For instance, enzymes that are involved in metabolism appear to be key effectors in RAS- and MYC-dependant tumorigenesis. While RAS-mutant cells are dependent on glycolysis (Clem et al., 2008), MYC-dependent cells have particular reliance on glutamine metabolism (Dang et al., 2009; Wise et al., 2008; Yuneva et al.,

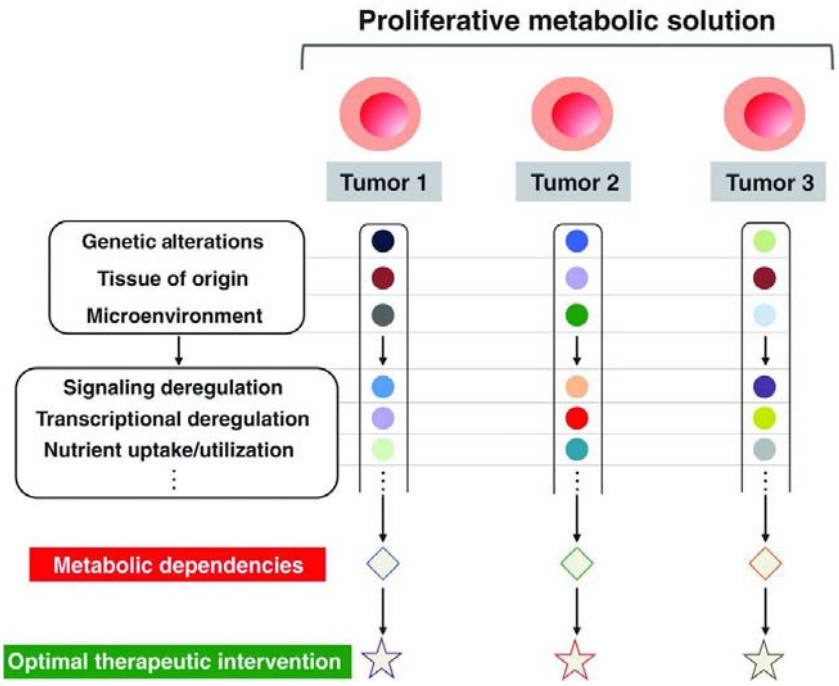

Figure 2.9 Rational design of potential therapies targeted to tumor metabolism.

Each tumor adopts a proliferative metabolic solution according to a set of intrinsic or extrinsic factors that dictates and compromises its progression and viability, resulting in a defined metabolic reprogramming profile. This profile implies the acquisition of a set of metabolic dependencies, which can include the activation or inhibition of particular metabolic reactions, pathways, isoforms of enzymes, etc. These metabolic dependencies represent potential vulnerabilities in the tumor survival strategies that might be targeted by delineating an optimal therapeutic intervention strategy. Reprinted from Cancer Discovery, Copyright © 2012, Cancer Discov 2(10): 881-898, Cantor, J. R. and D. M. Sabatini (2012). Cancer cell metabolism: one hallmark, many faces, with permission from AACR.

2007). But not only genetic alterations define a potential therapeutic intervention point within the metabolic network. A non-genetic component in the form of tumor microenvironment must additionally be considered as a component of metabolic reprogramming strategy. As an example, solid tumors are poorly vascularized, and therefore their surrounding environment can subject distinct regions of the tumor to spatial and temporal gradients of oxygenation, pH and nutrient availability (Tredan et al., 2007). All these conditions have also to be taken into consideration when delineating a therapeutic intervention based on tumor metabolism. Hence, genetic and non-genetic elements define a metabolic strategy for each tumor that implies the

acquisition of a set of metabolic dependencies, providing specific metabolic targets for an optimal therapeutic intervention (Figure 2.9) (Cantor and Sabatini, 2012).

The metabolic network has been targeted with therapeutic purposes in a number of tumors (Caro et al., 2012; Possemato et al., 2011; Wang et al., 2010) and many metabolic pathways and enzymes have been proposed as potential therapeutic intervention points (Butler et al., 2013). Targeting metabolic enzymes has been shown to be effective in the treatment of KRAS-mutant tumors *in vivo* (Clem et al., 2008). Since RAS-mutated tumors display a high glycolytic flux, inhibition of glycolysis by small-molecule inhibitors has been proposed. The enzyme 6-phosphofructokinase/fructose-2,6-biphosphatase 2 (PFK/FBPase 2 or PFKFB2) activates 6-phosphofructokinase (PKF1) by generating the allosteric activator fructose-2,6-biphosphate (F26BP), increasing flux through this step (Telang et al., 2006). Most isoforms of PFK/FBPase are bifunctional enzymes with both kinase and phosphatase activity, and can catalyze the destruction of the PFK/FBPase product reaction F26BP and decrease PFK1 activity (Yalcin et al., 2009b). The isoform PFK/FBPase 3 or PFKFB3 is expressed in many cancers and its expression has been documented to be regulated by some oncogenes such as RAS. Contrary to other PFK/FBPase isoforms, PFKFB3 has almost no phosphatase activity, enhancing the production of F26BP and promoting the Warburg effect. In addition, it has been shown to stimulate proliferation and to be required for anchorage-independent growth of RAS-driven tumors (Telang et al., 2006; Yalcin et al., 2009a). Small-molecule inhibitors of PFKFB3 have been reported to decrease levels of F26BP, to have cytostatic effect on RAS-transformed cancer cells and to impair the growth of xenograft tumors (Clem et al., 2008).

2.4.2 The PPP as potential cancer therapeutic target

Warburg effect is a metabolic trait widely displayed by most cancer cells. Therefore, glycolysis has been a very attractive pathway to be targeted in cancer treatment and has been explored as a potential therapeutic target (Pelicano et al., 2006). Likewise, other metabolic pathways with a pivotal role in tumor metabolic reprogramming have been proposed to be suitable targets (Butler et al., 2013; Vander Heiden, 2011). Among

them, the PPP has been considered a rational therapeutic target, since it meets two essential requirements of cancer cells: ribose synthesis for nucleotides production and NADPH synthesis for ROS protection lipogenesis. The main enzymes of the PPP, G6PD and TKT have been proposed as potential therapeutic targets (Boros et al., 1997; de Atauri et al., 2011; Rais et al., 1999; Ramos-Montoya et al., 2006).

A deficiency in G6PD is found in approximately 400 million people worldwide, with patients suffering mild anemia but no other serious health issues, which opens a potential therapeutic window for inhibition of this enzyme in cancer treatment. The reduction of G6PD levels seems to exert different effects on proliferation. In cancer cells, inhibition of G6PD leads to a clear decrease in proliferation (Li et al., 2009). Nevertheless, the complete absence of the enzyme in G6PD-deleted embryonic stem cells does not reduce proliferation, but makes cells more sensitive to strong antioxidants (Fico et al., 2004). On the other hand, G6PD inhibition in human foreskin fibroblast reduces cell growth and induces cellular senescence (Ho et al., 2000)

Also, the TKT enzyme has been explored as a potential therapeutic target. It has been observed that inhibition of the nonoxidative PPP pathway provokes a greater decrease in tumor proliferation than the inhibition of the oxidative branch. *In vivo* testing of the TKT inhibitor oxythiamine and the G6PD inhibitor dehydroepiandrosterone in C57BL/6 mice hosting Ehrlich's ascitic tumor cells revealed a 90.4 and a 46% decrease in the final tumor mass respectively after 3 days of treatment (Boros et al., 1997). Likewise, the inhibition of TKT or G6PD by oxythiamine and dehydroepiandrosterone respectively results in a cell cycle arrest in Ehrlich's ascites tumor *in vivo,* and the combined administration of both drugs resulted in a synergic effect (Rais et al., 1999). Moreover, it has been also reported that the ratio between oxidative and non-oxidative branches is critical in maintaining the metabolic efficiency in tumor cells (Ramos-Montoya et al., 2006).

In addition to G6PD and TKT, other enzymes of the PPP have been also described to be potential targets. Knockdown of 6-phosphogluconate dehydrogenase (6PGD) inhibits growth of lung cancer cells by senescence induction (Sukhatme and Chan, 2012). Also, inhibition of the nonoxidative-branch enzymes ribose-5-phosphate isomerase (RPIA)

and ribulose-phosphate 3-epimerase (RPE) decreases tumor growth in xenograft model of KRAS-induced pancreatic ductal adenocarcinoma (Ying et al., 2012). Taken together, these results indicate that inhibition of the PPP can be a potential therapeutic strategy to combat tumor progression in different cancer models.

The inhibition of the PPP, particularly the inhibition of the oxidative branch, is especially attractive since it also targets the ROS protection system of cancer cells. Targeting cancer cells with ROS mediated mechanism has been proposed as an interesting therapeutic approach. As mentioned earlier, cancer cells usually work with increased levels of ROS and acquire protective and compensating mechanisms by activation of ROS detoxification mechanisms. Moderate levels of ROS can promote many aspects of tumor biology. However, a delicate balance exists between ROS-producing and removing reactions. Since this equilibrium is forced in cancer cells, they are more sensitive to further external insults affecting this balance, promoting ROS formation, inhibiting ROS removal reactions or both actions simultaneously (Trachootham et al., 2009). Thus, given the role of G6PD in ROS detoxification, inhibition of this enzyme is likely to break this equilibrium, dismantling the ROS adaptive response and causing cell death. This hypothesis is fully supported by the fact that G6PD-deficient cells show enhanced oxidative stress and increased sensitivity to oxidative damage, indicating that G6PD plays a fundamental role controlling ROS levels, and that it might be a potential target in a ROS-based cancer therapy approach (Cheng et al., 2004; Gao et al., 2009a; Ho et al., 2000).

2.4.3 The tumor metabolism as therapeutic opportunity in cancer

One essential consideration when designing therapeutic strategies is in what extent a drug can perform its therapeutic function without affecting or damaging other healthy cells and tissues. This fact, commonly known as therapeutic window, is specially challenging when targeting cancer metabolic adaptations, since most of the cancer cells and normal proliferating cells rely on the same metabolic pathways. Although this is the case for some metabolic targets, the success of cytotoxic agents that target folate metabolism and DNA synthesis illustrates that a therapeutic window can exist for

anticancer drugs that target metabolic pathways. Most of the current therapeutic approaches are targeted to key proteins involved in signaling pathways and, with exception of gain-of-function mutations, no target is unique to cancer cells. Successful targeted therapies take advantage of the dependence of cancer cells on specific pathways. Similarly, metabolic dependencies of cancer cells can also be exploited for cancer treatment. To this end, a detailed and reliable knowledge of the metabolic phenotype of tumors both *in vitro* and *in vivo* is required. This ambitious goal can be achieved by an integrative approach, combining different *omics* targeted to reliably unveil the metabolic dependencies of tumors not only *in vitro* but also *in vivo* to establish a potential therapeutic window.

3. OBJECTIVES

3. OBJECTIVES

Over the last years, it has emerged a renewed interest in the field of metabolism, particularly in cancer metabolism. Great efforts have been focused on the association between mutated oncogenes or tumor suppressor genes and tumor metabolic profiles, in the search of metabolic dependencies that offer new potential venues for cancer treatment. The pursuit of discovering tumor metabolic alterations in which cancer cells rely on has represented the cornerstone of this interesting discipline. Thus, this thesis is part of this recent and promising scientific current and is intended to shed light on the metabolic alterations accompanying oncogene mutation and on potential metabolic pathways that might be of therapeutic interest in the future. Hence, the objectives of this thesis can be divided into two specific aims:

1. Analysis of the metabolic reprogramming of RAS oncogenic activation using stable transfected cell lines with mutated copies of K-RAS and H-RAS.

2. Validation of the pentose phosphate pathway as a potential therapeutic target and exploration of its role within tumor metabolism in colon and breast cancer cell models.

4. MATERIALS AND METHODS

4. MATERIALS AND METHODS

4.1 Cell Culture

Breast cancer cell line MCF7 was purchased from ATCC and cultured in MEM media without phenol red (Ref. 51200, Gibco) containing 10% Fetal Bovine Serum (FBS) (Ref. 7524, Sigma-Aldrich), 10 mM glucose (Sigma-Aldrich), 1 mM pyruvate (Biological Industries), 2 mM glutamine (Gibco), 0.1% antibiotic (Penicillin 10 Units/mL-Streptomycin 10 µg/mL, Gibco), 0.01 mg/mL insulin (Sigma-Aldrich) and 1% non-essential aminoacids (Biological Industries). HT29 and Caco-2 cell lines were cultured in DMEM (Ref. A14430, Gibco) containing 10% FBS (Ref. A15-151, PAA Laboratories), 10 mM glucose, 2 mM glutamine and 0.1% antibiotic. Cell lines SW620 and SW480 were kindly provided by Dr. G. Capellà (Bellvitge Biomedical Research Institute, Spain) and cultured in RPMI 1640 media (Ref. R0883, Sigma-Aldrich) supplemented with 10% FBS (Ref. A15-151, PAA Laboratories) and 0.1% antibiotic. Human colonocytes cell line NCM460 was provided by INCELL and cultured in M3Base media (Ref. M300A, INCELL) supplemented with 10% FBS (Ref. A15-151, PAA Laboratories) and 10 mM glucose. Human fibroblasts BJ and BJ-HRasV12 were kindly provided by Dr. R. Schäfer (Charité Universitätsmedizin Berlin, Germany). Both cell lines were immortalized and H-RasG12V cassette was expressed for BJ-HRasV12 cell line generation as described in Hahn *et al* 1999(Hahn et al., 1999). They were cultured in media consisted of DMEM (Ref. 11966, Gibco) and Medium 199 (Ref. M7653, Sigma-Aldrich) in 4:1 proportion containing 10% FBS (Ref. S0115, AG Biochrom), 10 mM glucose, 3 mM glutamine, 1 mM pyruvate, 0.085 mg/mL hygromycin B (Roche), 0.4 mg/mL puromycin (Sigma-Aldrich) and 1% antibiotic. BJ-HRasV12 cell line was routinely cultured in presence of 0.4 mg/mL of the selection antibiotic geneticin (Gibco). NIH3T3, K12- and K13- transfected cells were kindly provided by Dr. R. Mangues (Sant Pau Biomedical Research Institute, Spain) and cultured in DMEM (Ref. 5796, Sigma-Aldrich) in the presence of 10% FBS (Ref. A15-151, PAA Laboratories), 25 mM glucose and 4 mM glutamine. K12 and K13 cells were

cultured in the presence of 0.25 mg/mL of the selection antibiotic geneticin (Gibco). The transfectants contained a K-RAS minigene with a G:C to A:T mutation at the first position of codon 12 (K12 cells) and a G:C to A:T mutation at the second position of codon 13 (K13). All FBS used in this section were held at 56 °C for 30 min for inactivation before use. Also, all cell lines described in this section were cultured in humidified atmosphere at 37 °C and 5% CO_2.

4.2 Proliferation, viability and cell cycle analysis

Proliferation and viability assays were performed by flow citometry combining direct cell counting and propidium iodide (PI) staining. At the end of the experiment or as indicated elsewhere cells were tripsinized and resuspended in 500 µL of solution consisted of 450 µL of complete media, 45 µL of Flow-Count Fluorospheres (Beckman Coulter) and 5 µL of 1 mg/mL propidium iodide. Flow cytometer was adjusted to $1x10^4$ fluorospheres cut-off and total cell number was registered, allowing discrimination between dead and alive cells.

Viability was also assessed by MTT assay (Mosmann, 1983), which is based upon the principle of reduction of MTT ((3-(4,5-dimethylthiazol-2-yl)-2,5-diphenyltetrazolium bromide) into blue formazan pigments by viable mitochondria in healthy cells. Cells were seeded in a 96-well flat-bottom plate as indicated elsewhere and 24h later, media was replaced by fresh media containing the drug under study. At the end of the experiment, media was replaced by 0.5 mg/mL MTT solution and cells were incubated at 37 °C for 1h. Over this period, MTT was reduced to blue formazan. Then, media was removed and the formazan precipitate was dissolved in DMSO. Absorbance values were measured in an ELISA plate reader at 550 nm wavelength. Values were normalized to the absorbance of cells cultured in media without the drug under study (the proportional amount of drug vehicle was added to these wells).

For cell cycle analysis by flow citometry, cells were collected at the indicated time points and fixed with 70% cold ethanol prior to centrifugation and resuspension in buffer consisted of PBS, 0.01% (v/v) Triton X-100, 1 mg/mL propidium iodide, and 0.2 mg/mL

RNAse A (REAL Laboratories). For cell cycle phase distribution analysis the software FlowJo® was used, and the percentage of cells in G1, S and G2 was obtained.

4.3 siRNA transfection

MCF7 cell line was transfected using Metafectene (Biontex) according to the manufacturer's instructions. Briefly, $1x10^5$ cells were seeded in 6-well plates and after 24h, 60 nM of either control siRNA (siNEG) or siRNAs against TKT (siTKT) or G6PD (siG6PD) were transfected. RNAi sequences employed for each gene were purchased from Dharmacon and are listed as follows: siNEG, ON-TARGETplus Non-targeting siRNA D-001810-03-20 (sequence not provided by the manufacturer); siTKT, ON-TARGETplus J-004734-06-0010, GGAACUAGCCGCCAAUACA; siG6PD, ON-TARGETplus J-008181-06-0010, GAGAGUGGGUUUCCAGUAU.

HT29 cell line was transfected using RNAi/MAX (Invitrogen) following the manufacturer's instructions. Briefly, $5x10^4$ cells were seeded in 6-well plates and after 24h, 50 nM of G6PD siRNA pool (siG6PD, ON-TARGETplus SMARTpool, L-008181-02-0010) or control siRNA pool (siNEG, ON-TARGETplus Non-Targeting pool, D-001810-10-20) were transfected. The siG6PD pool includes the next sequences: ACAGAUACAAGAACGUGAA; CCGUGUACACCAACAUGAU; CAGAUAGGCUGGAACCGCA; AUUCACGAGUCCUGCAUGA. The sequences contained in the siNEG pool are not detailed by the manufacturer.

4.4 RNA isolation and gene expression analysis

RNA isolation was performed from fresh or frozen pellets or cultured plates using Trizol® reagent (Invitrogen) following manufacturer's instructions. Briefly, Trizol was added to samples and cell homogenates were mixed with chloroform and centrifuged, resulting in an upper aqueous phase, an interphase, and a lower organic phase. RNA was precipitated from the aqueous phase by adding cold isopropanol and centrifuging at 12000xg for 15 min at 4 °C. Next, supernatant was removed and pellet was washed

three times with cold 75% ethanol**.** After ethanol evaporation at room temperature, RNA was resuspended in RNAse-free water for subsequent quantification by Nanodrop. Next, cDNA was obtained using 1 µg of RNA, random primers (Roche) and M-MLV reverse transcriptase (Invitrogen) according to the manufacturer's indications. Gene expression analysis was performed by qPCR (ABI Prism 7700 Sequence Detector System, Applied Biosystems) in standard conditions provided by the manufacturer, employing Taqman® (Applied Biosystems) specific sequences for each gene (*G6PD:* Hs00166169_m1; *TKT:* Hs00169074_m1; *NFE2L2:* Hs00975961_g1; *HMDX1:* Hs01110250_m1; *NQO1:* Hs01045994_m1). Subsequently, expression was quantified by ΔΔCt method using *PPIA* (Hs99999904_m1) as reference gene.

4.5 Western Blot

Cell extracts were obtained from either fresh cells or frozen plates using lysis buffer consisted of 50 mM Tris-HCl pH 7.5, 1 mM EDTA, 1 mM DTT, 0.2% (v/v) Triton X-100, 0.2 mg/mL sodium deoxycolate and 1x protease inhibitor cocktail (Sigma-Aldrich). Protein concentration was determined by bicinchoninic acid assay (BCA). 10-30 µg of protein were separated by 10% SDS-PAGE and proteins were transferred to PVDF membrane. After 1h blocking in PBS containing 5% non-fat dried milk and 0.1% (v/v) Tween 20, membranes were incubated with primary antibodies according to the conditions indicated below. Then the membranes were rinsed with 0.1% (v/v) PBS-Tween followed by exposure to the appropriate horseradish peroxidase-conjugated secondary antibody visualized on Fujifilm X-ray film using chemiluminescence detection system (Millipore). The following antibodies were used: α-G6PD (Ref. ab993, Abcam, 1/10000), α-Actin (Ref. 691001, Millipore, 1/50000) and α-NRF2 (Ref. sc-365949, Santa Cruz, 1/100). α-G6PD and α-NRF2 were incubated O/N at 4 °C and α-Actin was incubated for 45 min at room temperature.

4.6 ROS levels measurement

Total intracellular ROS levels were determined by means of flow citometry using H_2DCFA probe (Invitrogen). Cells were incubated with 5 µM H_2DCFA in PBS for 30 min. After that, PBS was replaced by specific cell culture media, as appropriately described for each case in *Section 5,* and cells were incubated for 15 min at 37 °C and 5% CO_2. Next, cells were tripsinized and resuspended in a solution consisted of 50 µM H_2DCFA and 20 µg/mL propidium iodide. Internalized probe reacts with ROS and emits fluorescence when excited at 492 nm. Emitted fluorescence was recorded by flow citometry at 520 nm wavelength. For ROS analysis, only negative PI cells were considered.

4.7 Glutathione content

Total glutathione content was determined by glutathione reductase enzymatic method. Fresh cells were lysed with 5% SSA (5-sulfosalicylic acid) solution, vortexed and disrupted by two freezing/defreezing cycles in liquid N_2 and 37 °C water bath. 50 µL of this solution was separated for subsequent protein quantification by BCA assay. Cell extracts were held at 4 °C for 10 min and centrifuged at 10000xg for 10 min. For glutathione quantification, working solution consisted of 15 U/mL of glutathione reductase and 40 µg/mL of DTNB (5,5'-Dithiobis(2-nitrobenzoic acid)) dissolved in 100 mM K_2HPO_4/KH_2PO_4, 1 mM EDTA, pH 7 was prepared. Reaction was initiated by mixing 150 µL of working solution with up to 10 µL of cell extract or 10 µL of standard. Next, 150 µL of 40 mg/mL NADPH solution was added and the increase in absorbance was recorded at 340 nm wavelength. Total glutathione concentration was normalized by protein content determined by BCA method.

4.8 ATP/ADP ratio

Nucleotides were extracted from freshly cultured cells by addition of 10% $HClO_4$ to the plates, scrapping on ice and centrifugation for 5 min at 10000xg at 4 °C. Next, pH of

supernatant was neutralized with 5M K_2CO_3 and filtered using Microcon Centrifugal Filter Devices YM-10 10000 MWCO (Millipore) at 10000xg for 10 min. ATP and ADP detection and quantification were carried out by HPLC employing a Waters Acquity UPLC instrument equipped with a Kinetex Phenomenex column (2.6 µm C18 100 x 4.6 mm) coupled to a DAD detector at 260 nm wavelength. Sample separation was performed by applying a binary gradient at a flow rate of 0.5 mL/min at 35 °C. Solvent B consisted of 4 mM tetrabutylammonium hydrogensulphate in 0.05 M KH_2PO_4, pH 6.0. Solvent A consisted of methanol:solvent B mixture in proportion 30:70 (v/v). The table below shows the gradient used:

Time (min)	% A	% B
0	0	100
2.5	0	100
5	30	70
10	40	60
17	100	0
21	100	0
23	0	100
33	0	100

Retention time (RT) for ATP and ADP were 20.1 and 17.2 min respectively. ATP/ADP ratio was calculated by dividing ATP peak area by the corresponding one for ADP.

4.9 Oxygen consumption rate

Oxygen consumption rate was determined using Seahorse XF24 Extracellular Flux Analyzer instrument. $4x10^4$ cells were seeded in XF24 plates in complete media described in S*ection 4.1* and maintained at 37 °C and 5% CO_2. After 24h, media was replaced with non-buffered DMEM media supplemented exclusively with the carbon source indicated in each case for 30 min prior to oxygen consumption measurement. Over this period, cells were maintained in humidified atmosphere at 37 °C in non-CO_2 conditions. Oxygen measurements were carried out over 90 minutes divided into four periods. Within the first period, basal oxygen consumption was determined. The second

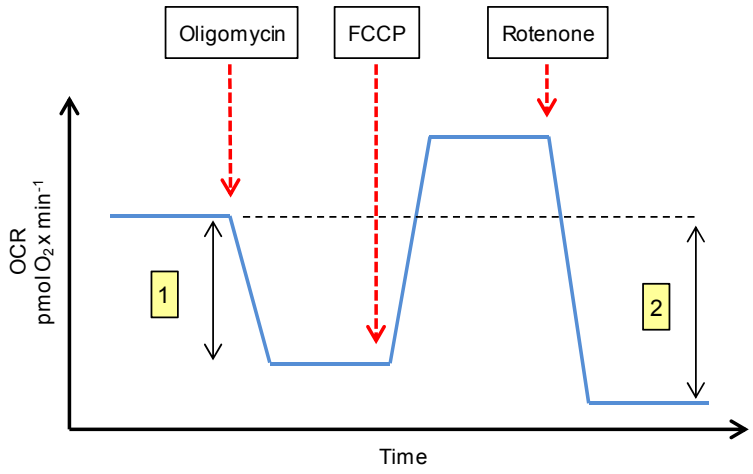

1: ATP-coupled respiration
2: Mitochondrial basal respiration

period begun with the injection of 1.5 µM solution of complex-V inhibitor oligomycin to determine the portion of oxygen consumption coupled to ATP production. It was calculated by subtracting oligomycin-insensitive oxygen consumption to basal oxygen consumption (see figure below). The third period started after addition of 0.5 µM solution of the uncoupler agent FCCP (Carbonyl cyanide 4-(trifluoromethoxy)phenylhydrazone) and finally, at the beginning of the fourth period, 0.5 µM solution of complex-I inhibitor rotenone was injected. The difference between basal and rotenone-insensitive oxygen consumption allowed for the calculation of basal mitochondrial oxygen consumption.

4.10 Biochemical assays

Glucose, lactate, glutamate and glutamine were determined by spectrophotometry (COBAS Mira Plus, Horiba ABX) from cell culture media by monitoring the production of NAD(P)H in specific reactions for each metabolite at 340 nm wavelength (de Atauri et al., 2011). Glucose concentration was measured using HK and G6PD coupled enzymatic reactions (commercial enzymatic kit). Lactate concentration was determined by LDH reaction, which was carried out at 37 °C by adding media sample to a cuvette

containing 1.55 mg/mL NAD and 87.7 U/mL LDH in 0.2M hydrazine 12 mM EDTA buffer, pH 9. Determination of glutamate concentration was done by its conversion to α-ketoglutarate through glutamate dehydrogenase (GLDH) reaction in the presence of ADP. This reaction was performed at 37 °C by adding media sample to a cuvette containing 2.41 mM ADP, 3.9 mM NAD and 39 U/mL of GLDH in 0.5M glycine/0.5M hydrazine buffer, pH 9. Glutamine was determined by its conversion first to glutamate through glutaminase (GLS) reaction and subsequently quantification of glutamate concentration as described above. GLS reaction was performed by adding media sample to a cuvette containing a mixture consisted of 90 mU/mL GLS in 111 mM acetate buffer, pH 5. Reaction was carried out for 90 min at 37 °C in agitation.

In order to calculate the consumption/production rate of each metabolite, media samples at the beginning and at the end of the experiment were taken and frozen for subsequent analysis. From the same plates, or parallel plates when required, cell numbers were determined through the procedure described in *Section 4.2* for normalization.

4.11 ^{13}C-assisted metabolomics

^{13}C-assited metabolomics experiments were carried out as indicated in each case in *Section 5*. In general, at the beginning of the experiment culture media was replaced by fresh media containing either 50% [1,2-$^{13}C_2$]-glucose (Sigma-Aldrich) or 100% [U-^{13}C]-glutamine (Sigma-Aldrich) and after the incubation period indicated in each case, media, pellets and cultured plates were collected. Media samples were frozen at -20 °C for ulterior determination of glucose, lactate, glutamate and glutamine concentrations as described in *Section 4.10*. Also, mass isotopomer distributions of glucose, lactate and glutamate were determined from media samples. Pellets were obtained by trypsinization and kept at -20 °C until used for analysis of mass isotopomer distribution of ribose and fatty acids. Cultured plates were frozen in liquid nitrogen and stored at –80 °C for mass isotopomer distribution analysis of TCA cycle intermediates. As stated

in *Section 4.10*, cell number was determined at each time point of the experiment following the procedure described in *Section 4.2*.

Analysis of ^{13}C-labeled intracellular and extracellular metabolites for mass isotopomer distribution analysis was done by gas chromatography coupled to mass spectrometry (GC-MS). GC-MS was performed using an Agilent 7890A GC equipped with a HP5 capillary column connected to an Agilent 5975C MS. Fatty acids GC-MS analysis was performed employing a GCMS-QP 2012 Shimadzu equipped with a bpx70 (SGE) column. In all cases, one microliter of sample was injected at 250 °C using helium as a carrier gas at a flow rate of 1 mL/min. Different procedures for metabolite isolation, derivatization and detection were used for each metabolite as described below.

4.11.1 Glucose

Glucose was isolated from cell culture media using a tandem set of Dowex-1X8/ Dowex-50WX8 ion-exchange columns, being glucose eluted with water. After that, water was evaporated to dryness under airflow and isolated glucose was held at 100 °C for 30 min with 2% (v/v) hydroxylamine hydrochloride in pyridine for derivatization. Then acetic anhydride was added for 1h more. Excess of reagent and solvent were removed by evaporation with N_2, and glucose derivative was dissolved in ethyl acetate for GC-MS analysis. GC-MS analysis was performed under chemical ionization mode. Sample injection was done at 250 °C and oven temperature was held at 230 °C for 2 min after injection and increased to 260 °C at 10 °C/min. Detector was run in SIM, recording ion abundance of C1-C6 molecule in the range of 327-336 m/z. RT was 3.8 min.

4.11.2 Lactate

Sample media was acidified by addition of HCl and shortly after ethyl acetate was added for lactate extraction and evaporated to dryness under N_2. Dried lactate was incubated at 75 °C for 1h in presence of dimethoxypropane and methanolic chloride. Next, n-propilamine was added to the reaction mixture, held at 100 °C for 1h and evaporated to dryness under N_2. Precipitate was then resuspended in dichloromethane and heptafluorobutyric anhydride at room temperature for 10 min. After that, sample

was evaporated to dryness under N_2 and resuspended in dichloromethane for GC-MS analysis. GC-MS analysis was performed under chemical ionization mode. Sample injection was done at 200 °C and oven temperature was held at 100 °C for 3 min after injection and increased to 160 °C at 20 °C/min. Detector was run in SIM recording ion abundance of C1-C3 molecule in the range of 327-332 m/z. RT was 5.4 min.

4.11.3 Glutamate

Sample media was passed through a 3-ml Dowex-50WX8 (H+) column. Aminoacids were eluted from the column with 2N NH_4OH, and the solution was evaporated to dryness by airflow. To further separate glutamate from glutamine, the aminoacid mixture was passed through a 3-ml Dowex-1X8 (acetate) column. Glutamine was washed with water, and glutamate was collected with 0.5N acetic acid. The acid-fraction containing glutamate was evaporated to dryness. Dried glutamate was therefore held at 100 °C for 1h in butanolic HCl. The excess of reagents was removed under N_2 and the precipitate was dissolved in methylene chloride. Reaction was completed with the addition of trifluoroacetic anhydride. Then, samples were dried under N_2, and the derivative was dissolved in methylene chloride for injection into GC-MS equipment. GC-MS analysis was performed under electron impact mode to yield two fragments corresponding to C2-C4 and C2-C5 glutamate fragments. Sample injection was done at 250 °C and oven temperature was held at 215 °C for 2 min after injection and increased to 225 °C at 9 °C/min and then to 233 °C at 3 °C/min. Detector was run in SIM mode recording ion abundance in the range of 151-157 m/z for C2-C4 and 197-203 m/z for C2-C5. RT was 3.9 min.

4.11.4 Ribose

Ribose from RNA was isolated from cultured cells using the aqueous phase after addition of Trizol® (Invitrogen) as described in *Section 4.4*. Purified RNA was hydrolyzed in 2N HCl for 2h at 100 °C and solvent was evaporated to dryness under airflow. RNA ribose was derivatized as previously described for glucose (see *Section 4.10.1*). GC-MS analysis was performed under chemical ionization mode. Sample injection was done at

250 °C and oven temperature was held at 150 °C for 1 min after injection, increased to 275 °C at 15 °C/min and finally to 300 °C at 40 °C/min. Detection was run in SIM recording ion abundance of C1-C5 molecule in the range of 256-261 m/z. RT was 5.3 min.

4.11.5 Palmitate

Fatty acids from cultured cells were extracted from the inter- and lower phase of Trizol extract as described above *(Section 4.4)* by adding 100% ethanol and 30% KOH. After that, samples were incubated at 70 °C overnight. Then, free fatty acids were extracted with petroleum ether, which was subsequently evaporated to dryness under N_2. Fatty acids were then derivatized adding 0.5N methanolic-HCl and held at 70 °C for 1h. GC-MS analysis was performed under chemical ionization mode. Sample injection was done at 250 °C and oven temperature was held for 1 min at 120 °C after injection and increased to 220 °C at 5 °C/min. Detector was run in SIM recording ion abundance in the range of 269-278 m/z. RT was 9.2 min.

4.11.6 TCA cycle intermediates

TCA cycle intermediates from cultured cells were extracted from liquid nitrogen frozen cultured plates by scrapping on ice with addition of 100% methanol:H_2O (1:1) mixture. Then, cell extracts were sonicated using a titanium probe (VibraCell, Sonics & Materials Inc., Tune: 50, Output: 30) and vortexed for 30 min at 4 °C. After that, samples were centrifuged and the upper aqueous phase was separated and evaporated to dryness under airflow at room temperature. TCA cycle intermediates were derivatized by addition of 2% (v/v) methoxyamine in pyridine and held at 37 °C for 90 min. Next, MBTSTFA + 1% TBDMCS was added and samples were incubated for 1h more at 55 °C and transferred to GC-MS vials. GC-MS analysis was under electron impact ionization. Sample injection was done at 270 °C and oven temperature was held at 100 °C for 3 min, increased to 165 °C at 10 °C/min, then to 225 °C at 2.5 °C/min, to 265 °C at 25 °C/min and finally to 300 °C at 7.5 °C/min. The following table shows the metabolites and m/z ranges monitored by SIM.

Metabolite	Empirical Formula	RT (min)	m/z range
Pyruvate	$C_6H_{12}O_3NSi$	8.2	173-177
Fumarate	$C_{12}H_{23}O4Si_2$	18.17	286-292
a-Ketoglutarate	$C_{14}H_{28}O_5NSi_2$	24.56	345-352
Malate	$C_{18}H_{39}O_5Si_3$	27.58	418-424
Aspartate	$C_{18}H_{40}O_4NSi_3$	28.90	417-423
Citrate	$C_{20}H_{39}O_6Si_3$	37.67	458-466

4.12 GC-MS data reduction

Spectral data obtained from a mass spectrometer simply represent the distribution of ions of a compound or its fragments with different molecular weights. The value for each observed m/z is the sum of experimental isotope incorporation, the presence of isotopes in heteroatoms, the presence of natural abundance of ^{13}C in the background, and, when corresponds, the ^{12}C isotope impurity in the ^{13}C-labeled precursor. Furthermore, the derivatizing reagents often contain isotopes which contribute to the mass isotopomer distribution of the derivatized compound as well. Correction for all such contributions is necessary before the amount of isotope incorporation and its distribution in the compound of interest can be determined. This correction was performed by using regression analysis employing in-house developed software. The algorithm used by Lee et al. corrects all the previous detailed contributions over the observed spectral intensities of each ion cluster, giving us the distribution of mass isotopomers in the metabolite of study due to incorporation of ^{13}C atoms from the tracer precursor. Results of the mass isotopomers in any of the ion clusters were reported as fractional enrichments of molecule isotopomers. These fractional enrichments are defined as the fraction of molecules having a certain number of isotope substitutions. They are designated as m0, m1, m2, etc., where the number indicates the number of labeled carbons in the molecule (see *Section 2.3.1.2.1*) corrected as described above. Note that the sum of all mass isotopomers of the ion clusters, $\sum_{i=n}^{i=0} m_i$ (n = number of carbons in the molecule or fragment), is equal to 1 or 100 %.

4.13 Mass isotopomer distribution analysis

4.13.1 Calculation of pathway-specific produced lactate

The amount of lactate produced from glucose, via glycolysis or PPP, and produced from other substrates, can be estimated by combining the concentration and the mass isotopomer distribution of lactate in cell culture media from cells cultured in the presence of 50% [1,2-$^{13}C_2$]-glucose. In order to calculate these fluxes, we assumed that BJ and MCF7 cells do not consume lactate, so this metabolite is only produced. Thus, as lactate present in the media at the beginning of the incubation period does not contain ^{13}C coming from the tracer, it will contribute to m0 pool of total lactate at the end of the incubation. Taking this into account, we have first estimated the mass isotopomer distribution of produced lactate (total lact-initial lac). To do this, first mass isotopomer distribution of lactate *($Lac_{Tot}(m0,m1,m2,m3)_{t=f}$ (%))* was multiplied per final concentration of lactate *($[Lac]_{t=f}$)* to obtain the absolute mass isotopomer distribution of total lactate in mM *($[Lac_{Tot}(m0,m1,m2,m3)]_{t=f}$ (mM))* at the end of the incubation period (t=f) (Eq. 4):

$$[Lac_{Tot}(m0,m1,m2,m3)]_{t=f}\ (mM) = Lac_{Tot}(m0,m1,m2,m3)_{t=f}\ (\%) * [Lac]_{t=f} \quad (4)$$

Next, initial lactate concentration *($[Lac]_{t=i}$)* was subtracted to the concentration of total lactate m0 *($[Lac_{Tot}(m0)]_{t=f}$ (mM)* to obtain the produced lactate in mM that does not contain ^{13}C *($[Lac_{Prod}(m0)]$ (mM))* (Eq. 5). The value of produced lactate in mM that contains one, two o three ^{13}C *($[Lac_{Prod}(m1,m2,m3)]$ (mM))* coincides with the measured values of m1, m2 and m3 in mM in total lactate ($[Lac_{Tot}(m1,m2,m3)]_{t=f}$ (mM)).

$$[Lac_{Prod}(m0)]\ (mM) = [Lac_{Tot}(m0)]_{t=f}\ (mM) - [Lac]_{t=i} \quad (5)$$

Next, relative mass isotopomer distribution of produced lactate *($Lac_{Prod}(m0,m1,m2,m3)$ (%))* was recalculated by dividing $[Lac_{Tot}(m0,m1,m2,m3)]_{t=f}$ (mM) values by total produced lactate *($[Lac_{Prod}]$ (mM))* (Eq. 6). Total produced lactate was estimated by subtracting initial lactate concentration to final lactate concentration (Eq. 7).

$$Lac_{Prod}(m0,m1,m2,m3)_{t=f}\ (\%) = [Lac_{Prod}(m0,m1,m2,m3)]_{t=f}\ (mM) / [Lac_{Prod}]\ (mM) \quad (6)$$

$$[Lac_{Prod}]\ (mM) = [Lac_{Tot}]_{t=f} - [Lac_{Tot}]_{t=i} \quad (7)$$

Following, glycolytic tax (GT), which is the percentage of produced lactate that comes from glucose through direct glycolysis, was calculated as follows:

$$GT = Lac_{Prod}(m2)_{t=f}\ (\%) * 2 / Glc(m2)_{t=i}\ (\%) \quad (8)$$

where $Glc(m2)_{t=i}$ is the percentage of [1,2-$^{13}C_2$]-glucose in the cell culture media at the beginning of the experiment. Next, maximum feasible amount of lactate coming from glycolysis *($[Lac_{ProdGlyc}]$)* was obtained by multiplying the GT per produced lactate *($[Lac_{Prod}]$ (mM))* (Eq. 9).

$$[Lac_{ProdGlyc}]\ (mM) = GT * [Lac_{Prod}]\ (mM) \quad (9)$$

In order to calculate the amount of lactate from glucose coming through the PPP, first, Pentose Cycle (PC) parameter was calculated following the next expression (Eq. 10) using values of mass isotopomer distribution of total lactate.

$$PC = \{Lac_{Tot}(m1)_{t=f} / Lac_{Tot}(m2)_{t=f}\} / \{3 + Lac_{Tot}(m1)_{t=f} / Lac_{Tot}(m2)_{t=f}\} \quad (10)$$

PC parameter is defined as the relative amount of glucose metabolized through glycolysis related to the glucose metabolized through PPP. A detailed description of this parameter and the deduction of the formula employed can be found in Lee *et al* 1998 (Lee et al., 1998).

Following, lactate from glucose coming through PPP was obtained by multiplying PC value per the maximum feasible amount of lactate coming from glycolysis *$[Lac_{ProdGlyc}]$* (Eq 11).

$$[Lac_{ProdPPP}]\ (mM) = PC * [Lac_{ProdGlyc}]\ (mM) \quad (11)$$

In order to calculate the amount of lactate coming from other sources different of glucose *($[Lac_{ProdOS}]$)*, the lactate produced from glycolysis *($[Lac_{ProdGlyc}]$ (mM))* and lactate coming from glucose through PPP *($[Lac_{ProdPPP}]$ (mM))* were subtracted to produced lactate *($[Lac_{Prod}]$ (mM))* (Eq 12).

$[Lac_{ProdOS}]$ (mM) = $[Lac_{Prod}]$ (mM) - $[Lac_{ProdGlyc}]$ (mM) - $[Lac_{ProdPPP}]$ (mM) (12)

4.13.2 Calculation of PC and PDH contribution to glucose entrance into the mitochondria

Glucose can enter into the TCA cycle via two major enzymes: PDH, which converts pyruvate into acetyl-CoA, or PC, which transforms pyruvate into oxaloacetate. Acetyl-CoA and oxaloacetate are combined in a reaction catalyzed by the enzyme citrate synthase that yields citrate, which is subsequently transformed into α-ketoglutarate, which is in equilibrium with glutamate. If a molecule of [1,2-$^{13}C_2$]-glucose enters into TCA cycle through PDH enzyme, it will yield [1,2-^{13}C]-acetyl-CoA, which will be eventually transformed into [4,5-$^{13}C_2$]-glutamate. On the other hand, if a molecule of [1,2-$^{13}C_2$]-glucose enters into TCA cycle through PC, it will yield [2,3-$^{13}C_2$]-glutamate. The pathway employed to enter glucose into TCA cycle can be assessed by analyzing the mass isotopomer distribution of glutamate molecule fragments C2-C4 and C2-C5 from cells cultured in the presence of [1,2-$^{13}C_2$]-glucose, as it is described in the table below:

	PDH	PC
	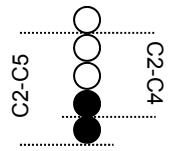	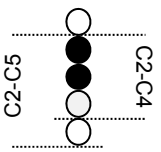
	[4,5-$^{13}C_2$]-Glutamate	[2,3-$^{13}C_2$]-Glutamate
C2-C5 fragment	m2	m2
C2-C4 fragment	m1	m2

Then, the relative contribution (%) of each pathway to glucose entrance into the TCA cycle was calculated as follows (Sanchez-Tena et al., 2013):

% PC = $Glu_{C2\text{-}C4}$(m2) / $Glu_{C2\text{-}C5}$(m2) (13)

% PDH = ($Glu_{C2\text{-}C5}$(m2)- $Glu_{C2\text{-}C4}$(m2))/ $Glu_{C2\text{-}C5}$(m2) (14)

4.13.3 Calculation of the glucose and glutamine contribution to synthesis of palmitate

The relative contribution of glucose or glutamine to palmitate synthesis was analyzed by firstly calculating the fraction of ^{13}C-acetyl-CoA *(q)* in total acetyl-CoA pool in cells cultured in the presence of 50% [1,2-$^{13}C_2$]-glucose or 100% [U-^{13}C]-glutamine (Boren et al., 2003; Lee et al., 1995). Fraction of ^{13}C-acetyl-CoA *(q)* was determined from the m4/m2 ratio of palmitate as follows:

$$Pal(m4)_{t=f}/Pal(m2)_{t=f} = (n - 1)/2 * (p/q) \quad (15)$$

where *n* is the number of acetyl units in the fatty acid under analysis (in our case, palmitate n=8), *q* is the labeled fraction, and *p* is the unlabeled fraction (p + q = 1).

In order to estimate the glucose or glutamine contribution to synthesis of palmitate, the theoretical fraction of ^{13}C-acetyl-CoA of cells cultured in the presence of the tracer must be estimated.

When cells were cultured in the presence of 50% [1,2-$^{13}C_2$]-glucose, this theoretical fraction of ^{13}C-acetyl-CoA was estimated using the next expression:

$$\text{Theoretical fraction of } ^{13}\text{C-acetyl-CoA} = Glc(m2)_{t=i}\ (\%)/2 \quad (16)$$

where $Glc(m2)_{t=i}$ is the percentage of [1,2-$^{13}C_2$]-glucose at the beginning of the ^{13}C-assisted metabolomics experiment. Since a molecule of glucose yields one ^{13}C-acetyl-CoA and one non-labeled acetyl-CoA, this theoretical fraction corresponds to the value of $Glc(m2)_{t=i}$ divided by 2.

The calculation of the theoretical fraction of ^{13}C-acetyl-CoA when using 100% [U-^{13}C]-glutamine is more complex. In this situation, acetyl-CoA can be produced via glutamine oxidative metabolism (GOM), which yields m0 acetyl-CoA, glutamine reductive metabolism (GRM), yielding m2 labeled acetyl-CoA, and malate dehydrogenase (MDH) - ME reactions, which can produce m2 labeled ^{13}C-acetyl-CoA (see Figure 4.1). Then, the theoretical fraction of ^{13}C-acetyl-CoA was assumed to be as follows:

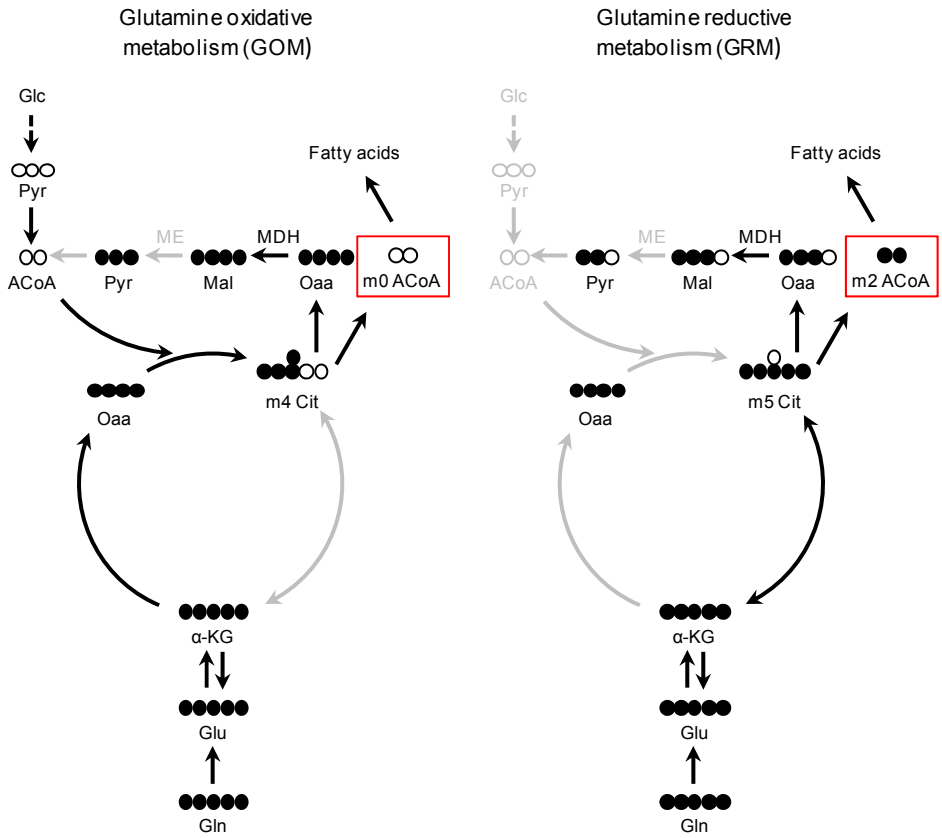

Figure 4.1 Glutamine contribution to acetyl-CoA synthesis

[U-^{13}C]-glutamine oxidative and reductive metabolism contribute differently to acetyl-CoA synthesis, yielding m0 and m2 labeled acetyl-CoA respectively. Black arrows indicate the pathway followed by glutamine carbons, while grey arrows denote inactive or non-used pathways. Note that malic enzyme (ME) reaction is shown as inactive in both cases, as described in *Section 4.13.3*, reducing therefore the contribution of malate dehydrogenase (MDH) and ME reactions to acetyl-CoA synthesis. Glc, glucose; Pyr, pyruvate; ACoA, acetyl-CoA; Mal, malate; Oaa, oxaloacetate; Cit, citrate; α-KG, α-ketoglutarate; Glu, glutamate; Gln, glutamine.

$$\text{Theoretical fraction of } ^{13}\text{C-acetyl-CoA} = (\text{GRM} + \text{ME}) / (\text{GRM} + \text{GOM} + \text{ME}) \quad (17)$$

In the conducted experiments culturing cells in the presence of 100% [U-^{13}C]-glutamine, less than 1% of ^{13}C incorporation in pyruvate was observed (see data shown in *Annex 10.1*, Table 10.1). Thus, the contribution of MDH and ME to total acetyl-CoA synthesis was neglected and the theoretical fraction of ^{13}C-acetyl-CoA was assumed to be as follows:

$$\text{Theoretical fraction of } ^{13}\text{C-acetyl-CoA} = \text{GRM} / (\text{GRM} + \text{GOM}) \quad (18)$$

In parallel, oxidative and reductive glutamine metabolism yield m4 and m5 labeled citrate respectively (Figure 4.1). Then, the relation between the fluxes through the oxidative and the reductive glutamine metabolism can be expressed as relation between m4 and m5 labeled citrate:

$$GOM/GRM = Cit(m4)_{t=f} / Cit(m5)_{t=f} \quad (19)$$

Thus equations 18 and 19 can be combined in order to obtain the theoretical fraction of ^{13}C-acetyl-CoA from 100% [U-^{13}C]-glutamine, resulting in the next expression:

$$\text{Theoretical fraction of } ^{13}\text{C-acetyl-CoA} = Cit(m5)_{t=f} / ((Cit(m5)_{t=f} + Cit(m4)_{t=f})) \quad (20)$$

Once the theoretical enrichment was calculated, the percentage or either glucose or glutamine used for palmitate synthesis was determined by using the expression:

$$\%\text{ of contribution} = q / \text{ Theoretical fraction of } ^{13}\text{C-acetyl-CoA} \quad (21)$$

4.14 Sugar phosphates determination

Hexose, pentose and triose phosphates were determined in cultured plates frozen in liquid nitrogen by LC-MS-MS using addition curve method as described in Vizan *et al* 2007 (Vizan et al., 2007). Briefly, frozen cultured plates at 80−90% of confluence were scraped at 4 °C by adding 2×1 mL of 100 mM acetic acid (extraction buffer) and 1 mL of 100 mM acetic acid containing 100 ng/µL of D-ribose as internal standard. From the cell homogenate, 50 µL was split for protein determination by the BCA protein assay. Cell extract was then centrifuged at 400xg for 10 min at 4 °C. The pellet was discarded, and supernatant was filtered through 0.22 µm filter and frozen at −80 °C until injection. In parallel, calibrators (F16BP, G6P, F6P, R5P, X5P, E4P, GAP, DHAP, PEP) were diluted in extraction buffer and added in increasing concentrations to extra plates following the same procedure used for samples to generate the addition curve. HPLC chromatography was performed using an Agilent 1100 quaternary pump equipped with a refrigerated autosampler. A Nucleodex β-OH HPLC column, 200 × 4 mm i.d. (Panreac) was used with a binary gradient at a flow rate of 0.75 mL/min. Solvent A consisted of 10

mM ammonium acetate, pH 4.0. Solvent B consisted of acetonitrile. MS and MS-MS experiments were carried out on an API 3000 triple quadrupole mass spectrometer. The MRM (multiple reaction monitoring) transitions were 339/97 for F16BP, 259/97 for G6P and F6P (hexose phosphates, HexP), 229/97 for R5P and X5P (pentose-phosphates, PenP), 169/97 for GAP and DHAP (triose phosphates, TrisP) and 167/79 for PEP.

4.15 Enzyme activities

Fresh cell culture plates were rinsed with PBS and scrapped in lysis buffer (20 mM Tris-HCl, pH 7.5, 1 mM dithiothreitol, 1 mM EDTA, 0.02% (v/v) Triton X-100, 0.02% (v/v) sodium deoxycholate) supplemented with protease inhibition cocktail (Sigma-Aldrich). Cell lysates were disrupted by sonication using titanium probe (VibraCell, Sonics & Materials Inc., Tune: 50, Output: 30) and immediately centrifuged at 12000×g for 20 min at 4 °C. The supernatant was separated and used for the determination of specific enzyme activities using a COBAS Mira Plus chemistry analyzer. All enzymatic activities were determined by monitoring NAD(P)H increment or decrement at 340 nm wavelength.

4.15.1 Glucose-6-phosphate dehydrogenase (G6PD, EC 1.1.1.49.)

G6PD activity was measured by adding samples to a cuvette containing 0.5 mM $NADP^+$ in 50 mM Tris-HCl, pH 7.6, at 37 °C. Reaction was initiated by the addition of G6P up to a final concentration of 2 mM.

4.15.2 Hexokinase (HK, EC 2.7.1.1)

HK specific activity was determined by coupling HK and G6PD reactions in the following conditions: 3.3 mM $NADP^+$, 14.8 mM ATP, 14.8 mM $MgCl_2$, 2.8 U/mL G6PD and 50 mM Tris-HCl, pH 7.6, at 37 °C. Reactions were initiated by the addition of glucose up to a final concentration of 10 mM.

4.15.3 Transketolase (TKT, EC 2.2.1.1.)

TKT specific activity was determined by adding samples to a cuvette containing 5 mM $MgCl_2$, 0.2 U/mL triose phosphate isomerase, 0.2 mM NADH, 0.1 mM thiamine pyrophosphate in 50 mM Tris-HCl, pH 7.6, at 37 °C. The reaction was initiated by the addition of a substrate mixture prepared by dissolving 50 mM R5P in 50 mM Tris-HCl, pH 7.6, in the presence of 0.1 U/mL ribulose-5-phosphate-3-epimerase and 1.7 mU/mL phosphoriboisomerase. The substrate mixture was continuously stirred and held at 37 °C for 1 h and then kept at -20 °C until use.

4.15.4 Pyruvate kinase (PK, EC 2.7.1.40)

PK specific activity was determined by coupling PK and LDH reactions in the following conditions: 0.8 mM NADH, 1.6 mM ADP, 12.1 mM $MgCl_2$, 36.8 mM KCl and 5.2 U/mL LDH in 20 mM KH_2PO_4/K_2HPO_4 buffer, pH 7.2, at 37 °C. Reactions were initiated by the addition of PEP up to a final concentration of 3.5 mM.

4.15.5 Lactate Dehydrogenase (LDH, EC 1.1.1.42)

LDH specific activity was measured by adding sample extracts to a cuvette containing 0.2 mM NADH in 100 mM KH_2PO_4/K_2HPO_4, pH 7.4, at 37 °C. Reaction was initiated by the addition of pyruvate up to a final concentration of 0.2 mM.

4.16 Statistical analysis

For statistical analysis parametric unpaired two-tailed independent sample Student's *t*-test was used. In figures, bars represent mean ± SD and number of replicates (n) is indicated in each case. One asterisk (*) denotes p-value<0.05 and two asterisks (**) denotes p-value<0.01 except in Chapter 5.1, where one asterisk (*) denotes p-value<0.1, two asterisks (**) denotes p-value<0.05 and three asterisks (***) p-value<0.01.

5. RESULTS AND DISCUSSION

Chapter 5.1

Carbon Metabolism and the Sign of Control Coefficients in Metabolic Adaptations Underlying *K-RAS* Transformation

This chapter corresponds to the published article (see *Appendix III*):

Benito A., de Atauri P., Vizán P., Zanuy M., Mangues R., Marín S., and Cascante M. (2011). Carbon metabolism and the sign of control coefficients in metabolic adaptations underlying *K-RAS* transformation. Biochimica et Biophysica Acta *6,* 746-754.

5.1.1 Brief introduction and scope

As described in the previous pages, signaling pathways control and reorganize metabolism to fulfill the specific energetic and biosynthetic requirements of cells for growth and proliferation. These requirements are especially important in proliferative and cancer cells. Besides, most of the oncogenic mutations in cancer are found in signaling pathways that regulate these processes, such as RAS signaling pathway, being the metabolic network rewired to support tumorigenesis. So far, no successful therapies targeting RAS exist and RAS-mutated tumors targeted with current therapies are often refractory (Linardou et al., 2009; Normanno et al., 2009). Since metabolic reprogramming is an essential step in tumors to progress, we sought to explore the K-RAS induced metabolic reprogramming and to identify the key enzymes that drive this metabolic transition.

Approximately 30% of human tumors are estimated to harbor activating mutations in one of the RAS isoforms K-RAS, N-RAS and H-RAS (Fernandez-Medarde and Santos,

2011). K-RAS is the most frequently mutated among the three isoforms and its mutation rate in all tumors is estimated to be 25-30% (Fernandez-Medarde and Santos, 2011). Moreover, and the RAS oncogenic mutations most commonly occur in codons 12, 13 and 61, all them located in the GTPase catalytic domain.

In order to unveil the key enzymes responsible for K-RAS induced metabolic reprogramming we employed RAS-transformed NIH-3T3 cells stably transfected with constitutively active *K-RAS* mutated at codon 12 or codon 13 (K12- and K13-transformed cells). NIH-3T3 cells have been used as a model system to explore characteristics associated with cell transformation, such as a higher aerobic glycolysis and changes of enzyme activities (Chiaradonna et al., 2006a; Chiaradonna et al., 2006b; Gaglio et al., 2009; Liu et al., 2010). Depending on the specific RAS mutation transfected, NIH-3T3 cells induce tumors with distinct survival strategies, associated with distinct transforming capabilities and aggressiveness (Guerrero et al., 2000; Guerrero et al., 2002).

In order to derive hypotheses about the driving enzymes that contribute to the reprogramming of carbon metabolism: i) metabolic adaptations were characterized in non-transformed and K12- and K13-transformed cells by means of experimentally measured external and internal metabolite concentrations; ii) the range of possible flux values was computed for each reaction using a flux spectrum approach and the data obtained from external metabolite variations; iii) control coefficients with fixed signs were identified by only a partial knowledge based on an established network structure, the flux distribution and the sign pattern of the regulatory dependences, which are described through the sign of elasticities and iv) control coefficients with fixed signs were used to identify the potential enzymes responsible for the observed increases and decreases in fluxes and concentrations that define KRAS-induced metabolic reprogramming in these cells.

5.1.2 Results

5.1.2.1. Metabolic adaptations in K12- and K13-transformed NIH-3T3 cells

5.1.2.1.1 System description

The scheme of the whole network under study is depicted in Figure 5.1.1. Fluxes are represented with letter *J*, where J_i refers to the steady state metabolic flux through the *ith* step; concentrations are represented with letter *x*, where x_i refers to the concentration of the *ith* metabolic intermediary; and activities are represented with letter *v*, where v_i refers to the rate of the isolated reaction of the *ith* step. Solid arrows (Figure 5.1.1) – reaction steps *A* to *Z* – refer to the principal carbon metabolism, including glycolysis, the PPP, the tricarboxylic acid (TCA) cycle and the main inputs and outputs. Some reactions were neglected and grouped into blocks – e.g. reaction step *F* refers to the block from glyceraldehyde-3-phosphate dehydrogenase (GAPDH) to enolase – and others were assumed to be involved in rapid

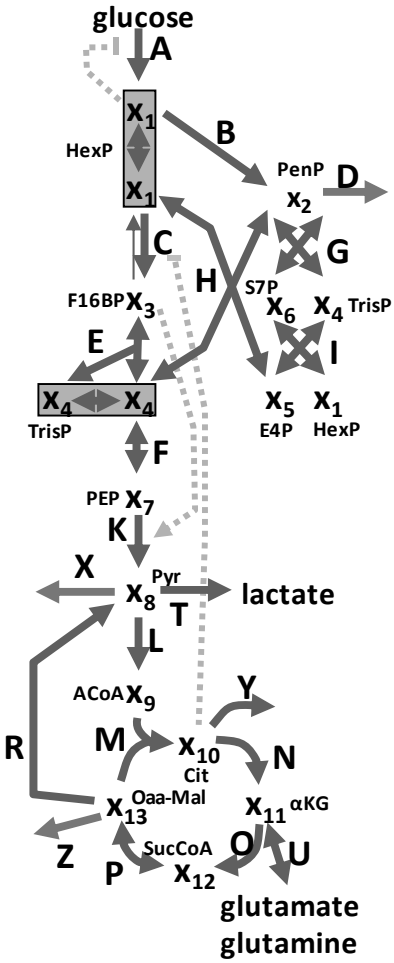

Figure 5.1.1. Network scheme.

Each arrow indicates a reversible or irreversible reaction step catalyzed by an enzyme (or transporter) or one block of enzymes. Grey dashed lines account for the regulatory circuits (inhibitions and activations). Acetyl-CoA – ACoA, citrate – Cit, dihydroxyacetone-phosphate – DHAP, erythrose-4-phosphate – E4P, fructose-1,6-bisphosphate – F16BP, fructose-6-phosphate – F6P, glucose-6-phosphate – G6P, glucose-6-phosphate dehydrogenase – G6PD, glyceraldehyde-3-phosphate – GAP, glyceraldehyde-3-phosphate dehydrogenase – GAPDH, hexokinase – HK, hexose phosphates – HexP, α-ketoglutarate – αKG, lactate dehydrogenase – LDH, malate – Mal, oxaloacetate – Oaa, pentose phosphates – PenP, pentose-phosphate pathway – PPP, phosphoenol pyruvate – PEP, phosphofructokinase – PFK, pyruvate – Pyr, pyruvate kinase – PK, ribose-5-phosphate – R5P, sedoheptulose-7-phosphate – S7P, succinate-CoA – SucCoA, transketolase – TKT, triose phosphates – TrisP.

equilibriums – e.g. glucose-6-phosphate isomerase -. Metabolites were combined into different pools: the pool x_1 for HexP refers to G6P and F6P; the pool x_2 for PenP refers to R5P; ribulose-5-phosphate and xylulose-5-phosphate; the pool x_4 for TrisP refers to dihydroxyacetone-phosphate (DHAP) and glyceraldehyde-3-phosphate dehydrogenase (GAP); and the pool x_{13} refers to oxaloacetate (Oaa) and malate (Mal). The rest of metabolic intermediates are F16BP (x_3), sedoheptulose-7-phosphate (x_6; S7P), erythrose-4-phosphate (x_5; E4P), PEP (x_7), Pyr (x_8), acetyl-CoA (x_9; ACoA), citrate (x_{10}; Cit), α-ketoglutarate (x_{11}; αKG) and succinate-CoA (x_{12}; SucCoA). In our system, the main fluxes in or out of the defined metabolic network correspond to experimentally measured glucose consumption (J_A), glutamate from glutamine consumption (J_U), and lactate production (J_T). Additional output exchanges connected to biosynthetic processes were not associated with a measured value (J_D, J_X, J_Y, J_Z).

5.1.2.1.2 Flux distributions

Under steady-state conditions, the flux balance associated with the stoichiometry constrains the dependences among fluxes (Kauffman et al., 2003; Llaneras and Pico, 2007; Schilling et al., 1999). In order to estimate the different flux distributions of non-transformed, K12- and K13-transformed cells, the fluxes for internal reactions can be expressed as dependent on a subset of fluxes including all output and input fluxes, e.g.:

$$
\begin{aligned}
&J_C = J_E = J_A - \tfrac{1}{3}(J_B + 2\times J_D),\\
&J_F = J_K = 2\times J_A - \tfrac{1}{3}(J_B + 5\times J_D),\\
&J_{Gf} = \tfrac{1}{3}(J_B - J_D) + J_{Gb},\\
&J_{Hf} = \tfrac{1}{3}(J_B - J_D) + J_{Hb},\\
&J_{If} = \tfrac{1}{3}(J_B - J_D) + J_{Ib},\\
&J_L = J_M = 2\times J_A - \tfrac{1}{3}(J_B + 5\times J_D) - J_T + J_U - J_X - J_Y - J_Z,\\
&J_N = 2\times J_A - \tfrac{1}{3}(J_B + 5\times J_D) - J_T + J_U - J_X - 2\times J_Y - J_Z,\\
&J_O = J_P = 2\times J_A - \tfrac{1}{3}(J_B + 5\times J_D) - J_T + 2\times J_U - J_X - 2\times J_Y - J_Z,\\
&J_R = J_U - J_Y - J_Z, \qquad (1)
\end{aligned}
$$

where J_{Gf}, J_{Hf}, J_{If} and J_{Gb}, J_{Hb}, J_{Ib} are the forward (J_{if}) and backward (J_{ib}) fluxes through the reversible reactions $J_G = J_{Gf} - J_{Gb}$, $J_H = J_{Hf} - J_{Hb}$, and $J_I = J_{If} - J_{Ib}$. An additional constraint was imposed based in our previous isotopomer-based analysis of non-transformed NIH-3T3 cells and K12- and K13-transformed cells (Vizan et al., 2005):

$$J_B = f_1 \times J_A \qquad (2)$$

where factor f_1 relates the oxidative branch of PPP (J_B) with the entry of glucose (J_A). This factor was set according to the measured ratios (Vizan et al., 2005): *0.063 ± 0.004* for non-transformed cells; *0.076 ± 0.012* for K12-transformed cells; and *0.153 ± 0.016* for K13-transformed cells. Thus, the flux through the oxidative branch of PPP was significantly lower than that descending through the glycolysis, and there was a significant increase of the flux through the PPP in transformed cells compared to non-transformed NIH-3T3 cells. Between transformed cells, K13 mutants routed more glucose to the oxidative branch of PPP than K12 mutants.

All these assumptions and measures are constraints limiting the space of solutions for the internal metabolic fluxes. Unfortunately, the complete system cannot be determined with the available measurements. Uncertainty is associated with the measured exchange fluxes (J_A, J_T, J_U) and, specially, with those not measured (J_X, J_Y, J_Z, J_D). An interval constraint satisfaction approach was applied as suggested by Llaneras and Picó (Llaneras and Pico, 2007) for cases where available measurements are insufficient and the complete flux distribution cannot be uniquely calculated. The feasible range of solutions satisfying all constraints was estimated for each reaction step. Initial lower and upper bounds for intervals were assigned to the flux through all reaction steps: 1) lower and upper bounds were assigned as the mean value ± 1.5 × standard deviation for measured fluxes J_A, J_T, and J_U; 2) a lower bound of zero was assumed for the irreversible fluxes J_B, J_D, J_K, J_L, J_M, J_N, J_O, J_R, J_S, J_X, J_Y, J_Z, which were assumed to have positive values ($0 < J_i$). For each cell type, the lower and upper bounds were constrained to satisfy the stoichiometric description of the system (Eq. 1) and the isotopomer-based constraint in (Eq. 2). These intervals of fluxes satisfying all constraints were calculated by two independent procedures: 1) iterative interval propagation, or 2) solving each minimum and maximum bound through linear programming, taking

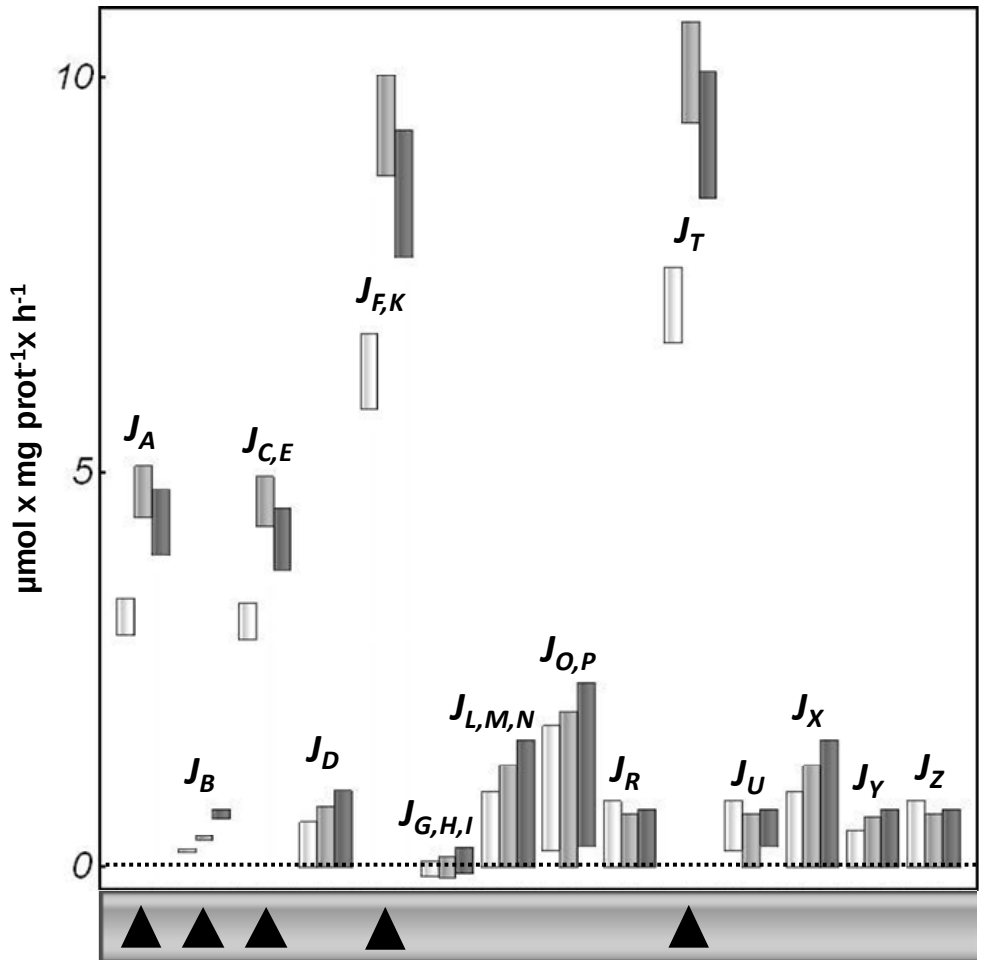

Figure 5.1.2. Comparison of fluxes.

Non-transformed NIH-3T3 cells (white); K12-transformed cells (light gray); and K13-transformed cells (dark gray). ▲) Increased flux in transformed cells with respect to non-transformed cells; and ▼) Decreased flux in transformed cells with respect to non-transformed cells. Some dependent fluxes are grouped together: *J_C and J_E ($J_{C,E}$); J_F and J_K ($J_{F,K}$), J_G, J_H and J_I ($J_{G,H,I}$) ; J_L, J_M and J_N ($J_{L,M,N}$); and J_O and J_P ($J_{O,P}$).*

advantage of the linear nature of the problem. The resulting flux distributions for non-transformed cells, K12- and K13-transformed cells are shown in Figure 5.1.2, which graphically depicts the interval ranges of flux values which satisfy all the constraints. As an example, for non-transformed cells, the initial intervals were $2.04 < J_A < 3.41$, $0 < J_B < \infty$, $-\infty < J_C < \infty$, $0 < J_D < \infty$, $-\infty < J_E < \infty$, $-\infty < J_F < \infty$, $0 < J_G < \infty$, …, $6.63 < J_T < 9.56$, $0.20 < J_U < 0.84$, …, and the final intervals satisfying all constraints (solution space)

computed with both iterative interval propagation and linear programming were 2.93 < J_A < 3.41, 0.18 < J_B < 0.21, 2.86 < J_C < 3.34, 0 < J_D < 0.57, 2.86 < J_E < 3.34, 5.80 < J_F < 6.75, -0.11 < J_G < 0.07, …, 6.63 < J_T < 7.59, 0.20 < J_U < 0.84, …. Even with the propagated uncertainty, substantial changes in flux distribution are detected in transformed cells with respect non-transformed cells, in particular for the flux pattern in glycolysis and the oxidative branch of the PPP.

5.1.2.1.3 Metabolite concentrations

Changes in fluxes were coupled with additional experimental measurement of key sugar phosphate concentrations. Thus, the concentrations of HexP (x_1), PenP (x_2), F16BP (x_3), TrisP (x_4), and PEP (x_7) were measured for non-transformed and transformed cells (K12 and K13) and are compared in Figure 5.1.3. All concentrations were found to be slightly decreased in transformed cells.

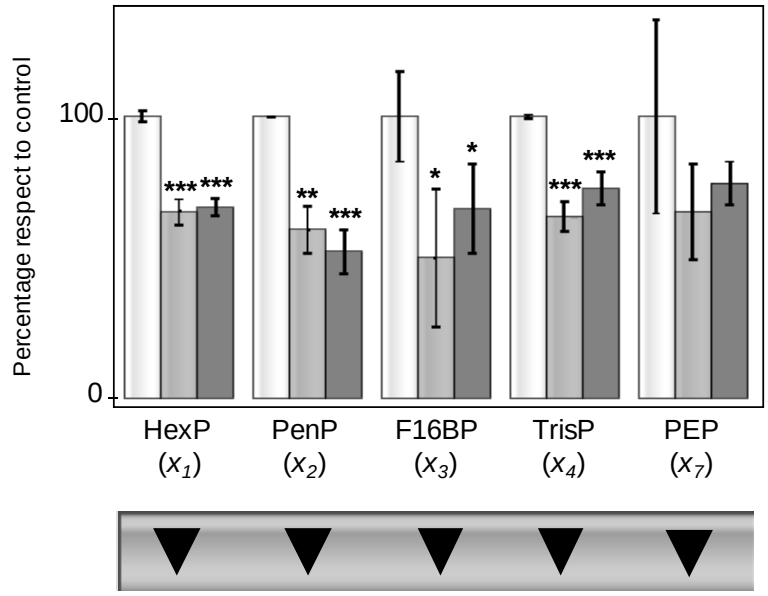

Figure 5.1.3. Comparison of measured concentrations.

Values for concentrations are proportional to the bar height for each chemical specie and error bars correspond tc standard deviations. See legend of Figure 5.1.2 for meaning of colours and triangles. As a reference for sugar phosphate concentrations, [F16BP] = 3.229 nmol·mg prot^{-1}, [HexP] = 1.799 nmol·mg prot^{-1}, [PenP] = 0.726 nmol·mg prot^{-1}, [TrisP] = 2.710 nmol·mg prot^{-1} and [PEP] = 0.457 nmol·mg prot^{-1} for non-transformed NIH-3T3 cells. p-values using two-tailed Student's *t*-test: *: p < 0.1, **: p < 0.05; ***: p < 0.01.

5.1.2.2. Predicted changes in fluxes and concentrations

5.1.2.2.1 The sign of control coefficients

In order to identify control coefficients with fixed signs, all regulatory dependences were considered. The matrix approach proposed by Cascante *et al* (Cascante et al., 1989a) was applied and is depicted in Figure 5.1.4. A matrix M^{-1} with all concentration control coefficients and all independent flux control coefficients can be derived from the inverse of a matrix *M* containing all elasticities and flux dependences. The sign of the elasticities is taken in order to derive the sign of the control coefficients. For example, the dependence of G6PD (reaction step B) on its substrate (HexP, x_1) corresponds to a positive elasticity ε_{B1}. In Figure 5.1.1, grey dashed lines account for the regulatory circuits – i.e. product (G6P, x_1) inhibition of HK (reaction step A) (Pelicano et al., 2006), inhibition of phosphofructokinase (PFK, reaction step C) by Cit (x_{10}) (Nakajima et al., 2002) and activation of PK (reaction step K) by F16BP (x_3) (Mazurek, 2011; Mazurek et al., 2007), which are associated with negative (ε_{A1}), negative (ε_{C10}) and positive (ε_{K3}) elasticities, respectively -. Reversibility is associated with negative elasticities with respect to products. Finally, reaction steps *D*, *X*, *Y* and *Z* describing the demand of synthetic processes were assumed to be saturated with respect to their respective substrates and then controlled by the demand; so, the elasticities ε_{D2}, ε_{X8}, ε_{Y10}, and ε_{Z13} were set to be zero. he sign of each control coefficient was analyzed by checking the positivity or negativity of the determinant |*M*| and the adjoint matrix in *Adj(M)* used for the derivation of the inverse:

$$M^{-1} = \frac{1}{|M|}\left(Adj(M)\right)^{\mathrm{T}} \qquad (3)$$

Since the determinant |M| was positive, the sign depended on the adjoint matrices. The matrix M^{-1} in Figure 5.1.4.B shows all control coefficients for independent fluxes and concentrations derived from this analysis. Control coefficients for the dependent fluxes can be derived by considering the dependences among fluxes in Eq. 1 and the control coefficients of independent fluxes (Cascante et al., 1989a; Cascante et al., 1989b), as

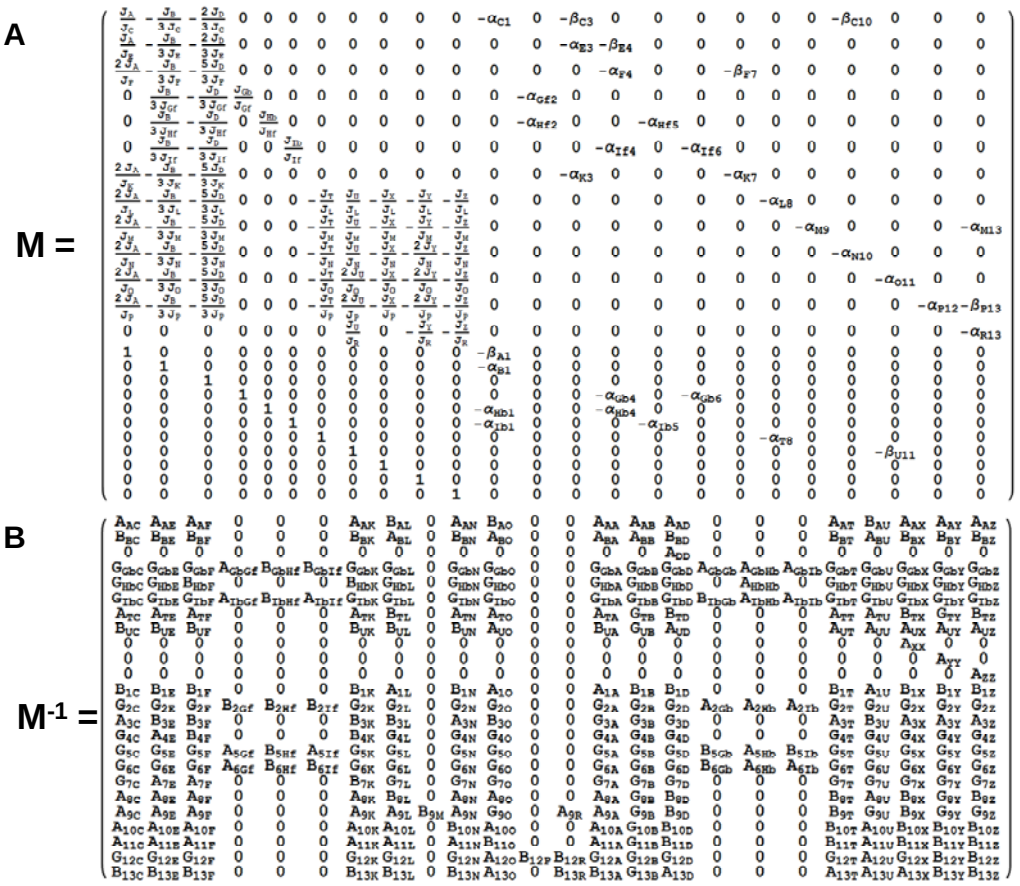

$$A_{CT} = \frac{J_A C_{AT}}{J_C} - \frac{J_B C_{BT}}{3J_C} - \frac{2J_D C_{DT}}{3J_C} = \frac{J_A A_{AT}}{J_C} - \frac{J_B B_{BT}}{3J_C}$$

Enzyme activities	J_A	J_B	$J^{f/b}_{G,H,I}$	$J_{C,E}$	$J_{F,K}$	J_T	J_L	x_1	x_2	x_3	x_4	x_7
v_A	+	+	+/-	±	+	+	+	+	±	±	±	±
v_B	(+)	+	+/-	(-)	(±)	(±)	(±)	(-)	±	(±)	(±)	(±)
v_C	+	-	-/+	+	+	+	+	-	±	+	±	±
v_E	+	-	-/+	+	+	+	+	-	±	-	+	+
$v^{f/b}_{G,H,I}$	*0*	*0*	*0*	*0*	*0*	*0*	*0*	*0*	*-/+*	*0*	*0*	*0*
v_F	+	-	-/+	+	+	+	+	-	±	-	-	+
v_K	+	-	-/+	+	+	+	+	-	±	-	-	-
v_T	+	-	-/+	+	+	+	-	-	±	+	±	±
v_L	-	+	+/-	-	-	-	+	+	±	-	±	±

Figure 5.1.4. Matrix estimation of the sign of control coefficients.

Elasticities with a magnitude of zero appear as *0*, while those positives are represented with a letter *α* ($\alpha_{ki} = \varepsilon_{ki} > 0$), and those negatives with a letter *β* ($\beta_{ki} = \varepsilon_{ki} > 0$); control coefficients with a magnitude of zero appear as *0*, while these positives are represented with the letter *A* ($A_{ki} = C_{ki} > 0$) or a symbol "+", and these negatives with the letter *B* ($B_{ki} = C_{ki} < 0$) or a symbol "-"; Those control coefficients with indeterminate signs are represented with a letter *G*

.../...

demonstrated in the example provided in Figure 5.1.4.C. A subset of control coefficients signs are presented in Figure 5.1.4.D in a table of dependences between the fluxes and concentrations and the main enzyme activities. Positive and negative symbols correspond to control coefficients with positive and negative signs, respectively. The signs in Figure 5.1.4.D collectively give a complete systemic predictive tool which can be used to evaluate the expected impact of changes in enzyme activities. Thus, the specific pattern of observed changes in fluxes and concentrations can be associated with increases or decreases in enzyme activities through analysis of the signs of control coefficients. For example, the observed decrease in the concentration of PEP (x_7) could correspond to an increase of PK activity (v_K), but never to a decrease.

5.1.2.2.2 The magnitude of the control coefficients

Analysis of the signs of metabolic control coefficients is sufficient if the aim is to predict the direction of changes in concentrations and fluxes. However, this previous analysis does not suffice if the objectives are to predict the magnitudes of these changes, and then the magnitude of the control coefficients is required. Unknown elasticities can be randomly sampled in order to derive feasible magnitudes for control coefficients (Wang et al., 2004). We have applied sampling procedures based on those described by Wang *et al* (Wang et al., 2004) in order to have an additional independent evaluation of the sign and mean magnitude of the control coefficients (results exactly match the computed signs). This analysis identified a subset of control coefficients which are always associated with small magnitudes. In the system considered (Figure 5.4.1) the PPP is a sub-network characterized by a flux which is much smaller than the main fluxes

.../...
(G_{ki} = C_{ki} > 0 or C_{ki} < 0) or a symbol "±". **A-B.** A matrix *M* (A) with the information containing both the stoichiometry and the regulatory properties of the analysed system (elasticities and ratios among fluxes), is inverted to obtain the matrix of control coefficients M^{-1} (B) for independent fluxes and concentrations. **C.** An example of estimation of a control coefficient of dependent fluxes from the previously estimated control coefficients of independent fluxes. **D.** Table of dependences connecting changes in fluxes and concentrations with changes in enzyme activities for a subset of analyzed control coefficients. Superscripts "f" and "b" refers to net direction of reversible reactions of the non-oxidative branch of PPP (*G,H,I*) following the forward or the backward directions, respectively. The net fluxes for the remaining reversible reactions are set to follow only the forward direction according to Figure 5.1.2. Symbols ("+","-","±") identified with a black circle refer to control coefficients of very low magnitude in comparison with the other ones.

through the rest of the network (J_B <<< J_C). The effect of changes in the activity throughout this sub-network will have minimal effect on the rest of the system, but these changes can have a significant effect on the concentrations and reaction steps inside the sub-network. The dependence of control coefficients on particular fluxes, such as J_B, can be easily identified by inspecting the adjoint matrices. Control coefficients identified with black circles in Figure 5.1.4.D are directly proportional to the value of J_B, which implies very small magnitudes due to the small flux through the oxidative branch of the PPP.

5.1.2.3. Testing and validation of hypotheses based on variations in enzyme activities

5.1.2.3.1 Specific activities

The specific activities of HK (v_A), G6PD (v_B), TKT (v_G, v_H), PK (v_K), and LDH (v_T) were measured for non-transformed and transformed (K12 and K13) cells and compared in Figure 5.1.5.A. Increases or decreases in specific activities observed during the metabolic adaptation associated with the K-RAS transformation were analysed. Clear changes were observed in G6PD and LDH in both K12- and K13-transformed cells and also in PK in K13-transformed cells. In addition, slight changes for TKT were detected in both K12- and K13-transformed cells and. There were no significant changes in the observed HK activities.

5.1.2.3.1 Do changes in measured activities satisfy the predictions for concentrations and fluxes?

The table of dependences in Figure 5.1.5.B identifies both satisfied and non-satisfied predictions of the sign of control coefficients for those activities with measured changes (v_B, v_G, v_H, v_K and v_T). Satisfied predictions, which are those where the direction of the changes in a concentration or flux is explained by the direction of the change in an enzyme activity, are marked in green. Otherwise, if the prediction is not satisfied, the sign of the control coefficients is marked in red. For example, the increase in LDH activity (v_T) could help to explain the measured increase in J_A, but not the increased in J_B,

which is satisfied by the increased G6PD activity (v_B). Predictions regarding TKT are more complicated because the slight decrease of TKT activity could contribute to a predicted decrease of PenP levels (x_2), but only if the net flux through the non-oxidative branch of PPP is following the backward direction to PenP as is shown in Figure 5.1.5.B.

Indeterminate signs (±) identify control coefficients that can be positive or negative, depending on the relative values of the elasticities and ratios between fluxes. For a set of such sign-indeterminate control coefficients, only a limited combination of positive and negative signs is possible. Indeterminate signs (±) marked in green were used in Figure 5.1.5.B to highlight that a specific and feasible combination of elasticities and fluxes can result in a combination of signs that satisfies the changes in fluxes and concentrations. For example, the measured decreases in x_2, x_4, and x_7 can be predicted by an increase in v_T activity, which is possible because the negative control coefficients for C_{2T}, C_{4T}, and C_{7T} can be obtained by selecting the appropriate elasticities.

5.1.3 Discussion

The existence of control coefficients with fixed or indeterminate signs is dependent on the topology of the metabolic pathway and location of regulatory loops (feedback, feed-forward), branches, etc. (Sen, 1996). The signs of the control coefficients estimated above (Figure 5.1.4) were obtained by assuming a model adapted to the available data, where the relevant topology and regulation are considered. Analysis of the signs of control coefficients in Figure 5.1.5.B provides a complete picture of the potential effect that any change in enzyme activities would have on systemic properties such as fluxes and metabolite concentrations. This picture confirms that the increased fluxes from glucose to lactate (J_A, J_C, J_E, J_F, J_K, J_T) and through the oxidative part of the PPP (J_B) (Figure 5.1.2), and the decreased concentrations of sugar phosphates (x_1, x_2, x_3, x_4, x_7) (Figure 5.1.3), observed in transformed cells, can be explained in part by the increased specific activities for G6PD (v_B), PK (v_K), LDH (v_T), and decreased activity of TKT (v_G,v_H) (Figure 5.1.5.A). Interestingly, the differences between the phenotypes of K12- and K13-tranformed cells (Guerrero et al., 2000; Guerrero et al., 2002) are reflected by the

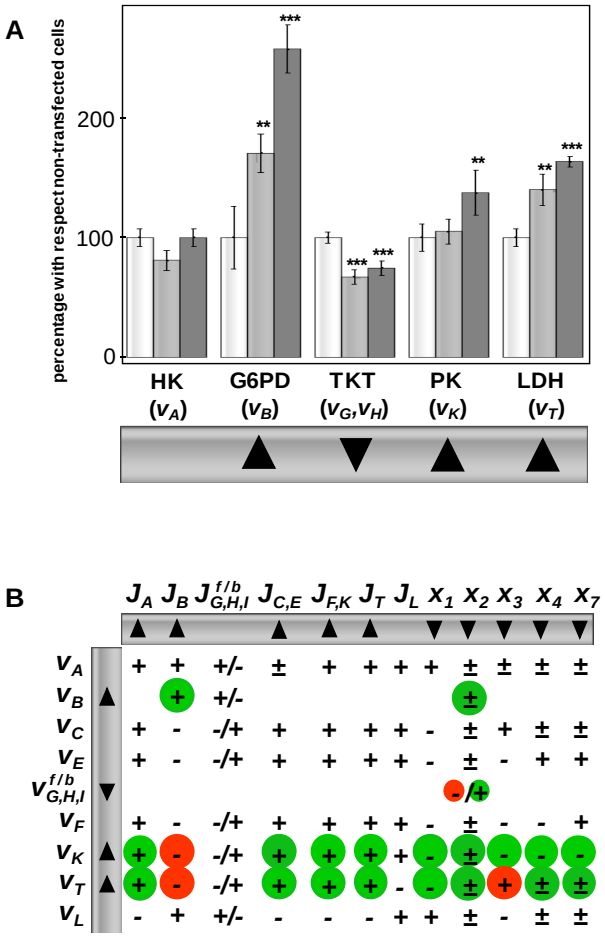

Figure 5.1.5. Specific activities and satisfied predictions.

A. Comparison of specific activities. See legend of Figures 5.1.2 and 5.1.3 for meaning of bar height, error bars, colours and triangles. As a reference for specific activities, HK = 130.17 mU·mg prot^{-1}, LDH = 2.83 U·mg prot^{-1}, G6PD = 215.02 mU·mg prot^{-1}, TKT = 35.72 mU·mg prot^{-1} and PK = 6.98 U·mg prot^{-1} for non-transformed NIH-3T3 cells. P-values using two-tailed Student's *t*-test: *: $p < 0.1$, **: $p < 0.05$; ***: $p < 0.01$. B. Satisfied predictions represented in the table of dependences connecting changes in fluxes and concentrations with changes in enzyme activities. See legend of Figure 5.1.4 for meaning of superscripts "f" and "b", and positive-negative symbols ("+","-","±"). Symbols marked in green or red refers to control coefficients that can or cannot explain, respectively, the observed change in a flux or concentration with respect to the direction of a measured change in an enzyme activity.

magnitude of the changes in fluxes and not by the sign of these changes. Changes in enzyme activities are also in the same direction (with the same sign of change) for both transformed cells with the exception of PK activity which is only increased significantly in the K13 cell line.

The measured changes in specific enzyme activities accounts for changes in the enzyme concentrations. It should be noted that *in vivo*, changes affecting an enzyme activity can be as a result of changes on its expression but also due to a variety of events including: changes in cofactors, post-transductional modification or changes in oligomerization state among others. One example of this is the case of PK. Among the different PK isoforms, the M2-PK isoenzyme is expressed in all proliferating cells, including embryonic, tumour and NIH-3T3 cells (Mazurek et al., 2007). The M2-PK isoenzyme occurs in a highly active tetrameric form and in a dimeric form with low affinity for PEP (Mazurek, 2011). The tetramer to dimer ratio of M2-PK is not static and depends on F16BP levels in addition to any effects due to other external mechanisms (Mazurek, 2011).

The measured changes of the specific activities for G6PD (v_B), PK (v_K), and LDH (v_T) satisfy the predictions based on the sign of the control coefficients. Interestingly, Figure 5.1.5.B shows that the set of observed changes in fluxes and concentrations accompanying K12- and K13-transformation cannot be attributed to the perturbation of a single enzyme activity. According to results depicted in Figure 5.1.5.B, simultaneous activation of G6PD and some of the glycolytic enzymes is required in order to fully explain the observed pattern of changes in fluxes and metabolite concentrations. The experimentally measured increase in G6PD and in some glycolytic enzymes (LDH (v_T) and PK (v_K)) confirms this prediction and helps to explain qualitatively almost all observed increases in fluxes and decreases in concentrations, although it is likely that other glycolytic enzyme activities could also be increased. The predictions of Figure 5.1.5.B are also in agreement with the available literature on tumour metabolism that suggests the action of transcription factors, as c-MYC and the hypoxia-inducible transcription factor 1 (HIF1), which are associated with the activation of oncogenes including transforming *RAS*. This leads to the reprogramming of different components of the cell metabolism, including higher expression for most of the genes encoding glycolytic enzymes (Gordan et al., 2007; Kim et al., 2007; Kim et al., 2004; Kroemer and Pouyssegur, 2008; Pelicano et al., 2006; Semenza, 2010; Vizán et al., 2008). Among the enhanced enzymes are mammalian isoforms of HK (HK1 and 2), PK (M2-PK) and LDH (LDH-A). We have also observed changes in LDH for both K12 and K13 cells in addition

to changes in PK for K13 cells. However, HK activity is not significantly altered by either of the two transformed cell lines. Interestingly, in the previous work of Guerrero *et al* (Guerrero et al., 2000; Guerrero et al., 2002) for the same K12- and K13-transformed NIH-3T3 cells used in the present study, they showed an increased expression of GAPDH for both transformed cell lines with respect to the non-transformed ones. From Figure 5.1.5.B we can predict that this increase of GAPDH (v_F) can also contribute to the observed metabolic phenotype of transformed cells.

Taking into account that control is distributed among the enzymes of glycolysis, it is not surprising that simultaneously increasing a number of different glycolytic enzymes is required in order to achieve a large increase in glycolytic flux. Thus, in a linear pathway, all the control coefficients are positive and their sum is equal to one (Fell, 1997), which means that, if the control is shared between several enzymes, then the magnitude of each individual control coefficient is expected to be quite low. A very low control coefficient indicates that in order to alter the flux significantly by using modifications of a single enzyme, a very large change in the enzyme concentration is required. However, a simultaneously balanced change in all glycolytic enzyme concentrations should result in both a directly proportional change in the glycolytic flux and also the absence of change in intermediate metabolites (Kacser and Acerenza, 1993). The observed slight decrease in all measured metabolites could be the consequence of increased external demands.

However, it is also interesting to notice that according to Figure 5.1.5.B the observed increase in the flux through the oxidative part of PPP is not predicted by an increase in measured glycolytic activities, but is clearly satisfied by an increase in G6PD activity. Comparing K12 and K13 cells, there is a perfect agreement between the higher G6PD activity and the higher flux through the oxidative part of the PPP. Regulation of the expression of G6PD is altered in many tumours, resulting in a significant increase in G6PD activity, and it has been suggested that G6PD may act as a potential oncogene (Kuo et al., 2000). Increased G6PD activity in NIH-3T3 cells, transfected with human G6PD cDNA, leads to tumorigenic transformations, dividing more quickly and inducing tumors in nude mice (Kuo et al., 2000). The decreased levels of PenP (x_2) are not

compatible with the increased activity of G6PD, but are compatible with an increased demand of ribose (reaction step D). Also, the decreased levels of PenP can be at least in part a consequence of the slight decrease in the TKT activity. The two key enzymes of the PPP, G6PD and TKT, were both previously identified as potential targets in cancer therapy (Boren et al., 2002; Boros et al., 1997; Comin-Anduix et al., 2001; Rais et al., 1999), and recently, the increased G6PD/TKT ratio was proposed as a tumour metabolome feature (Rais et al., 1999). The observed notorious increase of G6PD resulted in a higher G6PD/TKT ratio in both transformed cell lines with respect to non-transformed cells in agreement with the results of Montoya *et al* (Ramos-Montoya et al., 2006). Here, we have also found that this ratio is higher in K13 than in K12.

Finally, it is interesting to note the fact that metabolic adaptations observed in transformed cells require changes in more than one enzyme, which suggests that a multi-hit strategy would be required to counteract metabolic adaptations in transformed cells. These results support the suggestions of Moreno-Sanchez *et al* (Moreno-Sanchez et al., 2010) who proposed that a "multi-targeted MCA advised therapy" would be required to design efficient treatments in cancer based on the fact that control is shared among several steps in metabolic networks.

In summary, it can be concluded that, the study of flux distribution in combination with metabolic control analysis performed by analyzing solely the sign of fixed-sign control coefficients, is a reliable approach to identify the key enzymes involved in metabolic reprogramming. The use of this methodology has allowed us to, firstly, identify an increase in glycolysis and PPP fluxes as metabolic features of KRAS-induced metabolic reprogramming and, secondly, to propose G6PD, PK and LDH as the key enzymes responsible for this metabolic transition.

Chapter 5.2

Metabolic Reprogramming Induced by H-RAS Oncogenic Activation Assessed by ^{13}C-assisted Metabolomics

5.2.1 Brief introduction and scope

In the chapter 5.1 we have analyzed the metabolic reprogramming induced by K-RAS oncogenic activation employing NIH-3T3 cells transformed with K-RAS oncogene mutated either in codon 12 or 13 (K12- and K13-transformed cells). A feasible and accurate flux map distribution has been determined and key enzymes driving the metabolic transition from normal to transformed cells have been revealed. Although K-RAS isoforms is the RAS isoform most frequently mutated in human cancers, H-RAS has a mutation rate of 3% in human cancers (Takashima and Faller, 2013), being predominantly mutated in salivary gland (15%), urinary tract (11%), and cervix (9%) (Pylayeva-Gupta et al., 2011). Regardless of isoform type or codon location, all these activating mutations render RAS proteins constitutively activated, initiating intracellular signaling cascade autonomously and resulting in uncontrolled cell proliferation and abnormal cell survival.

The metabolic consequences of H-RAS oncogenic activation have been studied from different perspectives and using different systems. However, all the studies performed so far have examined HRas-induced metabolic reprogramming in a partial manner, considering only a fraction of the metabolic network. Regarding glycolysis, it has been reported that H-RAS oncogenic activation promotes an increase in glucose transporters, consumption of glucose and production of lactate (de Groof et al., 2009; Telang et al., 2007) and HIF1α levels (Chen et al., 2001). With regard to mitochondrial metabolism,

both increased (Telang et al., 2007) and decreased (Yang et al., 2010) mitochondrial metabolism has been described in HRas-mutated cells. On the other hand, some studies have also focused on lipid metabolism, concluding that H-RAS promotes an increased release of sphingosine (Kalas et al., 2012) and increased levels of acyl-CoA synthetase and phosphatidylethanolamine (Momchilova and Markovska, 1999).

All these studies provide independent pieces of evidence that reveal a portion of the metabolic effects derived from H-RAS oncogenic activation. Nevertheless, there is a lack of a deep and comprehensive metabolic approach to understand this process. Although these studies provide interesting metabolism-related information, only Telang and collaborators offered truly but limited metabolic data, obtained through ^{13}C-assisted metabolomics by using [U-^{13}C]-glucose (Telang et al., 2007).

Thus, with the aim to explore in great detail the metabolic reprogramming induced by the mutation HRasV12 in human cells, we assessed $BJ^{LT+/hTERT+/HRasV12-}$ (BJ) and $BJ^{LT+/hTERT+/HRasV12+}$ (BJ-HRasV12) cells through ^{13}C-assisted metabolomics using ^{13}C-glucose and ^{13}C-glutamine in parallel experiments. In order to achieve this aim: i) extracellular fluxes concerning the main metabolic substrates were determined and nutrient sensitivity analysis was performed; ii) ^{13}C-assisted metabolomics parallel experiments using [1,2-$^{13}C_2$]-glucose and [U-^{13}C]-glutamine were carried out and mass isotopomer distribution of several metabolites as well as state of different metabolic pathways were determined, and iii) mitochondrial metabolism was analyzed by measuring oxygen consumption rate in the presence of different carbon substrates.

5.2.2 Results

5.2.2.1 H-RAS oncogenic activation promotes global metabolic network reorganization

The intimate interconnection between signaling and metabolic events is of major relevance to ensure cell proliferation and survival. Such a tight relation is particularly essential in cancer, where oncogenes trigger a metabolic rewiring that guarantees the

fulfillment of the metabolic requirements. Glucose and glutamine account for the two major sources of energy and building blocks for synthesis of macromolecules. Then, we first determined how H-RAS oncogenic activation affected the metabolism of these two nutrients in BJ cells (Figure 5.2.1.A). We observed that H-RAS activation induced an increase of 80% in glucose uptake and 90% in lactate secretion. Likewise, we also found a 45% increase in glutamine consumption and a 30% increase in glutamate secretion, highlighting the importance of the mitochondrial metabolism in BJ-HRasV12 cells.

5.2.2.2 BJ-HRasV12 cells display increased sensitivity to glucose or glutamine deprivation

We next examined if the increased glucose and glutamine consumption induced by H-RAS resulted in increased sensitivity of BJ-HRasV12 cells to glucose or glutamine deprivation (Figure 5.2.1.B). Measurements of cell proliferation after 24h of culture in low glucose concentration (1 mM) or glutamine-free media showed that BJ-HRasV12 proliferation decreased around 60 and 80% respectively, whereas BJ cells experienced a

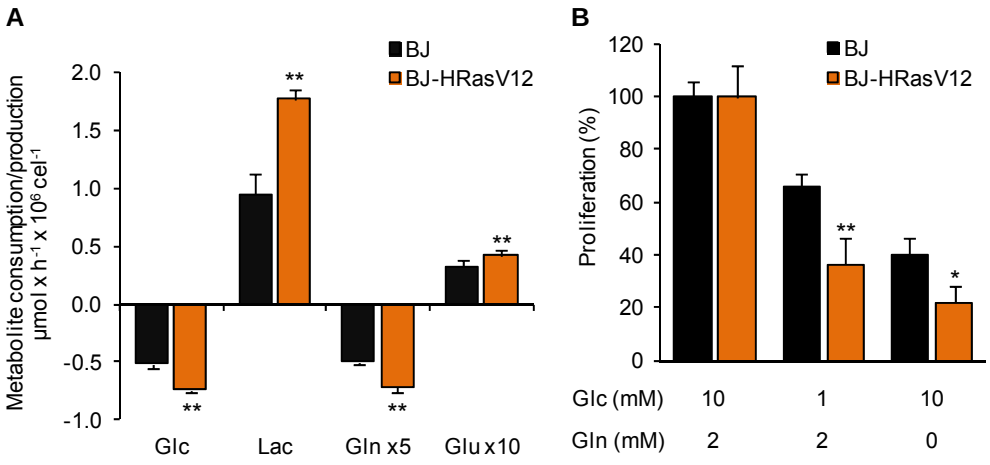

Figure 5.2.1. Extracellular fluxes and nutrient sensitivity analysis for BJ and BJ-HRasV12 cells

Metabolite consumption/production and cell proliferation were determined over a period of 24h. **A.** Glucose (Glc) and glutamine (Gln) consumptions and lactate (Lac) and glutamate (Glu) production. Bars represent mean ± SD of n=6. **B.** Cell proliferation under the indicated nutritional conditions. Cells were counted through flow citometry and relative increment in total cell number compared with cells grown in complete media is depicted. Concentration of each nutrient is shown below the plot. Bars represent mean ± SD of n=3. Significant differences compared with BJ cells were assessed by two-tailed Student's *t*-test. * $p<0.05$, ** $p<0.01$.

decrease of 40% and 60%. It is worth noting that both cell lines grow at similar rate when cultured in complete media (data not shown) (Hahn et al., 1999). Then, these results further support the enhanced nutrient requirements of BJ-HRasV12 cells described in the previous section.

5.2.2.3 ^{13}C-assisted metabolomics reveals a differential utilization of glucose- and glutamine-derived carbons in BJ-HRasV12 cells

Given the clear changes detected in the metabolism of glucose and glutamine, we sought to explore the fate of the carbons of both substrates as well as the utilization of the main metabolic pathways involved in central carbon metabolism in BJ and BJ-HRasV12 cells. To this end, we cultured BJ and BJ-HRasV12 cells in the presence of either [1,2-$^{13}C_2$]- glucose or [U-^{13}C]-glutamine and the mass isotopomer distribution of several metabolites was analyzed by GC-MS (see raw data in *Appendix I*).

5.2.2.3.1 H-RAS oncogenic activation induces an increase in lactate production

One of the main features of the Warburg effect is the increased conversion of glucose into lactate. The production of lactate from glucose through direct glycolysis or through PPP was quantified analyzing the mass isotopomer distribution of lactate in combination with the concentration of this metabolite in the cell culture media using data from experiments where up to 50% of [1,2-$^{13}C_2$]-glucose was used as tracer. [1,2-$^{13}C_2$]-glucose metabolized through direct glycolysis yields m2 lactate, whereas its metabolization through PPP yields m1 lactate. Then, pathway-specific production of lactate can be calculated based on this fact by using the equations described in *Section 4.13.1*. As shown in Figure 5.2.2.A, BJ-HRasV12 cells exhibited a 2-fold increase in the flux from glucose to lactate via glycolysis and via PPP. Also, lactate coming from other sources of carbon (OS) different than glucose was estimated using the methods described in the above-mentioned section. Results showed that BJ-HRasV12 exhibited over 2-fold increase in the flux of lactate from OS (Figure 5.2.2.A) indicating that BJ-HRasV12 cells can metabolize other substrates in a larger amount than BJ cells.

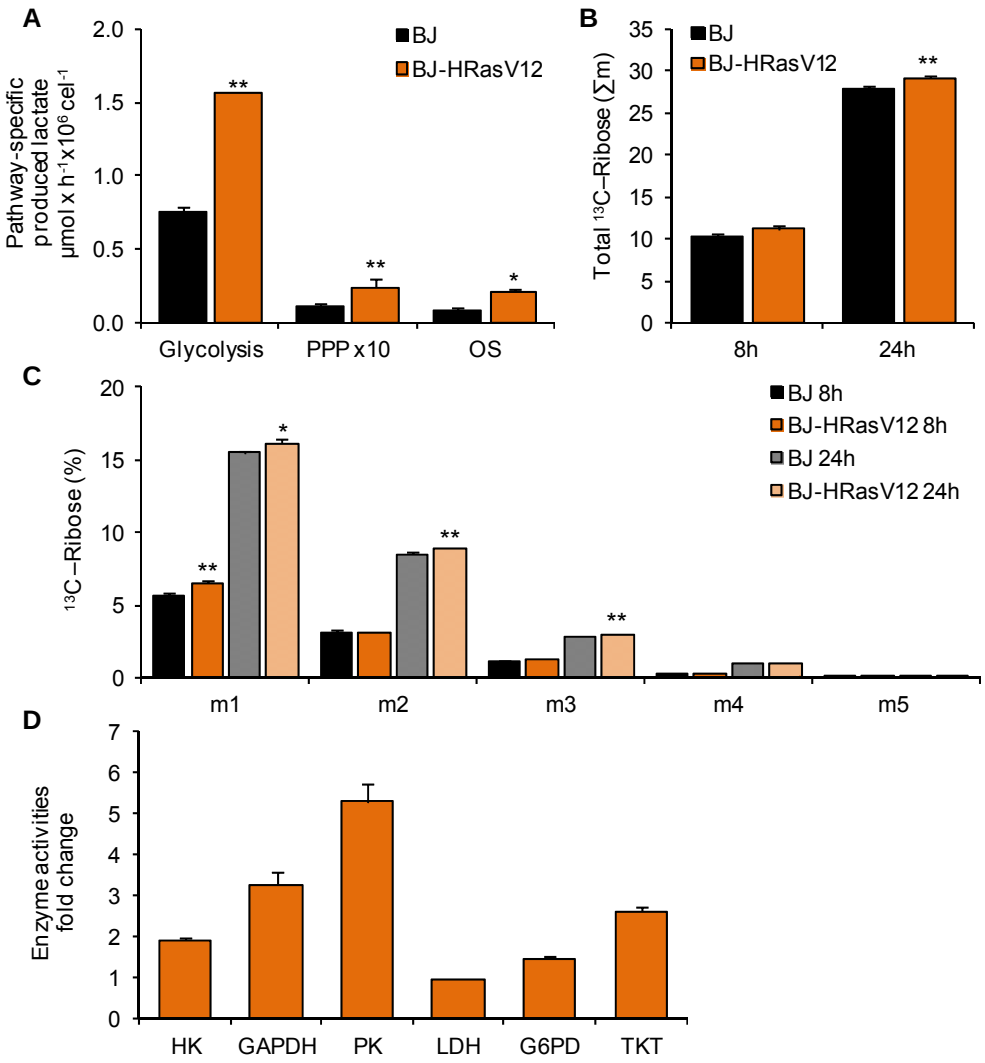

Figure 5.2.2. Glycolysis and PPP utilization in BJ and BJ-HRasV12

BJ and BJ-HRasV12 cells were cultured for 8 and 24h in the presence of 50% [1,2-$^{13}C_2$]-glucose. Media for lactate concentration and mass isotopomer distribution determinations and pellets for RNA ribose mass isotopomer analysis were taken at 8 and 24h. **A.** Pathway-specific produced lactate fluxes. Lactate production and mass isotopomer distribution of lactate were combined as described in *Section 4.13.1* to estimate the lactate produced from glucose through direct glycolysis or diverted through PPP and the lactate coming from other sources (OS). **B.** Total ^{13}C-ribose from RNA, represented as the sum of m1+m2+m3+m4 (∑m). **C.** Ribose mass isotopomer distribution. **D.** Specific activities of a panel of PPP and glycolytic enzymes. Data represents the BJ-HRasV12/BJ ratio. The value for each specific enzyme activity expressed in U x 10^6 cells^{-1} are as follows: HK (Hexokinase): BJ=23.74, BJ-HRasV12=45.31; GAPD (Glyceraldehyde-3-phosphate dehydrogenase): BJ=8.94, BJ-HRasV12=29.38; PK (Pyruvate Kinase): BJ=275.48, BJ-HRasV12=1463.39; LDH (Lactate dehydrogenase): BJ=1650.09, BJ-HRasV12=1622.35; G6PD (Glucose-6-phosphate dehydrogenase): BJ=33.74, BJ-HRasV12=49.57; TKT (Transketolase): BJ=1.65, BJ-HRasV12=4.34.. In all cases, bars represent mean ± SD of n=3. Significant differences compared with BJ were assessed by two-tailed Student's *t*-test. * $p<0.05$, ** $p<0.01$.

5.2.2.3.2 H-RAS oncogenic activation induces an increase in ribose synthesis

Since our results indicate that BJ-HRasV12 cells displayed increased lactate production not only through glycolysis but also through PPP, the mass isotopomer distribution of the end-product of this pathway, ribose, was analyzed. Ribose can be synthesized through the oxidative and the non-oxidative branches of PPP, resulting mainly in m1 and m2 labeled ribose respectively when up to 50% [1,2-$^{13}C_2$]-glucose is used as tracer. First, we observed that H-RAS oncogenic activation slightly enhanced the synthesis of ribose after 24h of incubation (Figure 5.2.2.B). Moreover, analysis of mass isotopomer distribution of ribose from RNA revealed an increase in m1 and m2 labeled ribose after 24h incubation, indicating that both oxidative and non-oxidative pathways were activated in BJ-HRasV12 cells (Figure 5.2.2.C). In order to investigate whether changes in fluxes are accompanied by changes at proteomic level, we examined a panel of enzyme activities involved in glycolysis and PPP (Figure 5.2.2.D). Key glycolytic enzymes such as HK, GAPDH and PK were found to be incremented in a range from 2- to 5-fold in BJ-HRasV12 cells compared to BJ cells. A striking exception was the case of LDH, which was found to be slightly diminished in BJ-HRasV12 cells. Likewise, the specific activity of the two key enzymes of PPP was determined. In consistence with the mass isotopomer distribution found in ribose, G6PD and TKT activities were found to be overactivated in BJ-HRasV12 cells. This data indicates that H-RAS oncogenic activation promotes not only an increase in metabolic fluxes but also changes in the concentration of the enzymes that participate in these pathways.

5.2.2.3.3. H-RAS oncogenic activation induces an increase of glucose-derived carbons in the TCA cycle

After characterizing the metabolic reprogramming in the upper part of the carbon metabolic network, we wanted to explore the glucose utilization in the mitochondria. Thus, we analyzed the mass isotopomer distribution of several TCA cycle intermediates. Since cells were cultured in the presence of [1,2-$^{13}C_2$]-glucose, TCA cycle metabolites were expected to mostly show m2 labeling as a result of the first turn in the TCA cycle

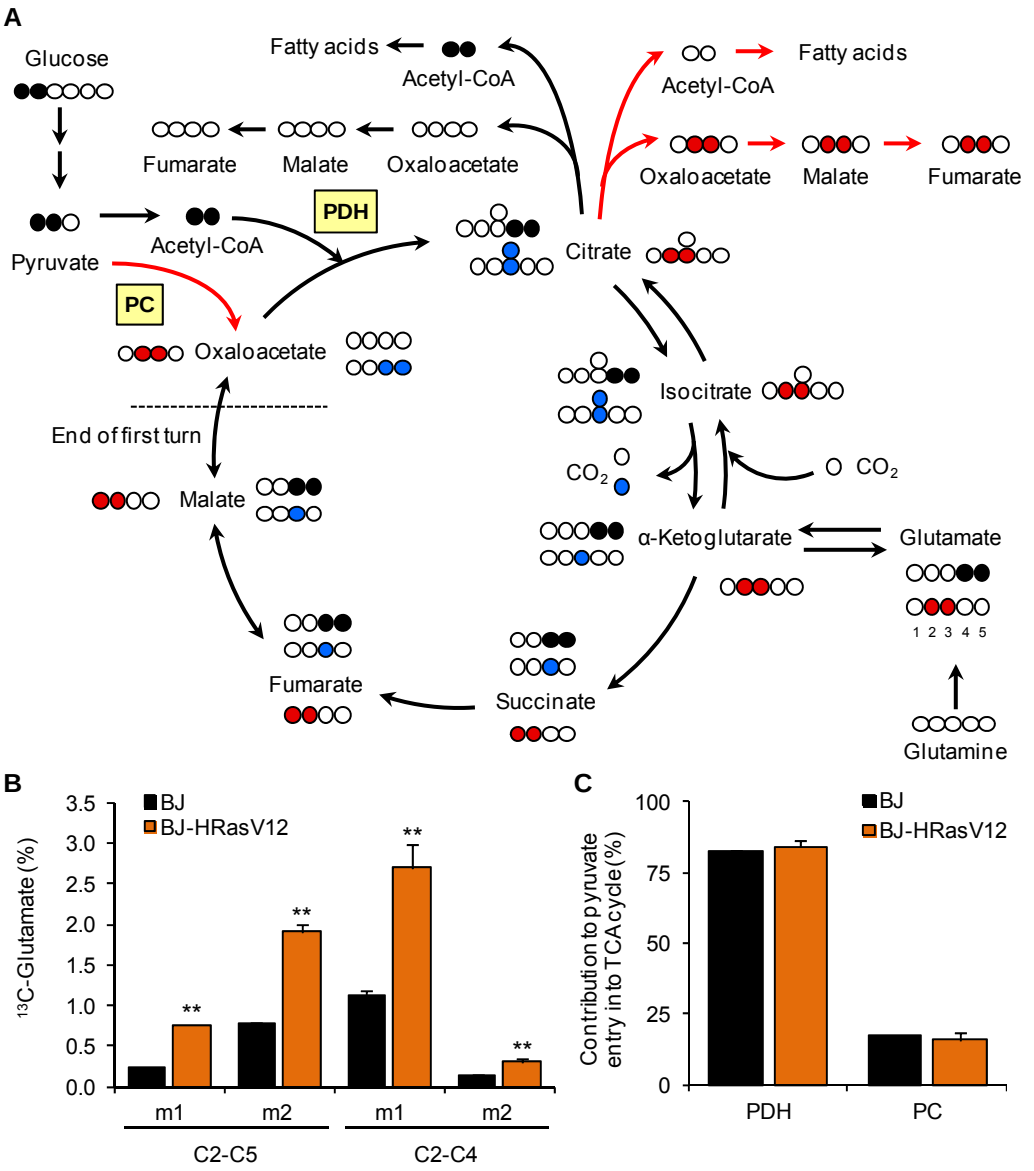

Figure 5.2.3. Glucose-derived carbons entrance into the TCA cycle

A. Carbon atom transition map for TCA cycle intermediates using 50% [1,2-$^{13}C_2$]-glucose as tracer. Pyruvate can enter into the TCA cycle via pyruvate dehydrogenase (PDH, black molecules) or pyruvate carboxylase (PC, red molecules). For each metabolite, black and red molecules represent the labeling pattern corresponding to the first turn, while blue molecules are the result of the reaction of a formed [1,2-$^{13}C_2$]-oxaloacetate with an unlabeled acetyl-CoA (second turn of TCA cycle). As an example, in the first turn, the initial labeled oxaloacetate coming from PC (red molecule) reacts with an unlabeled acetyl-CoA while, in the second turn (blue molecules), a labeled oxaloacetate coming from PC or PDH reacts with an unlabelled acetyl-CoA. Note the differential mass isotopomer distribution of glutamate according to the reaction employed to enter pyruvate into the mitochondria. **B.** Mass isotopomer distribution of C2-C5 and C2-C4 glutamate fragments. Cells were cultured as described in Figure 5.2.2

.../...

(Figure 5.2.3.A). [2,3-$^{13}C_2$]-pyruvate can enter into the TCA cycle via PDH, yielding a molecule of [1,2-^{13}C]-acetylCoA, or via PC, producing a molecule of [2,3-$^{13}C_2$]-oxaloacetate. The usage of these two reactions can be assessed by mass isotopomer distribution analysis of the glutamate molecule fragments C2-C5 and C2-C4 as described in *Section 4.11.2*. Thus, we observed an increase in m1 and m2 labeled C2-C5 and C2-C4 glutamate fragments in BJ-HRasV12 cells, indicating that these cells retained more label from glucose in glutamate than BJ cells (Figure 5.2.3.B). Nevertheless, no differences were found in the relative contribution of PDH and PC to glucose-derived carbons entrance into the mitochondria, being the former the main entrance pathway in both cell lines (Figure 5.2.3.C).

Furthermore, mass isotopomer distribution of other TCA cycle intermediates such as citrate, malate, fumarate and α-ketoglutarate were analyzed. In general, we observed that a greater extent of glucose-derived carbons is routed into the mitochondria in BJ-HRasV12 cells compared with BJ cells (Figure 5.2.4). The main differences were found in m2 labeling, which was clearly higher in the mutated cells in all the analyzed metabolites. Additionally, also m1, m3 and m4 labeling were significantly increased in BJ-HRasV12 cells, suggesting a more intense mitochondrial activity in these cells.

5.2.2.3.4 H-RAS oncogenic activation induces an increase of glutamine-derived carbons in the TCA cycle

Although a significant part of the glucose is routed into the mitochondria, glutamine is the main substrate employed in the mitochondrial metabolism. In order to understand how H-RAS alters mitochondrial and glutamine metabolism, we cultured cells in the presence of 100% [U-^{13}C]-glutamine. Glutamine is transformed in glutamate and subsequently deaminated to α-ketoglutarate, which is decarboxilated to fumarate in a process named oxidative glutamine metabolism (Figure 5.2.5.A black arrows). Then,

.../...
and media after 24h was used for glutamate mass isotopomer distribution analysis. Glutamate molecules were fragmented by EI ionization yielding C2-C5 and C2-C4 fragments. **C.** Relative contribution of PDH and PC to pyruvate entry into TCA cycle.C2-C5 and C2-C4 glutamate fragments mass isotopomer distribution for 24h was employed in the calculations, performed as described in *Section 4.13.2*. In all cases, bars represent mean ± SD of n=3. Significant differences in comparison with BJ cells were assessed by two-tailed Student's *t*-test. * $p<0.05$, ** $p<0.01$.

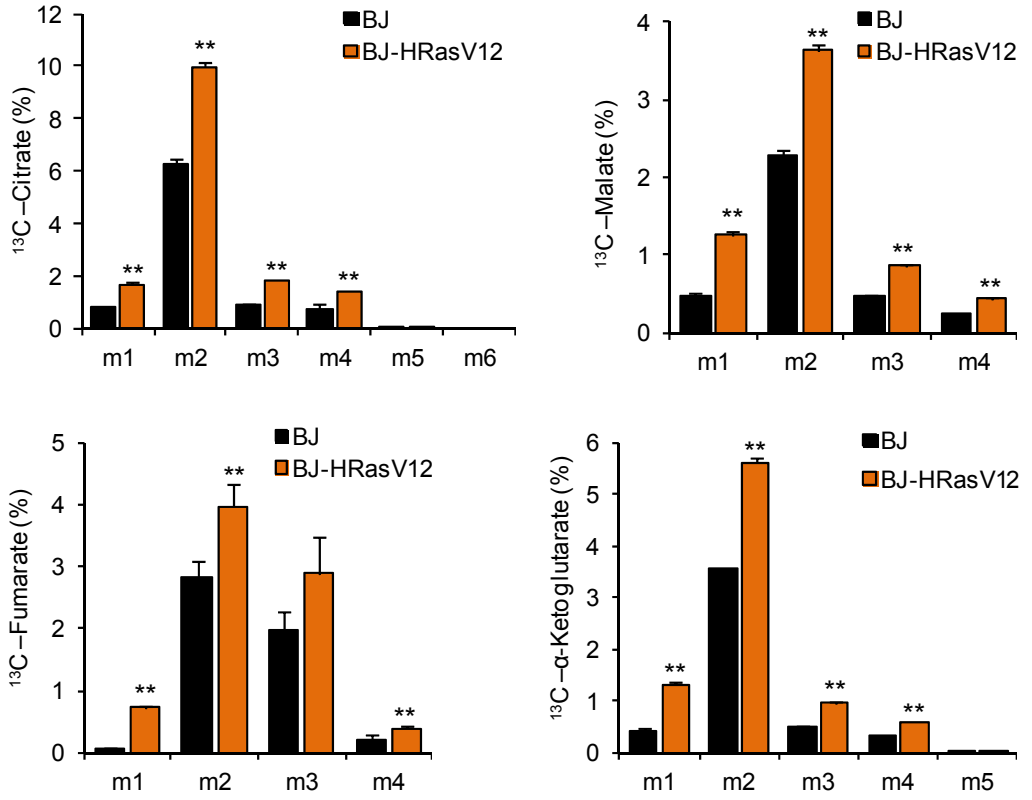

Figure 5.2.4. Glucose-derived carbons utilization in the TCA cycle

TCA cycle intermediates mass isotopomer distribution after 24h of culture in the presence of 50% [1,2-$^{13}C_2$]-glucose. Bars represent mean ± SD of n=3. Significant differences compared with BJ cells were assessed by two-tailed Student's *t*-test .* p<0.05, **p<0.01.

glutamine generates m4 labeled TCA cycle intermediates in the first turn (Figure 5.2.5.A, black molecules) and m2 labeled intermediates in the second turn (Figure 5.2.5.A, blue molecules). Alternatively, α-ketoglutarate can be carboxilated to isocitrate which is subsequently transformed to citrate in a process described as a glutamine reductive carboxilation (Figure 5.2.5.A red arrows and molecules). This process is characterized by the generation of m5 citrate and m3 labeled TCA cycle intermediates, such as malate, fumarate and α-ketoglutarate. As it is shown in Figure 5.2.5.B, we measured a robust and significant increase in m4 citrate, malate and fumarate, demonstrating an activated glutaminolysis in BJ-HRasV12 cells. Also, m5 and m3 citrate were incremented,

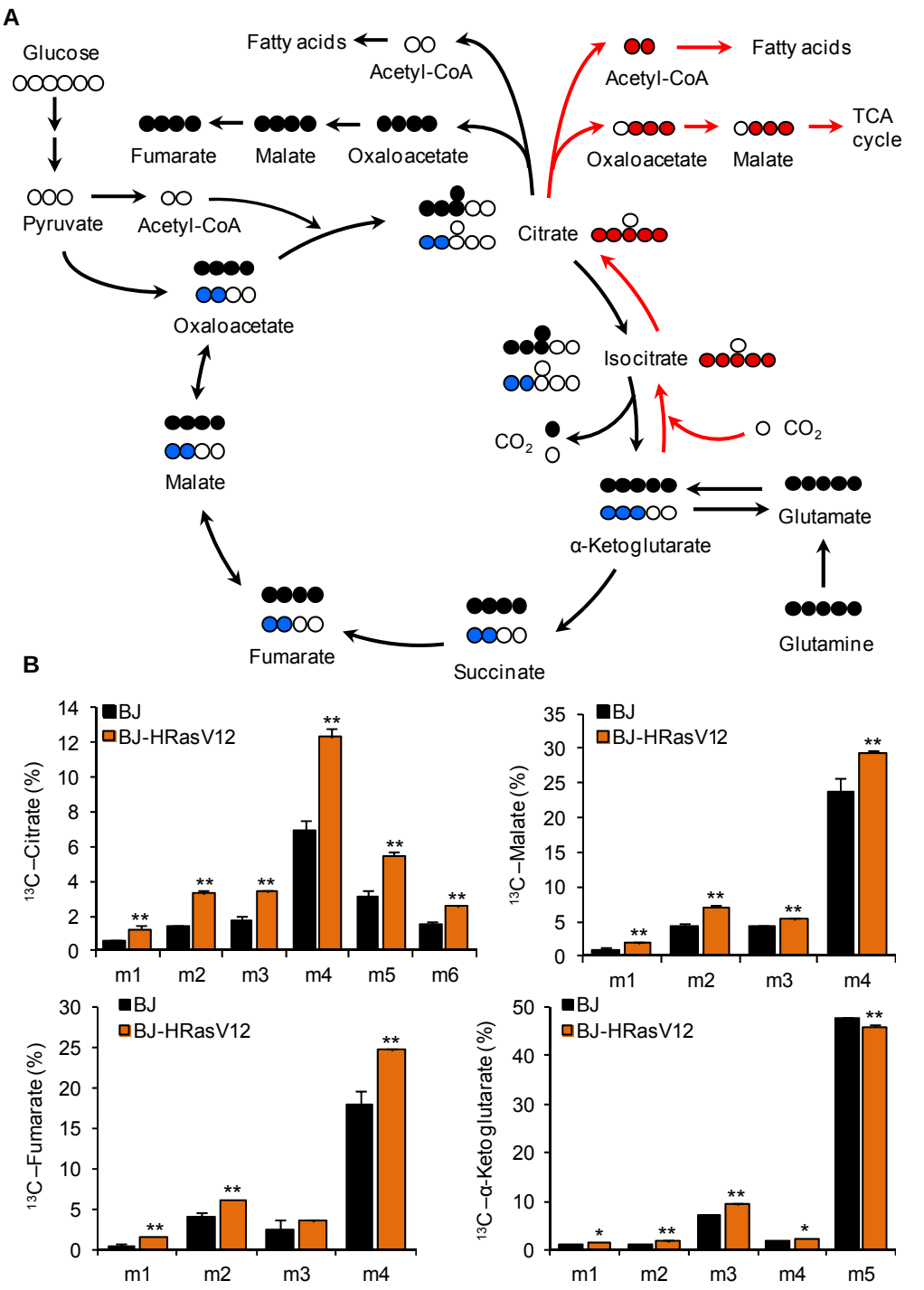

Figure 5.2.5. Glutamine-derived carbons utilization in the TCA cycle

A. Carbon atom transition map using [U-^{13}C]-glutamine as tracer. Oxidative (black molecules represent first round and blue molecules second round) and reductive (red molecules) glutamine metabolism are represented.

suggesting an enhanced glutamine reductive metabolism. In order to know if H-RAS induces changes in the relative use of the oxidative and reductive glutamine metabolism, the relative contribution of glutamine to citrate synthesis via oxidative or reductive metabolism was estimated by calculating m4/m5 citrate ratio. No differences were found in this ratio, which was 2.21 ± 0.06 and 2.25 ± 0.01 for BJ and BJ-HRasV12 cells, suggesting that H-RAS oncogenic activation enhances both reductive and oxidative glutamine metabolism.

5.2.2.4 BJ-HRasV12 cells show an enhanced mitochondrial metabolism and oxygen consumption

TCA cycle reactions are coupled to electron transport chain where oxygen is consumed. Thus, oxygen consumption measurement is a very reliable assay to explore the performance of mitochondrial metabolism. Keeping on searching the metabolic consequences of H-RAS oncogenic activation on glucose and glutamine metabolism, we determined the oxygen consumption rate (OCR) in BJ and BJ-HRasV12 cells in the presence of basal media (non-supplemented DMEM) or in the presence of media supplemented exclusively with glucose (10 mM) or glutamine (2 mM). We also used the complex-I inhibitor rotenone and complex-V inhibitor oligomycin to calculate the portion of oxygen consumed in the mitochondria and the portion of oxygen consumed associated to ATP production respectively (see *Section 4.9*). As shown in Figure 5.2.6.A we found that BJ-HRasV12 cells displayed an increased basal mitochondrial OCR either in basal media or in the presence of glutamine compared with BJ cells, indicating that the oncogenic activation of H-RAS conferred to BJ cells an increased capability of mitochondrial substrate oxidation. Additionally, this increase in oxidation of glutamine was found to be coupled to ATP production (Figure 5.2.6.B), indicating that this substrate represents a more important energetic source in BJ-HRasV12 cells. On the

Note that m3 labeled malate can be reintroduced into TCA cycle producing m3 labeled oxaloacetate, citrate and isocitrate and m2 labeled α-ketoglutarate, succinate and fumarate **B.** TCA cycle intermediates mass isotopomer distribution after 8 h of incubation with [U-^{13}C]-glutamine. Bars represent mean ± SD of n=3. Significant differences compared with BJ cells were assessed by two-tailed Student's *t*-test.* $p<0.05$, **$p<0.01$.

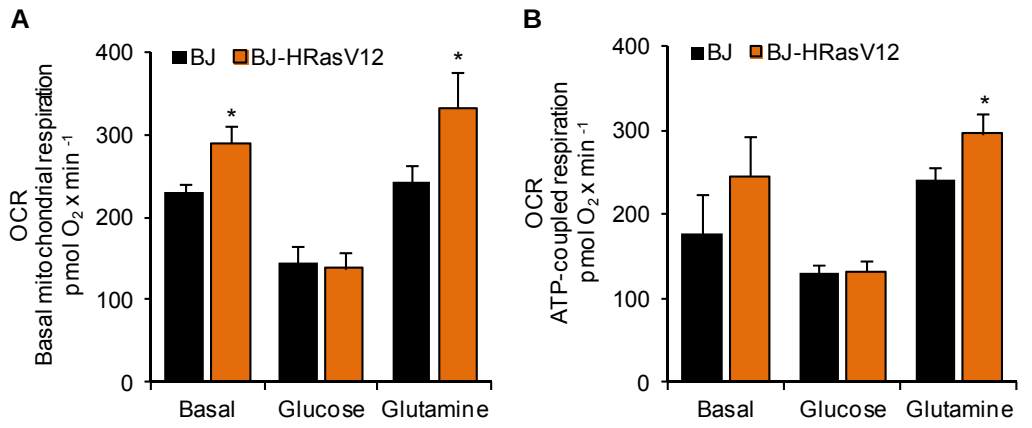

Figure 5.2.6 Oxygen consumption rate of BJ and BJ-HRasV12 cells

Oxygen consumption rate (OCR) was determined by Seahorse XF24 Extracellular Flux Analyzer instrument. $4x10^4$ cells/well were seeded in XF24 plates and, after 24h, media was replaced by non-buffered media supplemented with the indicted carbon sources prior to OCR determination. Basal media corresponds to non-supplemented DMEM. **A.** Basal mitochondrial respiration. It was determined by registering total oxygen consumption and subtracting the remaining portion of oxygen consumption after addition of complex-I inhibitor rotenone, as described in *Section 4.9.* **B.** ATP-coupled respiration. It was determined by registering total oxygen consumption and subtracting the remaining portion of oxygen consumption after addition of complex-V inhibitor oligomycin, as described in Section 4.9. Bars represent mean ± SD of n=3 independent experiments. Significant differences compared with BJ cells were assessed by two-tailed Student's *t*-test.* $p<0.05$, **$p<0.01$.

contrary, no differences between BJ and BJ-HRasV12 cells were detected in the OCR in the presence of glucose. Notably, OCR decreased in both cell lines in this condition, compared with assays performed in the presence of basal-media or glutamine, suggesting that mitochondrial metabolism is downregulated in the presence of glucose.

5.2.2.5 H-RAS oncogenic activation promotes lipogenesis

Mitochondrial metabolism is a source of precursors for synthesis of macromolecules such as lipids. Given the detected activation of mitochondrial metabolism, we explored the metabolic status of lipogenesis. Citrate can be exported to the cytoplasm and cleaved by ACLY to oxaloacetate and acetyl-CoA, which in turn is used for lipid synthesis. Palmitate is the first fatty acid synthesized in lipogenesis. Then, in order to examine the status of lipogenesis, we analyzed the mass isotopomer distribution of

palmitate in BJ and BJ-HRasV12 cells cultured in the presence of [1,2-$^{13}C_2$]-glucose or [U-^{13}C]-glutamine (Figure 5.2.7.A-B). A notable increase in m2 and m4 labeled palmitate was found in BJ-HRasV12 cells compared with BJ cells when they were cultured with [1,2-$^{13}C_2$]-glucose for 8h (Figure 5.2.7.A). Likewise, a parallel increase was also found when cells were cultured with [U-^{13}C]-glutamine for 8h (Figure 5.2.7.B). These results suggest that a greater amount of glucose- and glutamine-derived carbons is routed into lipogenesis in BJ-HRasV12 cells compared with BJ.

Next, we quantified the contribution of consumed glucose and glutamine to lipid synthesis in each cell line using the equations described in *Section 4.13.3*. Thus, our calculations showed that glucose contributed to lipid synthesis in a greater extent in BJ-HRasV12 cells than in BJ cells (Figure 5.2.7.C). Approximately, 35% of glucose was routed towards fatty acid synthesis in BJ cells, whereas it was around 42% in BJ-HRasV12 cells. On the contrary, although BJ-HRasV12 cells consumed a larger amount of glutamine, it contributed in a minor extent to lipid synthesis in these cells. BJ-HRasV12 cells routed into lipogenesis around 26% of the consumed glutamine, whereas this value was 33% in BJ cells. Hence, it suggests that part of the consumed glutamine has different fates in BJ-HRasV12 than in BJ cells.

In order to provide independent and parallel evidence for enhanced lipogenesis in BJ-HRasV12 cells and its importance in cell proliferation and viability, we cultured BJ and BJ-HRasV12 cells in the presence of 25 μM of C75 FAS inhibitor. An increased sensitivity of BJ-HRasV12 cells to lipogenesis impairment through FAS inhibition was observed, as shown in Figure 5.2.7.D, which is in consistence with the metabolic data, fully supporting an upregulation of lipogenesis in these cells. Taken together this data indicates that lipogenesis might play a pivotal role in H-RAS induced metabolic reprogramming.

5.2.3 Discussion

Our study provides an exhaustive characterization of the metabolic reprogramming induced by H-RAS oncogenic activation in BJ cells. Here, we have first shown that

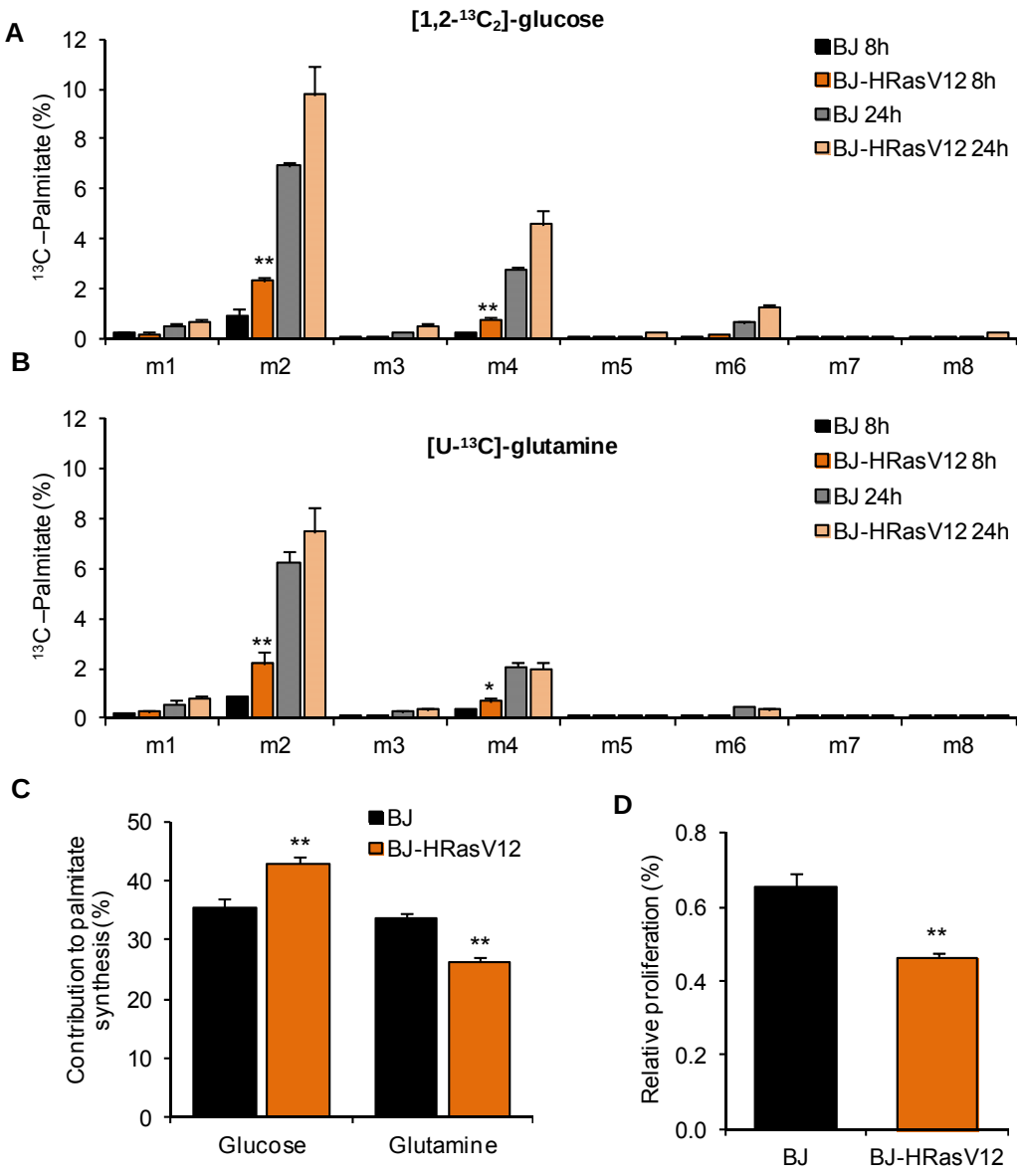

Figure 5.2.7. Fatty acid synthesis in BJ and BJ-HRasV12 cells

A-B. Mass isotopomer distribution of palmitate after incubation of cells with 50% [1,2-$^{13}C_2$]-glucose or [U-^{13}C]-glutamine over a period of 8 or 24h. **C.** Glucose and glutamine contribution to palmitate synthesis. These ratios were calculated as described in *Section 4.13.3* using data from 8h incubation. **D.** Cell viability in the presence of 25 μM of the fatty acid synthase (FAS) inhibitor C75. 1500 cells/p96 well were seeded and after 24h media was replaced by media containing increasing concentrations of the inhibitor. After 24h of incubation, cell viability was determined by MTT assay as described in *Section 4.2*. Results for each cell line were normalized to the absorbance of the corresponding cell line cultured in complete media. In all cases, bars represent mean ± SD of n=3. Significant differences compared with BJ cells were assessed by two-tailed Student's *t*-test.* $p<0.05$, **$p<0.01$.

H-RAS oncogenic activation promoted an increase in glucose consumption and glycolytic flux. This finding is in agreement with previous reports describing that Rat1 fibroblasts transformed with H-RAS (Chen et al., 2001) and overexpression of mutated N-RAS in 3T3-L1 mouse fibroblasts (Kozma et al., 1993) increase glucose uptake by upregulating glucose transporters. Additionally, K-RAS has also been demonstrated to upregulate glycolytic flux in inducible Kras(G12D)-driven pancreatic adenocarcinoma mouse model (Ying et al., 2012). One of the described mechanisms of action leading to this upregulation is by increasing the expression of the FB3 isoform of the enzyme PFK/FBPase (PFKFB3), producing high levels F26BP, the allosteric activator of PFK1, and subsequently increasing the glycolytic flux (Clem et al., 2008; Telang et al., 2006; Yalcin et al., 2009). Furthermore, different RAS isoforms also activate HIF1α expression, which in turn upregulates the expression of many glycolytic enzymes and promotes glucose shunt towards lactate by negatively regulating PDH flux, increasing then lactate secretion (Blum et al., 2005; Chun et al., 2010). Despite in the present work the levels of F26BP and HIF1α have not been tested, these two potential mechanisms are perfectly suitable to explain our results.

Moreover, our results indicated that BJ-HRasV12 cells display an activation of the PPP. This is fully supported by the increase in lactate produced from glucose via PPP, the percentage of m1 and m2 labeled ribose, and G6PD and TKT specific enzyme activities. Similar results have been reported in NIH3T3 mouse fibroblasts transfected with a mutated copy of K-RAS oncogene (de Atauri et al., 2011; Vizan et al., 2005). The observed increase in the use of oxidative branch of the PPP well might be intended to redox homeostasis maintenance. It has been documented that H-RAS and K-RAS oncogenic activation induce an increment in ROS levels (Dolado et al., 2007) (Hu et al., 2012) and the activation of the oxidative branch of the PPP might represent a compensatory mechanism activated in order to deal with oxidative stress (Recktenwald et al., 2008; Young et al., 2004). Additionally, the activation of the oxidative branch of the PPP provides cells with NADPH required for lipogenesis, which, as shown here, is also enhanced in BJ-HRasV12 cells. With regard to the nonoxidative branch, K-RAS has also been described to activate this branch of the PPP for ribose biosynthesis in pancreatic adenocarcinoma cancer cells (Ying et al., 2012). Thus, it seems that RAS

exerts a variety of effects on PPP, all of them converging in the partial or complete upregulation of this pathway.

BJ-HRasV12 cells also exhibited increased consumption of glutamine. The high dependence of K-RAS mutated cells on glutamine for proliferation and tumorigenicity has been highlighted previously in distinct cell models (Gaglio et al., 2009; Son et al., 2013; Weinberg et al., 2010). As mentioned above, taking into account the activation of HIF1α by RAS, it might be supposed that RAS induces a pseudohypoxic status. In hypoxia, it has been described that K-RAS mutated cell line H460 shows increased glutamine consumption compared with cells cultured in non-hypoxic conditions, suggesting that HIF1α activation can enhance glutamine consumption and might explain the observed phenotype (Metallo et al., 2012).

The increase in glucose and glutamine consumption in BJ-HRasV12 cells resulted in increased ^{13}C labeling in most of the metabolic intermediates analyzed, suggesting an increased flux from glucose and from glutamine to metabolic intermediates in BJ-HRasV12 compared with BJ cells. However, an integrative approach based on ^{13}C metabolic flux analysis (^{13}C-MFA) is still required to unmistakably determine increments or decrements in intracellular fluxes. Uptake of the different extracellular metabolites and mass isotopomer distribution of the intracellular ones must be combined, using computational approaches, to solidly reach this kind of conclusions.

Although BJ-HRasV12 cells exhibited greater ^{13}C labeling in most of the analyzed TCA cycle intermediates when cells were cultured in the presence ^{13}C substrates, only glutamine was proven to increase mitochondrial respiration. Despite the increase of glucose-derived carbons in the mitochondria in BJ-HRasV12 cells observed using [1,2-$^{13}C_2$]-glucose, no differences compared with BJ cells were detected in OCR in the presence of this substrate. On the contrary, the increase in glutamine-derived carbons in the mitochondria in BJ-HRasV12 cells paralleled the increase in OCR in the presence of this substrate. A more intense mitochondrial activity in both human HRas-mutated cells and KRas-mutated mouse model has been previously reported (Telang et al., 2007; Weinberg et al., 2010) and it has been suggested that mitochondrial activity is required for KRas-mediated tumorigenicity because it is the main source of ROS, which are

essential for this process (Weinberg et al., 2010). However, the role of RAS on mitochondrial metabolism still remains unclear. Coversely, it has been reported that activation of K-Ras(G12V) in human cells causes mitochondrial dysfunction, leading to decreased respiration, elevated glycolysis, and increased generation of ROS (Hu et al., 2012). Also, in mouse NIH3T3 fibroblasts transformed with H-Ras(Q61L) mitochondrial respiration was found to be suppressed (Yang et al., 2010). Taken together, this body of evidence suggests that the action of RAS on mitochondrial metabolism is very dependent on the cell system under study and the experimental techniques and conditions used. Differences between cell models (rodent or human), RAS isoforms (H-RAS or K-RAS), the presence of different metabolic substrates in the experiments (single carbon substrates vs. multiple carbon substrates) or the experimental procedures to reach conclusions on mitochondrial metabolism (OCR, TCA cycle labeled intermediates, glutamine consumption or ROS generation) might explain the differences found in the role of RAS in mitochondrial metabolism (Bellavia et al., 2012; Hamad et al., 2002; Santillo et al., 2001). Here, our study provides a complete and reliable picture of the effects of H-RAS oncogenic activation on mitochondrial metabolism, since we have carried out a comprehensive and integrative approach using human BJ cells transformed with genetically defined elements and combining several techniques that support our conclusions.

Mitochondrial metabolism is the main source of precursors required for lipid synthesis. According to the increase of ^{13}C labeling in TCA cycle intermediates, a subsequent increase of ^{13}C-palmitate was found when BJ-HRasV12 cells were cultured with both [1,2-$^{13}C_2$]-glucose or [U-^{13}C]-glutamine. Some previous evidences support an increased lipogenesis in HRas-mutated cells mediated by the action of PI3K pathway (Yang et al., 2002), which exerts part of the RAS effects on metabolism are mediated by PI3K/AKT pathway (Pylayeva-Gupta et al., 2011). This pathway induces the expression of SREBPs, which in turn enhances the expression of many lipogenic enzymes, providing a suitable mechanistic explanation for the increased lipogenesis observed in BJ-HRasV12 cells (Porstmann et al., 2005). Likewise, the inhibition of some components of this pathway has been proposed as potential therapeutic approach in RAS-mutated cells (Yang et al., 2002) and other tumors with mutations in the RAS downstream effectors PI3K or AKT

(Bauer et al., 2005; Hatzivassiliou et al., 2005). This fact is also fully supported by our results. As shown here, FAS inhibition using C75 inhibitor preferentially inhibited BJ-HRasV12 cells growth, indicating that H-RAS oncogenic activation renders cells more dependent on lipogenesis and suggesting that BJ-HRasV12 cells have an unavoidable increased requirement of lipids.

Interestingly, the portion of glucose and glutamine dedicated to lipid synthesis was different in BJ-HRasV12 in comparison with BJ cells. BJ-HRasV12 used proportionally more glucose for synthesis of palmitate. Conversely, BJ-HRasV12 cells, despite consuming more glutamine, routed less amount of this aminoacid into palmitate synthesis, suggesting that glutamine might have other fates in these cells. Recently it has been described that KRas-mutated pancreatic cancer cells metabolize glutamine through an alternative pathway in which glutamine-derived aspartate is converted into oxaloacetate which in turn is transformed into malate and then pyruvate through ME, increasing the NADPH/NADP ratio (Son et al., 2013). The existence of this metabolic route would allow KRas-mutated cells to obtain NADPH for lipid synthesis and also for maintenance of redox homeostasis under high ROS levels conditions, such as those described to exist when RAS is mutated. Thus, the activation of this pathway might offer an explanation about the decreased contribution of glutamine to palmitate synthesis despite being this aminoacid more largely consumed in BJ-HRasV12 cells.

In summary, H-RAS oncogenic activation reprograms glucose and glutamine metabolism by enhancing glycolytic and PPP fluxes as well as mitochondrial metabolism. Although both glucose- and glutamine-derived carbons are routed into the mitochondria in a greater extent in BJ-HRasV12 cells, glutamine is the main responsible for sustaining the activated mitochondrial metabolism in these cells, while glucose-derived carbons in the mitochondria are primarily used to fuel lipogenesis. In this sense, lipogenesis is overactivated in BJ-HRasV12 cells, which are more reliant on this pathway and more sensitive to FAS inhibition than BJ cells.

Chapter 5.3

The Role of G6PD in Colon Cancer Cell Line HT29 and its Regulation by Glutamine Availability and Proliferation Signaling Pathways

5.3.1 Brief Introduction and Scope

In the previous chapters we found that G6PD enzyme is upregulated in *RAS*-mutated cell lines. Also, additional unpublished observations of our group in tissue samples of colon cancer tumors demonstrated an imbalance of the PPP in favor of the oxidative PPP branch, controlled by the key enzyme G6PD. RAS signaling pathway is frequently mutated in colon cancer tumors, being mutations in RAS and BRAF genes among the most common (Phipps et al., 2013; Pylayeva-Gupta et al., 2011; Yokota et al., 2011). Herein, we sought to explore the role of G6PD in RAS pathway-activated cell lines, such as colon cancer cells, to study the potentiality of the oxidative branch of PPP as therapeutic intervention point in cells with activated RAS pathway. To achieve this goal, i) G6PD specific enzyme activity was determined in a panel of colon cancer cell lines displaying different status of the RAS signaling pathway, ii) G6PD was inhibited in the cell line that displayed the highest G6PD activity and the effect on proliferation and cell cycle was studied and, iii) regulation of G6PD by glutamine metabolism was studied in order to understand some of the processes observed.

5.3.2 Results

5.3.2.1 G6PD is overexpressed in RAS- and BRAF-mutated colon cancer cells

In order to explore the relation between RAS signaling pathway activation and G6PD activity, we examined the G6PD status in a panel of colon cancer cell lines consisted of four RAS pathway-activated cell lines (HT29, SW480, SW620 and HCT116) and one with no RAS pathway activation (Caco-2) in comparison with the normal colonocites cell line NCM460. The results shown in Figure 5.3.1.A clearly corroborated the relation between RAS pathway status and G6PD activity. While SW480 SW620, and HCT116 cells harbor mutations in *K-RAS* gene (Kobunai et al., 2010; Simi et al., 2008), HT29 cell line does not carry mutations in RAS gene (Ikediobi et al., 2006; Janakiraman et al., 2010), but mutation V600E in the RAS downstream effector *BRAF* is well documented in this cell line (Ikediobi et al., 2006; Loh et al., 2008; Oliveira et al., 2003; Tan et al., 2008). Thus, RAS pathway-activated cells displayed 1.5- to 2.6-fold increase in G6PD activity in comparison with NCM460 cell line. On the contrary, no activating mutations in RAS signaling pathway have been described in Caco-2 cells (Jarry et al., 2004).

As HT29 cell line displayed the highest G6PD activity among the cell lines examined and considering that *BRAF(V600E)* is one of the most well-documented mutations described in this cell line, we wondered if G6PD was effectively being regulated by BRAF. Then, HT29 cells were cultured in the presence of the highly selective BRAF inhibitor PLX4720 (Tsai et al., 2008) and G6PD expression and specific enzyme activity were examined. As shown in Figure 5.3.1.B-C, a prominent decrease in G6PD expression after 48 hour of incubation in the presence of the inhibitor was detected. In accordance to that, after 72 hours a decrease in G6PD activity was observed. These results indicate that the RAS downstream effector BRAF is also involved in the regulation of G6PD.

Although no mutations in RAS gene have been described in HT29 cells (Ikediobi et al., 2006), once confirmed the functional relation between BRAF and G6PD and given the high G6PD activity detected in HT29, we found interesting to study the role of this enzyme in these cells in greater detail. This decision was also based on two previous findings. On the one hand, HT29 cells synthesize around 70% of RNA ribose through

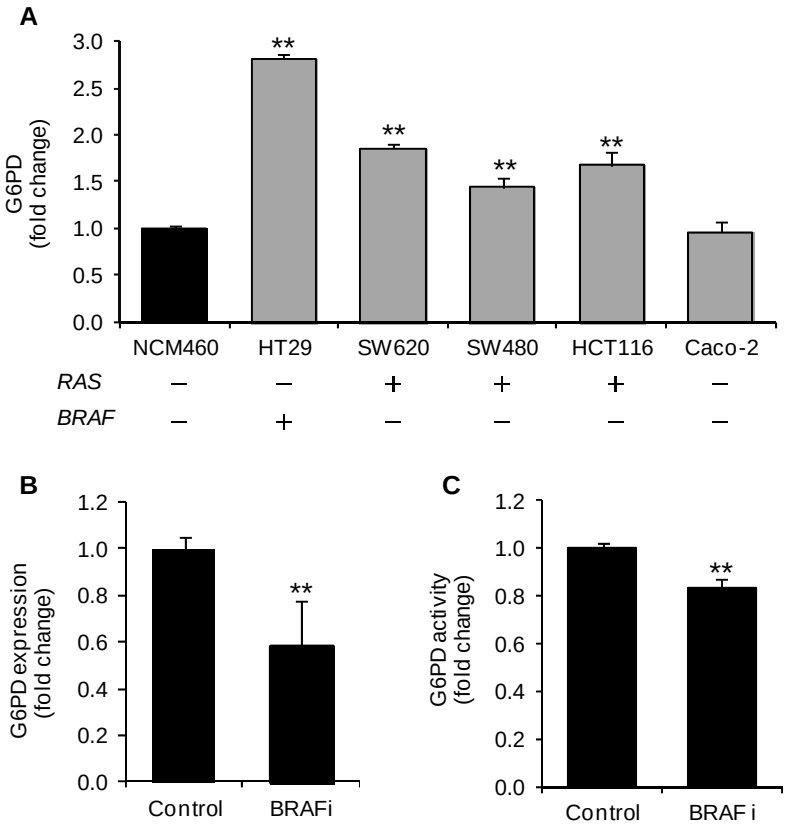

Figure 5.3.1 G6PD state in colon cancer cell lines and BRAF-mediated G6PD regulation

A. G6PD specific activity in a panel of colon cancer cell lines. Results are expressed as percentage of G6PD activity with respect to normal colonocites cell line NCM460. The presence (+) or absence (-) of mutation in *RAS* or *BRAF* genes is indicated below the plot. B-C. G6PD expression (B) and specific activities (C) in HT29 cell line after incubation with 10 μM of BRAF inhibitor PLX4720 (BRAFi) for 48 and 72 hours respectively. Results are expressed as fold change with respect to control. Bars represent mean ± SD of n=2 in A and C and n=5 in B. Significant differences compared with NCM460 in A and with control condition in B and C were assessed by two-tailed Student's *t*-test. * $p<0.05$, ** $p<0.01$.

the oxidative branch of the PPP (Alcarraz-Vizan et al., 2010). Likewise, unpublished data from our group has demonstrated an increment of the oxidative/nonoxidative ratio branch of PPP in HT29 cancer cells compared with the colonocytes cell line NCM460. Taken together, this body of evidence suggested that HT29 could be a good cell model to explore the role of G6PD in proliferation and survival in RAS pathway-activated colon cancer cells.

5.3.2.2 G6PD inhibition does not affect proliferation of BRAF-mutated cell line HT29

In order to test the dependence of HT29 cells on G6PD to proliferate, we inhibited this enzyme by means of interference RNA. Figure 5.3.2.A-C shows the strong inhibition of G6PD achieved at RNA, activity and protein levels in cells transfected with siRNA pool against G6PD (siG6PD cells) in comparison with cells transfected with a non-targeting siRNA pool (siNEG cells). Next, the effect of G6PD inhibition on proliferation was assessed. However, no differences in proliferation and viability (data not shown) were found between siNEG and siG6PD cells (Figure 5.3.2.D).

G6PD has also been described to be modulated along cell cycle progression, being its activity increased during late G1 and S phase. This suggests that it might play an essential role on cell cycle progression. Accordingly, the effect of G6PD inhibition on cell cycle was examined. As it was found in proliferation, no changes were detected in cell cycle phase distribution between siNEG and siG6PD cells (Figure 5.3.2.E).

G6PD plays a pivotal role in synthesis of macromolecules and maintenance of the reduced pool of glutathione for ROS counteraction. ROS is produced in many different physiological conditions, such as hypoxia (Chandel et al., 1998; Cheung et al., 2012; Rouschop et al., 2013). Then we hypothesized that G6PD might play a more essential role under conditions of high oxidative stress. To test this hypothesis, HT29 cells were transfected with siRNA pool against G6PD or non-targeting siRNA pool and cultured for 72h. At that point, hypoxia was induced by shifting transfected cells to 1% O_2 culture conditions for 72h more. On the contrary to what we expected, no significant differences were found in proliferation between siNEG and siG6PD cells (data not shown).

5.3.2.3 Glutamine availability regulates G6PD expression and activity

The oxidative branch of PPP provides the cell with NADPH required for many biosynthetic processes as well as for ROS homeostasis. However, other sources of NADPH exist in the cell, such as ME or IDH. These sources are primarily fueled with

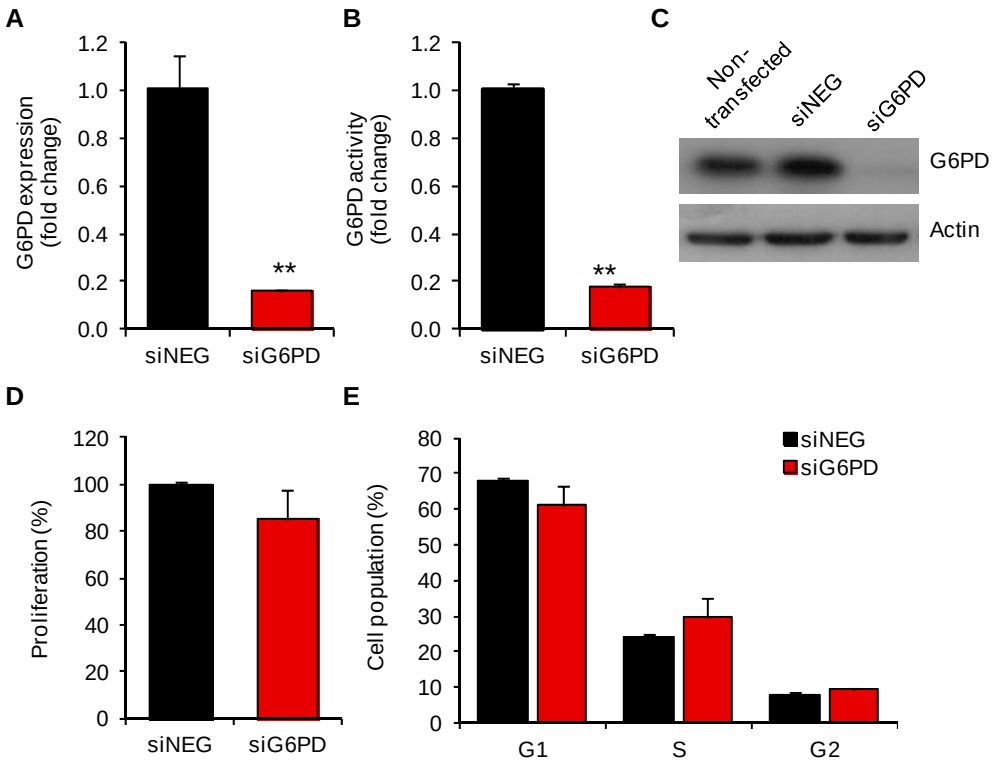

Figure 5.3.2 Role of G6PD in HT29 cell proliferation and cell cycle progression

A. G6PD expression 72 hours after transfection of siRNA targeting G6PD (siG6PD) or non-targeting siRNA (siNEG). **B-C.** G6PD specific activity (B) and protein levels (C) at 96 hours after transfection. Specific activity is expressed as fold change with respect to siNEG cells **D.** Effect of G6PD knockdown on cell proliferation. It was determined by cell counting through flow citometry at 144 hours after transfection. **E.** Cell cycle phase distribution 96 hours after transfection. In all cases, bars represent mean ± SD of n=3. Significant differences compared with siNEG were assessed by two-tailed Student's *t*-test. * $p<0.05$, ** $p<0.01$.

carbons coming from glutamine. In fact, it has been demonstrated in KRAS-driven pancreatic cancer cells that glutamine serves as a primary substrate for a set of reactions involving ME that lead to an increased NADPH/NADP ratio (Son et al., 2013). These results suggest that these glutamine-dependent reactions might be replacing the role of G6PD in NADPH production. As a consequence, G6PD might play an additional and more important role under glutamine-deprived conditions. Then, we studied the effects of G6PD knockdown under glutamine-deprived cell culture conditions. Our results showed that HT29 cell line was very dependent on glutamine for proliferation, but no significant differences between siNEG and siG6PD cells were found (Figure 5.3.3).

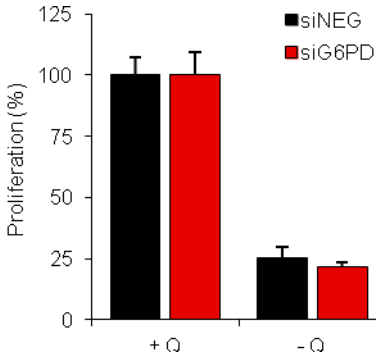

Figure 5.3.3 Role of G6PD in HT29 cell proliferation in the presence or absence of glutamine

The dependence of HT29 cell proliferation on G6PD under glutamine starvation was evaluated by replacing media by either complete media containing 2 mM glutamine (+Q) or glutamine-free media (-Q) at 72 hours after transfection of siRNA targeting G6PD (siG6PD) or non-targeting siRNA (siNEG). After 72 hours, cell number was determined by flow citometry and results are expressed as percentage with respect to +Q condition for each transfectant. Bars represent mean ± SD of n=3.

Throughout the experiments performed in the absence of glutamine, we detected that G6PD was overexpressed after 48h of glutamine withdrawal in non-transfected HT29 cells compared with cells cultured in complete media (Figure 5.3.4.A). In accordance, an increase in G6PD activity was also detected after 96h of glutamine deprivation (Figure 5.3.4.B). These results evidence a metabolic relation between G6PD and glutamine metabolism in this cell line.

5.3.2.4 G6PD regulation by glutamine availability involves NRF2 activation

In light of the glutamine-mediated regulation of G6PD, we wanted to know the potential mechanism that coordinates this process. It has been described that RAS pathway-activated cells display an enhanced levels of the transcription factor NRF2 (DeNicola et al., 2011). Furthermore, G6PD has been reported to be regulated by this transcription factor (Mitsuishi et al., 2012b) which in turn, is regulated by its inhibitor KEAP1. Under normal conditions, NRF2 is constantly ubiquitinated through KEAP1 and degraded in the proteasome (see Figure 1.7 in *Section 2.2.3*) Following exposure to oxidative stress, KEAP1 is inactivated and releases NRF2, which migrates into the nucleus and activates an antioxidant response program that involves several PPP genes (Mitsuishi et al., 2012a). Besides, glutamine deprivation has been correlated with an increase in ROS production (Son et al., 2013). Taken together, we reasoned that glutamine deprivation well might trigger a broad genetic program initiated by an increase in ROS intracellular levels and mediated by NRF2.

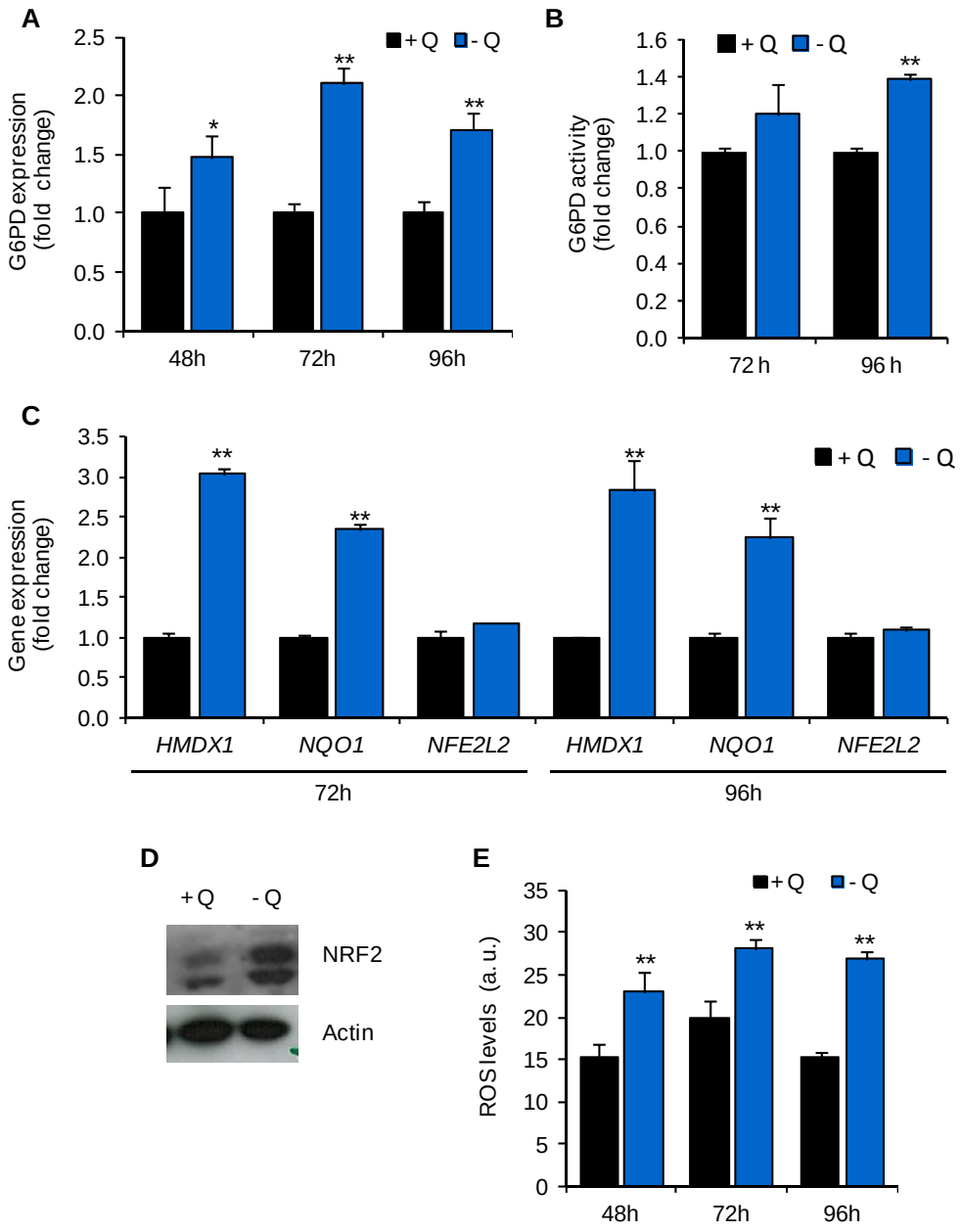

Figure 5.3.4 G6PD, NRF2-target genes and NRF2 levels under glutamine deprivation

HT29 cells were cultured for 48, 72 and 96h in complete media containing 2 mM glutamine (+Q) or glutamine-free media (-Q). **A.** G6PD expression. **B.** G6PD specific activity. **C.** Expression of the NRF2 target genes *HMDX1* and *NQO1*, and the NRF2-codifying gene *NFE2L2*. **D.** NRF2 protein levels in cells cultured in complete media (+Q) or glutamine-free media (-Q) for 24 hr **E.** ROS levels. In A, B and C values are expressed as fold change with respect to cells cultured in complete media. Bars represent mean ± SD of n=3. Significant differences compared with complete media condition were assessed by two-tailed Student's *t*-test. * p< 0.05 **p<0.01.

As a preliminary approach to explore NRF2 activation, we examined the status of some validated NRF2 target genes, such as *HMDX1* and *NQO1* (DeNicola et al., 2011; Mitsuishi et al., 2012b) and also the NRF2 codifying gene *NFE2L2* in HT29 cells cultured in complete media (+Q) or glutamine-free media (-Q) for 72 and 96h. Interestingly, in addition to G6PD, NRF2 target genes *HMDX1* and *NQO1* were also overexpressed in glutamine-free culture conditions, while *NFE2L2* was not (Figure 5.3.4.C). In order to verify that NRF2 was really activated, protein levels of this transcription factor were determined by western blotting. As shown in Figure 5.3.4.D, an increase in NRF2 protein levels was detected after culturing HT29 cells in glutamine-free media for 24h. It clearly indicates that glutamine deprivation activates a genetic response mediated by NRF2. Since KEAP1 release of NRF2 factor is produced after oxidation of KEAP1 cysteine residues under high ROS levels, we examined ROS levels after glutamine removal in order to provide a mechanistic explanation for NRF2 accumulation (Figure 5.3.4.E). Accordingly, a prominent increase in ROS levels was detected when cells were cultured without glutamine, suggesting that ROS production triggers NFR2 accumulation and the subsequent increase in NRF2-target genes expression.

5.3.3 Discussion

Here, we have shown that the levels of G6PD are associated to the genetic activation of RAS signaling pathway and regulated by glutamine availability. RAS proteins are involved in the transduction of proliferative signals from ligand-activated receptor to the nucleus. They activate a plethora of downstream effectors involved in many cellular processes (Pylayeva-Gupta et al., 2011), thereby existing several potential mechanisms to explain the relation between RAS signaling pathway and G6PD. Since BRAF is a downstream effector of RAS, here we assume that the oncogenic activation of BRAF and RAS result in a partially common metabolic phenotype.

G6PD expression and activity is controlled by, among others, the action of the transcription factor NRF2, which regulates G6PD promoter through its antioxidant response element (ARE) (Mitsuishi et al., 2012b). Recently, DeNicola and collaborators described the oncogene-induced NRF2 transcription in primary cells, tissues of mice

expressing K-Ras(G12D) and B-Raf(V619E), and in human pancreatic cancer (DeNicola et al., 2011). It promotes NRF2 overexpression and stabilization and the subsequent orchestration of a ROS detoxification program, involving G6PD upregulation. Thus, this mechanism provides a suitable explanation for the relation between G6PD and RAS signaling pathway.

NRF2 transcription factor is also activated in response to high ROS levels through the modification of the cysteine residues of its inhibitor KEAP1 (Mitsuishi et al., 2012b). In this regard, it has been documented that RAS signaling pathway activation via ectopic expression of different mutant isoforms of RAS leads to increased levels of oxidative stress (Chiaradonna et al., 2006; Maciag and Anderson, 2005), although some differences among RAS isoforms regarding effect of RAS on ROS levels have been detected (Santillo et al., 2001). Then, this increase in ROS levels might also trigger NRF2 activation and G6PD upregulation. Additional studies have also confirmed the relation between RAS signaling pathway and the oxidative branch of PPP (de Atauri et al., 2011; Vizan et al., 2005).

Furthermore, our results have shown that 80% inhibition of G6PD activity had no effect on cell proliferation and viability in BRAF-mutated HT29 cell line. G6PD plays an important role in redox homeostasis and anabolic metabolism. The absence of effect on cell proliferation and viability after G6PD inhibition may be explained on the basis of both physiological processes. In terms of redox homeostasis, HT29 has been described to express high levels of the CD44v protein, a variant of the cancer-stem-cell marker CD44 (Ishimoto et al., 2011). The high expression of this protein confers to the cell the capacity to maintain low levels of ROS by enhancing GSH synthesis and activating an antioxidant gene expression program involving ROS detoxification genes such as *GPX1*, *GPX2*, *PRDX1* and *PRDX2*. Consequently, G6PD may not be essential for redox homeostasis in cells expressing high levels of CD44v. In fact, not even in the challenging condition of glutamine withdrawal, in which there was a notable increase in ROS levels, we detected significant changes in proliferation when G6PD was inhibited. Regarding to the role of G6PD in anabolism, it is possible that cells circumvent the inhibition of G6PD by redirecting ribose synthesis flux through the nonoxidative branch of the PPP, which

would allow cells to obtain the required precursors for synthesis of macromolecules. In fact, it has been demonstrated in HT29 cell line that inhibition of TKT or G6PD enzymes with oxythiamine or dehydroepiandrosterone, respectively, leads to a compensatory response by enhancing ribose synthesis flux through the non-inhibited branch of PPP, highlighting the metabolic flexibility of this pathway (Ramos-Montoya et al., 2006). The role of the nonoxidative branch of the PPP in KRAS-mutated tumors has been also documented. In KRAS-mutated pancreatic tumors, ribose biogenesis is carried out by driving glycolysis intermediates via nonoxidative PPP and this pathway is essential for tumorigenic activity of pancreatic cancer cells (Ying et al., 2012). Similar results were found in additional studies in pancreatic cancer cells (Boros et al., 2005).

Another explanation for the absence of effect on HT29 cell proliferation and viability after G6PD inhibition lays on the role of P53. HT29 is a P53-deficient cell line that harbors the mutation P53(R273H). Wild-type P53 negatively regulates G6PD activity impairing active dimer formation by direct protein binding (Jiang et al., 2011). Although mutant P53(R273H) retains the capacity of binding to G6PD, it has lost the capacity of inhibiting G6PD activity (Jiang et al., 2011), what might result in a tremendously high G6PD activity in this cell line, as quantified here. In the presence of such a great amount of active G6PD enzyme, inhibition of enzyme activity around 80% by interference RNA might still left enough active G6PD as to maintain the oxidative PPP flux required for cell proliferation and survival. Accordingly, similar degree of G6PD inhibition in P53-proficient cell line HCT116, which displayed 50% of G6PD activity in comparison with HT29, led to a decrease of 30% in cell proliferation and survival (unpublished observations in our research group). In general, high G6PD activity leads to increased synthesis of the PPP metabolic intermediate 6-phosphogluconate (6PG), and this fact can be used to design a better approach for targeting PPP with therapeutic purposes. 6PG has been proposed as potential inhibitor of proliferation (Sukhatme and Chan, 2012) and its accumulation takes place when 6PGD enzyme is inhibited. As HT29 cell line has high levels of G6PD, it results in enhanced production of 6PG. Then, inhibition of 6PGD might result in a great accumulation of 6PG, which might lead to an inhibition of proliferation.

We have also demonstrated that glutamine withdrawal leads to an increase in ROS levels and subsequently to NRF2 stabilization. The increment in ROS levels in the absence of glutamine has been previously reported as consequence of the role of this aminoacid in fueling the mitochondrial reactions that convert aspartate into pyruvate (Son et al., 2013). These reactions involve the ME, a source of NADPH required for redox homeostasis. Nevertheless, the induction of NRF2 under this condition has not been studied before and may play a pivotal role in proliferation and survival under nutrient-limited conditions.

In summary, in this chapter we have demonstrated that G6PD is overactivated in colon cancer cells with oncogenic activation of the RAS signaling pathway. Nevertheless, G6PD seems to be dispensable for proliferation and survival in BRAF-mutated and P53-deficient HT29 colon cancer cell line. Interestingly, a new connection between PPP and glutamine metabolism has been unveiled, where G6PD is overexpressed in HT29 cells under glutamine-deprived conditions in a process that is accompanied with a concomitantly increase in ROS levels and NRF2 induction.

Chapter 5.4

The Pentose Phosphate Pathway as Potential Cancer Therapeutic Target and its Role in Tumor Metabolism in Breast Cancer Cell Line MCF7

5.4.1 Brief introduction and scope

In the previous chapter, we have inhibited G6PD in colon cancer cell line HT29 but no effects on cell proliferation and survival have been detected. Besides ribose synthesis, G6PD regulates ROS levels, and the balance between ROS production and removal has been demonstrated to be altered in some tumors and proposed as an attractive therapeutic target (Trachootham et al., 2009). An example of these tumors is the case of breast tumors, which display increased levels of ROS and a greater reliance on the ROS detoxification systems, which increases gradually as tumor progresses (Brown and Bicknell, 2001; Jerby et al., 2012; Kang, 2002; Portakal et al., 2000; Toyokuni et al., 1995). Since PPP is involved in ROS levels modulation, we tested the potential of the main enzymes of this pathway, G6PD and TKT, as therapeutic targets in the metastatic breast cancer cell model MCF7. Metastases of breast cancer display an increased expression of enzymes of the PPP such as G6PD and 6PGL (Chen et al., 2007). Additionally, advanced breast tumors display an increased need to detoxify ROS as demonstrated by the increased expression of the PPP enzymes detected in a genome-scale study based on the gene expression analysis of a large cohort of clinical samples (Jerby et al., 2012). Also, MCF7 cells have an increased expression of G6PD compared with the near-normal breast cancer cells MCF10 (Drabovich et al., 2012). Taken together, we reasoned that the PPP enzymes might be of potential therapeutic interest particularly in advanced breast cancer and we selected MCF7 cells, a cell model of metastatic breast cancer, to validate

this hypothesis. To this end i) G6PD and TKT were inhibited and its role in proliferation and survival was assessed, ii) the metabolic role of these enzymes was evaluated by performing a ^{13}C-assissted metabolomics experiment using [1,2-$^{13}C_2$]-glucose and iii) the metabolic relation between PPP and glutamine metabolism was explored to explain some of the results obtained.

5.4.2 Results

5.4.2.1 G6PD inhibition, but not TKT, decreases cell proliferation and survival

PPP has been hypothesized to play a critical role in tumor metabolism. In order to assess the dependence of MCF7 breast cancer cells on this pathway, we inhibited the main enzymes of PPP by means of siRNA targeted to TKT (siTKT) or G6PD (siG6PD). A non-targeting siRNA (siNEG) was used as a negative control in all experiments. As shown in Figures 5.4.1.A-B, both enzymes were effectively inhibited at mRNA level more than 75%, and specific enzyme activities were reduced around 50% at 96 hours after transfection in both cases.

PPP is an anabolic pathway that plays a fundamental role in cell growth. Then, we explored the role of TKT and G6PD in cell proliferation and survival. Notably, G6PD impairment reduced cell proliferation around 35%, while no effects were detected when TKT was inhibited (Figure 5.4.1.C, left). In accordance to that, G6PD knockdown resulted in a marked increase in cell death, as shown in Figure 5.4.1.C (right). Given that one of the essential roles of PPP is to provide cells with ribose for proliferation, we hypothesized that inhibition of these enzymes might influence on cell cycle progression. Cell cycle is classically divided into three different phases named G1, S and G2. G1 phase covers the period of time required for cell growth and macromolecules synthesis, such as DNA, lipids, etc, being this phase essential for a properly progression through the cell cycle and cell division. Accordingly, G6PD and TKT enzymes have been reported to be enhanced during late G1 and S phase and specific upregulation of the oxidative branch has been demonstrated (Vizan et al., 2009). Then, an arrest in G1 phase was expected when TKT and G6PD were inhibited. Effectively, a slight arrest in G1 phase

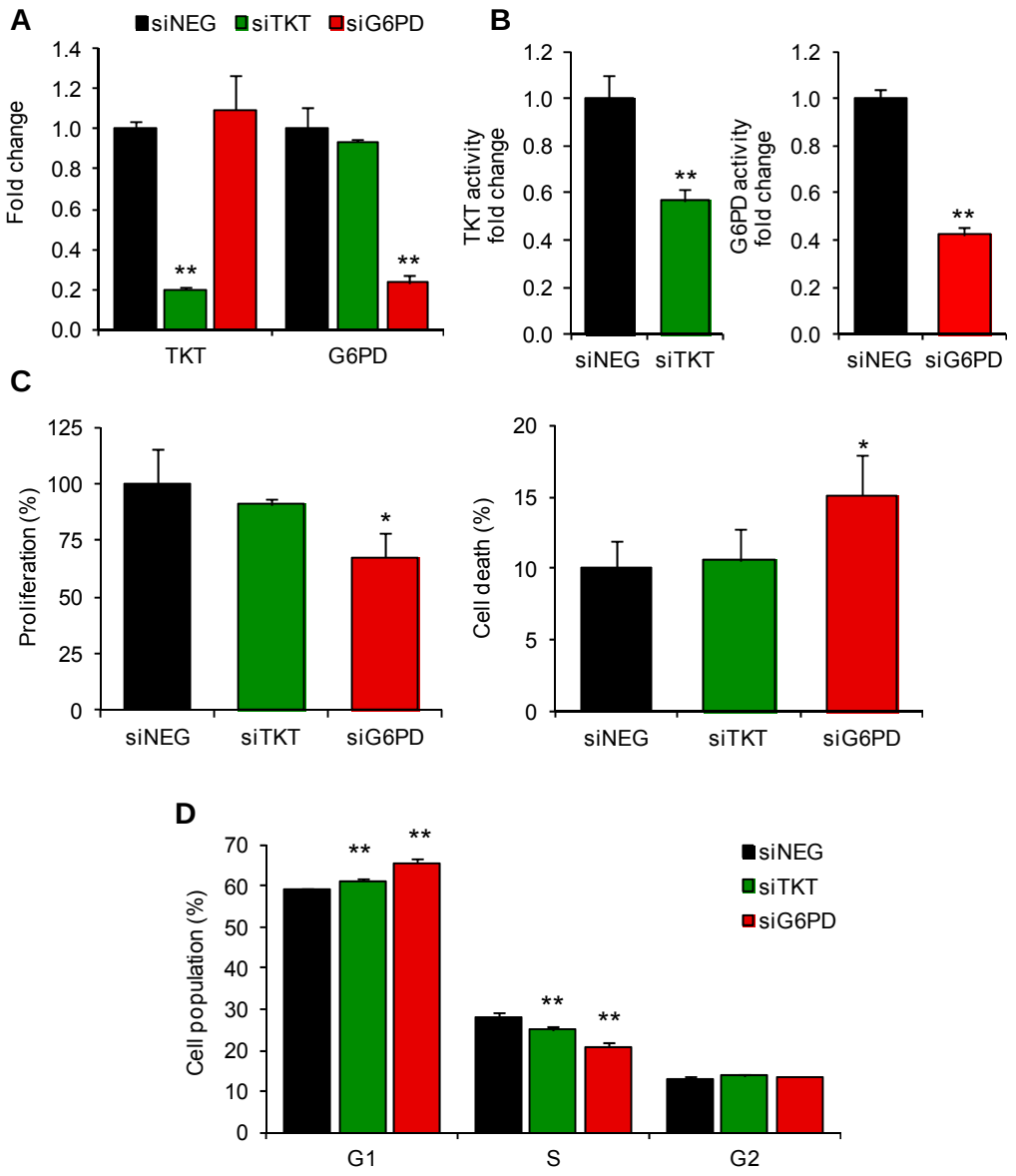

Figure 5.4.1. Role of PPP enzymes TKT and G6PD on cell proliferation and survival

A. TKT and G6PD mRNA expression 72 h after transfection of non-targeting siRNA (siNEG) or siRNA against TKT (siTKT) or G6PD (siG6PD). Fold change is calculated with respect to siNEG (mean ± SD of n=3). **B.** TKT (left) and G6PD (right) activity 120h after siTKT or siG6PD transfection respectively (mean ± SD of n=3). **C.** Effect of TKT and G6PD knockdown on cell proliferation (left) and survival (right). Cells were stained with propidium iodide and counted by flow citometry at 144 hours after siRNA transfection (mean ± SD of n=2 for siTKT and n=5 for siG6PD). **D.** Effect of TKT and G6PD knockdown on cell cycle progression. Cell cycle analysis was performed at 120 hours after siRNA transfection (mean ± SD of n=3). Significant differences compared with siNEG were assessed by two-tailed Student's *t*-test. * $p<0.05$, ** $p<0.01$

and a subsequent decrease in S phase were found when inhibiting any of the enzymes of the PPP (Figure 5.4.1.D).

As it has been mentioned earlier, PPP is also important in redox homeostasis, since the oxidative pathway is one of the main systems of NADPH production, which in turn is employed for maintaining the budget of reduced glutathione to counteract ROS production. As redox homeostasis plays an important role in cancer cell survival, particularly in breast cancer cells, the impact of inhibition of TKT and G6PD in ROS levels was assessed. Our results showed that G6PD depletion induced a clear increase in ROS intracellular levels (Figure 5.4.2). However, no changes were detected when TKT was inhibited, indicating that TKT does not participate in ROS levels regulation.

5.4.2.2 PPP inhibition promotes a whole-network metabolic reprogramming

PPP is involved in several essential processes in healthy and tumor cells. In order to obtain a deeper knowledge of the implications of this pathway in cancer cell metabolism, we performed a ^{13}C-assisted metabolomics experiment by using [1,2-$^{13}C_2$]-glucose. First, extracellular fluxes of glucose, lactate and glutamine were measured (Figure 5.4.3.A). TKT knockdown produced a decrease in glucose uptake of 20% which was in accordance with a decrease in lactate production of the same magnitude. On the

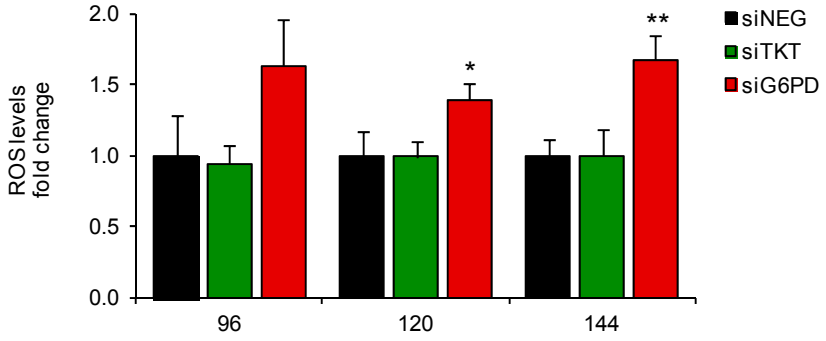

Figure 5.4.2. Role of PPP enzymes in redox homeostasis

Relative ROS levels measured by flow citometry using H_2DCFA probe at the indicated time points after transfection (mean ± SD; n=3). ROS levels are expressed as fold change with respect to siNEG. Significant differences compared with siNEG were assessed by two-tailed Student's *t*-test. * $p<0.05$, ** $p<0.01$

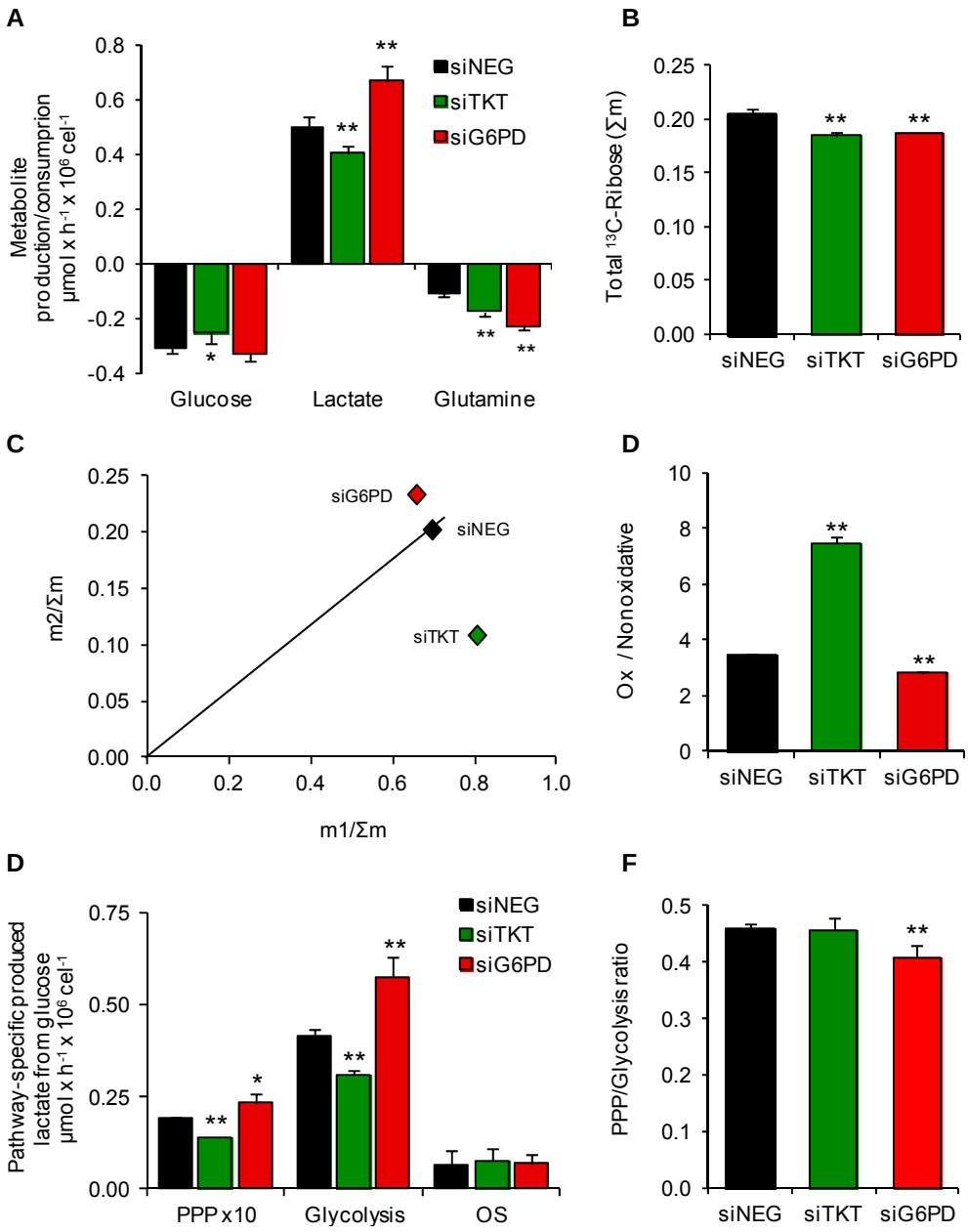

Figure 5.4.3. Metabolic role of TKT and G6PD enzymes

^{13}C-assisted metabolomics experiment was performed by replacing cell culture media by fresh media containing 50% [1,2-$^{13}C_2$]-glucose at 96 hours after transfection. Incubation with the tracer was carried out over a period of 24h and extracellular fluxes and mass isotopomer distribution of different metabolites were determined over this period. **A.** Main extracellular fluxes consisted of glucose and glutamine consumption and lactate production (mean ± SD of n=3) **B.** Total ^{13}C-Ribose represented as the sum of m1+m2+m3+m4 (∑m) (mean ± SD of n=3) **C.** Phase plane analysis for ribose synthesis. Ribose m1 and m2 were analyzed and plotted as percentage of total ^{13}C-Ribose (∑m)

.../...

contrary, G6PD depletion did not affect glucose consumption but an increase in lactate production of more than 30% was found. However, the most striking finding was that both TKT and G6PD knockdown cells increased glutamine consumption rate by more than 50%, being this increase more prominent for the latter (100%). Thus, although the flux through PPP has often been described to be small, these observations highlight the importance of this pathway in the global metabolic network. After that, we sought to determine in which extent the PPP was affected when TKT and G6PD were downregulated and whether other changes in metabolism were occurring.

As an approach to estimate the impact of these inhibitions on PPP, mass isotopomer distribution of ribose from RNA. First, the percentage of newly synthesized ribose (∑m) over the total ribose was determined (Figure 5.4.3.B) and a significant decrease in ribose synthesis was found in both TKT and G6PD knockdown cells. Glucose can be metabolized through either the oxidative or the nonoxidative branch of the PPP, yielding m1 or m2 labeled ribose respectively. Figure 5.4.3.C depicts the contribution of the oxidative and the nonoxidative PPP to ribose synthesis. TKT inhibition clearly promoted a decrease in utilization of nonoxidative pathway (m2/Σm) by around 50% and, simultaneously increased flux through the oxidative branch (m1/Σm). On the other hand, G6PD inhibition slightly affected the oxidative branch and no significant changes were found in the nonoxidative one. The calculation of the oxidative/nonoxidative ratio also corroborated these findings (Figure 5.4.3.D). Thus, a prominent increase in this ratio was found when TKT was inhibited while a small decrease was observed when G6PD was downregulated, suggesting that TKT exerts a higher control over the PPP. Additionally, to further asses the role of TKT and G6PD in PPP, mass isotopomer distribution of lactate from media was also analyzed. Lactate is mainly produced from glucose, even more in cancer cells. Since glucose can be either processed through direct

.../...

(mean ± SD of n=3) **D.** Oxidative vs. nonoxidative branch of PPP calculated as m1 ribose/ m2 ribose (mean ± SD of n=3) **E.** Pathway-specific produced lactate. Lactate produced flux from glucose via either PPP or glycolysis and from other sources (OS) was calculated using lactate production in combination with mass isotopomer distribution of lactate as described in section 4.13.1 (mean ± SD of n=3). **F.** The ratio between PPP and glycolysis fluxes was calculated by dividing the values for PPP by glycolysis for each condition (mean ± SD of n=3). Significant differences compared with siNEG were assessed by two-tailed Student's *t*-test * $p<0.05$, ** $p<0.01$.

glycolysis or diverted into PPP and reintroduced in glycolysis, the carbons of the end-product of glycolysis lactate contains information of the route followed by glucose carbons. Then, mass isotopomer distribution of lactate when cells are incubated with [1,2-$^{13}C_2$]-glucose integrates information of the glucose-derived carbon flow. Using lactate production in combination with lactate mass isotopomer distribution, pathway-specific production of lactate from glucose can be estimated as described in *Section 4.13.1*, (Figure 5.4.3.E). The results clearly indicated a decrease in glycolytic flux when TKT was inhibited whereas the opposite result was obtained for G6PD knockdown. Likewise, data showed a very small flux of glucose transformed into lactate through PPP in all conditions, indicating than most of the glucose-derived ribose is used for biosynthetic purposes instead of being reincorporated into glycolysis and finally transformed into lactate. A decrease in flux from glucose to lactate via PPP was observed when TKT was inhibited and, paradoxically, a small increase was detected when G6PD was depleted. It was expected that G6PD knockdown led to a decreased flux from glucose to lactate via PPP, since its inhibition blocks the entrance of G6P into PPP. Nevertheless, when ratio PPP/glycolysis fluxes was calculated no changes were detected when TKT was inhibited and a decrease was observed in G6PD knockdown cells (Figure 5.4.3.F), confirming a blockade of oxidative PPP flux in relation to glycolytic flux. Taken together, these results indicate that TKT inhibition led to a decrease in glucose consumption which impacted in a balanced manner in glycolysis and PPP flux, since PPP/glycolysis ratio was maintained. However, G6PD enhances both glycolytic and PPP in a different magnitude, provoking a decrease in PPP/glycolysis ratio. This result is in accordance with the metabolic role of G6PD shunting carbons from glycolysis intermediates into the PPP. Besides, lactate produced from other sources (OS) different from glucose was calculated in each condition, although no differences were detected (Figure 5.4.3.E)

Cancer cells display higher requirements of lipids to sustain proliferation. Since the oxidative branch of PPP is one of the main sources of NADPH as reducing equivalents, we studied the impact of these inhibitions on lipid synthesis by analyzing palmitate production from glucose (Figure 5.4.4). Remarkably, lipid synthesis was clearly impaired

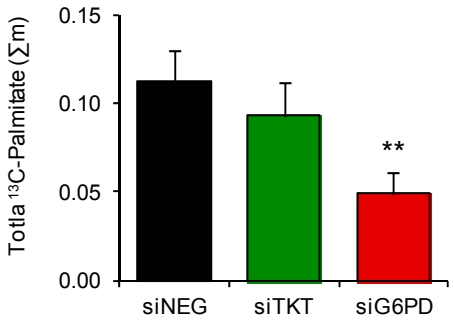

Figure 5.4.4. Role of PPP enzymes in lipid synthesis

^{13}C-assisted metabolomics experiment was performed by replacing cell culture media by fresh media containing 50% [1,2-$^{13}C_2$]-glucose at 96 hours after transfection. Incubation with the tracer was carried out over a period of 24h and total ^{13}C-Palmitate was measured and represented as sum of m1+m2+…+m6 (∑m) (mean ± SD of n=3). Significant differences compared with siNEG were assessed by two-tailed Student's *t*-test. * p<0.05, **p<0.01

after G6PD knockdown by more than 50%, whereas no changes were detected when TKT was inhibited.

5.4.2.3 PPP and glutaminolysis are functionally interconnected

One of the most unexpected findings observed in the previous results was the marked increase in glutamine consumption when TKT and G6PD were impaired, which suggested an interconnection between PPP and glutamine metabolism. As it is for PPP, also glutaminolysis is involved in NADPH production, since it supplies carbons required for TCA cycle reactions that can generate malate, which is subsequently oxidized by malic enzyme into pyruvate producing reducing power in the form of NADPH. Additionally, NADP-dependent isocitrate dehydrogenase isoforms are fueled with glutamine-derived metabolites, so replenishment of the TCA cycle intermediates is critical for NADPH generation and redox homeostasis. Then, at least in case of G6PD knockdown, we reasoned that the observed increase in glutamine uptake might be intended to counteract ROS production by activating NADPH-generating reactions. To test this hypothesis, G6PD and TKT knockdown cells were grown in the absence (-Q) or presence (+Q) of glutamine and intracellular levels of ROS were determined. As shown in Figure 5.4.5.A, no additional increase in ROS levels was detected when G6PD was inhibited and transfected cells were cultured in the absence of glutamine compared with those cultured in the presence of glutamine, indicating that the observed increase in glutamine uptake was not intended to ROS counteraction.

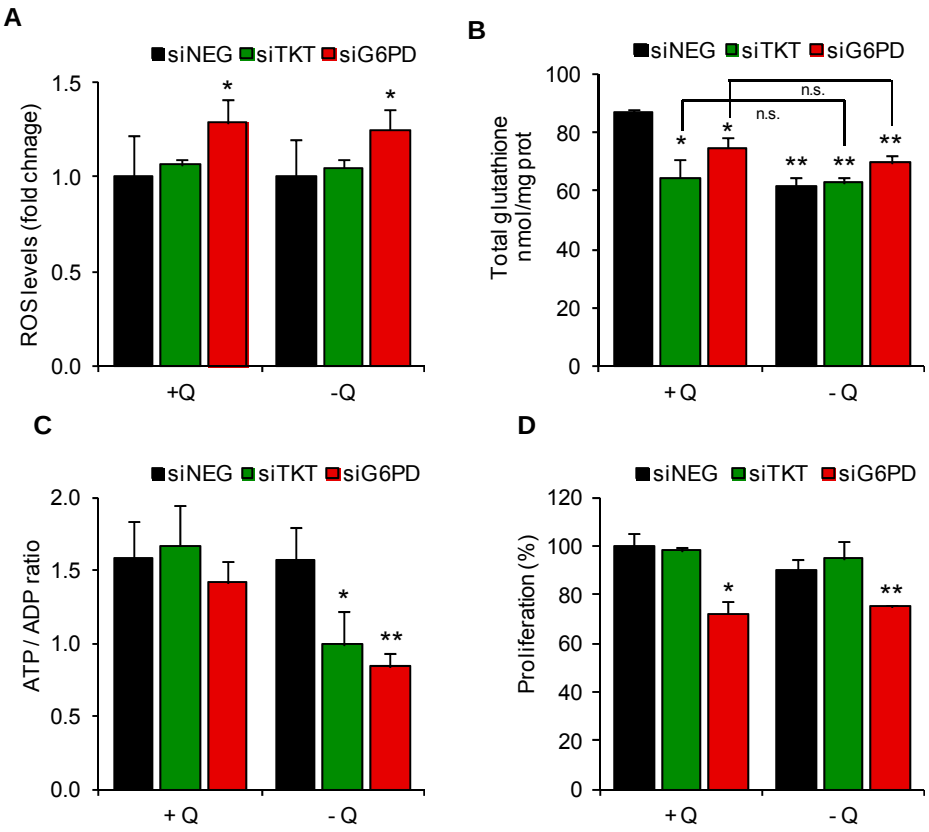

Figure 5.4.5. Role of glutamine under PPP inhibition

To determine the role of PPP enzymes in the presence or absence of glutamine, 96 hours after transfection, media was replaced by complete (+Q) or glutamine-free (-Q) media for 16 h and ROS levels (A), glutathione content (B) and ATP/ADP ratio (C) were determined. **A.** ROS levels expressed as fold change compared with siNEG in each condition (mean± SD of n=6 from two independent experiments). **B.** Total glutathione content (mean ± SD of n=3). **C.** ATP/ADP ratio (mean ± SD of n=3). **D.** Relative cell proliferation. 72 hours after transfection media was replaced by fresh complete or glutamine-free media and cells were counted by flow citometry after 72 hours. Results are expressed as percentage of siNEG in complete media (mean ± SD of n=3). Significant differences compared with +Q siNEG (B and D) or with siNEG in each condition (A and C) were assessed by two-tailed Student's *t*-test * $p<0.05$, ** $p<0.01$, n.s, denotes non-significant differences,

Glutamine is also used to produce glutathione, an antioxidant tripeptide involved in redox homeostasis. It is synthesized from cysteine, glycine and glutamate, being the latter a direct product of glutamine metabolism. Then, we hypothesized that the increase in glutamine uptake might be directed towards glutathione synthesis in order to maintain redox homeostasis. To elucidate the contribution of glutamine to glutathione budget when PPP was impaired, total levels of glutathione were measured

when TKT or G6PD were inhibited in the absence or presence of glutamine (Figure 5.4.5. B). A decrease in total glutathione levels was found in siNEG condition without glutamine in comparison with the same condition in the presence of glutamine, indicating that glutamine significantly contributes to glutathione synthesis. Also a decrease in glutathione was found when TKT or G6PD were depleted in the presence of glutamine. Nevertheless, no additional decrease in glutathione levels was found when glutamine was removed from media and PPP was inhibited, what points out that the increase in glutamine consumption was not intended to increase glutathione budget.

As the results obtained so far suggested that the increase in glutamine uptake observed was not primarily involved in redox homeostasis, we explored other potential mechanisms that could explain this process. One of the fates of glutamine is the production of ATP by oxidative phosphorilation in the mitochondria. Considering that glutamine is one of the main energetic substrates, we wanted to know if TKT and G6PD knockdown cells were more dependent on glutamine for energetic purposes. Then, we examined ATP/ADP ratio under presence or absence of glutamine in control and knockdown cells (Figure 5.4.5.D). Notably, we detected a significant decrease in the energetic status when TKT or G6PD were inhibited in the absence of glutamine, suggesting that PPP inhibition renders cells more dependent on glutamine metabolism for energy production.

Taking into account the energetic utilization of glutamine as demonstrated above, we reasoned that it might play an essential role in proliferation when PPP enzymes were inhibited. Then, cells were transfected and cultured in the absence or presence of glutamine (Figure 5.4.5.D). According to the results obtained so far, we speculated that TKT and G6PD knockdown cells should be more sensitive to glutamine deprivation. As demonstrated previously, we observed a decrease in proliferation when G6PD was inhibited in the presence of glutamine. However, we did not find any additional difference when either TKT or G6PD were inhibited in glutamine-free media. Note that siNEG cells neither showed a significant decrease in proliferation under glutamine deprivation, demonstrating that MCF7 cells are glutamine-independent to proliferate. These facts indicate that, although glutamine consumption increased when PPP was

inhibited and it was primarily used to sustain ATD/ADP ratio, glutamine was not essential for proliferation. It suggests that this cell line displays a high level of metabolic flexibility in order to adapt to changing nutritional conditions.

5.4.3 Discussion

Our study provides several insights into the role of PPP in the metabolism of MCF7 breast cancer cell line. Previous studies suggest the importance of this pathway in breast cancer tumors, especially in those in advanced state such as MCF7 cell line (Drabovich et al., 2012; Jerby et al., 2012). Here, we have first shown that G6PD plays a pivotal role in cell proliferation and survival, while TKT seems to be dispensable in these processes. We have also demonstrated that the inhibition of G6PD led to a significant decrease in cell growth and viability. The high dependency of this cell line on this pathway is clearly supported by the fact that just 50% inhibition of G6PD specific activity led to a 35% decrease in cell proliferation. Several reports have also corroborated the role of G6PD in cell proliferation (Ho et al., 2000; Li et al., 2009), although the exact mechanism by which G6PD is important for cell proliferation is still unclear. G6PD is the key in the synthesis of ribose via oxidative pathway. However, we have demonstrated here that the impact of G6PD on ribose synthesis is low whereas it is high on ROS levels, suggesting that G6PD plays a more crucial role in redox homeostasis than in ribose synthesis in MCF7 cell line. This idea has been documented in other study concluding that G6PD is dispensable for pentose synthesis but essential for defense against oxidative stress (Pandolfi et al., 1995). In addition, G6PD ablation renders cell more sensitive to the action of oxidative agents, indicating the essential role of this enzyme in protection against oxidative damage (Cheng et al., 2004; Gao et al., 2009). Then, it is more likely that cell death caused by G6PD inhibition is due to ROS homeostasis deregulation. G6PD is involved in NADPH production, which is used for maintenance of the reduced pool of glutathione which in turn is responsible for ROS levels. Thus, measurement of NADP/NADPH ratio would provide valuable and more direct information of the consequences of G6PD inhibition. As indicated by ROS levels, a decrease in NADPH levels is highly probable. This fact is also supported by the observed

decrease in the synthesis of fatty acids, for which NADPH is essentially required. Not only might the damage produced by high levels of ROS be the cause of decreased cell proliferation and survival, but also a limited amount of reducing equivalents in the form of NADPH. The assessment of cell proliferation and survival in the presence of the antioxidant N-acetyl-cysteine or palmitate would provide additional evidence of the mechanism involved in G6PD-inhibition induced cell death. It is worth of noting that although G6PD had the greatest impact on cell proliferation and ROS levels maintenance, TKT inhibition showed the highest impact on pathway-specific ribose synthesis. Levels of total newly synthesized ribose were similarly decreased in both TKT and G6PD inhibited cells, but TKT showed a greater regulatory capacity over the non-oxidative pathway than G6PD over the oxidative one. This fact can be related to the protein level of each enzyme in the cell. It is described that G6PD usually works at around 2% of its total maximum rate (Riganti et al., 2012), what indicates that the enzyme is in excess in the cell and its inhibition will have a low impact on the synthesis of the end-product of the pathway catalyzed. This is corroborated by the fact that 50% inhibition of G6PD specific enzyme activity provoked a slight decrease in m1 ribose. On the contrary, the results indicated that TKT probably works at its maximum rate in the cell, since 50% inhibition of the enzyme provoked a proportional inhibition in m2 ribose. Additionally, TKT inhibition also increased m1 ribose. It can be due to either the impossibility of reintroducing ribose synthesized by the oxidative branch into glycolysis or to a compensatory activation of the flux through the oxidative branch, what resulted in m1 ribose accumulation. Taken together, all these findings suggest that although both oxidative and nonoxidative pathways are tightly connected, the functions of controlling ROS levels and synthesizing ribose might be partially decoupled.

One of the most striking findings in this study is the uncovered link between PPP and glutaminolysis. The results provided here clearly demonstrate that the increase in glutamine consumption was because of energy requirements. In the case of TKT inhibition, the observed decrease in glucose consumption and lactate production well might be associated to a decrease in glycolytic ATP production. In MCF7 cells, the contribution of glucose to total ATP turnover has been estimated to be around 30 % (Guppy et al., 2002). TKT inhibition might entail a reduction of the network dimension

and consequently a decrease in the amount of glucose than can be uptaken. In order to compensate this situation and sustain the level of ATP, additional sources of energy must be used in a greater extent, such as glutamine, even more if there are no changes in cell proliferation.

In the case of G6PD, we detected no changes in glucose consumption but an increase in glucose-derived lactate production. In fact, glycolytic flux was incremented (Figure 5.4.3.E), suggesting that less carbons are routed into the mitochondria. This result can be explained on the basis of HIF activation. The increment in ROS levels can stabilize and activate HIF dependent signaling pathway (Chandel et al., 1998), which upregulates glycolysis and divert glycolytic flux away from mitochondria by PDH complex inactivation (Kim et al., 2006; Papandreou et al., 2006). This reasoning is supported by the increased lactate levels in G6PD knockdown cells despite of neither increase in glucose consumption nor increase in lactate from other sources (Figure 4.4.3.E). Since MCF7 cell line produces around 80% of ATP by oxidative phosphorylation in the mitochondria (Guppy et al., 2002), it is likely that the inhibition of pyruvate entry into the mitochondria by inactivation of PDH complex led to an increased use of other energetic substrates such as glutamine. Under these circumstances, glutamine would play a determining role in maintaining ATP levels as demonstrated by the decrease in ATP/ADP ratio of G6PD inhibited cells in the absence of glutamine.

Despite the energetic role of glutamine under PPP inhibition, it is timely to note that simultaneous glutamine depletion and G6PD or TKT knockdown did not cause an additional decrease in cell proliferation. In fact, MCF7 cells displayed low sensitivity to glutamine deprivation in terms of cell proliferation and ATP levels (Kung et al., 2011), suggesting that this cell line has a certain metabolic flexibility to maintain energy homeostasis. Then, although glutamine turns into a more important source of energy when G6PD or TKT are inhibited, the lack of this aminoacid might be replaced by an increased consumption of other nutrients in order to sustain proliferation.

In summary, PPP plays a pivotal role in several cellular processes in MCF7 cells. On the one hand, G6PD is important in proliferation and survival as well as in regulating ROS levels in these cells. However, it exerts a low regulation over ribose synthesis flux

through the oxidative branch of PPP. On the other hand, TKT seems to be dispensable for proliferation, but it exerts a high control over ribose synthesis flux through the nonoxidative branch of PPP. The inhibition of each enzyme entails a different metabolic response. Whereas G6PD inhibition enhances glycolytic flux and promotes lactate secretion, TKT impairment reduces glucose consumption and glycolytic flux. Nevertheless, the inhibition of each enzyme increases the consumption of glutamine, which is used to maintain energy homeostasis although it is not essential for cell proliferation.

6. GENERAL DISCUSSION

6. GENERAL DISCUSSION

Throughout the different chapters of this thesis, the metabolic adaptations induced by RAS oncogenic activation and the potential of metabolism as a new field of therapeutic opportunities have been explored. In this regard, we have unveiled the essential traits of the metabolic reprogramming induced by mutated RAS and explored the PPP enzymes as potential therapeutic targets in colon and breast cancer cells.

In the Chapters 5.1 and 5.2, the metabolic reprogramming induced by RAS oncogenic activation has been studied using two different cell models: NIH3T3 mouse fibroblasts transfected with a mutated copy of the *K-RAS* gene in either codon 12 (K12-transfected cells) or 13 (K13-transfected cells) (Chapter 5.1) and human BJ cells transfected with a copy of *H-RAS* mutated in codon 12 (Chapter 5.2). Although the experimental approaches carried out to study each situation have been different, some conclusions can be reached about the metabolic reprogramming induced by mutated RAS. It is worth of noting that the work presented in Chapter 5.1 is a continuation of the work published by Vizan *et al*, in which NIH3T3 K12 and K13 cells were studied at metabolic level using ^{13}C-assisted metabolomics (Vizan et al., 2005).

In Chapters 5.1 and 5.2, the results have shown a parallel metabolic phenotype between K-RAS and H-RAS oncogenic activation with regard to glycolysis and PPP, although the magnitude of the change in PPP has been determined to be higher in KRas-transfected NIH3T3 cells. However, the proteomic changes at enzymatic level accompanying these metabolic phenotypes were different in the situations considered. Both systems display an increase in G6PD and PK (only in K13) enzyme activity. However, HK was activated in BJ-HRasV12 cells while it changed in neither NIH3T3 K12 nor K13. Similarly, LDH increased substantially in NIH3T3 K12 and K13 compared with control NIH3T3, but it decreased slightly in BJ-HRasV12 compared with BJ. These results suggest that different metabolic changes can result in a similar metabolic phenotype. In other words, a high

glycolytic flux can be obtained by upregulating different steps of glycolysis. This observation can be explained on the basis of MCA. The dependencies matrix shown in figure 5.1.4.D clearly exemplifies how an increase in LDH flux *(J_T)* can be achieved by activating not only LDH *(v_T)* but also PK *(v_K)* or GAPDH *(v_F),* demonstrating that different metabolic mechanisms can take place to induce an increase in a metabolic flux. In a parallel manner, different enzymes or combinations of them can be modified to result in increased glycolytic flux.

With regard to mitochondrial metabolism in K-RAS and H-RAS mutated cells, the lack of parallel data for each system complicates the comparison. In NIH3T3 K12 and K13 cells, no differences in mitochondrial metabolism have been found in the analysis performed in Chapter 5.1, although previously published data showed that K-RAS induced an increase in glucose-derived carbons in the TCA cycle intermediate glutamate (Vizan et al., 2005). However, other authors using also NIH3T3 KRas-transfected cells concluded that K-RAS activation induces mitochondrial dysfunction and decreases mitochondrial respiration (Chiaradonna et al., 2006a; Chiaradonna et al., 2006b; Gaglio et al., 2011). On the other hand, in BJ-HRasV12 cells a substantial increase in mitochondrial metabolism has been detected in BJ-HRasV12 cells compared with BJ. This increase is supported by an increase of glucose- and glutamine-derived carbons in TCA cycle intermediates as well as an enhanced consumption of glutamine and O_2 in the presence of this aminoacid.

The differences found between KRas-transfected NIH3T3 and HRas-transfected BJ cells well might be attributed to the origin of the cells employed as well as to the transfected RAS isoform. Similar differences to the ones presented here have been reported previously in other studies. A study performed using human KRas-transfected cells indicated that K-RAS oncogenic activation leads to mitochondrial dysfunction (Hu et al., 2012). Additionally, studies with mouse H-RAS mutated transfectants suggest that RAS oncogenic activation also leads to mitochondrial dysfunction (Yang et al., 2010), and to an impairment of mitochondrial respiration combined with a gradual acquisition of the Warburg effect after an initial activation of mitochondrial metabolism (de Groof et al., 2009). On the contrary, human HRasV12-expressing cells have been reported to

increase mitochondrial metabolism (Telang et al., 2007). Taken together, these findings suggest that, whereas glycolytic phenotype is a robust metabolic change induced by RAS activation, changes in mitochondria are more fragile and sensitive to the cell model employed and the RAS isoform transfected. In these regard, despite of the high degree of sequence homology between RAS isoforms, H-RAS, K-RAS and N-RAS proteins exert different downstream activities, in part because of the ability of RAS isoforms to localize in different cellular microdomains (Bellavia et al., 2012; Omerovic et al., 2007). This different intracellular compartmentalization could help RAS isoforms to contact different downstream effectors finally leading to different biological outcomes and partially different metabolic phenotypes. As an example, it has been proposed that *K-RAS* and *H-RAS* genes differently regulate the redox state of the cell (Bellavia et al., 2012). This fact suggests that different isoforms of RAS could regulate mitochondrial metabolism in various ways, leading to different mitochondrial phenotypes.

The activation of the PPP in RAS-mutated cancer cells prompted us to validate this finding in other RAS-pathway activated cells, such as colon cancer cells. After finding that RAS-pathway activated colon cancer cells displayed increased levels of G6PD, this enzyme was inhibited in BRAF-mutated cell line HT29. Nevertheless, no changes were observed in cell proliferation and survival when G6PD was impaired in this cell line. Therefore, since G6PD plays a pivotal role in regulating ROS levels, the inhibition of PPP was performed in a cell line with high levels of oxidative stress, such as breast cancer cell line MCF7. In this model, G6PD inhibition induced a notable decrease in cell proliferation, whereas TKT inhibition provoked no changes. As a whole, the results suggest that different cancer cells have distinct metabolic dependencies. MCF7 breast cancer cells displayed a greater reliance on the oxidative branch of the PPP than HT29 colon cancer cells. It suggests that the metabolism of each cell line is tuned in a different way in order to cover their metabolic requirements. Then, it can be deduced from the obtained results that G6PD inhibition in HT29 either did not affect any essential process or a metabolic reorganization took place in order to circumvent G6PD inhibition. Thus, when G6PD is inhibited, HT29 cells might use nonoxidative PPP branch to synthesize ribose and use glutamine to produce NADPH, as discussed in Chapter 5.3. On the other hand, our results indicate that MCF7 cells mainly use oxidative branch of

PPP to synthesize ribose for RNA, but little impact on ribose synthesis was found on ribose synthesis when G6PD was inhibited. However, a greater change was observed in ROS, suggesting that ROS and ribose synthesis might be decoupled and most of the ribose synthesized through the oxidative branch of PPP might be reintroduced into glycolysis instead of using for RNA synthesis. Therefore, it would indicate that the primary use of this pathway is to synthesize NADPH instead of ribose.

On the contrary to HT29, when G6PD was inhibited in MCF7 cells, a decrease in cell proliferation was found, indicating that the metabolism of these could not be readapted to avoid this metabolic insult. Then, the results presented here reveal a metabolic fragility in this cell model.

The different consequences of G6PD inhibition in MCF7 and HT29 might also be explained on the basis of P53 state in each cell model. HT29 is a P53-deficient cell line that harbors P53(R273H) mutation, whereas MCF7 is a P53-proficient cell line. As discussed in Chapter 5.3, wild-type P53 binds to G6PD and impairs dimer formation, inhibiting G6PD activity. P53(R272H) mutant maintains the capability of binding to G6PD but it cannot inhibit the enzymatic activity. Therefore, according to this regulatory system, the concentration of active G6PD enzyme in HT29 is expected to be higher than in MCF7. Consequently, the higher is the concentration of the enzyme, the more difficult is the total inhibition of the reaction or flux. When G6PD is overactivated due to P53 mutation, it might be more interesting to inhibit the enzyme 6PGD. A high G6PD activity leads to the production of high 6PG, which has been proposed to display an inhibitory growth effect in P53-mutated cell line H1975 (Sukhatme and Chan, 2012). Therefore, blockade of the 6PDG reaction would lead to a rapid accumulation of this metabolite and subsequent inhibition of proliferation. In addition, this option would be even more interesting in cancer cells with high glycolytic flux, since enhanced glycolysis provides high amounts of PPP precursors.

Furthermore, a very interesting metabolic relation between PPP and glutamine metabolism has been unveiled in this thesis. In MCF7 cells, inhibition of PPP enzymes G6PD and TKT led to an increase in glutamine consumption whereas HT29 cells cultured in the absence of glutamine experienced an increase in G6PD expression and activity.

However, whether the response observed in each case is intended to fulfill the same requirement is unclear. In P53-proficient MCF7 cells, the inhibition of G6PD led to increased ROS levels and glutamine consumption. A potential mechanism to explain this response might be based on P53 activation. Under high oxidative stress conditions, P53 is activated and results in increased expression of the P53 target gene glutaminase 2, which increases the intracellular levels of glutamate, α-ketoglutarate, reduced glutathione and mitochondrial ATP production (Hu et al., 2010; Suzuki et al., 2010). As shown in Chapter 5.4, our results support the idea that glutamine enhances ATP production, since G6PD inhibition in MCF7 cells cultured in glutamine-free media displayed a decreased ATP/ADP ratio. On the other hand, HT29 cells cultured in glutamine-free media resulted in increased ROS levels. In this case, despite the observed increase in ROS, the fact that HT29 is a P53-decificent cell line together with the absence of glutamine in cell culture media make unfeasible the activation of the same mechanism triggered in MCF7 cells. However, NRF2-mediated response involving G6PD upregulation was detected, which might be intended to restore NADPH levels. The importance of maintaining NADPH homeostasis in cancer cells has been previously reported by Jeon and colaborators (Jeon et al., 2012). Therein, NADPH generation through PPP is impaired under glucose deprivation. Under these conditions, AMP-kinase induces alternative routes to maintain NADPH levels and inhibit cell death. The inhibition of the acetyl-CoA carboxylases 1 and 2 (ACC1 and ACC2) by AMPK maintains NADPH levels by decreasing NADPH consumption in fatty-acid synthesis and increasing NADPH generation by means of fatty acid oxidation. In a parallel manner, glutamine deprivation well might induce a NRF2-mediated metabolic reorganization in HT29 cells by activating oxidative PPP flux to provide cells with NADPH. This mechanism might be positively influenced by P53 mutation in HT29. P53 has been reported to negatively regulate NRF2-dependent transcription of antioxidant genes (Faraonio et al., 2006). Thus, the absence of functional P53 would boost NRF2-mediated response, enhancing the upregulation of NRF2 target genes such as G6PD.

In summary, in this thesis we have provided and extensive and deep body of evidence of the metabolic reprogramming induced by RAS oncogenic activation as well as explored the role of PPP enzymes in cancer cell metabolism. The study of the RAS-

induced metabolic reprogramming has revealed a variety of metabolic changes which can potentially represent specific metabolic dependencies of RAS-mutated cells and tumors. On the other hand, the inhibition of G6PD might be a promising therapeutic intervention point in some tumors according to the levels of oxidative stress or the mutational status of other regulatory proteins, such as P53. Furthermore we have also provided new knowledge to understand the regulation of metabolic processes, such as the interplay between PPP and glutamine metabolism. Collectively, all the results provided in this thesis, fully support the intimate relationship between oncogenes and metabolism and highlight the importance of metabolism in cancer cell proliferation and survival.

7. CONCLUSIONS

7. CONCLUSIONS

1. The study of flux distribution in combination with metabolic control analysis performed by analyzing solely the sign of fixed-sign control coefficients, is a reliable approach to identify the key enzymes involved in metabolic reprogramming. The use of this methodology has allowed us to identify an increase in glycolysis and PPP fluxes as metabolic features of KRAS-induced metabolic reprogramming and to propose G6PD, PK and LDH as the key enzymes responsible for this metabolic transition.

2. H-RAS oncogenic activation reprograms glucose and glutamine metabolism by enhancing glycolytic and PPP fluxes as well as mitochondrial metabolism. Glutamine is responsible for sustaining the activated mitochondrial metabolism in BJ-HRasV12, while glucose-derived carbons in the mitochondria are primarily used to fuel lipogenesis. Moreover, lipogenesis is overactivated in BJ-HRasV12 cells, which are more sensitive to FAS inhibition than BJ cells.

3. G6PD enzyme is overactivated in colon cancer cells with oncogenic activation of the RAS signaling pathway. Nevertheless, G6PD seems to be dispensable for proliferation and survival in BRAF-mutated HT29 cell line. Furthermore, a new connection between PPP and glutamine metabolism has been unveiled, as G6PD is overexpressed in HT29 cells under glutamine-deprived conditions by a mechanism involving a concomitantly increase in ROS levels and NRF2 induction.

4. G6PD enzyme is important in proliferation, survival and regulation of ROS levels in breast cancer MCF7 cells. However, it exerts a low regulation over ribose synthesis flux through the oxidative branch of PPP. G6PD inhibition enhances glycolytic flux, promotes lactate secretion and increases glutamine consumption, which is used to maintain energy homeostasis, although it is not essential for cell proliferation.

5. TKT enzyme is dispensable for proliferation of breast cancer MCF7 cells, but it exerts a high control over ribose synthesis flux through the nonoxidative branch of PPP. TKT impairment reduces glycolytic flux and increases the consumption of glutamine, which is intended to maintain energy homeostasis but it is not essential for cell proliferation.

8. RESUMEN EN ESPAÑOL / SUMMARY IN SPANISH

8. RESUMEN EN ESPAÑOL / SUMMARY IN SPANISH

8.1 INTRODUCCIÓN

8.1.1 Visión general de las bases del cáncer

El cáncer es un término genérico que incluye un elevado número de enfermedades en las cuales las células de los tejidos proliferan descontroladamente y son capaces de invadir otros tejidos dando lugar a la formación de metástasis. Para el desarrollo y la progresión de un tumor es necesario que las células tumorales adquieran ciertas capacidades a lo largo del proceso cancerígeno. Estas capacidades se pueden clasificar en: generación de señales de crecimiento, insensibilidad a las señales de inhibición de la proliferación, evasión de la apoptosis, capacidad de invasión y metástasis, potencial ilimitado de replicación y capacidad de estimulación de procesos angiogénicos (Hanahan and Weinberg, 2011). Recientemente se han incorporado dos nuevas capacidades, que son la evasión del sistema inmunitario y la reprogramación del metabolismo, permitiendo esta última satisfacer las necesidades energéticas y biosintéticas particulares de la célula tumoral.

8.1.2 Metabolismo tumoral

El metabolismo es el conjunto de reacciones químicas que posibilitan la vida y que tienen lugar dentro de las células de los organismo vivos. Todas las células de nuestro cuerpo requieren de la aportación de nutrientes, los cuales pueden ser empleados en reacciones que tienen como finalidad la obtención de energía (catabolismo) o bien en procesos de síntesis de macromoléculas necesarios para la proliferación (anabolismo). Estas necesidades nutricionales son particularmente altas en células proliferantes, ya

que deben duplicar todo su material ante de dividirse. Por tanto, dado que el cáncer es una enfermedad basada en la proliferación descontrolada de las células de los tejidos, no es de extrañar que el metabolismo de las células tumorales se vea particularmente alterado.

Las primeras observaciones de la existencia de un metabolismo diferencial en células tumorales tuvo lugar a principios del siglo XX, cuando Otto Warburg demostró que muestras de tumores presentaban un consumo de glucosa mayor que los tejidos normales y, que incluso en presencia de oxígeno, metabolizaban la glucosa a través de glucólisis anaerobia en lugar de fosforilación oxidativa (Jones and Schulze, 2011; Warburg et al., 1927). Esta característica del metabolismo tumoral es comúnmente conocida como efecto Warburg.

Durante los últimos años, el estudio del metabolismo tumoral, pese a haber sido considerado como un efecto colateral derivado de la activación de oncogenes o inactivación de genes supresores de tumores, ha cobrado especial relevancia. Muchas de las vías de señalización implicadas en la proliferación y supervivencia celular y que se encuentran frecuentemente mutadas en cáncer, como PI3K/AKT o RAS, ejercen parte de sus efectos mediante la regulación del entramado metabólico, siendo éstos esenciales para la correcta ejecución de las señales transmitidas por estas vías. Por tanto, las vías de señalización que controlan tanto la proliferación y la supervivencia como el metabolismo se encuentran íntimamente relacionadas y esta conexión es esencial para que los procesos celulares se sucedan de manera apropiada y coordinada.

8.1.2.1 Obtención de ATP: bioenergética de la célula tumoral y el efecto Warburg

Tal como describió Warburg, la mayoría de células tumorales metabolizan la glucosa principalmente mediante glucólisis aeróbica en lugar de fosforilación oxidativa. Dado que la glucólisis aeróbica menos eficiente que la fosforilación oxidativa en la producción de ATP por molécula de glucosa, las razones por las cuales las células tumorales adoptan este metabolismo glucolítico constituyen todavía hoy un tema controvertido.

Algunas ventajas para la célula tumoral que podrían derivarse de este fenotipo metabólico serían la utilización de una ruta metabólica de producción de energía rápida para un sustrato que puede ser limitante en algunas condiciones, la obtención de elevadas concentraciones de intermediarios glucolíticos necesarios para procesos biosintéticos, una menor dependencia del oxígeno en condiciones de hipoxia que se pueden dar habitualmente en tumores sólidos y una posible protección frente al desencadenamiento de procesos apoptóticos originados en la mitocondria.

El efecto Warburg se encuentra regulado por algunos de los oncogenes más frecuentemente mutados en cáncer como *c-MYC* (Dang et al., 2009; Shim et al., 1997), *RAS* (Chun et al., 2010) o *P53* (Kondoh et al., 2005; Pilkis et al., 1981; Vousden and Ryan, 2009), los cuales modulan la expresión de muchas de las enzimas glucolíticas.

Aunque la glucosa es el principal sustrato energético, también otros nutrientes pueden ser metabolizados con finalidad energética. Uno de los más relevantes es la glutamina, que además de participar en numerosos procesos biosintéticos, también puede ser oxidada en el ciclo de los ácidos tricarboxílicos (TCA, del inglés *Tricarboxylic Acid*) para dar lugar a la síntesis de ATP mediante fosforilación oxidativa. De hecho, algunos estudios demuestran el papel esencial de la glutamina en la proliferación y supervivencia de células tumorales (DeBerardinis and Cheng, 2010; DeBerardinis et al., 2007).

8.1.2.2 Proliferación celular: procesos biosintéticos en el metabolismo tumoral

La proliferación celular conlleva duplicar todo el material celular, incrementando las necesidades de la célula de precursores metabólicos para la síntesis de macromoléculas. Se ha propuesto que las células proliferantes, y en particular las células tumorales, en lugar de maximizar los procesos de obtención de energía mediante el uso de la fosforilación oxidativa mitocondrial, deben maximizar la capacidad de producción de sustratos precursores de macromoléculas para poder proliferar (DeBerardinis et al., 2008). Así, la mitocondria actuaría como centro biosintético donde se producen muchos de los precursores necesarios. Asimismo, las células tumorales presentan elevadas

necesidades de lípidos para duplicar sus membranas, hecho que comporta una salida de metabolitos del ciclo de TCA, en este caso de citrato para la síntesis de ácidos grasos. Dicha salida de metabolitos del ciclo de TCA constituye el proceso conocido como cataplerosis. Las células tumorales presentan frecuentemente una sobreactivación de las vías metabólicas encargadas de las síntesis de ácidos grasos, las cuales son reguladas por señales de proliferación frecuentemente alteradas en cáncer (Santos and Schulze, 2012). Para evitar el vaciado del ciclo del CAT, los procesos catapleróticos deben ser compensados con la entrada de otros metabolitos en el ciclo de TCA en el proceso inverso a la cataplerosis conocido como anaplerosis. El principal metabolito que cubre esta función en células proliferantes y en especial en células tumorales es la glutamina. Este aminoácido participa en multitud de procesos biosintéticos de manera directa, mediante la donación de sus grupos nitrogenados para la síntesis de nucleótidos así como a través de su conversión a glutamato y α-cetoglutarato, participando en la síntesis de aminoácidos, glutatión, ATP y equivalentes reducidos en forma de NADPH (DeBerardinis and Cheng, 2010). Además la glutamina también contribuye a la síntesis de lípidos no solo a través del metabolismo oxidativo mitocondrial sino también mediante el proceso de carboxilación reductiva, a través de la cual el α-cetoglutarato derivado de la glutamina es transformado en isocitrato a través de la carboxilación mediada por la isocitrato deshidrogenasa y la posterior transformación catalizada por la aconitasa, siendo esta carboxilación reductiva especialmente relevante en condiciones de hipoxia (Metallo et al., 2012).

Los procesos biosintéticos requieren tanto de precursores metabólicos como de coenzimas reducidos en forma de NADPH, siendo éste último imprescindible para la síntesis de ácidos grasos, aminoácidos, nucleótidos y el mantenimiento de los niveles intracelulares de glutatión reducido. Una de las rutas metabólicas más implicadas tanto en la síntesis de macromoléculas como de NADPH es la ruta de las pentosas fosfato (PPP, del inglés *Pentose Phosphate Pathway*) (Riganti et al., 2012). Esta vía metabólica se divide en dos ramas. Por un lado, la rama oxidativa, compuesta por las enzimas glucosa-6-fosfato deshidrogenasa (G6PD) y 6-fosfogluconato deshidrogenasa (6PGD), tiene como finalidad la síntesis de NADPH y de ribosa-5-fosfato (R5P). Por otro lado, la rama no oxidativa, está catalizada por la transcetolasa (TKT) y la transaldolasa (TALDO) y

se encarga tanto de la síntesis de R5P como del reciclaje del exceso de pentosas hacia la glucólisis. Ambas ramas de la PPP han sido relacionadas con diversos aspectos del fenotipo tumoral. Se ha descrito que la vía oxidativa se encuentra sobreactivada en ciertos tipos de cáncer (Kekec et al., 2009; Langbein et al., 2008) así como en procesos de transformación por oncogenes (de Atauri et al., 2011), y que su sobreexpresión se correlaciona con una mayor proliferación y permite la formación de tumores en ratones atímicos (Kuo et al., 2000; Leopold et al., 2003; Tian et al., 1998). Por otro lado, se ha demostrado que algunos tumores emplean preferentemente la vía no oxidativa para la síntesis de ribosa (Boros et al., 1997; Ying et al., 2012).

En el contexto del metabolismo tumoral, la PPP está regulada por algunos de los oncogenes y genes supresores de tumores más importantes, como *RAS*, *PI3K, AKT* o *P53* (de Atauri et al., 2011; Jiang et al., 2011; Mitsuishi et al., 2012b; Vizan et al., 2005; Ying et al., 2012).

8.1.2.3 Mantenimiento del estado redox

Como consecuencia del metabolismo celular se producen una serie de subproductos que deben ser eliminados o neutralizados para evitar su toxicidad. Algunos de estos subproductos son las denominadas Especies Reactivas de Oxígeno (ROS, del inglés *Reactive Oxygen Species*) y el incremento de su concentración en la célula da lugar a lo que se conoce como estrés oxidativo.

El estrés oxidativo está asociado con numerosos procesos que tienen lugar en la célula tumoral. Los niveles de ROS son finamente regulados mediante procesos de producción y eliminación, ya que a bajas concentraciones promueven la proliferación celular pero un incremento descontrolado resulta altamente tóxico para la célula (Boonstra and Post, 2004; Trachootham et al., 2009). Así, el crecimiento tumoral se ha asociado con elevados niveles de ROS (Kawanishi et al., 2006; Szatrowski and Nathan, 1991), los cuales inducen efectos sobre el fenotipo tumoral a diferentes niveles, incluyendo proliferación, viabilidad, apoptosis y progresión del ciclo celular, metabolismo energético, movilidad y adhesión celular, y angiogénesis (Sosa et al., 2013). Un ejemplo de ello lo encontramos

en los tumores de mama, que elevados niveles de estrés oxidativo (Brown and Bicknell, 2001; Kang, 2002; Portakal et al., 2000; Toyokuni et al., 1995).

Los mecanismos tumorales que conducen a unos niveles elevados de ROS no están totalmente claros. Sin embargo, la activación de oncogenes, defectos en el metabolismo, un mal funcionamiento de la mitocondria o pérdida del gen supresor de tumores *P53* son factores intrínsecos que causan un incremento de los niveles de ROS (Cook et al., 2004). Un ejemplo paradigmático de éstos es la activación del oncogén *RAS*, que ha sido relacionada con el incremento de los niveles de estrés oxidativo (Irani et al., 1997; Weinberg et al., 2010). Además, existen otros factores extrínsecos que pueden afectar a los niveles de ROS intracelular (Cook et al., 2004).

Dado que las células tumorales presentan niveles de ROS incrementados, parece lógico que al mismo tiempo hayan desarrollado mecanismos adaptativos para controlarlos y neutralizar los potenciales efectos tóxicos. En el caso de células con RAS mutado se ha descrito la activación de una variedad de mecanismos relacionados con esta finalidad, como la activación de la vía oxidativa de la PPP (de Atauri et al., 2011; Vizan et al., 2005), la síntesis de niveles elevados de antioxidantes como peroxiredoxina-3 y tiorredoxina peroxidasa C (Young et al., 2004) o la activación del sistema de detoxificación KEAP1-NRF2 (DeNicola et al., 2011) entre otros (Trachootham et al., 2006).

El mantenimiento de los niveles de ROS mediante el sistema de detoxificación KEAP1-NRF2 es particularmente interesante. Los niveles del factor de transcripción NRF2 se encuentran frecuentemente elevados en varios tipos de tumores y se ha demostrado que este factor de transcripción está involucrado en la adquisición de propiedades malignas por parte de las células tumorales (Kim et al., 2010; Singh et al., 2006; Solis et al., 2010; Wang et al., 2008). Existen diversos mecanismos que conducen a una sobreactivación de NFR2 (Mitsuishi et al., 2012a), entre los que destaca la señalización mediada por oncogenes, como por ejemplo *RAS* (DeNicola et al., 2011). Una fracción importante de los genes regulados por NRF2 corresponde a genes del metabolismo, como so los que codifican para las enzimas G6PD, fosfoglicerato deshidrogenasa (PGD), TKT, TALDO, enzima málico (ME) e isocitrato deshidrogenasa (IDH) (Mitsuishi et al., 2012b). Estos genes no sólo están involucrados en el control redox sino también en

la síntesis de una gran variedad de intermediarios metabólicos necesarios para la síntesis de macromoléculas. Así pues, NRF2 ejerce una acción dual en el metabolismo tumoral, participando simultáneamente en el control de los niveles de estrés oxidativo y en la síntesis de macromoléculas.

Las implicaciones del metabolismo en el mantenimiento de la homeostasis redox van más allá de las mediadas por NRF2. Una de las ventajas que se ha asociado al efecto Warburg es que una menor utilización de la mitocondria reduciría los niveles de ROS procedentes del metabolismo oxidativo. Además, el incremento de la concentración de los intermediarios glucolíticos permitiría disponer de mayor concentración de sustratos para la vía oxidativa de la PPP, cuyo papel en la protección frente al estrés oxidativo ha sido ampliamente documentado (Cheng et al., 2004; Gao et al., 2009a; Ho et al., 2000). En este aspecto juega un papel importante la enzima glucolítica piruvato quinasa M2 (PKM2), que bajo elevadas concentraciones de ROS reduce su actividad y disminuye el flujo glucolítico, provocando la acumulación de intermediarios glucolíticos que permiten incrementar el flujo a través de la vía oxidativa de la PPP (Anastasiou et al., 2011). También el metabolismo de la glutamina participa en el mantenimiento de la homeostasis redox aportando intermediarios que participan en reacciones en las que se produce NADPH, como la reacción catalizada por el ME (DeBerardinis et al., 2007).

A nivel mecanístico, cabe mencionar que los procesos para el control de los niveles de estrés oxidativo expuestos anteriormente son en parte inducidos por algunos oncogenes, como por ejemplo *RAS* (Mazurek et al., 2001; Son et al., 2013). Así, algunos de los oncogenes que inducen el efecto Warburg y la generación de ROS simultáneamente, como RAS, activan un programa metabólico dual con el objetivo de proveer a la célula tumoral con los precursores metabólicos necesarios y la protección frente a elevados niveles de ROS, cubriendo así dos requisitos esenciales para la progresión tumoral.

8.1.3 Estudio del metabolismo tumoral

El auge de la biología molecular durante los últimos años ha propiciado que el estudio del metabolismo tumoral se haya centrado principalmente en la regulación de ciertas reacciones metabólicas y/o enzimas por oncogenes o genes supresores de tumores. Aunque la biología tumoral, por si misma o en combinación con otras disciplinas como la transcriptómica o la proteómica, genera información valiosa para el estudio del metabolismo, ésta no es suficiente para un estudio detallado del mismo. Para ello, datos bioquímicos y metabólicos son esenciales. Por tanto, dada la extensión y la complejidad del entramado metabólico, el estudio del metabolismo se debe llevar a cabo desde un perspectiva integrada, estudiando sus diferentes niveles de regulación mediante herramientas experimentales y computacionales. Posiblemente, la Biología de Sistemas Computacional sea la disciplina más involucrada en este tipo de estudios (Borodina and Nielsen, 2005; Cascante and Marin, 2008; Hiller and Metallo, 2012). Asimismo, el estudio del metabolismo queda también integrado dentro de la disciplina conocida como metabolómica, la cual tiene como objeto el estudio y la cuantificación de todos los metabolitos de un organismo. (Fiehn, 2002). Sin embargo, el funcionamiento de la red metabólica no puede ser estudiado tan sólo mediante el análisis de la concentración de metabolitos, que es consecuencia de la transformación y transporte de los mismos a través de reacciones metabólicas, en lo que se conoce como flujos metabólicos. Con el objetivo de superar estas limitaciones, el análisis de la distribución de flujos metabólicos y los cambios asociados a ellos son explorados a nivel celular en una nueva disciplina emergente llamada flujómica (Cascante and Marin, 2008; Winter and Kromer, 2013).

8.1.3.1 Flujómica: el análisis de los flujos metabólicos

Los flujos metabólicos intracelulares pueden ser estudiados a diferentes niveles, desde el análisis de balance de flujos (FBA, del inglés *Flux Balance Analysis*), basado principalmente en la estequiometria de todas las reacciones metabólicas del sistema en estudio (Orth et al., 2010), hasta el uso de precursores de las vías metabólicas marcados con ^{13}C, en lo que se conoce como análisis de flujos metabólicos basado en ^{13}C (^{13}C-

MFA, del inglés *^{13}C-Metabolic Flux Analysis*) (Sauer, 2006). El uso de sustratos marcados con ^{13}C ofrece datos adicionales para la restricción del espacio de soluciones (valores posibles de flujos) obtenido mediante métodos de FBA. La aproximación experimental más común para llevar a cabo ^{13}C-MFA es la metabolómica basada en ^{13}C. En estos experimentos las células son cultivadas en presencia de sustratos metabólicos marcados con ^{13}C (trazador), los cuales son metabolizados por las células y dan lugar a la formación de metabolitos que contienen átomos de ^{13}C procedentes del trazador. Dependiendo de la vía metabólica a través de la cual ha sido metabolizado el trazador, los átomos de ^{13}C son incorporados en diferente número y posición en los nuevos metabolitos, produciendo metabolitos con una distribución isotopomérica distinta, tanto en número de ^{13}C (isotopómero de masa) como en posición del ^{13}C dentro de la molécula (isotopómero de posición). En los experimentos de metabolómica basada en ^{13}C se pueden utilizar una gran variedad de trazadores dependiendo de las rutas metabólicas a estudiar (Metallo et al., 2009). Entre los trazadores más comunes se encuentran aquellos derivados de la glucosa (^{13}C-glucosa) o la glutamina (^{13}C-glutamina), que han sido ampliamente utilizados con distintas distribuciones isotopoméricas, como por ejemplo la [1,2-$^{13}C_2$]-glucosa (Marin et al., 2003; Vizan et al., 2009), la [U-^{13}C]-glucosa (Gaglio et al., 2011), la [U-^{13}C]-glutamina, [1-^{13}C]-glutamina o la [5-^{13}C]-glutamina (Metallo et al., 2012).

Una vez finalizado el experimento, los metabolitos intracelulares y/o extracelulares son analizados mediante cromatografía de gases o cromatografía de líquidos acoplada a espectrometría de masas (GC-MS o LC-MS, del inglés, G*as or Liquid Chromatography coupled to Mass Spectrometry*) o bien mediante resonancia magnética nuclear (NMR, del inglés *Nuclear Magnetic Resonance*) para determinar la presencia de ^{13}C y, si es posible, su posición en la molécula. Así pues, se obtiene la distribución isotopomérica de los distintos metabolitos marcados con ^{13}C. Dicha distribución, en combinación con medidas de los flujos extracelulares relacionados con el trazador y/o otros sustratos, puede ser utilizada para determinar algunos flujos intracelulares, o bien la relación entre algunos de ellos, mediante el uso de fórmulas matemáticas simples basadas en el conocimiento previo de la red metabólica en estudio. Esta aproximación es conocida como MIDA (Análisis de la Distribución de Isotopoméros de Masa, del inglés, *Mass*

Isotopomer Distribution Analysis) (Alcarraz-Vizan et al., 2010; Marin et al., 2003; Ramos-Montoya et al., 2006).

Además, la distribución de isotopómeros de masa de los metabolitos, puede ser introducida en modelos computacionales que simulan de manera detallada el funcionamiento de la red metabólica, permitiendo estimar de manera más precisa los flujos intracelulares (Hiller and Metallo, 2012; Selivanov et al., 2006; Selivanov et al., 2004).

8.1.3.2 Análisis de control metabólico: identificación de las enzimas clave

En los sistemas metabólicos es frecuente la existencia de reacciones limitantes. Estas reacciones son particularmente relevantes, ya que variaciones en las enzimas que las catalizan cambian el flujo de la correspondiente vía metabólica en la que participan. El Análisis de Control Metabólico (MCA, del inglés *Metabolic Control Analysis*) es una aproximación matemática aplicada al estudio de los mecanismos reguladores de las redes metabólicas (Fell, 1997; Kacser and Burns, 1973). El análisis de MCA se lleva a cabo mediante la determinación de los coeficientes de sensibilidad, los cuales estiman en qué medida la perturbación de un parámetro (del sistema K_m, V_{max}, concentración de enzima…) afecta al valor en estado estacionario de una variable del sistema (flujo, concentración de un metabolito), siendo los más importantes los coeficientes de control (Fell, 1997; Kacser and Burns, 1973). En MCA, la elasticidad (ε_{qk}) es el parámetro de sensibilidad de la velocidad de una reacción aislada (v_q) con respecto a los cambios en la concentración (x_k) de uno de sus sustratos, un inhibidor o cualquier otro efector cinético de la reacción aislada (Ecuación 1 en *Sección 2.3.2*) (Cornish-Bowden, 2000; Fell, 1997).

Igualmente, el coeficiente de control de flujo o concentración es una propiedad del sistema definida como la sensibilidad de la concentración de un metabolito (x_g) o un flujo (J_q) en estado estacionario a cambios en un parámetro p, normalmente la concentración de enzima (v_k) (Ecuaciones 2 y 3 en *Sección 2.3.2*) .

Cuanto mayor sea el coeficiente de control de una enzima, mayor será su contribución al control y a la regulación de la vía metabólica, siendo el flujo de dicha vía o la concentración o actividad del metabolito en cuestión más sensible a cambios en la actividad de esta enzima.

Se han propuesto diferentes aproximaciones para la derivación de los coeficientes de control a partir de las elasticidades (Cascante et al., 1989a; Cascante et al., 1989b; Fell and Sauro, 1985; Reder, 1988; Westerhoff and Kell, 1987). Sin embargo, el signo de los coeficientes de control (positivo o negativo) puede ser suficiente para predecir si un flujo o concentración se incrementará o reducirá cuando la actividad de una enzima del sistema determinada cambie. Los coeficientes de control pueden ser de signo fijo, indeterminado o cero, dependiendo de la estructura de la red metabólica y las regulaciones, reflejadas principalmente en el signo positivo o negativo de las elasticidades: las elasticidades con respecto a los sustratos y activadores son siempre positivas mientras que las elasticidades con respecto a los inhibidores son siempre negativas (o productos en reacciones reversibles). Los coeficientes de control positivos indican que cambios en la concentración de un metabolito (x_g) o flujo (J_q) seguirán la misma dirección que cambios en la actividad de la enzima (v_k). Por el contrario, los coeficientes de control negativos indican que cambios en v_k inducirán un cambio en sentido inverso en x_g o J_q. Así, los coeficientes de control de signo fijo se pueden utilizar para evaluar qué enzimas del entramado metabólico podrían explicar los incrementos o decrementos observados en flujos y concentraciones o bien predecir posibles cambios tras el aumento o disminución de alguna actividad enzimática.

8.1.4 El metabolismo tumoral como potencial diana antitumoral

8.1.4.1 La reprogramación metabólica inducida por oncogenes como potencial diana terapéutica en cáncer

La reprogramación metabólica inducida por oncogenes conlleva que las células tumorales desarrollen una elevada dependencia de ciertos procesos metabólicos y/o enzimas, ofreciendo por tanto un conjunto de posibles dianas terapéuticas. La mutación

de ciertos oncogenes, como *RAS* o *MYC*, induce profundos cambios en el metabolismo que permiten a la célula dotarse de los recursos metabólicos necesarios para el proceso tumorigénico. Por ejemplo, se ha demostrado que ciertas enzimas son proteínas clave y esenciales para la progresión de tumores con RAS o c-MYC mutados (Dang et al., 2009; Gao et al., 2009b; Son et al., 2013; Telang et al., 2006). Los tumores con RAS mutado presentan especial dependencia de la glucólisis (Telang et al., 2006) y de una ruta alternativa del metabolismo de la glutamina en la cual el aspartato derivado de la glutamina es convertido en oxaloacetato por la transaminasa GOT, el cual es transformado en malato y después en piruvato mediante el ME, produciendo NADPH. (Son et al., 2013). Por otro lado, los tumores con c-MYC mutado son especialmente dependientes del metabolismo de la glutamina (Dang et al., 2009; Gao et al., 2009b). Así pues, estas dependencias metabólicas constituyen potenciales puntos de intervención terapéutica.

8.1.4.2 La PPP como potencial diana antitumoral

La PPP participa en dos procesos clave del metabolismo tumoral: la síntesis de ribosa y la síntesis de NADPH, éste último necesario para el mantenimiento del glutatión reducido y la lipogénesis. Por ello, las enzimas clave de la PPP, G6PD y TKT, han sido postuladas como potenciales dianas antitumorales. Por una lado, se ha descrito que la inhibición de la G6PD disminuye la proliferación en fibroblastos y líneas tumorales (Ho et al., 2000; Li et al., 2009), así como del tumor ascítico de Ehrlich en modelos *in vivo* (Boros et al., 1997; Rais et al., 1999). Por otro lado, también se ha demostrado que la inhibición de la TKT disminuye la proliferación tumoral *in vitro*, en células de adenocarcinoma de páncreas, e *in vivo* en ratones con tumor ascítico de Ehrlich (Boros et al., 1997; Rais et al., 1999). Conjuntamente, estos resultados indican que la inhibición de la PPP es una potencial estrategia terapéutica para combatir la progresión tumoral.

8.2. RESULTADOS Y DISCUSIÓN

8.2.1. El metabolismo del carbono y el signo de los coeficientes de control en las adaptaciones metabólicas inducidas por K-RAS

El oncogén *K-RAS* se encuentra mutado en aproximadamente el 25% de los tumores (Fernandez-Medarde and Santos, 2011). Dado el papel fundamental que juega el metabolismo en la progresión tumoral, conocer las adaptaciones metabólicas inducidas por la mutación de este oncogén y las enzimas clave que las promueven puede contribuir sustancialmente a desvelar mecanismos esenciales para la progresión de tumores con *K-RAS* mutado. En este capítulo, se han empleado células de ratón NIH3T3 transfectadas con el oncogén *K-RAS* mutado en los codones 12 (K12) y 13 (K13). Para determinar las principales diferencias metabólicas entre las células no transfectadas, las K12 y las K13, i) se determinaron experimentalmente las concentraciones de metabolitos extra- e intracelulares, ii) se definió el sistema metabólico de estudio, así como sus regulaciones, y se obtuvo el intervalo de valores posibles para cada reacción que conforma el sistema, iii) se identificaron los coeficientes de control de signo fijo y iv) se emplearon estos coeficientes de control para identificar las enzimas potencialmente responsables de los cambios en los flujos observados en las células K12 y K13 respecto a las células no transfectadas.

Para determinar los flujos intra- y extracelulares se midieron experimentalmente los principales flujos de entrada y salida de la célula (glucosa, lactato, glutamina y glutamato) y la concentración de algunos metabolitos intracelulares (hexosas fosfato, pentosas fosfato, triosas fosfato, fructosa-1,6-bifosfato y fosfoenolpiruvato). Posteriormente se determinó el sistema metabólico de estudio (Figura 5.1.1) y se obtuvo el mapa de flujos metabólicos correspondiente a cada tipo celular mediante FBA, usando la metodología sugerida por Llaneras y Picó (Llaneras and Pico, 2007) conocida como intervalo de satisfacción de restricciones (*interval constraint satisfaction approach*). Asimismo, en el análisis también se usaron restricciones isotopoméricas correspondientes a la relación entre los flujos glucolítico y a través de la PPP (Vizan et al., 2005). La distribución de flujos resultante se muestra en la Figura 5.1.2, donde se

observa un incremento de los flujos en las reacciones de la glucólisis y de la vía oxidativa de la PPP en las células K12 y K13 respecto a las células no transfectadas. En concordancia con estos resultados, se observó que las concentraciones de los intermediarios metabólicos de estas de estas vías estaban disminuidas en las células mutadas (Figura 5.1.3).

Para determinar las enzimas responsables de la reprogramación metabólica observada, se empleó el análisis de los coeficientes de control de signo fijo. Con el objetivo de identificar estos coeficientes de control, en el sistema metabólico utilizado se aplicó la aproximación matricial propuesta por Cascante *et al* mostrada en la figura 5.1.4.A-B (Cascante et al., 1989a; Cascante et al., 1989b). El signo de los coeficientes de control de flujo y concentración obtenidos son presentados en la tabla de dependencias de la Figura 5.1.4.D y conjuntamente ofrecen una herramienta predictiva que puede ser empleada para evaluar el impacto de cambios en actividades enzimáticas sobre los flujos y concentraciones, o bien, para hipotetizar qué cambios enzimáticos permiten explicar los cambios observados en los flujos y concentraciones. Teniendo en cuenta la matriz de dependencias mostrada en la Figura 5.1.4.D, se determinó experimentalmente la actividad específica de varias enzimas y se comprobó si los cambios en ellas concordaban con la distribución de flujos previamente obtenida (Figura 5.1.5.B). Se detectaron incrementos en las actividades específicas de las enzimas G6PD, PK y LDH, mientras que la actividad de la TKT se encontró disminuida y no se detectaron cambio en la actividad HK. En la Figura 5.1.5.B, los cambios en las actividades enzimáticas que dan lugar a cambios en los flujos que satisfacen la distribución observada de los mismos, se encuentran indicados en verde. Por el contrario, aquellos que no la satisfacen se encuentran marcados en rojo. Así pues, estos resultados nos permiten confirmar que el incremento observado en los flujos de la glucólisis y de la vía oxidativa de la PPP, así como la disminución de las concentraciones de azúcares fosfato en las células K12 y K13 respecto a las células no transfectadas, podrían ser explicados por el incremento de la actividad específica de las enzimas G6PD, PK y LDH y la disminución de la actividad TKT. Además, tal como se observa en la Figura 5.1.5.B, para explicar completamente el fenotipo metabólico observado en las células K12 y K13 son

necesarios cambios simultáneos en varias enzimas, como la G6PD y algunas enzimas glucolíticas.

8.2.2. Estudio de la reprogramación metabólica inducida por la activación oncogénica de H-RAS mediante el uso de la metabolómica basada en ^{13}C

En el capítulo 5.1 se ha analizado la reprogramación metabólica inducida por la activación oncogénica de *K-RAS* empleando células de ratón NIH3T3 transformadas con el oncogén *K-RAS* mutado en el codón 12 (K12) o 13 (K13). Aunque la isoforma K-RAS es la más frecuentemente mutada en cáncer, H-RAS se encuentra mutada en un 3% de los tumores, siendo los más frecuentes los de glándula salival (15%), tracto urinario (11%) y cérvix (9%)(Pylayeva-Gupta et al., 2011).

Las consecuencias metabólicas de la activación oncogénica de *H-RAS* han sido estudiadas desde diferentes perspectivas y empleando diferentes sistemas. Sin embargo, todos los estudios llevados a cabo hasta el momento han analizado la reprogramación metabólica inducida por la activación oncogénica de *H-RAS* de una manera parcial, considerando sólo una parte de la red metabólica y estudiando solo una porción de los metabólicos derivados de esta activación (Chen et al., 2001; de Groof et al., 2009; Kalas et al., 2012; Momchilova and Markovska, 1999; Telang et al., 2007; Yang et al., 2010). Así pues, esta reprogramación metabólica no ha sido estudiada desde una perspectiva global y profunda.

Por tanto, con el objetivo de explorar en detalle la reprogramación metabólica inducida por la mutación HRasV12, en este capítulo se utilizaron células $BJ^{LT+/hTERT+/HRasV12-}$ (BJ) y $BJ^{LT+/hTERT+/HRasV12+}$ (BJ-HRasV12) en combinación con técnicas de metabolómica basada en ^{13}C. Así pues, para realizar el estudio: i) se determinaron los flujos extracelulares correspondientes a los principales sustratos metabólicos y se determinó la sensibilidad de cada línea a la falta de ciertos nutrientes, ii) se realizaron experimentos de metabolómica basada en ^{13}C utilizando como trazadores la [1,2-$^{13}C_2$]-glucosa y la [U-^{13}C]-glutamina en paralelo y se analizó la distribución isotopomérica de distintos

metabolitos así como el funcionamiento de diferentes rutas metabólicas, y iii) se analizó el metabolismo mitocondrial mediante la determinación de la tasa de consumo de oxígeno en presencia de diferentes nutrientes.

La glucosa y la glutamina representan las dos principales fuentes de energía y precursores para la síntesis de macromoléculas. Por tanto, se exploró el efecto de la activación oncogénica de H-RAS sobre el metabolismo de estos dos sustratos metabólicos. Así, se observó que la activación de H-RAS inducía un incremento en el consumo de glucosa y glutamina así como en la producción de lactato y glutamato (Figura 5.2.1.A). Además, las células BJ-HRasV12 presentaron mayor sensibilidad a la depleción de estos nutrientes (Figura 5.2.1.B).

A continuación, se exploró más en profundidad el metabolismo de la glucosa y la glutamina mediante la realización de experimentos de metabolómica basada en ^{13}C utilizando en paralelo la [1,2-$^{13}C_2$]-glucosa y la [U-^{13}C]-glutamina como trazadores.

El experimento realizado con [1,2-$^{13}C_2$]-glucosa reveló que las células BJ-HRasV12 presentan un incremento en el flujo de glucosa a lactato vía glucólisis y vía PPP (Figura 5.2.2.A). Además, también presentan un incremento en el flujo de producción de lactato procedente de otras fuentes distintas de la glucosa.

Con el objetivo de evaluar el efecto de la mutación H-RasV12 sobre la PPP, se llevó a cabo el análisis de la distribución de isotopómeros de masa de la ribosa aislada de RNA. Primero se observó que las células BJ-HRasV12 sintetizaron más ribosa que las células BJ (Figura 5.2.2.B). Además, el análisis de la distribución isotopomérica de este metabolito mostró una activación tanto de la vía oxidativa como de la vía no oxidativa de la PPP. Con la finalidad de explicar los resultados obtenidos en cuanto a activación del flujo glucolítico y de la PPP, se determinó la actividad enzimática de algunas de las enzimas involucradas en estas vías (Figura 5.2.2.D). Enzimas clave como la HK, la gliceraldehido-3-fosfato deshidrogenasa (GAPDH) y la PK se encontraron incrementadas entre un 20 y un 400%. Asimismo, también se encontraron incrementadas las actividades de las enzimas de la PPP, G6PD y TKT. Sin embargo, paradójicamente la actividad LDH se encontró disminuida en las células BJ-HRasV12.

Posteriormente, se analizó también la distribución isotopomérica de varios metabolitos del ciclo de TCA para estudiar los efectos de la activación oncogénica de H-RAS sobre el metabolismo mitocondrial (Figura 5.2.3.A). El análisis de la distribución de isotopómeros de masa del glutamato reveló, en primer lugar, un incremento del porcentaje de moléculas de glutamato con carbonos procedentes de la glucosa en la células BJ-HRasV12 con respecto a las células BJ (Figura 5.2.3.B). En segundo lugar, también se constató que ambas líneas celulares emplean principalmente la enzima piruvato deshidrogenasa (PDH), en lugar de la piruvato carboxilasa (PC), para introducir los carbonos procedentes de la glucosa en la mitocondria (Figura 5.2.3.C). De manera análoga al glutamato, también se determinó un mayor porcentaje de carbonos procedentes de la glucosa en otros metabolitos del ciclo de TCA, como α-cetoglutarato, malato o fumarato (Figura 5.2.4).

La glutamina es uno de los principales sustratos metabólicos mitocondriales. Por tanto, para profundizar en el efecto de la activación oncogénica de H-RAS sobre el metabolismo mitocondrial y de la glutamina, las células fueron cultivadas en presencia de [U-^{13}C]-glutamina. Los resultados mostraron un incremento significativo en la marca de ^{13}C en todos los metabolitos del ciclo de TCA analizados en las células BJ-HRasV12 en comparación con las células BJ (Figura 5.2.4.B), indicando una activación del metabolismo mitocondrial y de la glutamina en las células mutadas.

Con el objetivo de complementar los resultados obtenidos a nivel de metabolismo mitocondrial, se analizó el consumo de oxígeno en presencia de diferentes sustratos metabólicos. Tal como se muestra en la Figura 5.2.6.A, se detectó que las células BJ-HRasV12 presentan un incremento en la respiración mitocondrial basal en medio basal (sin suplementar) y en presencia de glutamina en comparación con las células BJ, indicando que la activación oncogénica de H-RAS confiere a las células BJ una capacidad incrementada para la oxidación de glutamina en la mitocondria. Además, se detectó que el incremento en la respiración de glutamina estaba asociado a la producción de ATP (Figura 5.2.6.B), lo que sugiere que este sustrato es una fuente energética más importante en las células BJ-HRasV12 que en las BJ.

El metabolismo mitocondrial es una importante fuente de precursores para la síntesis de macromoléculas, como por ejemplo lípidos. Con la finalidad de estudiar los posibles cambios inducidos por la mutación H-RasV12 en la síntesis de lípidos, se analizó la distribución isotopomérica del palmitato, el primer ácido graso sintetizado en la lipogénesis. Así pues, se detectó en este ácido graso un incremento del porcentaje de carbonos procedentes tanto de glucosa como de glutamina en las células BJ-HRasV12 en comparación con las BJ (Figura 5.2.7.A-B). Además, el cálculo del porcentaje de cada nutriente que contribuye a la síntesis de lípidos permitió determinar que la glucosa consumida contribuye en mayor medida a la síntesis de ácidos grasos en las células BJ-HRasV12 (Figura 5.2.7.C). Por el contrario, aunque las células BJ-HRasV12 consumen una mayor cantidad de glutamina, ésta contribuye en menor medida a la síntesis de lípidos en comparación con las células BJ. Este hecho sugiere que parte de la glutamina consumida tiene un destino distinto en las células BJ-HRasV12 comparado con las BJ.

Además, la inhibición de la lipogénesis mediante el uso del inhibidor de la enzima ácido graso sintasa (FAS) C75 provocó una mayor inhibición de la proliferación en las células BJ-HRasV12 que en las BJ, en concordancia con los datos metabólicos previamente obtenidos y corroborando que esta vía metabólica juega un papel importante en la transformación mediada por H-RAS (Figura 5.2.7.D).

8.2.3. El papel de la G6PD en la línea celular de cáncer de colon HT29 y su regulación por la disponibilidad de glutamina y por las vías de señalización que estimulan la proliferación

En los capítulos anteriores se ha determinado que la actividad de la enzima G6PD y el flujo a través de la vía oxidativa de la PPP se encuentran incrementados en líneas celulares con la vía de RAS sobreactivada. Además, observaciones no publicadas realizadas en nuestro grupo de investigación han puesto de manifiesto un desbalance en el uso de la PPP a favor de la vía oxidativa en células de cáncer de colon. Por otro lado, la vía de RAS se encuentra frecuentemente activada en tumores de colon, principalmente a través de mutaciones en los genes *RAS* y *BRAF* (Phipps et al., 2013;

Pylayeva-Gupta et al., 2011; Yokota et al., 2011). En este capítulo, se exploró el papel de la G6PD como potencial punto de intervención terapéutica en líneas celulares con la vía de RAS sobreactivada, como es el caso de algunas líneas de cáncer de colon. Para ello i) se determinó la actividad G6PD en un panel de líneas celulares de cáncer de colon con diferente estado de activación de los genes *RAS* y *BRAF*, ii) se procedió a la inhibición de la G6PD en la línea de cáncer de colon que mostró una mayor actividad de esta enzima y se estudió el efecto sobre la proliferación y el ciclo celular, y iii) se profundizó en la regulación de este enzima por el metabolismo de la glutamina.

La actividad G6PD se encontró incrementada en todas las líneas celulares de cáncer de colon con mutaciones en *RAS* o *BRAF* en comparación con la línea celular control NCM460 (Figura 5.3.1.A), siendo la línea HT29 la que presentó un nivel más elevado. Dado que esta línea celular no presentaba mutaciones en *RAS* sino en *BRAF* (Ikediobi et al., 2006; Janakiraman et al., 2010; Loh et al., 2008; Oliveira et al., 2003; Tan et al., 2008), se validó el efecto de esta mutación sobre la G6PD con la finalidad de confirmar la relación entre ambos fenómenos. La inhibición de BRAF mediante el inhibidor químico PLX4720 indujo una inhibición de la expresión y de la actividad G6PD en comparación a la condición control, confirmando así dicha relación (Figura 5.3.1.B-C). Dado que la línea HT29 presentaba la mayor actividad de G6PD, se empleó esta línea celular para evaluar el papel de esta enzima en la proliferación, viabilidad y ciclo celular. Para ello se llevó a cabo la inhibición de la G6PD mediante RNAi (Figura 5.3.2.A-B-C), la cual no produjo cambios en ninguno de los aspectos examinados en comparación con las células transfectadas con el siRNA control (Figura 5.3.2.D-E).

La enzima G6PD se encuentra involucrada en la síntesis de NADPH. Por otro lado, algunos estudios sugieren que la glutamina puede ser utilizada para sintetizar NADPH, proporcionando carbonos al TCA para reacciones que sintetizan NADPH, como el ME. Por tanto, se evaluó el papel de la G6PD en la proliferación en ausencia de glutamina en busca de un efecto sinérgico entre la deprivación de glutamina y la inhibición de la G6PD. Sin embargo, no se detectaron cambios significativos entre las células transfectadas con el siRNA contra G6PD y las transfectadas con el siRNA control en presencia o ausencia de glutamina (Figura 5.3.3).

En los experimentos en ausencia de glutamina se detectó que las células no transfectadas sobreexpresaban la G6PD, tanto a nivel de RNA como de actividad, poniendo de relevancia la existencia de una relación metabólica entre ambas vías (Figura 5.3.4.A-B). Así pues, se procedió a estudiar en más profundidad esta relación. Se determinó que la falta de glutamina induce no solo la sobreexpresión de G6PD, sino también la transcripción de los genes *HMDX1* y *NQD1*, todos ellos genes diana del factor de transcripción NRF2 (Figura 5.3.4.C). Por tanto, se comprobó el nivel de proteína de este factor de transcripción y se constató un incremento de su expresión en ausencia de glutamina (Figura 5.3.4.E). Dado que el mecanismo principal de activación de NRF2 es mediante un incremento de los niveles de ROS intracelulares, se examinaron los niveles de ROS en ausencia y en presencia de glutamina (Figura 5.3.4.E). Así, se determinó que la falta de glutamina induce un incremento los niveles de ROS que podría explicar la activación de NRF2 y la consiguiente sobreexpresión de los genes diana analizados, entre ellos la enzima G6PD.

8.2.4 La vía de las pentosas fosfato como potencial diana antitumoral y su papel en el metabolismo tumoral en células de cáncer de mama MCF7

En este capítulo se examinó el potencial de las principales enzimas de la PPP, la G6PD y la TKT, como dianas antitumorales en células de cáncer de mama metastásico MCF7. Estudios previos demuestran que las células de cáncer mama, y en particular las células de cáncer mama avanzado, presentan elevados niveles de estrés oxidativo y una elevada dependencia de las vías de detoxificación de ROS (Brown and Bicknell, 2001; Jerby et al., 2012; Kang, 2002; Portakal et al., 2000; Toyokuni et al., 1995), por lo que, dado que una de las principales funciones de la PPP es controlar el nivel redox intracelular, es interesante explorar esta vía metabólica como potencial diana antitumoral en este tipo de tumores. Para ello i) se inhibieron las enzimas TKT y G6PD en la línea celular MCF7 mediante RNAi y se analizó la proliferación, viabilidad y ciclo celular, ii) se analizó el papel metabólico de estas enzimas mediante técnicas de metabolómica basada en ^{13}C utilizando como trazador la [1,2-$^{13}C_2$]-glucosa y iii) se

exploró la relación de la PPP con otras rutas metabólicas como el metabolismo de la glutamina, con la finalidad de explicar algunos de los resultados obtenidos.

Para determinar la importancia de la G6PD y la TKT en la proliferación, viabilidad y ciclo celular, ambas enzimas fueron inhibidas mediante RNAi en la línea celular MCF7 (Figura 5.4.1.A-B). Nuestros resultados mostraron que la inhibición de un 50% de la actividad G6PD reduce la proliferación celular en aproximadamente un 50%, disminuyendo al mismo tiempo la viabilidad en comparación con células transfectadas con un siRNA control (Figura 5.4.1.C). Por el contrario, la inhibición de la TKT no produjo efectos significativos sobre la proliferación ni la viabilidad. Asimismo, en ambas inhibiciones se detectó un leve incremento en la fracción de células en fase G1 y una disminución de la proporción en fase S (Figura 5.4.1.D). Dado que una de las funciones principales de la PPP es mantener la homeostasis redox, se determinaron los niveles de ROS en la inhibición de ambas enzimas y se observó que la inhibición de la G6PD induce un incremento en los niveles de ROS intracelulares en comparación con las células transfectadas con el siRNA control, mientras que no se detectaron cambios asociados a la inhibición de la TKT (Figura 5.4.2).

Con el objetivo de profundizar en los cambio metabólicos inducidos por la inhibición de ambas enzimas, se llevó a cabo un experimento de metabolómica basada en ^{13}C empleando [1,2-$^{13}C_2$]-glucosa. Este experimento reveló que la inhibición de la G6PD incrementa la producción de lactato y el consumo de glutamina (Figura 5.4.3.A). Por el contrario, la inhibición de la TKT reduce el consumo de glucosa y la producción de lactato pero aumenta el consumo de glutamina, aunque en menor magnitud que el observado en el caso de la G6PD. En ambas inhibiciones se observó un descenso en la síntesis *de novo* de ribosa (Figura 5.4.3.B). Analizando los efectos sobre la PPP en más profundidad, se observó que la inhibición de la G6PD redujo levemente (10%) la cantidad de ribosa sintetizada por la vía oxidativa. Sin embargo, la inhibición de la TKT disminuyó de manera notable (50%) la síntesis a través de la vía no oxidativa, al mismo tiempo que aumentaba el porcentaje de ribosa sintetizada por la vía oxidativa (Figura 5.4.3.C-D). Ello indica que la TKT ejerce un mayor control sobre la rama de la PPP en la que participa que la G6PD sobre su respectiva en células MCF7.

Por otro lado, los resultados también mostraron que la inhibición de la TKT induce una disminución proporcional tanto del flujo glucolítico como del flujo de lactato sintetizado a través de la PPP, mientras que, por el contrario, en el caso de la G6PD se produjo un incremento no proporcional de ambos flujos (Figura 5.4.3.E). Así la inhibición de la G6PD disminuyó el ratio entre los flujos PPP/glucólisis (Figura 5.4.3.F), indicando un bloqueo de la entrada de carbonos procedentes de la glucólisis en la vía oxidativa de la PPP.

La PPP es una las principales rutas metabólicas que sintetizan NADPH, necesario, entre otras cosas, para la síntesis de lípidos. Así pues, se examinó la síntesis de palmitato mediante el análisis de la incorporación de ^{13}C en este ácido graso (Figura 5.4.4). Los resultados revelaron una notable disminución de la síntesis de palmitato bajo la inhibición de la G6PD mientras que no se detectaron cambios cuando se inhibió la TKT.

Uno de los resultados más sorprendentes obtenidos fue el incremento del consumo de glutamina asociado a la inhibición de ambas enzimas. La glutamina interviene en funciones energéticas, anabólicas y de mantenimiento redox. Para profundizar en la relación entre el metabolismo de la glutamina y la PPP, se llevaron a cabo inhibiciones de la TKT y la G6PD en presencia y ausencia de glutamina y se analizaron los niveles de ROS, glutatión y el ratio ATP/ADP. Estos ensayos pusieron de manifiesto que el incremento observado en el consumo de glutamina es necesario para el mantenimiento de la homeostasis energética (ratio ATP/ADP) (Figura 5.4.5.C). Así pues, ya que la homeostasis energética es importante en la proliferación y supervivencia celular, se estudió el efecto de la deprivación de glutamina en combinación con la inhibición de la TKT y la G6PD sobre la proliferación celular. Sin embargo, si bien se confirmó la disminución de la proliferación cuando la G6PD es inhibida, no se encontraron diferencias adicionales cuando la TKT o la G6PD fueron inhibidas en ausencia de glutamina (Figura 5.4.5.D).

8.3. CONCLUSIONES

1. La combinación del estudio de la distribución de flujos con el MCA basado en el análisis de los signos de los coeficientes de control de signo fijo, es una aproximación válida para identificar las enzimas clave involucradas en la reprogramación metabólica inducida por K-RAS. El uso de esta metodología nos ha permitido identificar un incremento en los flujos glucolítico y a través de la PPP como características básicas de la reprogramación metabólica inducida por K-RAS, así como proponer la G6PD, la PK y la LDH como enzimas clave responsables de dicha reprogramación.

2. La activación oncogénica de H-RAS reprograma el metabolismo de la glucosa y la glutamina a través del incremento de los flujos glucolítico y a través de la PPP así como del metabolismo mitocondrial. La glutamina es responsable de la activación del metabolismo mitocondrial en las células BJ-HRasV12, mientras que los carbonos procedentes de la glucosa que llegan a la mitocondria son principalmente utilizados en la lipogénesis. Además, la lipogénesis se encuentra sobreactivada en las células BJ-HRasV12, las cuales son más sensibles que las células BJ a la inhibición de la enzima FAS.

3. La enzima G6PD se encuentra sobreactivada en células de cáncer de colon con la vía de señalización de RAS activada. Sin embargo, G6PD no es esencial para la proliferación y supervivencia de la línea celular HT29 que tiene BRAF mutado (efector *downstream* de RAS). Además, se ha identificado una nueva conexión entre la PPP y el metabolismo de la glutamina en células HT29, según la cual la G6PD se sobreexpresa en condiciones de deprivación de glutamina a través de un mecanismo en el que tiene lugar el incremento de los niveles de ROS y la activación del factor de transcripción NRF2.

4. La enzima G6PD es importante en la proliferación, supervivencia y regulación de los niveles de ROS en células de cáncer de mama MCF7. Sin embargo, regula de manera poco significativa el flujo de síntesis de ribosa a través de la vía oxidativa de la PPP.

La inhibición de la G6PD aumenta el flujo glucolítico, promueve la secreción de lactato e incrementa el consumo de glutamina, siendo este último metabolito utilizado para mantener la homeostasis energética, aunque no es esencial para la proliferación celular.

5. La enzima TKT no es esencial para la proliferación de la línea celular de cáncer de mama MCF7, pero sin embargo regula de manera significativa el flujo de síntesis de ribosa a través de la vía no oxidativa de la PPP. La inhibición de la TKT reduce el flujo glucolítico e incrementa el consumo de glutamina, siendo este último metabolito utilizado para mantener la homeostasis energética pero no es imprescindible para la proliferación celular.

9. REFERENCES

9. REFERENCES

Adams, J. M., and Cory, S. (2007). The Bcl-2 apoptotic switch in cancer development and therapy. Oncogene *26*, 1324-1337.

Adekola, K., Rosen, S. T., and Shanmugam, M. (2012). Glucose transporters in cancer metabolism. Curr Opin Oncol *24*, 650-654.

Agius, L. (1998). The physiological role of glucokinase binding and translocation in hepatocytes. Adv Enzyme Regul *38*, 303-331.

Ahn, W. S., and Antoniewicz, M. R. (2013). Parallel labeling experiments with [1,2-(13)C]glucose and [U-(13)C]glutamine provide new insights into CHO cell metabolism. Metab Eng *15*, 34-47.

Al Zaid Siddiquee, K., Arauzo-Bravo, M. J., and Shimizu, K. (2004). Metabolic flux analysis of pykF gene knockout Escherichia coli based on 13C-labeling experiments together with measurements of enzyme activities and intracellular metabolite concentrations. Appl Microbiol Biotechnol *63*, 407-417.

Alcarraz-Vizan, G., Boren, J., Lee, W. N., and Cascante, M. (2010). Histone deacetylase inhibition results in a common metabolic profile associated with HT29 differentiation. Metabolomics 6, 229-237.

Anastasiou, D., Poulogiannis, G., Asara, J. M., Boxer, M. B., Jiang, J. K., Shen, M., Bellinger, G., Sasaki, A. T., Locasale, J. W., Auld, D. S., et al. (2011). Inhibition of pyruvate kinase M2 by reactive oxygen species contributes to cellular antioxidant responses. Science 334, 1278-1283.

Antoniewicz, M. R. (2013). C metabolic flux analysis: optimal design of isotopic labeling experiments. Curr Opin Biotechnol.

Antoniewicz, M. R., Kelleher, J. K., and Stephanopoulos, G. (2006). Determination of confidence intervals of metabolic fluxes estimated from stable isotope measurements. Metab Eng 8, 324-337.

Antoniewicz, M. R., Kelleher, J. K., and Stephanopoulos, G. (2007). Elementary metabolite units (EMU): a novel framework for modeling isotopic distributions. Metab Eng 9, 68-86.

Asensio, C., Levoin, N., Guillaume, C., Guerquin, M. J., Rouguieg, K., Chretien, F., Chapleur, Y., Netter, P., Minn, A., and Lapicque, F. (2007). Irreversible inhibition of glucose-6-phosphate dehydrogenase by the coenzyme A conjugate of ketoprofen: a key to oxidative stress induced by non-steroidal anti-inflammatory drugs? Biochem Pharmacol 73, 405-416.

Au, S. W., Gover, S., Lam, V. M., and Adams, M. J. (2000). Human glucose-6-phosphate dehydrogenase: the crystal structure reveals a structural NADP(+) molecule and provides insights into enzyme deficiency. Structure 8, 293-303.

Baldazzi, V., Ropers, D., Markowicz, Y., Kahn, D., Geiselmann, J., and de Jong, H. (2010). The carbon assimilation network in Escherichia coli is densely connected and largely sign-determined by directions of metabolic fluxes. PLoS Comput Biol 6, e1000812.

Barata, J. T., Silva, A., Brandao, J. G., Nadler, L. M., Cardoso, A. A., and Boussiotis, V. A. (2004). Activation of PI3K is indispensable for interleukin 7-mediated viability, proliferation, glucose use, and growth of T cell acute lymphoblastic leukemia cells. J Exp Med 200, 659-669.

Bauer, D. E., Hatzivassiliou, G., Zhao, F., Andreadis, C., and Thompson, C. B. (2005). ATP citrate lyase is an important component of cell growth and transformation. Oncogene 24, 6314-6322.

Baxter, C. J., Liu, J. L., Fernie, A. R., and Sweetlove, L. J. (2007). Determination of metabolic fluxes in a non-steady-state system. Phytochemistry 68, 2313-2319.

Beckers, A., Organe, S., Timmermans, L., Scheys, K., Peeters, A., Brusselmans, K., Verhoeven, G., and Swinnen, J. V. (2007). Chemical inhibition of acetyl-CoA carboxylase induces growth arrest and cytotoxicity selectively in cancer cells. Cancer Res 67, 8180-8187.

Bellavia, M., Gioviale, M. C., Damiano, G., Palumbo, V. D., Spinelli, G., Buscemi, G., and Lo Monte, A. I. (2012). Dissecting the different biological effects of oncogenic Ras isoforms in cancer cell lines: Could stimulation of oxidative stress be the one more weapon of H-Ras?: Regulation of oxidative stress and Ras biological effects. Med Hypotheses.

Bensinger, S. J., and Christofk, H. R. (2012). New aspects of the Warburg effect in cancer cell biology. Semin Cell Dev Biol 23, 352-361.

Berwick, D. C., Hers, I., Heesom, K. J., Moule, S. K., and Tavare, J. M. (2002). The identification of ATP-citrate lyase as a protein kinase B (Akt) substrate in primary adipocytes. J Biol Chem 277, 33895-33900.

Berx, G., and van Roy, F. (2009). Involvement of members of the cadherin superfamily in cancer. Cold Spring Harb Perspect Biol 1, a003129.

Blasco, M. A. (2005). Telomeres and human disease: ageing, cancer and beyond. Nat Rev Genet 6, 611-622.

Blum, R., Jacob-Hirsch, J., Amariglio, N., Rechavi, G., and Kloog, Y. (2005). Ras inhibition in glioblastoma down-regulates hypoxia-inducible factor-1alpha, causing glycolysis shutdown and cell death. Cancer Res 65, 999-1006.

Bonnet, S., Archer, S. L., Allalunis-Turner, J., Haromy, A., Beaulieu, C., Thompson, R., Lee, C. T., Lopaschuk, G. D., Puttagunta, L., Harry, G., et al. (2007). A mitochondria-K+ channel axis is suppressed in cancer and its normalization promotes apoptosis and inhibits cancer growth. Cancer Cell 11, 37-51.

Boonstra, J., and Post, J. A. (2004). Molecular events associated with reactive oxygen species and cell cycle progression in mammalian cells. Gene 337, 1-13.

Boren, J., Cascante, M., Marin, S., Comin-Anduix, B., Centelles, J. J., Lim, S., Bassilian, S., Ahmed, S., Lee, W. N., and Boros, L. G. (2001). Gleevec (STI571) influences metabolic enzyme activities and glucose carbon flow toward nucleic acid and fatty acid synthesis in myeloid tumor cells. J Biol Chem 276, 37747-37753.

Boren, J., Lee, W. N., Bassilian, S., Centelles, J. J., Lim, S., Ahmed, S., Boros, L. G., and Cascante, M. (2003). The stable isotope-based dynamic metabolic profile of butyrate-induced HT29 cell differentiation. J Biol Chem 278, 28395-28402.

Boren, J., Montoya, A. R., de Atauri, P., Comin-Anduix, B., Cortes, A., Centelles, J. J., Frederiks, W. M., Van Noorden, C. J., and Cascante, M. (2002). Metabolic control analysis aimed at the ribose synthesis pathways of tumor cells: a new strategy for antitumor drug development. Mol Biol Rep 29, 7-12.

Borodina, I., and Nielsen, J. (2005). From genomes to in silico cells via metabolic networks. Curr Opin Biotechnol 16, 350-355.

Boros, L. G., Lee, P. W. N., Brandes, J. L., Cascante, M., Muscarella, P., Schirmer, W. J., Melvin, W. S., and Ellison, E. C. (1998). Nonoxidative pentose phosphate pathways and their direct role in ribose synthesis in tumors: is cancer a disease of cellular glucose metabolism? Medical Hypotheses 50, 55-59.

Boros, L. G., Lerner, M. R., Morgan, D. L., Taylor, S. L., Smith, B. J., Postier, R. G., and Brackett, D. J. (2005). [1,2-13C2]-D-glucose profiles of the serum, liver, pancreas, and DMBA-induced pancreatic tumors of rats. Pancreas 31, 337-343.

Boros, L. G., Puigjaner, J., Cascante, M., Lee, W.-N. P., Brandes, J. L., Bassilian, S., Yusuf, F. I., Williams, R. D., Muscarella, P., Melvin, W. S., and Schirmer, W. J. (1997a). Oxythiamine and Dehydroepiandrosterone Inhibit the Nonoxidative Synthesis of Ribose and Tumor Cell Proliferation. Cancer Res 57, 4242-4248.

Boros, L. G., Puigjaner, J., Cascante, M., Lee, W. N., Brandes, J. L., Bassilian, S., Yusuf, F. I., Williams, R. D., Muscarella, P., Melvin, W. S., and Schirmer, W. J. (1997b). Oxythiamine and dehydroepiandrosterone inhibit the nonoxidative synthesis of ribose and tumor cell proliferation. Cancer Res 57, 4242-4248.

Brimacombe, K. R., Anastasiou, D., Hong, B. S., Tempel, W., Dimov, S., Veith, H., Auld, D. S., Vander Heiden, M. G., Thomas, C. J., Park, H. W., et al. (2010). ML285 affects reactive oxygen species' inhibition of pyruvate kinase M2.

Brown, N. S., and Bicknell, R. (2001). Hypoxia and oxidative stress in breast cancer. Oxidative stress: its effects on the growth, metastatic potential and response to therapy of breast cancer. Breast Cancer Res 3, 323-327.

Burgess, S. C., He, T., Yan, Z., Lindner, J., Sherry, A. D., Malloy, C. R., Browning, J. D., and Magnuson, M. A. (2007). Cytosolic phosphoenolpyruvate carboxykinase does not solely control the rate of hepatic gluconeogenesis in the intact mouse liver. Cell Metab 5, 313-320.

Burkhart, D. L., and Sage, J. (2008). Cellular mechanisms of tumour suppression by the retinoblastoma gene. Nat Rev Cancer 8, 671-682.

Butler, E. B., Zhao, Y., Munoz-Pinedo, C., Lu, J., and Tan, M. (2013). Stalling the engine of resistance: targeting cancer metabolism to overcome therapeutic resistance. Cancer Res 73, 2709-2717.

Cantor, J. R., and Sabatini, D. M. (2012). Cancer cell metabolism: one hallmark, many faces. Cancer Discov 2, 881-898.

Caro, P., Kishan, A. U., Norberg, E., Stanley, I. A., Chapuy, B., Ficarro, S. B., Polak, K., Tondera, D., Gounarides, J., Yin, H., et al. (2012). Metabolic signatures uncover distinct targets in molecular subsets of diffuse large B cell lymphoma. Cancer Cell 22, 547-560.

Cascante, M., Boros, L. G., Comin-Anduix, B., de Atauri, P., Centelles, J. J., and Lee, P. W. (2002). Metabolic control analysis in drug discovery and disease. Nature biotechnology 20, 243-249.

Cascante, M., Centelles, J. J., Veech, R. L., Lee, W. N., and Boros, L. G. (2000). Role of thiamin (vitamin B-1) and transketolase in tumor cell proliferation. Nutr Cancer 36, 150-154.

Cascante, M., Franco, R., and Canela, E. I. (1989a). Use of implicit methods from general sensitivity theory to develop a systematic approach to metabolic control. I. Unbranched pathways. Math Biosci 94, 271-288.

Cascante, M., Franco, R., and Canela, E. I. (1989b). Use of implicit methods from general sensitivity theory to develop a systematic approach to metabolic control. II. Complex systems. Math Biosci 94, 289-309.

Cascante, M., and Marin, S. (2008). Metabolomics and fluxomics approaches. Essays Biochem 45, 67-81.

Clem, B., Telang, S., Clem, A., Yalcin, A., Meier, J., Simmons, A., Rasku, M. A., Arumugam, S., Dean, W. L., Eaton, J., et al. (2008). Small-molecule inhibition of 6-phosphofructo-2-kinase activity suppresses glycolytic flux and tumor growth. Mol Cancer Ther 7, 110-120.

Collins, J. M., Neville, M. J., Pinnick, K. E., Hodson, L., Ruyter, B., van Dijk, T. H., Reijngoud, D. J., Fielding, M. D., and Frayn, K. N. (2011). De novo lipogenesis in the differentiating human adipocyte can provide all fatty acids necessary for maturation. J Lipid Res 52, 1683-1692.

Comin-Anduix, B., Boren, J., Martinez, S., Moro, C., Centelles, J. J., Trebukhina, R., Petushok, N., Lee, W. N., Boros, L. G., and Cascante, M. (2001). The effect of thiamine supplementation on tumour proliferation. A metabolic control analysis study. Eur J Biochem 268, 4177-4182.

Cook, J. A., Gius, D., Wink, D. A., Krishna, M. C., Russo, A., and Mitchell, J. B. (2004). Oxidative stress, redox, and the tumor microenvironment. Semin Radiat Oncol 14, 259-266.

Cornish-Bowden, A. (2000). Fundamentals of enzyme kinetics, Third edn (London: Portland Press).

Coy, J. F., Dressler, D., Wilde, J., and Schubert, P. (2005). Mutations in the transketolase-like gene TKTL1: clinical implications for neurodegenerative diseases, diabetes and cancer. Clin Lab 51, 257-273.

Crown, S. B., and Antoniewicz, M. R. (2013). Parallel labeling experiments and metabolic flux analysis: Past, present and future methodologies. Metab Eng 16, 21-32.

Chandel, N. S., Maltepe, E., Goldwasser, E., Mathieu, C. E., Simon, M. C., and Schumacker, P. T. (1998). Mitochondrial reactive oxygen species trigger hypoxia-induced transcription. Proc Natl Acad Sci U S A 95, 11715-11720.

Chen, C., Pore, N., Behrooz, A., Ismail-Beigi, F., and Maity, A. (2001). Regulation of glut1 mRNA by hypoxia-inducible factor-1. Interaction between H-ras and hypoxia. J Biol Chem 276, 9519-9525.

Chen, E. I., Hewel, J., Krueger, J. S., Tiraby, C., Weber, M. R., Kralli, A., Becker, K., Yates, J. R., 3rd, and Felding-Habermann, B. (2007). Adaptation of energy metabolism in breast cancer brain metastases. Cancer Res 67, 1472-1486.

Cheng, M. L., Ho, H. Y., Wu, Y. H., and Chiu, D. T. (2004). Glucose-6-phosphate dehydrogenase-deficient cells show an increased propensity for oxidant-induced senescence. Free Radic Biol Med 36, 580-591.

Cheung, E. C., Ludwig, R. L., and Vousden, K. H. (2012). Mitochondrial localization of TIGAR under hypoxia stimulates HK2 and lowers ROS and cell death. Proc Natl Acad Sci U S A 109, 20491-20496.

Chiaradonna, F., Gaglio, D., Vanoni, M., and Alberghina, L. (2006a). Expression of transforming K-Ras oncogene affects mitochondrial function and morphology in mouse fibroblasts. Biochim Biophys Acta 1757, 1338-1356.

Chiaradonna, F., Sacco, E., Manzoni, R., Giorgio, M., Vanoni, M., and Alberghina, L. (2006b). Ras-dependent carbon metabolism and transformation in mouse fibroblasts. Oncogene 25, 5391-5404.

Chun, S. Y., Johnson, C., Washburn, J. G., Cruz-Correa, M. R., Dang, D. T., and Dang, L. H. (2010). Oncogenic KRAS modulates mitochondrial metabolism in human colon cancer cells by inducing HIF-1alpha and HIF-2alpha target genes. Mol Cancer 9, 293.

Dang, C. V., Le, A., and Gao, P. (2009). MYC-induced cancer cell energy metabolism and therapeutic opportunities. Clin Cancer Res 15, 6479-6483.

Davies, M. A., and Samuels, Y. (2010). Analysis of the genome to personalize therapy for melanoma. Oncogene 29, 5545-5555.

de Atauri, P., Benito, A., Vizan, P., Zanuy, M., Mangues, R., Marin, S., and Cascante, M. (2011). Carbon metabolism and the sign of control coefficients in metabolic

adaptations underlying K-ras transformation. Biochim Biophys Acta 1807, 746-754.

de Groof, A. J., te Lindert, M. M., van Dommelen, M. M., Wu, M., Willemse, M., Smift, A. L., Winer, M., Oerlemans, F., Pluk, H., Fransen, J. A., and Wieringa, B. (2009). Increased OXPHOS activity precedes rise in glycolytic rate in H-RasV12/E1A transformed fibroblasts that develop a Warburg phenotype. Mol Cancer 8, 54.

DeBerardinis, R. J., and Cheng, T. (2010). Q's next: the diverse functions of glutamine in metabolism, cell biology and cancer. Oncogene 29, 313-324.

DeBerardinis, R. J., Lum, J. J., Hatzivassiliou, G., and Thompson, C. B. (2008). The biology of cancer: metabolic reprogramming fuels cell growth and proliferation. Cell Metab 7, 11-20.

Deberardinis, R. J., Lum, J. J., and Thompson, C. B. (2006). Phosphatidylinositol 3-kinase-dependent modulation of carnitine palmitoyltransferase 1A expression regulates lipid metabolism during hematopoietic cell growth. J Biol Chem 281, 37372-37380.

DeBerardinis, R. J., Mancuso, A., Daikhin, E., Nissim, I., Yudkoff, M., Wehrli, S., and Thompson, C. B. (2007). Beyond aerobic glycolysis: transformed cells can engage in glutamine metabolism that exceeds the requirement for protein and nucleotide synthesis. Proc Natl Acad Sci U S A 104, 19345-19350.

DeNicola, G. M., Karreth, F. A., Humpton, T. J., Gopinathan, A., Wei, C., Frese, K., Mangal, D., Yu, K. H., Yeo, C. J., Calhoun, E. S., et al. (2011). Oncogene-induced Nrf2 transcription promotes ROS detoxification and tumorigenesis. Nature 475, 106-109.

Denkert, C., Budczies, J., Weichert, W., Wohlgemuth, G., Scholz, M., Kind, T., Niesporek, S., Noske, A., Buckendahl, A., Dietel, M., and Fiehn, O. (2008). Metabolite profiling of human colon carcinoma--deregulation of TCA cycle and amino acid turnover. Mol Cancer 7, 72.

Denko, N. C. (2008). Hypoxia, HIF1 and glucose metabolism in the solid tumour. Nat Rev Cancer.

Dolado, I., Swat, A., Ajenjo, N., De Vita, G., Cuadrado, A., and Nebreda, A. R. (2007). p38alpha MAP kinase as a sensor of reactive oxygen species in tumorigenesis. Cancer Cell 11, 191-205.

Drabovich, A. P., Pavlou, M. P., Dimitromanolakis, A., and Diamandis, E. P. (2012). Quantitative analysis of energy metabolic pathways in MCF-7 breast cancer cells by selected reaction monitoring assay. Mol Cell Proteomics.

Eagle, H. (1955). Nutrition needs of mammalian cells in tissue culture. Science 122, 501-514.

Edinger, A. L., and Thompson, C. B. (2002). Akt maintains cell size and survival by increasing mTOR-dependent nutrient uptake. Mol Biol Cell 13, 2276-2288.

Eggleston, L. V., and Krebs, H. A. (1974). Regulation of the pentose phosphate cycle. Biochem J 138, 425-435.

Elstrom, R. L., Bauer, D. E., Buzzai, M., Karnauskas, R., Harris, M. H., Plas, D. R., Zhuang, H., Cinalli, R. M., Alavi, A., Rudin, C. M., and Thompson, C. B. (2004). Akt stimulates aerobic glycolysis in cancer cells. Cancer Res 64, 3892-3899.

Faraonio, R., Vergara, P., Di Marzo, D., Pierantoni, M. G., Napolitano, M., Russo, T., and Cimino, F. (2006). p53 suppresses the Nrf2-dependent transcription of antioxidant response genes. J Biol Chem 281, 39776-39784.

Fell, D. A. (1997). Understanding the control of metabolism, (London: Portland Press).

Fell, D. A., and Sauro, H. M. (1985). Metabolic control and its analysis. Additional relationships between elasticities and control coefficients. Eur J Biochem 148, 555-561.

Ferlay, J., Shin, H., Bray, F., Forman, D., Mathers, C., and Parkin, D. (2010). GLOBOCAN 2008 v2.0, Cancer Incidence and Mortality Worldwide: IARC CancerBase No. 10 [Internet]. In, (International Agency for Research on Cancer. Available from: http://globocan.iarc.fr, accessed on day/month/year).

Fernandez-Medarde, A., and Santos, E. (2011). Ras in cancer and developmental diseases. Genes Cancer 2, 344-358.

Ferrara, N. (2009). Vascular endothelial growth factor. Arteriosclerosis, thrombosis, and vascular biology 29, 789-791.

Fico, A., Paglialunga, F., Cigliano, L., Abrescia, P., Verde, P., Martini, G., Iaccarino, I., and Filosa, S. (2004). Glucose-6-phosphate dehydrogenase plays a crucial role in protection from redox-stress-induced apoptosis. Cell Death Differ 11, 823-831.

Fiehn, O. (2002). Metabolomics--the link between genotypes and phenotypes. Plant Mol Biol 48, 155-171.

Fritz, V., Benfodda, Z., Rodier, G., Henriquet, C., Iborra, F., Avances, C., Allory, Y., de la Taille, A., Culine, S., Blancou, H., et al. Abrogation of de novo lipogenesis by stearoyl-CoA desaturase 1 inhibition interferes with oncogenic signaling and blocks prostate cancer progression in mice. Mol Cancer Ther 9, 1740-1754.

Furuta, E., Pai, S. K., Zhan, R., Bandyopadhyay, S., Watabe, M., Mo, Y. Y., Hirota, S., Hosobe, S., Tsukada, T., Miura, K., et al. (2008). Fatty acid synthase gene is up-regulated by hypoxia via activation of Akt and sterol regulatory element binding protein-1. Cancer Res 68, 1003-1011.

Gaglio, D., Metallo, C. M., Gameiro, P. A., Hiller, K., Danna, L. S., Balestrieri, C., Alberghina, L., Stephanopoulos, G., and Chiaradonna, F. (2011). Oncogenic K-Ras decouples glucose and glutamine metabolism to support cancer cell growth. Mol Syst Biol 7, 523.

Gaglio, D., Soldati, C., Vanoni, M., Alberghina, L., and Chiaradonna, F. (2009). Glutamine deprivation induces abortive s-phase rescued by deoxyribonucleotides in k-ras transformed fibroblasts. PLoS One 4, e4715.

Gameiro, P. A., Yang, J., Metelo, A. M., Perez-Carro, R., Baker, R., Wang, Z., Arreola, A., Rathmell, W. K., Olumi, A., Lopez-Larrubia, P., et al. (2013). In vivo HIF-mediated reductive carboxylation is regulated by citrate levels and sensitizes VHL-deficient cells to glutamine deprivation. Cell Metab 17, 372-385.

Ganan-Gomez, I., Wei, Y., Yang, H., Boyano-Adanez, M. C., and Garcia-Manero, G. (2013). Oncogenic functions of the transcription factor Nrf2. Free Radic Biol Med.

Gao, L. P., Cheng, M. L., Chou, H. J., Yang, Y. H., Ho, H. Y., and Chiu, D. T. (2009a). Ineffective GSH regeneration enhances G6PD-knockdown Hep G2 cell sensitivity to diamide-induced oxidative damage. Free Radic Biol Med 47, 529-535.

Gao, P., Tchernyshyov, I., Chang, T. C., Lee, Y. S., Kita, K., Ochi, T., Zeller, K. I., De Marzo, A. M., Van Eyk, J. E., Mendell, J. T., and Dang, C. V. (2009b). c-Myc suppression of miR-23a/b enhances mitochondrial glutaminase expression and glutamine metabolism. Nature.

Gordan, J. D., Thompson, C. B., and Simon, M. C. (2007). HIF and c-Myc: sibling rivals for control of cancer cell metabolism and proliferation. Cancer Cell 12, 108-113.

Guerrero, S., Casanova, I., Farre, L., Mazo, A., Capella, G., and Mangues, R. (2000). K-ras codon 12 mutation induces higher level of resistance to apoptosis and predisposition to anchorage-independent growth than codon 13 mutation or proto-oncogene overexpression. Cancer Res 60, 6750-6756.

Guerrero, S., Figueras, A., Casanova, I., Farre, L., Lloveras, B., Capella, G., Trias, M., and Mangues, R. (2002). Codon 12 and codon 13 mutations at the K-ras gene induce different soft tissue sarcoma types in nude mice. FASEB J 16, 1642-1644.

Guppy, M., Greiner, E., and Brand, K. (1993). The role of the Crabtree effect and an endogenous fuel in the energy metabolism of resting and proliferating thymocytes. Eur J Biochem 212, 95-99.

Guppy, M., Leedman, P., Zu, X., and Russell, V. (2002). Contribution by different fuels and metabolic pathways to the total ATP turnover of proliferating MCF-7 breast cancer cells. Biochem J 364, 309-315.

Hahn, W. C., Counter, C. M., Lundberg, A. S., Beijersbergen, R. L., Brooks, M. W., and Weinberg, R. A. (1999). Creation of human tumour cells with defined genetic elements. Nature 400, 464-468.

Hamad, N. M., Elconin, J. H., Karnoub, A. E., Bai, W., Rich, J. N., Abraham, R. T., Der, C. J., and Counter, C. M. (2002). Distinct requirements for Ras oncogenesis in human versus mouse cells. Genes Dev 16, 2045-2057.

Hanahan, D., and Folkman, J. (1996). Patterns and emerging mechanisms of the angiogenic switch during tumorigenesis. Cell 86, 353-364.

Hanahan, D., and Weinberg, R. A. (2011). Hallmarks of cancer: the next generation. Cell 144, 646-674.

Hatzivassiliou, G., Zhao, F., Bauer, D. E., Andreadis, C., Shaw, A. N., Dhanak, D., Hingorani, S. R., Tuveson, D. A., and Thompson, C. B. (2005). ATP citrate lyase inhibition can suppress tumor cell growth. Cancer Cell 8, 311-321.

Hellerstein, M. K., and Neese, R. A. (1992). Mass isotopomer distribution analysis: a technique for measuring biosynthesis and turnover of polymers. Am J Physiol 263, E988-1001.

Hiller, K., and Metallo, C. M. (2012). Profiling metabolic networks to study cancer metabolism. Curr Opin Biotechnol.

Ho, H. Y., Cheng, M. L., Lu, F. J., Chou, Y. H., Stern, A., Liang, C. M., and Chiu, D. T. (2000). Enhanced oxidative stress and accelerated cellular senescence in glucose-6-phosphate dehydrogenase (G6PD)-deficient human fibroblasts. Free Radic Biol Med 29, 156-169.

Holleran, A. L., Briscoe, D. A., Fiskum, G., and Kelleher, J. K. (1995). Glutamine metabolism in AS-30D hepatoma cells. Evidence for its conversion into lipids via reductive carboxylation. Mol Cell Biochem 152, 95-101.

Hornberg, J. J., Bruggeman, F. J., Bakker, B. M., and Westerhoff, H. V. (2007). Metabolic control analysis to identify optimal drug targets. Prog Drug Res 64, 171, 173-189.

Hu, L. H., Yang, J. H., Zhang, D. T., Zhang, S., Wang, L., Cai, P. C., Zheng, J. F., and Huang, J. S. (2007). The TKTL1 gene influences total transketolase activity and cell proliferation in human colon cancer LoVo cells. Anticancer Drugs 18, 427-433.

Hu, W., Zhang, C., Wu, R., Sun, Y., Levine, A., and Feng, Z. (2010). Glutaminase 2, a novel p53 target gene regulating energy metabolism and antioxidant function. Proc Natl Acad Sci U S A 107, 7455-7460.

Hu, Y., Lu, W., Chen, G., Wang, P., Chen, Z., Zhou, Y., Ogasawara, M., Trachootham, D., Feng, L., Pelicano, H., et al. (2012). K-ras(G12V) transformation leads to mitochondrial dysfunction and a metabolic switch from oxidative phosphorylation to glycolysis. Cell Res.

Hynes, N. E., and MacDonald, G. (2009). ErbB receptors and signaling pathways in cancer. Curr Opin Cell Biol 21, 177-184.

Ikediobi, O. N., Davies, H., Bignell, G., Edkins, S., Stevens, C., O'Meara, S., Santarius, T., Avis, T., Barthorpe, S., Brackenbury, L., et al. (2006). Mutation analysis of 24 known cancer genes in the NCI-60 cell line set. Mol Cancer Ther 5, 2606-2612.

Irani, K., Xia, Y., Zweier, J. L., Sollott, S. J., Der, C. J., Fearon, E. R., Sundaresan, M., Finkel, T., and Goldschmidt-Clermont, P. J. (1997). Mitogenic signaling mediated by oxidants in Ras-transformed fibroblasts. Science 275, 1649-1652.

Ishimoto, T., Nagano, O., Yae, T., Tamada, M., Motohara, T., Oshima, H., Oshima, M., Ikeda, T., Asaba, R., Yagi, H., et al. (2011). CD44 variant regulates redox status in cancer cells by stabilizing the xCT subunit of system xc(-) and thereby promotes tumor growth. Cancer Cell 19, 387-400.

Janakiraman, M., Vakiani, E., Zeng, Z., Pratilas, C. A., Taylor, B. S., Chitale, D., Halilovic, E., Wilson, M., Huberman, K., Ricarte Filho, J. C., et al. (2010). Genomic and biological characterization of exon 4 KRAS mutations in human cancer. Cancer Res 70, 5901-5911.

Jarry, A., Masson, D., Cassagnau, E., Parois, S., Laboisse, C., and Denis, M. G. (2004). Real-time allele-specific amplification for sensitive detection of the BRAF mutation V600E. Mol Cell Probes 18, 349-352.

Jeon, S. M., Chandel, N. S., and Hay, N. (2012). AMPK regulates NADPH homeostasis to promote tumour cell survival during energy stress. Nature 485, 661-665.

Jerby, L., Wolf, L., Denkert, C., Stein, G. Y., Hilvo, M., Oresic, M., Geiger, T., and Ruppin, E. (2012). Metabolic associations of reduced proliferation and oxidative stress in advanced breast cancer. Cancer Res 72, 5712-5720.

Jiang, P., Du, W., Wang, X., Mancuso, A., Gao, X., Wu, M., and Yang, X. (2011). p53 regulates biosynthesis through direct inactivation of glucose-6-phosphate dehydrogenase. Nat Cell Biol 13, 310-316.

Jones, N. P., and Schulze, A. (2011). Targeting cancer metabolism - aiming at a tumour's sweet-spot. Drug Discov Today.

Jones, R. G., and Thompson, C. B. (2009). Tumor suppressors and cell metabolism: a recipe for cancer growth. Genes Dev 23, 537-548.

Junttila, M. R., and Evan, G. I. (2009). p53--a Jack of all trades but master of none. Nat Rev Cancer 9, 821-829.

Kacser, H., and Acerenza, L. (1993). A universal method for achieving increases in metabolite production. Eur J Biochem 216, 361-367.

Kacser, H., and Burns, J. A. (1973). The control of flux. Symp Soc Exp Biol 27, 65-104.

Kalas, W., Rybka, J., Swiderek, E., Ziolo, E., Rybka, W., Gamian, A., Rak, J., and Strzadala, L. (2012). H-Ras increases release of sphingosine resulting in down-regulation of TSP-1 in non-transformed cells. Int J Exp Pathol.

Kan, Z., Jaiswal, B. S., Stinson, J., Janakiraman, V., Bhatt, D., Stern, H. M., Yue, P., Haverty, P. M., Bourgon, R., Zheng, J., et al. (2010). Diverse somatic mutation patterns and pathway alterations in human cancers. Nature 466, 869-873.

Kang, D. H. (2002). Oxidative stress, DNA damage, and breast cancer. AACN Clin Issues 13, 540-549.

Kauffman, K. J., Prakash, P., and Edwards, J. S. (2003). Advances in flux balance analysis. Curr Opin Biotechnol 14, 491-496.

Kawanishi, S., Hiraku, Y., Pinlaor, S., and Ma, N. (2006). Oxidative and nitrative DNA damage in animals and patients with inflammatory diseases in relation to inflammation-related carcinogenesis. Biol Chem 387, 365-372.

Kekec, Y., Paydas, S., Tuli, A., Zorludemir, S., Sakman, G., and Seydaoglu, G. (2009). Antioxidant enzyme levels in cases with gastrointesinal cancer. Eur J Intern Med 20, 403-406.

Kikuchi, H., Pino, M. S., Zeng, M., Shirasawa, S., and Chung, D. C. (2009). Oncogenic KRAS and BRAF differentially regulate hypoxia-inducible factor-1alpha and -2alpha in colon cancer. Cancer Res 69, 8499-8506.

Kilburn, D. G., Lilly, M. D., and Webb, F. C. (1969). The energetics of mammalian cell growth. J Cell Sci 4, 645-654.

Kim, J. W., Gao, P., Liu, Y. C., Semenza, G. L., and Dang, C. V. (2007). Hypoxia-inducible factor 1 and dysregulated c-Myc cooperatively induce vascular endothelial growth factor and metabolic switches hexokinase 2 and pyruvate dehydrogenase kinase 1. Mol Cell Biol 27, 7381-7393.

Kim, J. W., Tchernyshyov, I., Semenza, G. L., and Dang, C. V. (2006). HIF-1-mediated expression of pyruvate dehydrogenase kinase: a metabolic switch required for cellular adaptation to hypoxia. Cell Metab 3, 177-185.

Kim, J. W., Zeller, K. I., Wang, Y., Jegga, A. G., Aronow, B. J., O'Donnell, K. A., and Dang, C. V. (2004). Evaluation of myc E-box phylogenetic footprints in glycolytic genes by chromatin immunoprecipitation assays. Mol Cell Biol 24, 5923-5936.

Kim, Y. R., Oh, J. E., Kim, M. S., Kang, M. R., Park, S. W., Han, J. Y., Eom, H. S., Yoo, N. J., and Lee, S. H. (2010). Oncogenic NRF2 mutations in squamous cell carcinomas of oesophagus and skin. J Pathol 220, 446-451.

Kobunai, T., Watanabe, T., Yamamoto, Y., and Eshima, K. (2010). The frequency of KRAS mutation detection in human colon carcinoma is influenced by the sensitivity of assay methodology: a comparison between direct sequencing and real-time PCR. Biochem Biophys Res Commun 395, 158-162.

Kondoh, H., Lleonart, M. E., Gil, J., Wang, J., Degan, P., Peters, G., Martinez, D., Carnero, A., and Beach, D. (2005). Glycolytic enzymes can modulate cellular life span. Cancer Res 65, 177-185.

Kotaka, M., Gover, S., Vandeputte-Rutten, L., Au, S. W., Lam, V. M., and Adams, M. J. (2005). Structural studies of glucose-6-phosphate and NADP+ binding to human glucose-6-phosphate dehydrogenase. Acta Crystallogr D Biol Crystallogr 61, 495-504.

Kozma, L., Baltensperger, K., Klarlund, J., Porras, A., Santos, E., and Czech, M. P. (1993). The ras signaling pathway mimics insulin action on glucose transporter translocation. Proc Natl Acad Sci U S A 90, 4460-4464.

Krockenberger, M., Honig, A., Rieger, L., Coy, J. F., Sutterlin, M., Kapp, M., Horn, E., Dietl, J., and Kammerer, U. (2007). Transketolase-like 1 expression correlates with subtypes

of ovarian cancer and the presence of distant metastases. Int J Gynecol Cancer 17, 101-106.

Kroemer, G., and Pouyssegur, J. (2008). Tumor cell metabolism: cancer's Achilles' heel. Cancer Cell 13, 472-482.

Kung, H. N., Marks, J. R., and Chi, J. T. (2011). Glutamine synthetase is a genetic determinant of cell type-specific glutamine independence in breast epithelia. PLoS Genet 7, e1002229.

Kuo, W., Lin, J., and Tang, T. K. (2000). Human glucose-6-phosphate dehydrogenase (G6PD) gene transforms NIH 3T3 cells and induces tumors in nude mice. Int J Cancer 85, 857-864.

Langbein, S., Frederiks, W. M., zur Hausen, A., Popa, J., Lehmann, J., Weiss, C., Alken, P., and Coy, J. F. (2008). Metastasis is promoted by a bioenergetic switch: new targets for progressive renal cell cancer. Int J Cancer 122, 2422-2428.

Langbein, S., Zerilli, M., Zur Hausen, A., Staiger, W., Rensch-Boschert, K., Lukan, N., Popa, J., Ternullo, M. P., Steidler, A., Weiss, C., et al. (2006). Expression of transketolase TKTL1 predicts colon and urothelial cancer patient survival: Warburg effect reinterpreted. Br J Cancer 94, 578-585.

Lee, W. N., Boros, L. G., Puigjaner, J., Bassilian, S., Lim, S., and Cascante, M. (1998). Mass isotopomer study of the nonoxidative pathways of the pentose cycle with [1,2-13C2]glucose. Am J Physiol 274, E843-851.

Lee, W. N., Byerley, L. O., Bassilian, S., Ajie, H. O., Clark, I., Edmond, J., and Bergner, E. A. (1995). Isotopomer study of lipogenesis in human hepatoma cells in culture: contribution of carbon and hydrogen atoms from glucose. Anal Biochem 226, 100-112.

Leopold, J. A., Walker, J., Scribner, A. W., Voetsch, B., Zhang, Y. Y., Loscalzo, A. J., Stanton, R. C., and Loscalzo, J. (2003). Glucose-6-phosphate dehydrogenase modulates vascular endothelial growth factor-mediated angiogenesis. J Biol Chem 278, 32100-32106.

Levine, A. J., and Puzio-Kuter, A. M. (2010). The control of the metabolic switch in cancers by oncogenes and tumor suppressor genes. Science 330, 1340-1344.

Li, D., Zhu, Y., Tang, Q., Lu, H., Li, H., Yang, Y., Li, Z., and Tong, S. (2009). A new G6PD knockdown tumor-cell line with reduced proliferation and increased susceptibility to oxidative stress. Cancer Biother Radiopharm 24, 81-90.

Li, F., Wang, Y., Zeller, K. I., Potter, J. J., Wonsey, D. R., O'Donnell, K. A., Kim, J. W., Yustein, J. T., Lee, L. A., and Dang, C. V. (2005). Myc stimulates nuclearly encoded mitochondrial genes and mitochondrial biogenesis. Mol Cell Biol 25, 6225-6234.

Linardou, H., Dahabreh, I. J., Bafaloukos, D., Kosmidis, P., and Murray, S. (2009). Somatic EGFR mutations and efficacy of tyrosine kinase inhibitors in NSCLC. Nat Rev Clin Oncol 6, 352-366.

Liou, G. Y., and Storz, P. (2010). Reactive oxygen species in cancer. Free Radic Res 44, 479-496.

Liu, X., Wang, X., Zhang, J., Lam, E. K., Shin, V. Y., Cheng, A. S., Yu, J., Chan, F. K., Sung, J. J., and Jin, H. C. (2010). Warburg effect revisited: an epigenetic link between glycolysis and gastric carcinogenesis. Oncogene 29, 442-450.

Loh, K., Chia, J. A., Greco, S., Cozzi, S. J., Buttenshaw, R. L., Bond, C. E., Simms, L. A., Pike, T., Young, J. P., Jass, J. R., et al. (2008). Bone morphogenic protein 3 inactivation is an early and frequent event in colorectal cancer development. Genes Chromosomes Cancer 47, 449-460.

Lowe, S. W., Cepero, E., and Evan, G. (2004). Intrinsic tumour suppression. Nature 432, 307-315.

Llaneras, F., and Pico, J. (2007). An interval approach for dealing with flux distributions and elementary modes activity patterns. J Theor Biol 246, 290-308.

Maciag, A., and Anderson, L. M. (2005). Reactive oxygen species and lung tumorigenesis by mutant K-ras: a working hypothesis. Exp Lung Res 31, 83-104.

Mal, M., Koh, P. K., Cheah, P. Y., and Chan, E. C. (2012). Metabotyping of human colorectal cancer using two-dimensional gas chromatography mass spectrometry. Anal Bioanal Chem.

Malumbres, M., and Barbacid, M. (2003). RAS oncogenes: the first 30 years. Nat Rev Cancer 3, 459-465.

Marin, S., Chiang, K., Bassilian, S., Lee, W. N., Boros, L. G., Fernandez-Novell, J. M., Centelles, J. J., Medrano, A., Rodriguez-Gil, J. E., and Cascante, M. (2003). Metabolic strategy of boar spermatozoa revealed by a metabolomic characterization. FEBS Lett 554, 342-346.

Mazurek, S. (2011). Pyruvate kinase type M2: a key regulator of the metabolic budget system in tumor cells. Int J Biochem Cell Biol 43, 969-980.

Mazurek, S., Drexler, H. C., Troppmair, J., Eigenbrodt, E., and Rapp, U. R. (2007). Regulation of pyruvate kinase type M2 by A-Raf: a possible glycolytic stop or go mechanism. Anticancer Res 27, 3963-3971.

Mazurek, S., Zwerschke, W., Jansen-Durr, P., and Eigenbrodt, E. (2001). Metabolic cooperation between different oncogenes during cell transformation: interaction between activated ras and HPV-16 E7. Oncogene 20, 6891-6898.

Menendez, J. A., and Lupu, R. (2007). Fatty acid synthase and the lipogenic phenotype in cancer pathogenesis. Nat Rev Cancer 7, 763-777.

Metallo, C. M., Gameiro, P. A., Bell, E. L., Mattaini, K. R., Yang, J., Hiller, K., Jewell, C. M., Johnson, Z. R., Irvine, D. J., Guarente, L., et al. (2012). Reductive glutamine metabolism by IDH1 mediates lipogenesis under hypoxia. Nature 481, 380-384.

Metallo, C. M., Walther, J. L., and Stephanopoulos, G. (2009). Evaluation of 13C isotopic tracers for metabolic flux analysis in mammalian cells. J Biotechnol 144, 167-174.

Mitsuishi, Y., Motohashi, H., and Yamamoto, M. (2012a). The Keap1-Nrf2 system in cancers: stress response and anabolic metabolism. Front Oncol 2, 200.

Mitsuishi, Y., Taguchi, K., Kawatani, Y., Shibata, T., Nukiwa, T., Aburatani, H., Yamamoto, M., and Motohashi, H. (2012b). Nrf2 redirects glucose and glutamine into anabolic pathways in metabolic reprogramming. Cancer Cell 22, 66-79.

Momchilova, A., and Markovska, T. (1999). Phosphatidylethanolamine and phosphatidylcholine are sources of diacylglycerol in ras-transformed NIH 3T3 fibroblasts. Int J Biochem Cell Biol 31, 311-318.

Moreno-Sanchez, R., Saavedra, E., Rodriguez-Enriquez, S., Gallardo-Perez, J. C., Quezada, H., and Westerhoff, H. V. (2010). Metabolic control analysis indicates a change of strategy in the treatment of cancer. Mitochondrion 10, 626-639.

Mosmann, T. (1983). Rapid colorimetric assay for cellular growth and survival: application to proliferation and cytotoxicity assays. J Immunol Methods 65, 55-63.

Mullen, A. R., Wheaton, W. W., Jin, E. S., Chen, P. H., Sullivan, L. B., Cheng, T., Yang, Y., Linehan, W. M., Chandel, N. S., and DeBerardinis, R. J. (2012). Reductive carboxylation supports growth in tumour cells with defective mitochondria. Nature 481, 385-388.

Nakajima, H., Raben, N., Hamaguchi, T., and Yamasaki, T. (2002). Phosphofructokinase deficiency; past, present and future. Curr Mol Med 2, 197-212.

Noh, K., Wahl, A., and Wiechert, W. (2006). Computational tools for isotopically instationary 13C labeling experiments under metabolic steady state conditions. Metab Eng 8, 554-577.

Normanno, N., Tejpar, S., Morgillo, F., De Luca, A., Van Cutsem, E., and Ciardiello, F. (2009). Implications for KRAS status and EGFR-targeted therapies in metastatic CRC. Nat Rev Clin Oncol 6, 519-527.

Oliveira, C., Pinto, M., Duval, A., Brennetot, C., Domingo, E., Espin, E., Armengol, M., Yamamoto, H., Hamelin, R., Seruca, R., and Schwartz, S., Jr. (2003). BRAF mutations characterize colon but not gastric cancer with mismatch repair deficiency. Oncogene 22, 9192-9196.

Omerovic, J., Laude, A. J., and Prior, I. A. (2007). Ras proteins: paradigms for compartmentalised and isoform-specific signalling. Cell Mol Life Sci 64, 2575-2589.

Orth, J. D., Thiele, I., and Palsson, B. O. (2010). What is flux balance analysis? Nature biotechnology 28, 245-248.

Owen, O. E., Kalhan, S. C., and Hanson, R. W. (2002). The key role of anaplerosis and cataplerosis for citric acid cycle function. J Biol Chem 277, 30409-30412.

Palaskas, N., Larson, S. M., Schultz, N., Komisopoulou, E., Wong, J., Rohle, D., Campos, C., Yannuzzi, N., Osborne, J. R., Linkov, I., et al. (2011). 18F-fluorodeoxy-glucose positron emission tomography marks MYC-overexpressing human basal-like breast cancers. Cancer Res 71, 5164-5174.

Pandolfi, P. P., Sonati, F., Rivi, R., Mason, P., Grosveld, F., and Luzzatto, L. (1995). Targeted disruption of the housekeeping gene encoding glucose 6-phosphate dehydrogenase (G6PD): G6PD is dispensable for pentose synthesis but essential for defense against oxidative stress. Embo J 14, 5209-5215.

Papandreou, I., Cairns, R. A., Fontana, L., Lim, A. L., and Denko, N. C. (2006). HIF-1 mediates adaptation to hypoxia by actively downregulating mitochondrial oxygen consumption. Cell Metab 3, 187-197.

Parlo, R. A., and Coleman, P. S. (1986). Continuous pyruvate carbon flux to newly synthesized cholesterol and the suppressed evolution of pyruvate-generated CO2 in tumors: further evidence for a persistent truncated Krebs cycle in hepatomas. Biochim Biophys Acta 886, 169-176.

Paul Lee, W. N., Wahjudi, P. N., Xu, J., and Go, V. L. (2010). Tracer-based metabolomics: concepts and practices. Clin Biochem 43, 1269-1277.

Pelicano, H., Martin, D. S., Xu, R. H., and Huang, P. (2006). Glycolysis inhibition for anticancer treatment. Oncogene 25, 4633-4646.

Perry, G., Raina, A. K., Nunomura, A., Wataya, T., Sayre, L. M., and Smith, M. A. (2000). How important is oxidative damage? Lessons from Alzheimer's disease. Free Radic Biol Med 28, 831-834.

Pfeiffer, T., Schuster, S., and Bonhoeffer, S. (2001). Cooperation and competition in the evolution of ATP-producing pathways. Science 292, 504-507.

Phipps, A. I., Buchanan, D. D., Makar, K. W., Win, A. K., Baron, J. A., Lindor, N. M., Potter, J. D., and Newcomb, P. A. (2013). KRAS-mutation status in relation to colorectal cancer survival: the joint impact of correlated tumour markers. Br J Cancer 108, 1757-1764.

Pilkis, S. J., El-Maghrabi, M. R., McGrane, M. M., Pilkis, J., and Claus, T. H. (1981). The role of fructose 2,6-bisphosphate in regulation of fructose-1,6-bisphosphatase. J Biol Chem 256, 11489-11495.

Plas, D. R., Talapatra, S., Edinger, A. L., Rathmell, J. C., and Thompson, C. B. (2001). Akt and Bcl-xL promote growth factor-independent survival through distinct effects on mitochondrial physiology. J Biol Chem 276, 12041-12048.

Pollak, N., Dolle, C., and Ziegler, M. (2007). The power to reduce: pyridine nucleotides--small molecules with a multitude of functions. Biochem J 402, 205-218.

Porstmann, T., Griffiths, B., Chung, Y. L., Delpuech, O., Griffiths, J. R., Downward, J., and Schulze, A. (2005). PKB/Akt induces transcription of enzymes involved in cholesterol and fatty acid biosynthesis via activation of SREBP. Oncogene 24, 6465-6481.

Portakal, O., Ozkaya, O., Erden Inal, M., Bozan, B., Kosan, M., and Sayek, I. (2000). Coenzyme Q10 concentrations and antioxidant status in tissues of breast cancer patients. Clin Biochem 33, 279-284.

Possemato, R., Marks, K. M., Shaul, Y. D., Pacold, M. E., Kim, D., Birsoy, K., Sethumadhavan, S., Woo, H. K., Jang, H. G., Jha, A. K., et al. (2011). Functional genomics reveal that the serine synthesis pathway is essential in breast cancer. Nature 476, 346-350.

Pylayeva-Gupta, Y., Grabocka, E., and Bar-Sagi, D. (2011). RAS oncogenes: weaving a tumorigenic web. Nat Rev Cancer 11, 761-774.

Rais, B., Comin, B., Puigjaner, J., Brandes, J. L., Creppy, E., Saboureau, D., Ennamany, R., Lee, W. N., Boros, L. G., and Cascante, M. (1999). Oxythiamine and

dehydroepiandrosterone induce a G1 phase cycle arrest in Ehrlich's tumor cells through inhibition of the pentose cycle. FEBS Lett 456, 113-118.

Ramos-Montoya, A., Lee, W. N., Bassilian, S., Lim, S., Trebukhina, R. V., Kazhyna, M. V., Ciudad, C. J., Noe, V., Centelles, J. J., and Cascante, M. (2006). Pentose phosphate cycle oxidative and nonoxidative balance: A new vulnerable target for overcoming drug resistance in cancer. Int J Cancer 119, 2733-2741.

Rathmell, J. C., Fox, C. J., Plas, D. R., Hammerman, P. S., Cinalli, R. M., and Thompson, C. B. (2003). Akt-directed glucose metabolism can prevent Bax conformation change and promote growth factor-independent survival. Mol Cell Biol 23, 7315-7328.

Recktenwald, C. V., Kellner, R., Lichtenfels, R., and Seliger, B. (2008). Altered detoxification status and increased resistance to oxidative stress by K-ras transformation. Cancer Res 68, 10086-10093.

Reder, C. (1988). Metabolic control theory: a structural approach. J Theor Biol 135, 175-201.

Riganti, C., Gazzano, E., Polimeni, M., Aldieri, E., and Ghigo, D. (2012). The pentose phosphate pathway: an antioxidant defense and a crossroad in tumor cell fate. Free Radic Biol Med 53, 421-436.

Rodriguez-Prados, J. C., Traves, P. G., Cuenca, J., Rico, D., Aragones, J., Martin-Sanz, P., Cascante, M., and Bosca, L. (2010). Substrate fate in activated macrophages: a comparison between innate, classic, and alternative activation. J Immunol 185, 605-614.

Roos, S., Jansson, N., Palmberg, I., Saljo, K., Powell, T. L., and Jansson, T. (2007). Mammalian target of rapamycin in the human placenta regulates leucine transport and is down-regulated in restricted fetal growth. J Physiol 582, 449-459.

Rouschop, K. M., Dubois, L. J., Keulers, T. G., van den Beucken, T., Lambin, P., Bussink, J., van der Kogel, A. J., Koritzinsky, M., and Wouters, B. G. (2013). PERK/eIF2alpha signaling protects therapy resistant hypoxic cells through induction of glutathione synthesis and protection against ROS. Proc Natl Acad Sci U S A 110, 4622-4627.

Salter, M., Knowles, R. G., and Pogson, C. I. (1994). Metabolic control. Essays Biochem 28, 1-12.

Samuels, Y., Wang, Z., Bardelli, A., Silliman, N., Ptak, J., Szabo, S., Yan, H., Gazdar, A., Powell, S. M., Riggins, G. J., et al. (2004). High frequency of mutations of the PIK3CA gene in human cancers. Science 304, 554.

Sanchez-Tena, S., Alcarraz-Vizan, G., Marin, S., Torres, J. L., and Cascante, M. (2013). Epicatechin gallate impairs colon cancer cell metabolic productivity. J Agric Food Chem 61, 4310-4317.

Santillo, M., Mondola, P., Seru, R., Annella, T., Cassano, S., Ciullo, I., Tecce, M. F., Iacomino, G., Damiano, S., Cuda, G., et al. (2001). Opposing functions of Ki- and Ha-Ras genes in the regulation of redox signals. Curr Biol 11, 614-619.

Santos, C. R., and Schulze, A. (2012). Lipid metabolism in cancer. FEBS J 279, 2610-2623.

Sauer, L. A., and Dauchy, R. T. (1983). Ketone body, glucose, lactic acid, and amino acid utilization by tumors in vivo in fasted rats. Cancer Res 43, 3497-3503.

Sauer, L. A., Stayman, J. W., 3rd, and Dauchy, R. T. (1982). Amino acid, glucose, and lactic acid utilization in vivo by rat tumors. Cancer Res 42, 4090-4097.

Sauer, U. (2006). Metabolic networks in motion: 13C-based flux analysis. Mol Syst Biol 2, 62.

Scheffzek, K., Ahmadian, M. R., Kabsch, W., Wiesmuller, L., Lautwein, A., Schmitz, F., and Wittinghofer, A. (1997). The Ras-RasGAP complex: structural basis for GTPase activation and its loss in oncogenic Ras mutants. Science 277, 333-338.

Schilling, C. H., Schuster, S., Palsson, B. O., and Heinrich, R. (1999). Metabolic pathway analysis: basic concepts and scientific applications in the post-genomic era. Biotechnol Prog 15, 296-303.

Schwartzenberg-Bar-Yoseph, F., Armoni, M., and Karnieli, E. (2004). The tumor suppressor p53 down-regulates glucose transporters GLUT1 and GLUT4 gene expression. Cancer Res 64, 2627-2633.

Sears, R., Leone, G., DeGregori, J., and Nevins, J. R. (1999). Ras enhances Myc protein stability. Mol Cell 3, 169-179.

Selivanov, V. A., Marin, S., Lee, P. W., and Cascante, M. (2006). Software for dynamic analysis of tracer-based metabolomic data: estimation of metabolic fluxes and their statistical analysis. Bioinformatics 22, 2806-2812.

Selivanov, V. A., Meshalkina, L. E., Solovjeva, O. N., Kuchel, P. W., Ramos-Montoya, A., Kochetov, G. A., Lee, P. W., and Cascante, M. (2005). Rapid simulation and analysis of isotopomer distributions using constraints based on enzyme mechanisms: an example from HT29 cancer cells. Bioinformatics 21, 3558-3564.

Selivanov, V. A., Puigjaner, J., Sillero, A., Centelles, J. J., Ramos-Montoya, A., Lee, P. W., and Cascante, M. (2004). An optimized algorithm for flux estimation from isotopomer distribution in glucose metabolites. Bioinformatics 20, 3387-3397.

Selivanov, V. A., Vizan, P., Mollinedo, F., Fan, T. W., Lee, P. W., and Cascante, M. (2010). Edelfosine-induced metabolic changes in cancer cells that precede the overproduction of reactive oxygen species and apoptosis. BMC Syst Biol 4, 135.

Semenza, G. L. (2010). Defining the role of hypoxia-inducible factor 1 in cancer biology and therapeutics. Oncogene 29, 625-634.

Sen, A. K. (1996). On the sign pattern of metabolic control coefficients. J Theor Biol 182, 269-275.

Sherr, C. J., and McCormick, F. (2002). The RB and p53 pathways in cancer. Cancer Cell 2, 103-112.

Shim, H., Dolde, C., Lewis, B. C., Wu, C. S., Dang, G., Jungmann, R. A., Dalla-Favera, R., and Dang, C. V. (1997). c-Myc transactivation of LDH-A: implications for tumor metabolism and growth. Proc Natl Acad Sci U S A 94, 6658-6663.

Simi, L., Pratesi, N., Vignoli, M., Sestini, R., Cianchi, F., Valanzano, R., Nobili, S., Mini, E., Pazzagli, M., and Orlando, C. (2008). High-resolution melting analysis for rapid detection of KRAS, BRAF, and PIK3CA gene mutations in colorectal cancer. Am J Clin Pathol 130, 247-253.

Singh, A., Bodas, M., Wakabayashi, N., Bunz, F., and Biswal, S. (2010). Gain of Nrf2 function in non-small-cell lung cancer cells confers radioresistance. Antioxid Redox Signal 13, 1627-1637.

Singh, A., Boldin-Adamsky, S., Thimmulappa, R. K., Rath, S. K., Ashush, H., Coulter, J., Blackford, A., Goodman, S. N., Bunz, F., Watson, W. H., et al. (2008). RNAi-mediated silencing of nuclear factor erythroid-2-related factor 2 gene expression in non-small cell lung cancer inhibits tumor growth and increases efficacy of chemotherapy. Cancer Res 68, 7975-7984.

Singh, A., Misra, V., Thimmulappa, R. K., Lee, H., Ames, S., Hoque, M. O., Herman, J. G., Baylin, S. B., Sidransky, D., Gabrielson, E., et al. (2006). Dysfunctional KEAP1-NRF2 interaction in non-small-cell lung cancer. PLoS Med 3, e420.

Soga, T. (2013). Cancer metabolism: key players in metabolic reprogramming. Cancer Sci 104, 275-281.

Solis, L. M., Behrens, C., Dong, W., Suraokar, M., Ozburn, N. C., Moran, C. A., Corvalan, A. H., Biswal, S., Swisher, S. G., Bekele, B. N., et al. (2010). Nrf2 and Keap1

abnormalities in non-small cell lung carcinoma and association with clinicopathologic features. Clin Cancer Res 16, 3743-3753.

Som, P., Atkins, H. L., Bandoypadhyay, D., Fowler, J. S., MacGregor, R. R., Matsui, K., Oster, Z. H., Sacker, D. F., Shiue, C. Y., Turner, H., et al. (1980). A fluorinated glucose analog, 2-fluoro-2-deoxy-D-glucose (F-18): nontoxic tracer for rapid tumor detection. J Nucl Med 21, 670-675.

Son, J., Lyssiotis, C. A., Ying, H., Wang, X., Hua, S., Ligorio, M., Perera, R. M., Ferrone, C. R., Mullarky, E., Shyh-Chang, N., et al. (2013). Glutamine supports pancreatic cancer growth through a KRAS-regulated metabolic pathway. Nature.

Sosa, V., Moline, T., Somoza, R., Paciucci, R., Kondoh, H., and ME, L. L. (2013). Oxidative stress and cancer: an overview. Ageing Res Rev 12, 376-390.

Staiger, W. I., Coy, J. F., Grobholz, R., Hofheinz, R. D., Lukan, N., Post, S., Schwarzbach, M. H., and Willeke, F. (2006). Expression of the mutated transketolase TKTL1, a molecular marker in gastric cancer. Oncol Rep 16, 657-661.

Stubbs, M., and Griffiths, J. R. (2009). The altered metabolism of tumors: HIF-1 and its role in the Warburg effect. Adv Enzyme Regul.

Sukhatme, V. P., and Chan, B. (2012). Glycolytic cancer cells lacking 6-phosphogluconate dehydrogenase metabolize glucose to induce senescence. FEBS Lett.

Suzuki, S., Tanaka, T., Poyurovsky, M. V., Nagano, H., Mayama, T., Ohkubo, S., Lokshin, M., Hosokawa, H., Nakayama, T., Suzuki, Y., et al. (2010). Phosphate-activated glutaminase (GLS2), a p53-inducible regulator of glutamine metabolism and reactive oxygen species. Proc Natl Acad Sci U S A 107, 7461-7466.

Swietach, P., Vaughan-Jones, R. D., and Harris, A. L. (2007). Regulation of tumor pH and the role of carbonic anhydrase 9. Cancer Metastasis Rev 26, 299-310.

Swinnen, J. V., Vanderhoydonc, F., Elgamal, A. A., Eelen, M., Vercaeren, I., Joniau, S., Van Poppel, H., Baert, L., Goossens, K., Heyns, W., and Verhoeven, G. (2000). Selective activation of the fatty acid synthesis pathway in human prostate cancer. Int J Cancer 88, 176-179.

Szatrowski, T. P., and Nathan, C. F. (1991). Production of large amounts of hydrogen peroxide by human tumor cells. Cancer Res 51, 794-798.

Takashima, A., and Faller, D. V. (2013). Targeting the RAS oncogene. Expert Opin Ther Targets.

Talmadge, J. E., and Fidler, I. J. (2010). AACR centennial series: the biology of cancer metastasis: historical perspective. Cancer Res 70, 5649-5669.

Tan, Y. H., Liu, Y., Eu, K. W., Ang, P. W., Li, W. Q., Salto-Tellez, M., Iacopetta, B., and Soong, R. (2008). Detection of BRAF V600E mutation by pyrosequencing. Pathology 40, 295-298.

Telang, S., Lane, A. N., Nelson, K. K., Arumugam, S., and Chesney, J. (2007). The oncoprotein H-RasV12 increases mitochondrial metabolism. Mol Cancer 6, 77.

Telang, S., Yalcin, A., Clem, A. L., Bucala, R., Lane, A. N., Eaton, J. W., and Chesney, J. (2006). Ras transformation requires metabolic control by 6-phosphofructo-2-kinase. Oncogene 25, 7225-7234.

Tian, W. N., Braunstein, L. D., Pang, J., Stuhlmeier, K. M., Xi, Q. C., Tian, X., and Stanton, R. C. (1998). Importance of glucose-6-phosphate dehydrogenase activity for cell growth. J Biol Chem 273, 10609-10617.

Toyokuni, S., Okamoto, K., Yodoi, J., and Hiai, H. (1995). Persistent oxidative stress in cancer. FEBS Lett 358, 1-3.

Trachootham, D., Alexandre, J., and Huang, P. (2009). Targeting cancer cells by ROS-mediated mechanisms: a radical therapeutic approach? Nat Rev Drug Discov 8, 579-591.

Trachootham, D., Zhou, Y., Zhang, H., Demizu, Y., Chen, Z., Pelicano, H., Chiao, P. J., Achanta, G., Arlinghaus, R. B., Liu, J., and Huang, P. (2006). Selective killing of oncogenically transformed cells through a ROS-mediated mechanism by beta-phenylethyl isothiocyanate. Cancer Cell 10, 241-252.

Tredan, O., Galmarini, C. M., Patel, K., and Tannock, I. F. (2007). Drug resistance and the solid tumor microenvironment. J Natl Cancer Inst 99, 1441-1454.

Tsai, J., Lee, J. T., Wang, W., Zhang, J., Cho, H., Mamo, S., Bremer, R., Gillette, S., Kong, J., Haass, N. K., et al. (2008). Discovery of a selective inhibitor of oncogenic B-Raf kinase with potent antimelanoma activity. Proc Natl Acad Sci U S A 105, 3041-3046.

Vander Heiden, M. G. (2011). Targeting cancer metabolism: a therapeutic window opens. Nat Rev Drug Discov 10, 671-684.

Vizan, P., Alcarraz-Vizan, G., Diaz-Moralli, S., Rodriguez-Prados, J. C., Zanuy, M., Centelles, J. J., Jauregui, O., and Cascante, M. (2007). Quantification of intracellular phosphorylated carbohydrates in HT29 human colon adenocarcinoma cell line

using liquid chromatography-electrospray ionization tandem mass spectrometry. Anal Chem 79, 5000-5005.

Vizan, P., Alcarraz-Vizan, G., Diaz-Moralli, S., Solovjeva, O. N., Frederiks, W. M., and Cascante, M. (2009). Modulation of pentose phosphate pathway during cell cycle progression in human colon adenocarcinoma cell line HT29. Int J Cancer 124, 2789-2796.

Vizan, P., Boros, L. G., Figueras, A., Capella, G., Mangues, R., Bassilian, S., Lim, S., Lee, W. N., and Cascante, M. (2005). K-ras codon-specific mutations produce distinctive metabolic phenotypes in NIH3T3 mice [corrected] fibroblasts. Cancer Res 65, 5512-5515.

Vizán, P., Mazurek, S., and Cascante, M. (2008). Robust metabolic adaptation underlying tumor progression. Metabolomics 4, 1-12.

Vousden, K. H., and Ryan, K. M. (2009). p53 and metabolism. Nat Rev Cancer 9, 691-700.

Wamelink, M. M., Struys, E. A., and Jakobs, C. (2008). The biochemistry, metabolism and inherited defects of the pentose phosphate pathway: a review. J Inherit Metab Dis 31, 703-717.

Wang, J. B., Erickson, J. W., Fuji, R., Ramachandran, S., Gao, P., Dinavahi, R., Wilson, K. F., Ambrosio, A. L., Dias, S. M., Dang, C. V., and Cerione, R. A. (2010). Targeting mitochondrial glutaminase activity inhibits oncogenic transformation. Cancer Cell 18, 207-219.

Wang, L., Birol, I., and Hatzimanikatis, V. (2004). Metabolic control analysis under uncertainty: framework development and case studies. Biophys J 87, 3750-3763.

Wang, R., An, J., Ji, F., Jiao, H., Sun, H., and Zhou, D. (2008). Hypermethylation of the Keap1 gene in human lung cancer cell lines and lung cancer tissues. Biochem Biophys Res Commun 373, 151-154.

Warburg, O., Wind, F., and Negelein, E. (1927). THE METABOLISM OF TUMORS IN THE BODY. J Gen Physiol 8, 519-530.

Ward, P. S., and Thompson, C. B. (2012). Metabolic reprogramming: a cancer hallmark even warburg did not anticipate. Cancer Cell 21, 297-308.

Weinberg, F., Hamanaka, R., Wheaton, W. W., Weinberg, S., Joseph, J., Lopez, M., Kalyanaraman, B., Mutlu, G. M., Budinger, G. R., and Chandel, N. S. (2010). Mitochondrial metabolism and ROS generation are essential for Kras-mediated tumorigenicity. Proc Natl Acad Sci U S A 107, 8788-8793.

Westerhoff, H. V., and Kell, D. B. (1987). Matrix method for determining steps most rate-limiting to metabolic fluxes in biotechnological processes. Biotechnol Bioeng 30, 101-107.

Wieman, H. L., Wofford, J. A., and Rathmell, J. C. (2007). Cytokine stimulation promotes glucose uptake via phosphatidylinositol-3 kinase/Akt regulation of Glut1 activity and trafficking. Mol Biol Cell 18, 1437-1446.

Winter, G., and Kromer, J. O. (2013). Fluxomics - connecting 'omics analysis and phenotypes. Environ Microbiol 15, 1901-1916.

Wise, D. R., DeBerardinis, R. J., Mancuso, A., Sayed, N., Zhang, X. Y., Pfeiffer, H. K., Nissim, I., Daikhin, E., Yudkoff, M., McMahon, S. B., and Thompson, C. B. (2008). Myc regulates a transcriptional program that stimulates mitochondrial glutaminolysis and leads to glutamine addiction. Proc Natl Acad Sci U S A 105, 18782-18787.

Wise, D. R., Ward, P. S., Shay, J. E., Cross, J. R., Gruber, J. J., Sachdeva, U. M., Platt, J. M., DeMatteo, R. G., Simon, M. C., and Thompson, C. B. (2011). Hypoxia promotes isocitrate dehydrogenase-dependent carboxylation of alpha-ketoglutarate to citrate to support cell growth and viability. Proc Natl Acad Sci U S A 108, 19611-19616.

Xu, X., Zur Hausen, A., Coy, J. F., and Lochelt, M. (2009). Transketolase-like protein 1 (TKTL1) is required for rapid cell growth and full viability of human tumor cells. Int J Cancer 124, 1330-1337.

Yalcin, A., Clem, B. F., Simmons, A., Lane, A., Nelson, K., Clem, A. L., Brock, E., Siow, D., Wattenberg, B., Telang, S., and Chesney, J. (2009a). Nuclear targeting of 6-phosphofructo-2-kinase (PFKFB3) increases proliferation via cyclin-dependent kinases. J Biol Chem 284, 24223-24232.

Yalcin, A., Telang, S., Clem, B., and Chesney, J. (2009b). Regulation of glucose metabolism by 6-phosphofructo-2-kinase/fructose-2,6-bisphosphatases in cancer. Exp Mol Pathol 86, 174-179.

Yang, D., Wang, M. T., Tang, Y., Chen, Y., Jiang, H., Jones, T. T., Rao, K., Brewer, G. J., Singh, K. K., and Nie, D. (2010a). Impairment of mitochondrial respiration in mouse fibroblasts by oncogenic H-RAS(Q61L). Cancer Biol Ther 9, 122-133.

Yang, L., Pang, Y., and Moses, H. L. (2010b). TGF-beta and immune cells: an important regulatory axis in the tumor microenvironment and progression. Trends Immunol 31, 220-227.

Yang, Y. A., Han, W. F., Morin, P. J., Chrest, F. J., and Pizer, E. S. (2002). Activation of fatty acid synthesis during neoplastic transformation: role of mitogen-activated protein kinase and phosphatidylinositol 3-kinase. Exp Cell Res 279, 80-90.

Ying, H., Kimmelman, A. C., Lyssiotis, C. A., Hua, S., Chu, G. C., Fletcher-Sananikone, E., Locasale, J. W., Son, J., Zhang, H., Coloff, J. L., et al. (2012). Oncogenic Kras Maintains Pancreatic Tumors through Regulation of Anabolic Glucose Metabolism. Cell 149, 656-670.

Yokota, T., Ura, T., Shibata, N., Takahari, D., Shitara, K., Nomura, M., Kondo, C., Mizota, A., Utsunomiya, S., Muro, K., and Yatabe, Y. (2011). BRAF mutation is a powerful prognostic factor in advanced and recurrent colorectal cancer. Br J Cancer 104, 856-862.

Yoon, S., Lee, M. Y., Park, S. W., Moon, J. S., Koh, Y. K., Ahn, Y. H., Park, B. W., and Kim, K. S. (2007). Up-regulation of acetyl-CoA carboxylase alpha and fatty acid synthase by human epidermal growth factor receptor 2 at the translational level in breast cancer cells. J Biol Chem 282, 26122-26131.

Young, T. W., Mei, F. C., Yang, G., Thompson-Lanza, J. A., Liu, J., and Cheng, X. (2004). Activation of antioxidant pathways in ras-mediated oncogenic transformation of human surface ovarian epithelial cells revealed by functional proteomics and mass spectrometry. Cancer Res 64, 4577-4584.

Yuneva, M., Zamboni, N., Oefner, P., Sachidanandam, R., and Lazebnik, Y. (2007). Deficiency in glutamine but not glucose induces MYC-dependent apoptosis in human cells. J Cell Biol 178, 93-105.

Zhang, P., Singh, A., Yegnasubramanian, S., Esopi, D., Kombairaju, P., Bodas, M., Wu, H., Bova, S. G., and Biswal, S. (2010). Loss of Kelch-like ECH-associated protein 1 function in prostate cancer cells causes chemoresistance and radioresistance and promotes tumor growth. Mol Cancer Ther 9, 336-346.

Zhang, S., Yang, J. H., Guo, C. K., and Cai, P. C. (2007). Gene silencing of TKTL1 by RNAi inhibits cell proliferation in human hepatoma cells. Cancer Lett 253, 108-114.

APPENDIX I

APPENDIX I: SUPPLEMENTARY DATA FOR MASS ISOTOPOMER DISTRIBUTION OF METABOLITES PRESENTED IN CHAPTER 5.2

Metabolite	Cells	Tracer	Incubation Time (h)	m0 (%) mean	m0 (%) SD	m1 (%) mean	m1 (%) SD	m2 (%) mean	m2 (%) SD	m3 (%) mean	m3 (%) SD	m4 (%) mean	m4 (%) SD	m5 (%) mean	m5 (%) SD	m6 (%) mean	m6 (%) SD	∑m (%) mean	∑m (%) SD
Ribose	BJ																		
		[1,2-$^{13}C_2$]-Glc	8	89.79	*0.42*	5.67	*0.14*	3.07	*0.21*	1.11	*0.04*	0.33	*0.04*	0.03	*0.01*			10.21	*0.42*
			24	72.10	*0.22*	15.48	*0.06*	8.53	*0.14*	2.84	*0.01*	0.98	*0.02*	0.08	*0.02*			27.90	*0.22*
		[U-^{13}C]-Gln	8	99.98	*0.00*	0.00	*0.00*	0.01	*0.01*	0.01	*0.01*	0.00	*0.01*	0.00	*0.00*			0.02	*0.00*
			24	99.89	*0.18*	0.10	*0.18*	0.00	*0.00*	0.00	*0.00*	0.01	*0.01*	0.00	*0.00*			0.11	*0.18*
	BJ-HRasV12																		
		[1,2-$^{13}C_2$]-Glc	8	88.79	*0.28*	6.52	*0.15*	3.12	*0.09*	1.26	*0.06*	0.27	*0.02*	0.03	*0.01*			11.21	*0.28*
			24	70.83	*0.38*	16.12	*0.33*	8.94	*0.05*	3.02	*0.04*	1.00	*0.02*	0.09	*0.02*			29.17	*0.38*
		[U-^{13}C]-Gln	8	99.18	*0.73*	0.32	*0.56*	0.08	*0.11*	0.00	*0.01*	0.20	*0.32*	0.22	*0.38*			0.82	*0.73*
			24	97.72	*2.05*	2.13	*1.97*	0.09	*0.08*	0.01	*0.01*	0.04	*0.01*	0.01	*0.01*			2.28	*2.05*
Pyruvate	BJ																		
		[1,2-$^{13}C_2$]-Glc	8	88.20	*0.89*	0.65	*0.09*	10.51	*0.73*	0.65	*0.07*							11.80	*0.89*
			24	84.34	*0.25*	0.63	*0.11*	14.25	*0.11*	0.78	*0.08*							15.66	*0.25*
		[U-^{13}C]-Gln	8	98.96	*0.64*	0.27	*0.15*	0.36	*0.41*	0.41	*0.10*							1.04	*0.64*
			24	98.91	*0.37*	0.29	*0.14*	0.21	*0.08*	0.59	*0.15*							1.09	*0.37*
	BJ-HRasV12																		
		[1,2-$^{13}C_2$]-Glc	8	85.68	*0.75*	0.75	*0.14*	12.74	*0.79*	0.82	*0.09*							14.32	*0.75*
			24	83.05	*0.10*	0.75	*0.01*	15.33	*0.06*	0.87	*0.04*							16.95	*0.10*
		[U-^{13}C]-Gln	8	98.71	*0.37*	0.40	*0.10*	0.34	*0.32*	0.55	*0.06*							1.29	*0.37*
			24	98.81	*0.24*	0.37	*0.06*	0.10	*0.11*	0.72	*0.11*							1.19	*0.24*

Metabolite	Cells	Tracer	Incubation Time (h)	m0 (%)		m1 (%)		m2 (%)		m3 (%)		m4 (%)		m5 (%)		m6 (%)		∑m (%)	
				mean	SD	mean	SD	mean	SD	mean	SD	mean	SD	mean	SD	mean	SD	mean	SD
Lactate	BJ																		
		[1,2-$^{13}C_2$]-Glc	8	90.31	*0.09*	0.35	*0.09*	8.87	*0.20*	0.48	*0.03*							9.69	*0.09*
			24	84.42	*0.15*	0.65	*0.11*	14.14	*0.12*	0.79	*0.05*							15.58	*0.15*
		[U-^{13}C]-Gln	8	99.72	*0.04*	0.09	*0.02*	0.03	*0.01*	0.16	*0.02*							0.28	*0.04*
			24	99.23	*0.20*	0.24	*0.18*	0.11	*0.03*	0.42	*0.02*							0.77	*0.20*
	BJ-HRasV12																		
		[1,2-$^{13}C_2$]-Glc	8	87.76	*0.04*	0.50	*0.08*	11.14	*0.08*	0.61	*0.01*							12.24	*0.04*
			24	83.03	*0.15*	0.72	*0.15*	15.38	*0.18*	0.87	*0.03*							16.97	*0.15*
		[U-^{13}C]-Gln	8	99.75	*0.05*	0.07	*0.02*	0.03	*0.01*	0.15	*0.03*							0.25	*0.05*
			24	99.29	*0.02*	0.20	*0.03*	0.12	*0.01*	0.39	*0.01*							0.71	*0.02*
Citrate	BJ																		
		[1,2-$^{13}C_2$]-Glc	8	95.38	*1.44*	0.35	*0.03*	1.81	*0.18*	0.71	*0.19*	0.98	*0.59*	0.45	*0.32*	0.33	0.24	4.62	*1.44*
			24	91.16	*0.17*	0.85	*0.05*	6.24	*0.21*	0.87	*0.05*	0.77	*0.17*	0.01	*0.01*	0.00	0.00	8.74	*0.17*
		[U-^{13}C]-Gln	8	84.79	*1.32*	0.52	*0.07*	1.38	*0.08*	1.74	*0.25*	6.92	*0.57*	3.13	*0.33*	1.52	0.15	15.21	*1.32*
			24	60.25	*7.60*	2.74	*1.69*	6.46	*1.96*	4.04	*0.70*	16.01	*2.63*	4.16	*0.54*	2.26	0.31	35.66	*7.60*
	BJ-HRasV12																		
		[1,2-$^{13}C_2$]-Glc	8	93.74	*0.75*	0.57	*0.13*	3.70	*0.57*	1.18	*0.07*	0.65	*0.05*	0.13	*0.04*	0.04	0.04	6.26	*0.75*
			24	84.84	*0.39*	1.70	*0.08*	9.97	*0.23*	1.83	*0.05*	1.42	*0.05*	0.10	*0.01*	0.00	0.00	15.03	*0.39*
		[U-^{13}C]-Gln	8	71.73	*1.27*	1.24	*0.19*	3.32	*0.20*	3.39	*0.13*	12.30	*0.54*	5.47	*0.26*	2.55	0.10	28.27	*1.27*
			24	53.76	*6.56*	5.87	*1.64*	10.19	*2.04*	5.46	*0.64*	20.64	*1.77*	5.07	*0.27*	2.79	0.19	50.02	*6.56*

Metabolite	Cells	Tracer	Incubation Time (h)	m0 (%)		m1 (%)		m2 (%)		m3 (%)		m4 (%)		m5 (%)		m6 (%)		∑m (%)	
				mean	SD	mean	SD	mean	SD	mean	SD	mean	SD	mean	SD	mean	SD	mean	SD
α-Ketoglutarate	BJ																		
		[1,2-$^{13}C_2$]-Glc	8	97.82	*0.32*	0.28	*0.19*	1.19	*0.06*	0.37	*0.05*	0.21	*0.04*	0.13	*0.01*			2.18	*0.32*
			24	95.18	*0.12*	0.41	*0.07*	3.58	*0.02*	0.49	*0.03*	0.34	*0.02*	0.00	*0.00*			4.82	*0.12*
		[U-^{13}C]-Gln	8	40.96	*0.10*	1.29	*0.03*	1.23	*0.00*	7.09	*0.08*	1.70	*0.01*	47.72	*0.02*			59.04	*0.10*
			24	24.01	*2.65*	4.00	*1.69*	4.03	*1.04*	15.17	*1.79*	3.55	*0.26*	49.24	*3.03*			75.99	*2.65*
	BJ-HRasV12																		
		[1,2-$^{13}C_2$]-Glc	8	97.04	*0.33*	0.20	*0.22*	2.13	*0.07*	0.34	*0.03*	0.24	*0.01*	0.05	*0.01*			2.96	*0.33*
			24	91.47	*0.15*	1.31	*0.05*	5.61	*0.08*	0.96	*0.03*	0.60	*0.02*	0.05	*0.01*			8.53	*0.15*
		[U-^{13}C]-Gln	8	39.02	*0.06*	1.62	*0.02*	1.85	*0.01*	9.31	*0.00*	2.29	*0.02*	45.92	*0.01*			60.98	*0.06*
			24	24.96	*1.08*	4.89	*1.69*	4.64	*0.98*	15.80	*1.52*	3.74	*0.21*	45.98	*3.32*			75.04	*1.08*
Glutamate																			
C2-C4	BJ																		
		[1,2-$^{13}C_2$]-Glc	8	99.71	*0.25*	0.22	*0.20*	0.03	*0.04*	0.04	*0.03*							0.29	*0.25*
			24	98.65	*0.05*	1.13	*0.05*	0.14	*0.00*	0.09	*0.01*							1.35	*0.05*
		[U-^{13}C]-Gln	8	18.35	*0.33*	0.66	*0.06*	2.66	*0.02*	78.34	*0.38*							81.65	*0.33*
			24	19.96	*0.07*	2.04	*0.30*	5.57	*0.54*	72.44	*0.16*							80.04	*0.07*
	BJ-HRasV12																		
		[1,2-$^{13}C_2$]-Glc	8	99.40	*0.13*	0.48	*0.09*	0.05	*0.02*	0.06	*0.03*							0.60	*0.13*
			24	96.82	*0.30*	2.70	*0.28*	0.30	*0.04*	0.17	*0.16*							3.18	*0.30*
		[U-^{13}C]-Gln	8	18.66	*0.50*	0.89	*0.46*	2.14	*0.99*	78.31	*0.81*							81.34	*0.50*
			24	20.38	*0.64*	3.22	*0.34*	8.23	*0.57*	68.18	*0.81*							79.62	*0.64*

Metabolite	Cells	Tracer	Incubation Time (h)	m0 (%) mean	m0 (%) SD	m1 (%) mean	m1 (%) SD	m2 (%) mean	m2 (%) SD	m3 (%) mean	m3 (%) SD	m4 (%) mean	m4 (%) SD	m5 (%) mean	m5 (%) SD	m6 (%) mean	m6 (%) SD	∑m (%) mean	∑m (%) SD
Glutamate																			
C2-C5	BJ																		
		[1,2-$^{13}C_2$]-Glc	8	99.75	*0.01*	0.12	*0.06*	0.09	*0.00*	0.00	*0.00*	0.03	*0.05*					0.25	*0.01*
			24	98.92	*0.02*	0.24	*0.01*	0.77	*0.02*	0.03	*0.00*	0.03	*0.01*					1.08	*0.02*
		[U-^{13}C]-Gln	8	17.35	*0.27*	0.20	*0.00*	1.35	*0.02*	2.57	*0.14*	78.54	*0.19*					82.65	*0.27*
			24	18.89	*0.08*	1.31	*0.05*	5.03	*0.18*	2.32	*0.07*	72.45	*0.38*					81.11	*0.08*
	BJ-HRasV12																		
		[1,2-$^{13}C_2$]-Glc	8	99.66	*0.11*	0.11	*0.08*	0.20	*0.01*	0.01	*0.00*	0.02	*0.02*					0.34	*0.11*
			24	96.36	*1.25*	0.76	*0.02*	1.91	*0.11*	0.15	*0.02*	0.83	*1.11*					3.64	*1.25*
		[U-^{13}C]-Gln	8	17.69	*0.49*	0.33	*0.03*	2.00	*0.10*	1.80	*1.10*	78.19	*0.57*					82.31	*0.49*
			24	19.49	*0.51*	2.93	*0.12*	8.14	*0.41*	1.46	*0.86*	67.98	*0.62*					80.51	*0.51*
Fumarate	BJ																		
		[1,2-$^{13}C_2$]-Glc	8	99.08	*0.25*	0.14	*0.19*	0.76	*0.06*	0.00	*0.00*	0.03	*0.01*					0.92	*0.25*
			24	94.90	*0.57*	0.05	*0.04*	2.84	*0.24*	1.99	*0.28*	0.22	*0.06*					5.10	*0.57*
		[U-^{13}C]-Gln	8	75.00	*3.76*	0.52	*0.35*	4.06	*0.47*	2.50	*1.31*	17.92	*1.76*					25.00	*3.76*
			24	54.97	*2.71*	2.64	*0.90*	11.67	*2.29*	6.20	*0.60*	24.52	*1.21*					45.03	*2.71*
	BJ-HRasV12																		
		[1,2-$^{13}C_2$]-Glc	8	99.54	*0.33*	0.04	*0.03*	0.43	*0.30*	0.00	*0.00*	0.00	*0.00*					0.46	*0.33*
			24	92.04	*0.90*	0.72	*0.05*	3.97	*0.34*	2.88	*0.60*	0.38	*0.07*					7.96	*0.90*
		[U-^{13}C]-Gln	8	64.14	*0.21*	1.50	*0.06*	6.12	*0.10*	3.52	*0.21*	24.72	*0.08*					35.86	*0.21*
			24	53.48	*2.26*	3.59	*1.34*	12.32	*1.77*	5.07	*0.52*	25.54	*1.04*					46.52	*2.26*

Metabolite	Cells	Tracer	Incubation Time (h)	m0 (%) mean	m0 (%) SD	m1 (%) mean	m1 (%) SD	m2 (%) mean	m2 (%) SD	m3 (%) mean	m3 (%) SD	m4 (%) mean	m4 (%) SD	m5 (%) mean	m5 (%) SD	m6 (%) mean	m6 (%) SD	∑m (%) mean	∑m (%) SD
Malate	BJ																		
		[1,2-$^{13}C_2$]-Glc	8	98.81	*0.06*	0.24	*0.06*	0.73	*0.06*	0.11	*0.04*	0.10	*0.01*					1.19	*0.06*
			24	96.54	*0.11*	0.47	*0.04*	2.28	*0.06*	0.46	*0.01*	0.25	*0.02*					3.46	*0.11*
		[U-^{13}C]-Gln	8	66.71	*2.80*	0.96	*0.31*	4.29	*0.41*	4.32	*0.25*	23.72	*1.90*					33.29	*2.80*
			24	55.24	*2.18*	4.01	*1.23*	9.72	*0.89*	5.07	*0.33*	25.95	*2.41*					44.76	*2.18*
	BJ-HRasV12																		
		[1,2-$^{13}C_2$]-Glc	8	97.78	*0.06*	0.30	*0.03*	1.42	*0.11*	0.32	*0.09*	0.18	*0.02*					2.22	*0.06*
			24	93.82	*0.14*	1.25	*0.05*	3.64	*0.08*	0.86	*0.02*	0.44	*0.02*					6.18	*0.14*
		[U-^{13}C]-Gln	8	56.14	*0.91*	1.88	*0.15*	7.14	*0.18*	5.40	*0.25*	29.43	*0.34*					43.86	*0.91*
			24	52.10	*0.87*	5.13	*1.48*	11.04	*1.13*	5.25	*0.20*	26.47	*1.67*					47.90	*0.87*
Palmitate	BJ																		
		[1,2-$^{13}C_2$]-Glc	8	98.52	*0.36*	0.22	*0.07*	0.93	*0.24*	0.02	*0.01*	0.25	*0.07*	0.00	*0.00*	0.04	*0.02*	1.48	*0.36*
			24	88.63	*0.37*	0.52	*0.08*	6.92	*0.15*	0.27	*0.05*	2.78	*0.07*	0.11	*0.00*	0.66	*0.02*	11.37	*0.37*
		[U-^{13}C]-Gln	8	98.44	*0.05*	0.23	*0.05*	0.84	*0.03*	0.02	*0.00*	0.34	*0.02*	0.01	*0.00*	0.09	*0.01*	1.56	*0.05*
			24	90.16	*0.81*	0.57	*0.15*	6.24	*0.48*	0.28	*0.04*	2.07	*0.18*	0.10	*0.01*	0.48	*0.03*	9.84	*0.81*
	BJ-HRasV12																		
		[1,2-$^{13}C_2$]-Glc	8	96.45	*0.16*	0.20	*0.05*	2.32	*0.13*	0.05	*0.01*	0.78	*0.07*	0.02	*0.01*	0.14	*0.00*	3.55	*0.16*
			24	82.62	*2.12*	0.71	*0.10*	9.78	*1.17*	0.54	*0.06*	4.56	*0.57*	0.26	*0.04*	1.26	*0.15*	17.38	*2.12*
		[U-^{13}C]-Gln	8	96.61	*0.73*	0.26	*0.05*	2.18	*0.49*	0.07	*0.02*	0.68	*0.17*	0.02	*0.01*	0.15	*0.04*	3.39	*0.73*
			24	88.93	*1.48*	0.80	*0.13*	7.45	*0.99*	0.34	*0.04*	1.98	*0.26*	0.09	*0.01*	0.35	*0.04*	11.07	*1.48*

Mass isotopomer distribution of analyzed metabolites in BJ and BJ-HRasV12 cells

BJ and BJ H-RasV12 cells were cultured in the presence of 50% [1,2-$^{13}C_2$]-Glc (glucose) or 100% [U-^{13}C]-Gln (glutamine) in parallel experiments for 8 and 24 hours. Mass isotopomer distribution of each metabolite was analyzed as described in *Section 4.11.* Ribose, pyruvate, citrate, α-ketoglutarate, fumarate, malate and palmitate were extracted from pellets or cell cultured plates while lactate and glutamate were obtained from media. For palmitate, m/z corresponding from m0 to m8 were monitored, but only m1 to m6 were used for calculation of ∑m. Values are expressed as percentage of each mass isotopomer and denote mean ± SD of n=3.

APPENDIX II

APPENDIX II: SUPPLEMENTARY DATA FOR MASS ISOTOPOMER DISTRIBUTION OF METABOLITES PRESENTED IN CHAPTER 5.4

		m0 (%)		m1 (%)		m2 (%)		m3 (%)		m4 (%)		m5 (%)		m6 (%)		Σm (%)	
Metabolite	**Condition**	**mean**	**SD**	**mean**	**SD**	**mean**	**SD**	**mean**	**SD**	**mean**	**SD**	**mean**	**SD**	**mean**	**SD**	**mean**	**SD**
Ribose																	
	siNEG	79.55	*0.18*	14.25	*0.18*	4.11	*0.06*	1.68	*0.17*	0.38	*0.51*					20.42	*0.51*
	siTKT	81.49	*0.35*	14.89	*0.35*	1.99	*0.05*	1.47	*0.05*	0.13	*0.28*					18.47	*0.28*
	siG6PD	81.29	*0.04*	12.28	*0.04*	4.35	*0.03*	1.56	*0.11*	0.51	*0.14*					18.70	*0.14*
Lactate																	
	siNEG	89.32	*0.35*	1.35	*0.05*	9.33	*0.30*									10.68	*0.35*
	siTKT	91.84	*0.16*	1.02	*0.03*	7.13	*0.19*									8.16	*0.16*
	siG6PD	90.08	*0.63*	1.12	*0.08*	8.80	*0.57*									9.92	*0.63*
Palmitate																	
	siNEG	88.54	*1.77*	0.95	*0.35*	6.09	*0.84*	0.80	*0.14*	2.58	*0.36*	0.26	*0.03*	0.60	*0.09*	11.28	*1.78*
	siTKT	90.54	*1.94*	0.98	*0.06*	4.91	*1.10*	0.72	*0.13*	2.00	*0.44*	0.23	*0.05*	0.47	*0.13*	9.30	*1.89*
	siG6PD	95.08	*1.25*	0.49	*0.08*	2.64	*0.70*	0.35	*0.08*	1.06	*0.29*	0.09	*0.03*	0.24	*0.06*	4.86	*1.23*

Mass isotopomer distribution of analyzed metabolites in siNEG, siTKT and siG6PD transfected cells

MCF7 cells were transfected with non-targeting siRNA (siNEG) or siRNA against TKT (siTKT) or G6PD (siG6PD) and after 96 hours, media was replaced by fresh media containing 50% [1,2-$^{13}C_2$]-glucose and incubated for 24h. Mass isotopomer distribution of each metabolite at the end of incubation was analyzed as described in *Section 4.11*. For palmitate, m/z corresponding from m0 to m8 were monitored, but only m1 to m6 were used for calculation of ∑m. Values are expressed as percentage of each mass isotopomer and denote mean ± SD of n=3.

APPENDIX III

PAGES 223-234

Biochimica et Biophysica Acta 1807 (2011) 746–754

Contents lists available at ScienceDirect

Biochimica et Biophysica Acta

journal homepage: www.elsevier.com/locate/bbabio

Carbon metabolism and the sign of control coefficients in metabolic adaptations underlying K-*ras* transformation ☆

Pedro de Atauri [a,1], Adrian Benito [a,1], Pedro Vizán [a,2], Miriam Zanuy [a], Ramón Mangues [b], Silvia Marín [a], Marta Cascante [a,*]

[a] Department of Biochemistry and Molecular Biology, University of Barcelona, (associated to CSIC, IBUB, IDIBAPS, XRQTC), 08028 Barcelona, Spain
[b] Oncogenesis and Antitumor Drug Group, Networking Research Center on Bioengineering, Biomaterials and Nanomedicine (CIBER-BBN) and Biomedical Research Institute Sant Pau (IIB-Sant Pau), Barcelona, Spain

ARTICLE INFO

Article history:
Received 15 July 2010
Received in revised form 29 November 2010
Accepted 30 November 2010
Available online 23 December 2010

Keywords:
Metabolic control analysis
Control coefficient signs
Carbon metabolism
K-Ras cell transformation

ABSTRACT

Metabolic adaptations are associated with changes in enzyme activities. These adaptations are characterized by patterns of positive and negative changes in metabolic fluxes and concentrations of intermediate metabolites. Knowledge of the mechanism and parameters governing enzyme kinetics is rarely available. However, the signs—increases or decreases—of many of these changes can be predicted using the signs of metabolic control coefficients. These signs require the only knowledge of the structure of the metabolic network and a limited qualitative knowledge of the regulatory dependences, which is widely available for carbon metabolism. Here, as a case study, we identified control coefficients with fixed signs in order to predict the pattern of changes in key enzyme activities which can explain the observed changes in fluxes and concentrations underlying the metabolic adaptations in oncogenic K-*ras* transformation in NIH-3T3 cells. The fixed signs of control coefficients indicate that metabolic changes following the oncogenic transformation—increased glycolysis and oxidative branch of the pentose-phosphate pathway, and decreased concentration in sugar-phosphates—could be associated with increases in activity for glucose-6-phosphate dehydrogenase, pyruvate kinase and lactate dehydrogenase, and decrease for transketolase. These predictions were validated experimentally by measuring specific activities. We conclude that predictions based on fixed signs of control coefficients are a very robust tool for the identification of changes in enzyme activities that can explain observed metabolic adaptations in carbon metabolism. This article is part of a Special Issue entitled: Bioenergetics of Cancer.

1. Introduction

Metabolic concentrations and fluxes are the constrained components characterizing the collective action of cell metabolism, which are modulated by enzymatic activities. However, we have partial knowledge of the components of cell metabolism and the constraints relating them. Specially, we have limited knowledge of the kinetic properties of the enzymes and their regulation. Moreover, the observed heterogeneity in cell populations, associated with phenomena like protein crowding, interactions between glycolytic enzymes, and reversible associations with structural proteins or organelles [1,2] should alter both components and constraints. These limitations are likely to make systems in part unpredictable, specifically the magnitude of the changes following alterations in the activity of enzymes. Interestingly, the predicted sign of changes in metabolite concentrations and metabolic fluxes following changes in enzyme activity is likely to be more robust and allows their prediction without requiring accurate kinetic information. Metabolic control analysis (MCA) [3–5] is one framework which permits the prediction of the signs of concentration and flux changes.

In the framework of MCA, systemic properties of the whole network are described as a function of the properties of enzymes isolated from the system. Steady state fluxes and metabolite concentrations are systemic properties. Enzyme rates, by contrast,

Abbreviations: ACoA, acetyl-CoA; Cit, citrate; DHAP, dihydroxyacetone-phosphate; E4P, erythrose-4-phosphate; F16BP, fructose-1,6-bisphosphate; F6P, fructose-6-phosphate; G6P, glucose-6-phosphate; G6PD, glucose-6-phosphate dehydrogenase; GAP, glyceraldehyde-3-phosphate; GAPDH, glyceraldehyde 3-phosphate dehydrogenase; HK, hexokinase; HexP, hexose phosphates; αKG, α-ketoglutarate; LDH, lactate dehydrogenase; Mal, malate; MCA, metabolic control analysis; Oaa, oxaloacetate; PenP, pentose phosphates; PPP, pentose-phosphate pathway; PEP, phosphoenol pyruvate; PFK, phosphofructokinase; Pyr, pyruvate; PK, pyruvate kinase; R5P, ribose-5-phosphate; S7P, sedoheptulose-7-phosphate; SucCoA, succinate-CoA; TKT, transketolase; TrisP, triose phosphates

☆ This article is part of a Special Issue entitled: Bioenergetics of Cancer.

* Corresponding author. Tel.: +34 4021593; fax: +34 4021559.
E-mail addresses: pde_atauri@ub.edu (P. de Atauri), adriabenito@ub.edu (A. Benito), Pedro.Vizan@cancer.org.uk (P. Vizán), mzanuy@ub.edu (M. Zanuy), rmangues@hsp.santpau.es (R. Mangues), silviamarin@ub.edu (S. Marín), martacascante@ub.edu (M. Cascante).
[1] These authors contributed equally to this work.
[2] Present address: Laboratory of Developmental Signalling, Cancer Research UK London Research Institute, London WC2A 3LY, United Kingdom.

0005-2728/$ – see front matter © 2010 Elsevier B.V. All rights reserved.
doi:10.1016/j.bbabio.2010.11.015

are properties of the isolated enzymes, and depend on the specific mechanism and parameters governing the enzyme kinetics. Under MCA, an *elasticity* ε_{qk} is the parameter sensitivity of the rate v_q of an isolated reaction—at steady state conditions—with respect to changes in the concentration x_k of one of its substrate, inhibitor or any other kinetic effectors of the isolated reaction [3,4]:

$$\varepsilon_{qk} = \frac{\partial \ln v_q}{\partial \ln x_k} \tag{1}$$

Similarly, a *control coefficient* is a system property defined as the sensitivity of a metabolite concentration x_g or a flux J_q with respect to changes in some parameter p—usually the enzyme concentration—which will in principle be proportional to the rate v_k when the enzyme is isolated, and then associated to the enzyme activity [3,4]:

$$C_{gk} = \frac{\partial \ln x_g}{\partial \ln p} \Big/ \frac{\partial \ln v_k}{\partial \ln p} = \frac{\partial \ln x_g}{\partial \ln v_k} \tag{2}$$

$$C_{qk} = \frac{\partial \ln J_q}{\partial \ln p} \Big/ \frac{\partial \ln v_k}{\partial \ln p} = \frac{\partial \ln J_q}{\partial \ln v_k} \tag{3}$$

Different approaches have been proposed for describing the control coefficients, including methods based on matrices [6–10] and those based on graph theoretical procedures [11,12]. These methods allow the derivation of large expressions describing the control coefficients, whose sign and magnitude are a function of the pathway stoichiometry, the elasticities, and the ratios of fluxes in branched pathways. In systems with moiety conservations, concentrations are also required [8,10]. The sign of a control coefficient—positive or negative—is sufficient to predict whether a flux or concentration will increase or decrease when an enzyme activity is changed. Positive control coefficient indicates that changes in x_g or J_q will follow the same pattern as changes in v_k. This means an increase of v_k will induce an increase of x_g or J_q, while decreasing v_k will also decrease the value of x_g or J_q. Negative control coefficient, on the contrary, indicates that changes in v_k will induce an inverse effect on the changes in x_g or J_q.

Some control coefficients have fixed signs, irrespective of the magnitudes of the elasticities and fluxes, and then they are either always positive or always negative [13,14]. Other control coefficients are sign-indeterminate, meaning they can be positive or negative, and some control coefficients are always zero. The classification into these types of control coefficients requires the only knowledge of the metabolic network structure and the direction of regulatory dependencies of the network, which basically refers to the positive or negative sign of the elasticities: i) elasticities with respect to substrates or activators are always positive; ii) elasticities with respect to inhibitors—or products in reversible reactions—are always negative. The fixed sign will be maintained while both structure and qualitative regulatory dependencies are maintained. Each control coefficient predicts changes in fluxes and concentrations resulting from the change of one enzyme activity. In general, the predictive value of this normalized derivative is accurate for infinitesimal changes of the enzyme activity and decays for larger changes due to the redistribution of the elasticities and fluxes. The prediction of the sign of a sign-fixed control coefficient is a positive or negative direction that is not modified for large changes.

In the present work, we take advantage of sign-fixed control coefficients to derive hypotheses about the enzyme activities which are modified in order to achieve specific changes in glycolytic and pentose phosphate pathway (PPP) fluxes and concentrations. As a case study of metabolic reprogramming, we have analyzed the transformation with mutated *K-ras* oncogenes of a mouse embryonic fibroblast cell line NIH-3T3. Oncogenic Ras-transformed NIH-3T3 cells have been used as a model system to explore characteristics associated with cell transformation, such as a higher aerobic glycolysis and changes of enzyme activities [15–18]. Ras proteins are a family of small GTPases activated in response to extracellular stimuli and leading to the activation of several signalling cascades [19–21]. Among the different isoforms, K-Ras is the Ras protein which plays a major role in cancer. NIH-3T3 cells stably transfected with constitutively active K-*ras* mutated at codon 12 or codon 13 (K12- and K13-transformed cells) induce tumours with distinct survival strategies, associated with distinct transforming capabilities and aggressiveness [22,23]. Previously, we measured significant changes in carbon metabolism of K12- and K13-transformed cells based on stable-isotope (^{13}C) tracer-based technologies [24]. Interestingly, both mutants showed an increased utilization of the oxidative branch of the PPP, higher for K13 cells, compared with non-transformed NIH-3T3 cells.

In order to derive hypotheses about the enzyme activities that contribute to the reprogramming of carbon metabolism: 1) we characterized metabolic adaptations in non-transformed and K12- and K13-transformed cells by means of experimentally measured external and internal metabolite concentrations; and 2) we computed the network flux distribution using a constraint based approach and the data obtained of external metabolite variations; 3) we identified control coefficients with fixed signs in order to predict the pattern of changes in enzyme activities which can explain the observed increases or decreases in fluxes and concentrations; and 4) finally, we measured specific activities of key enzymes in order to validate the predictions on the enzyme activity increases or decreases compatible with the observed flux and concentration changes.

2. Materials and methods

A combination of experimental and mathematical–computational methods was applied including the measurement of glucose uptake (J_A), lactate production (J_T), and glutamate–glutamine uptake (J_U) together with measurements of sugar phosphate concentrations and enzyme specific activities. All measures were replicated in independent experiments. Mathematical–computational methods were performed using *Mathematica* [25].

2.1. Cell lines and culture

NIH-3T3 cells were obtained from the American Type Cell Culture (ATCC). The transfectants contained a K-*ras* minigene with a G:C → A:T mutation at the first position of codon 12 (K12 cells) and a G:C → A:T mutation at the second position of codon 13 (K13). All lines were maintained in Dulbecco's Modified Eagle Medium (DMEM) in the presence of 10% FBS, 25 mM D-glucose and 4 mM L-glutamine, at 37 °C in 95% air–5% CO_2. Geneticin© Selective Antibiotic (GIBCO) was used as a selective antibiotic in K12 and K13 cells.

For biochemical and enzyme activity measurements, cells were seeded in p100 dishes at different densities between $0.8 \cdot 10^6$ and $1.2 \cdot 10^6$ cells/cm^2. 24 h after seeding, incubation medium was removed and cells were incubated for 72 h with DMEM containing 10% FBS, 25 mM D-glucose and 4 mM L-glutamine. At the end of the incubations, media for biochemical analysis were removed and frozen at −20 °C until processing. Cells for sugar phosphates determination were immediately frozen in liquid nitrogen and kept at −80 °C until processing. Cells for activity measurements were washed with PBS and scrapped in a lysis buffer as detailed below. Cell counting was performed with a haemocytometer.

2.2. Protein concentration

Protein concentration of cell extracts was determined using the BCA Protein Assay (Pierce Biotechnology, Rockford, IL).

2.3. Measurements of media metabolites consumption and production

Glucose, lactate, glutamate, and glutamine concentrations were determined from frozen medium samples as previously described [26–28] using a Cobas Mira Plus chemistry analyzer (ABX). The rates of the medium metabolites consumption/production—glucose consumption (J_A), lactate production (J_T) and glutamate from glutamine consumption (J_U)—are derived from the total measured consumptions/production of metabolites and corrected according to the measured cell proliferation, assuming exponential growth and constant consumption or production. The rate of glutamate from glutamine consumption is derived from the measured rates of glutamine consumption and glutamate accumulation. All the values are expressed in micromol of metabolite consumed or produced per milligram of protein and hour (μmol mg prot^{-1} h^{-1}).

2.4. Sugar phosphates determination

Hexose, pentose and triose phosphates were determined in cell monolayers frozen in liquid nitrogen using addition curve methods as described [29]. The MRM (multiple reaction monitoring) transitions were 339/97 for fructose-1,6-bisphosphate (F16BP), 259/97 for glucose-6-phosphate (G6P) and fructose-6-phosphate (F6P) (hexose phosphates) (HexP), 229/97 for ribose-5-phosphate (R5P) and xylulose-5-phosphate (pentose-phosphates) (PenP), 169/97 for glyceraldehyde-3-phosphate (GAP) and dihydroxyacetone phosphate (triose phosphates) (TrisP) and 167/79 for phosphoenol pyruvate (PEP). Sugar phosphate concentrations are expressed as nanomol per milligram of protein (nmol mg prot^{-1}).

2.5. Enzyme activity determinations

Activities of the glycolytic enzymes hexokinase (HK), pyruvate kinase (PK), and lactate dehydrogenase (LDH), and PPP enzymes glucose-6-phosphate dehydrogenase (G6PD) and transketolase (TKT), were determined from cell culture extracts. Enzyme activities are expressed as milliunits per milligram of protein (mU mg prot^{-1}).

Preparation of cell extracts for enzyme activity determination. Cell cultures were washed with PBS and scrapped in lysis buffer (20 mM Tris–HCl, pH 7.5, 1 mM dithiothreitol, 1 mM EDTA, 0.02% Triton X-100, 0.02% sodium deoxycholate) supplemented with protease and phosphatase inhibition cocktails. Cell lysates were disrupted by sonication (3 cycles of 5 s) and immediately ultracentrifuged at 105,000 ×*g* for 1 h at 4 °C. The supernatant was separated and used for the determination of enzyme activities using a Cobas Mira Plus chemistry analyzer (HORIBA ABX, Montpellier, France). All enzymatic activities were determined by monitoring NADH/NADPH increment or decrement at a wavelength of 340 nm.

A strong decrease of the mitochondrial Complex I activity has been recently reported in K-*ras* transformed cells [30]. The conditions of extract preparation using a soft lysis buffer as well as soft sonication have been optimised to minimise the extraction of mitochondrial Complex I activity and other membrane-bound enzymes. The absence of unspecific coenzyme (NADH or NADPH) consumption/production has been checked before the addition of the reaction substrate for all the enzyme activities measured.

Glucose-6-phosphate dehydrogenase (G6PD, EC 1.1.1.49) activity was measured as described in Tian et al. [31]. Briefly, samples were added to a cuvette containing 0.5 mM $NADP^+$ in 50 mM Tris–HCl, pH 7.6 at 37 °C. Reactions were initiated by the addition of G6P up to a final concentration of 2 mM.

Hexokinase (HK, EC 2.7.1.1) activity was determined by coupling HK reaction to G6PD enzyme in the following conditions: 3.3 mM $NADP^+$, 14.8 mM ATP, 14.8 mM $MgCl_2$, 2.8 U/mL G6PD and 50 mM Tris–HCl, pH 7.6 at 37 °C. Reactions were initiated by the addition of glucose to a final concentration of 10 mM.

Transketolase (TKT, EC 2.2.1.1) activity was determined using the enzyme linked method described by Smeets and colleagues [32]. Briefly, samples were added to a cuvette containing 5 mM $MgCl_2$, 0.2 U/ml triose phosphate isomerase, 0.2 mM NADH, 0.1 mM thiamine pyrophosphate in 50 mM Tris–HCl, and pH 7.6 at 37 °C. The reaction was initiated by the addition of a substrate mixture in 1:2 proportion (substrate mixture : final volume) prepared by dissolving 50 mM R5P in 50 mM Tris–HCl, pH 7.6 with 0.1 U/ml ribulose-5-phosphate-3-epimerase and 1.7 mU/ml phosphoriboisomerase. The substrate mixture was continuously stirred and heated for 1 h at 37 °C and then kept at −20 °C until use.

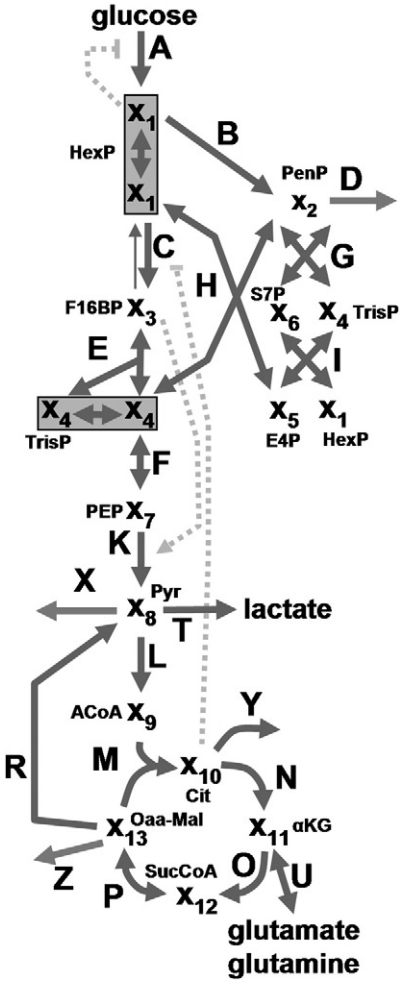

Fig. 1. Network scheme. Each arrow indicates a reversible or irreversible reaction step catalyzed by an enzyme (or transporter) or one block of enzymes. Grey dashed lines account for the regulatory circuits (inhibitions and activations).

Pyruvate kinase (PK, EC 2.7.1.40) activity was determined by coupling the PK reaction to the LDH enzyme in the following conditions: 0.8 mM NADH, 1.6 mM ADP, 12.1 mM $MgCl_2$, 36.8 mM KCl, 5.2 U/mL LDH in 20 mM phosphate buffer, pH 7.2 at 37 °C. Reactions were initiated by the addition of PEP up to a final concentration of 3.5 mM.

Lactate Dehydrogenase (LDH, EC 1.1.1.27) activity was measured at 37 °C by adding sample extracts to a cuvette containing 0.2 mM of NADH and 100 mM phosphate buffer, pH 7.4. Reaction was initiated by the addition of pyruvate (Pyr) up to a final concentration of 0.2 mM.

2.6. Isotopomer abundances

^{13}C labelled substrates generate for each metabolic product a set of different labelled molecules—*isotopomers*—that differ only in the labelling state of their individual carbon atoms. In a previous paper [24] 50% [1,2-^{13}C]-D-glucose was used as tracer and the generation of ^{13}C labeled products was measured retaining for each product the relative abundances of the non-labelled isotopomer form (m0), and

the isotopomers with one ^{13}C (m1), two ^{13}C (m2), three ^{13}C (m3), etc. The isotopomer abundances of lactate are here applied to describe the ratio of fluxes through oxidative PPP (J_B) with respect to the entry of glucose (J_A) [33]: $f1 = J_B/J_A = 3\times(m1/m2)/(3+(m1/m2))$.

2.7. Statistical analysis

Two-tailed Student's t-test was performed in order to compare metabolite concentrations and activities of non-transfected against K12- and K13-transfected cells. Differences were considered significant for $p<0.1$.

3. Results

3.1. Metabolic adaptations in K12- and K13-transformed NIH-3T3 cells

3.1.1. System description

The scheme of the whole network under study is depicted in Fig. 1. Fluxes are represented with letter *J*, where J_i refers to the steady state metabolic flux through the *i*th step; concentrations are represented with letter *x*, where x_i refers to the concentration of the *i*th metabolic intermediary; and activities are represented with letter *v*, where v_i refers to the rate of the isolated reaction of the *i*th step. Solid arrows (Fig. 1)—reaction steps *A* to *Z*—refer to the principal carbon metabolism, including glycolysis, the PPP, the tricarboxylic acid cycle and the main inputs and outputs. Some reactions were neglected and grouped into blocks—e.g. reaction step *F* refers to the block from glyceraldehyde 3-phosphate dehydrogenase (GAPDH) to enolase—and others were assumed to be involved in rapid equilibriums—e.g. glucose-6-phosphate isomerase. Metabolites were combined into different pools: the pool x_1 for HexP refers to G6P and F6P; the pool x_2 for PenP refers to R5P; ribulose-5-phosphate and xylulose-5-phosphate; the pool x_4 for TrisP refers to dihydroxyacetone-phosphate (DHAP) and GAP; and the pool x_{13} refers to oxaloacetate (Oaa) and malate (Mal). The rest of metabolic intermediaries are F16BP (x_3), sedoheptulose-7-phosphate (x_6; S7P), erythrose-4-phosphate (x_5; E4P), PEP (x_7), Pyr (x_8), acetyl-CoA (x_9; ACoA), citrate (x_{10}; Cit), α-ketoglutarate (x_{11}; αKG) and succinate-CoA (x_{12}; SucCoA). In our system, the main fluxes in or out of the defined metabolic network correspond to experimentally measured glucose consumption (J_A), glutamate from glutamine consumption (J_U), and lactate production (J_T). Additional output exchanges connected to biosynthetic processes were not associated with a measured value (J_D, J_X, J_Y, J_Z).

3.1.2. Flux distributions

Under steady-state conditions, the flux balance associated with the stoichiometry constrains the dependences among fluxes [34–36]. In order to estimate the different flux distributions of non-transformed, K12- and K13-transformed cells, the fluxes for internal reactions can be expressed as dependent on a subset of fluxes including all output and input fluxes, e.g.:

$$\begin{aligned}
J_C &= J_E = J_A - {}^1/_3\,(J_B + 2\times J_D),\\
J_F &= J_K = 2\times J_A - {}^1/_3\,(J_B + 5\times J_D),\\
J_{Gf} &= {}^1/_3(J_B - J_D) + J_{Gb},\\
J_{Hf} &= {}^1/_3\,(J_B - J_D) + J_{Hb},\\
J_{If} &= {}^1/_3\,(J_B - J_D) + J_{Ib},\\
J_L &= J_M = 2\times J_A - {}^1/_3\,(J_B + 5\times J_D) - J_T + J_U - J_X - J_Y - J_Z,\\
J_N &= 2\times J_A - {}^1/_3(J_B + 5\times J_D) - J_T + J_U - J_X - 2\times J_Y - J_Z,\\
J_O &= J_P = 2\times J_A - {}^1/_3\,(J_B + 5\times J_D) - J_T + 2\times J_U - J_X - 2\times J_Y - J_Z,\\
J_R &= J_U - J_Y - J_Z,
\end{aligned} \tag{4}$$

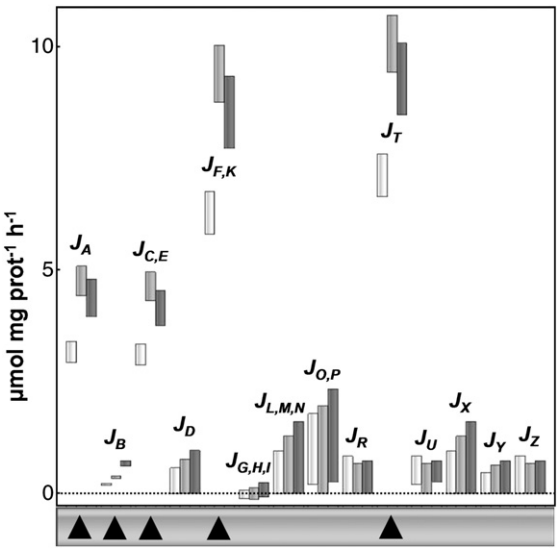

Fig. 2. Comparison of fluxes. Non-transformed NIH-3T3 cells (white); K12-transformed cells (light gray); and K13-transformed cells (dark gray). ▲) Increased flux in transformed cells with respect to non-transformed cells; and ▼) Decreased flux in transformed cells with respect to non-transformed cells. Some dependent fluxes are grouped together: J_C *and* J_E ($J_{C,E}$); J_F *and* J_K ($J_{F,K}$); J_G, J_H *and* J_I ($J_{G,H,I}$) ; J_L, J_M *and* J_N ($J_{L,M,N}$); *and* J_O *and* J_P ($J_{O,P}$).

where J_{Gf}, J_{Hf}, J_{If} and J_{Gb}, J_{Hb}, J_{Ib} are the forward (J_{if}) and backward (J_{ib}) fluxes through the reversible reactions $J_G = J_{Gf} - J_{Gb}$, $J_H = J_{Hf} - J_{Hb}$, and $J_I = J_{If} - J_{Ib}$. An additional constraint was imposed based in our previous isotopomer-based analysis of non-transformed NIH-3T3 cells and K12- and K13-transformed cells [24] (see Section 2.6):

$$J_B = f_1 \times J_A \tag{5}$$

where factor f_1 relates the oxidative branch of PPP (J_B) with the entry of glucose (J_A). This factor was set according to the measured ratios [24]: 0.063 ± 0.004 for non-transformed cells; 0.076 ± 0.012 for K12-transformed cells; and 0.153 ± 0.016 for K13-transformed cells. Thus, the flux through the oxidative branch of PPP was significantly lower than that descending through the glycolysis, and there was a significant increase of the flux through the PPP in transformed cells compared to non-transformed NIH-3T3 cells. Between transformed cells, K13 mutants routed more glucose to the oxidative branch of PPP than K12 mutants.

All these assumptions and measures are constraints limiting the space of solutions for the internal metabolic fluxes. Unfortunately, the complete system cannot be determined with the available measurements. Uncertainty is associated with the measured exchange fluxes (J_A, J_T, J_U) and, specially, with those not measured (J_X, J_Y, J_Z, J_D). An interval constraint satisfaction approach was applied as suggested by Llaneras and Picó [37] for cases where available measurements are insufficient and the complete flux distribution cannot be uniquely calculated. The feasible range of solutions satisfying all constraints was estimated for each reaction step. Initial lower and upper bounds for intervals were assigned to the flux through all reaction steps: 1) lower and upper bounds were assigned as the mean value ± 1.5 × standard deviation for measured fluxes J_A, J_T, and J_U; 2) a lower bound of zero was assumed for the irreversible fluxes $J_B, J_D, J_K, J_L, J_M, J_N, J_O, J_R, J_S, J_X, J_Y, J_Z$, which were assumed to have positive values ($0 < J_i$). For each cell type, the lower and upper bounds were constrained to satisfy the stoichiometric description of the system Eq. (4) and the isotopomer-based constraint in Eq. (5). These intervals of fluxes satisfying all constraints were calculated by two independent procedures: 1) iterative interval propagation, or 2) solving each minimum and maximum bound through linear programming, taking

advantage of the linear nature of the problem. The resulting flux distributions for non-transformed cells, K12- and K13-transformed cells are shown in Fig. 2, which graphically depicts the interval ranges of flux values which satisfy all the constraints. As an example, for non-transformed cells, the initial intervals were $2.04<J_A<3.41$, $0<J_B<\infty$, $-\infty<J_C<\infty$, $0<J_D<\infty$, $-\infty<J_E<\infty$, $-\infty<J_F<\infty$, $0<J_G<\infty$, ..., $6.63<J_T<9.56$, $0.20<J_U<0.84$,..., and the final intervals satisfying all constraints (solution space) computed with both iterative interval propagation and linear programming were $2.93<J_A<3.41$, $0.18<J_B<0.21$, $2.86<J_C<3.34$, $0<J_D<0.57$, $2.86<J_E<3.34$, $5.80<J_F<6.75$, $-0.11<J_G<0.07$, ..., $6.63<J_T<7.59$, $0.20<J_U<0.84$, ... Even with the propagated uncertainty, substantial changes in flux distribution are detected in transformed cells with respect non-transformed cells, in particular for the flux pattern in glycolysis and the oxidative branch of the PPP.

3.1.3. Metabolite concentrations

Changes in fluxes were coupled with additional experimental measurement of key sugar phosphate concentrations. Thus, the concentrations of HexP (x_1), PenP (x_2), F16BP (x_3), TrisP (x_4), and PEP (x_7) were measured for non-transformed and transformed cells (K12 and K13) and are compared in Fig. 3. All concentrations were found to be slightly decreased in transformed cells.

3.2. Predicted changes in fluxes and concentrations

3.2.1. The sign of control coefficients

In order to identify control coefficients with fixed signs, all regulatory dependences were considered. The matrix approach proposed by Cascante et al. [9,10] was applied and is depicted in Fig. 4. A matrix M^{-1} with all concentration control coefficients and all independent flux control coefficients can be derived from the inverse of a matrix M containing all elasticities and flux dependences. The sign of the elasticities is taken in order to derive the sign of the control coefficients. For example, the dependence of G6PD (reaction step B) on its substrate (HexP, x_1) corresponds to a positive elasticity ε_{B1}. In Fig. 1, grey dashed lines account for the regulatory circuits—i.e. product (G6P, x_1) inhibition of HK (reaction step A) [38], inhibition of phosphofructokinase (PFK, reaction step C) by Cit (x_{10}) [39] and activation of PK (reaction step K) by F16BP (x_3) [40,41], which are associated with negative (ε_{A1}), negative (ε_{C10}) and positive (ε_{K3})

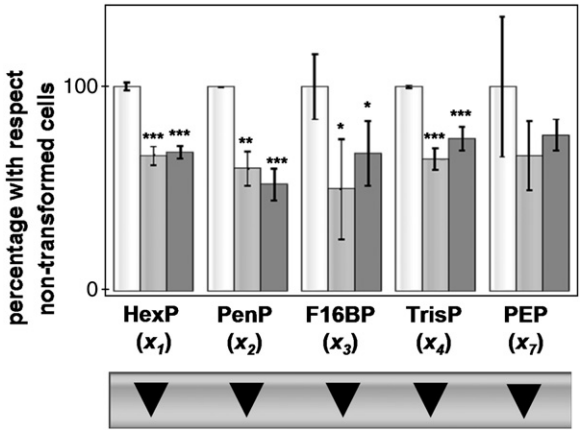

Fig. 3. Comparison of measured concentrations. Values for concentrations are proportional to the bar height for each chemical specie and error bars correspond to standard deviations. See legend of Fig. 2 for meaning of colours and triangles. As a reference for sugar phosphate concentrations, [F16BP] = 3.229 nmol mg prot^{-1}, [HexP] = 1.799 nmol mg prot^{-1}, [PenP] = 0.726 nmol mg prot^{-1}, [TrisP] = 2.710 nmol mg prot^{-1} and [PEP] = 0.457 nmol mg prot^{-1} for non-transformed NIH-3T3 cells. P-values using two-tailed Student's t-test: *: $p<0.1$, **: $p<0.05$; ***: $p<0.01$.

elasticities, respectively. Reversibility is associated with negative elasticities with respect to products. Finally, reaction steps D, X, Y and Z describing the demand of synthetic processes were assumed to be saturated with respect to their respective substrates and then controlled by the demand; so, the elasticities ε_{D2}, ε_{X8}, ε_{Y10}, and ε_{Z13} were set to be zero.

The sign of each control coefficient was analyzed by checking the positivity or negativity of the determinant $|M|$ and the adjoint matrices in $Adj(M)$ used for the derivation of the inverse:

$$M^{-1} = \frac{1}{|M|}(Adj(M))^{\mathrm{T}} \tag{6}$$

Since the determinant |M| was positive, the sign depended on the adjoint matrices. The matrix M^{-1} in Fig. 4b shows all control coefficients for independent fluxes and concentrations derived from this analysis. Control coefficients for the dependent fluxes can be derived by considering the dependences among fluxes in Eq. (4) and the control coefficients of independent fluxes [9,10], as demonstrated in the example provided in Fig. 4c. A subset of control coefficients signs are presented in Fig. 4d in a table of dependences between the fluxes and concentrations and the main enzyme activities. Positive and negative symbols correspond to control coefficients with positive and negative signs, respectively. The signs in Fig. 4d collectively give a complete systemic predictive tool which can be used to evaluate the expected impact of changes in enzyme activities. Thus, the specific pattern of observed changes in fluxes and concentrations can be associated with increases or decreases of enzyme activities through analysis of the signs of control coefficients. For example, the observed decrease in the concentration of PEP (x_7) could correspond to an increase of PK activity (v_K), but never due to a decrease.

3.2.2. The magnitude of the control coefficients

The analysis of the signs of metabolic control coefficients is sufficient if the aim is to predict the direction of changes in concentrations and fluxes. However, this previous analysis does not suffice if the objectives are to predict the magnitudes of these changes, and then the magnitude of the control coefficients is required. Unknown elasticities can be randomly sampled in order to derive feasible magnitudes for control coefficients [42]. We have applied sampling procedures based on those described by Wang et al. [42] in order to have an additional independent evaluation of the sign and mean magnitude of the control coefficients (results exactly match the computed signs). This analysis identified a subset of control coefficients which are always associated with small magnitudes. In the system considered (Fig. 1) the PPP is a sub-network characterized by a flux which is much smaller than the main fluxes through the rest of the network ($J_B \lll J_C$). The effect of changes in the activity throughout this sub-network will have minimal effect on the rest of the system, but these changes can have a significant effect on the concentrations and reaction steps inside the sub-network. The dependence of control coefficients on particular fluxes, such as J_B, can be easily identified by inspecting the adjoint matrices. Control coefficients identified with black circles in Fig. 4d are directly proportional to the value of J_B, which implies very small magnitudes due to the small flux through the oxidative branch of the PPP.

3.3. Testing and validation of hypotheses based on variations in enzyme activities

3.3.1. Specific activities

The specific activities of HK (v_A), G6PD (v_B), TKT (v_G, v_H), PK (v_K), and LDH (v_T) were measured for non-transformed and transformed (K12 and K13) cells and compared in Fig. 5a. Increases or decreases in specific activities observed during the metabolic adaptation associated with the K-*ras* transformation were analysed. Clear changes were observed for

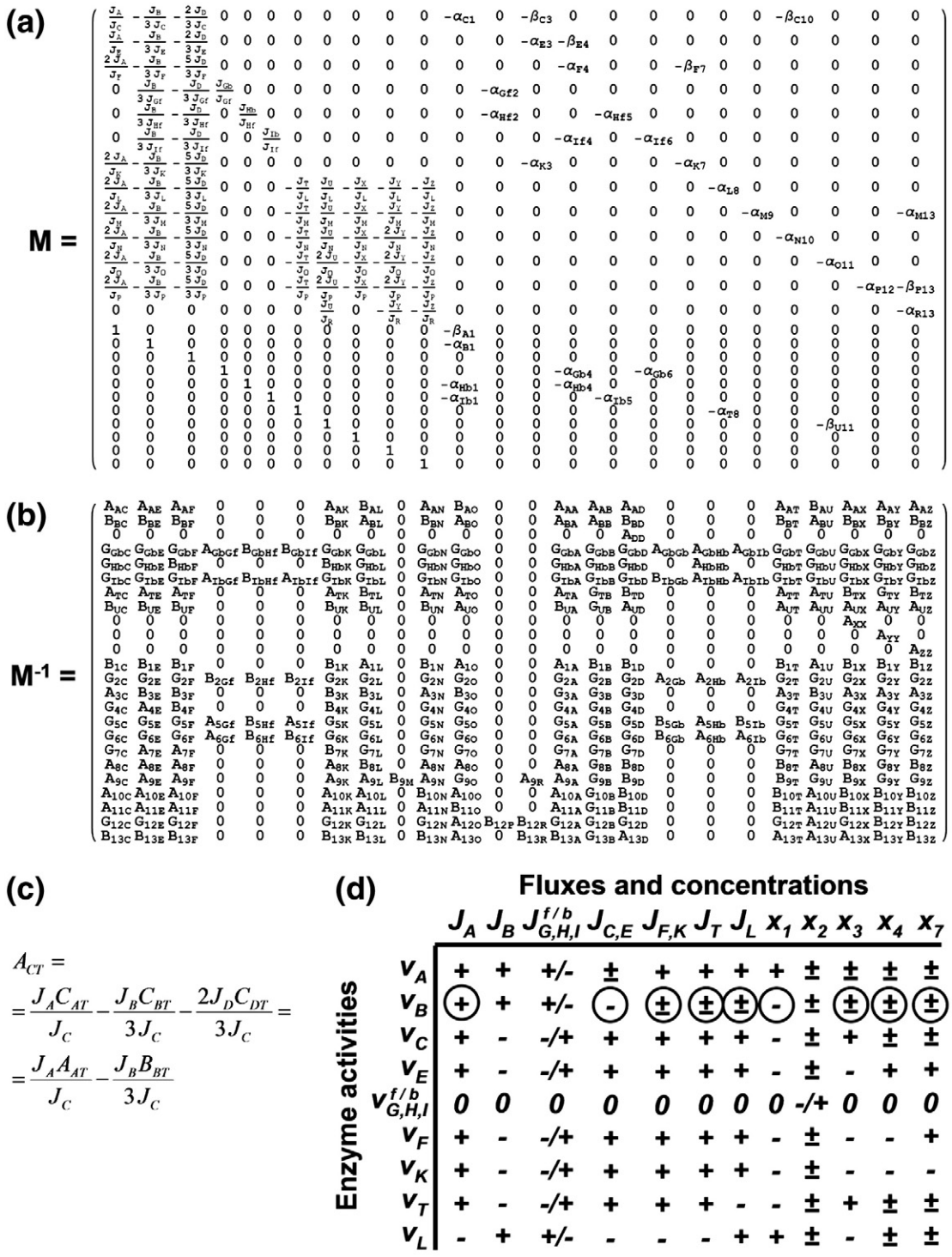

Fig. 4. Matrix estimation of the sign of control coefficients. For details about the method see [9,10]. Elasticities with a magnitude of zero appear as *0*, while those positives are represented with a letter α ($\alpha_{ki}=\varepsilon_{ki}>0$), and those negatives with a letter β ($\beta_{ki}=\varepsilon_{ki}<0$); control coefficients with a magnitude of zero appear as *0*, while these positives are represented with the letter *A* ($A_{ki}=C_{ki}>0$) or a symbol "+", and these negatives with the letter *B* ($B_{ki}=C_{ki}<0$) or a symbol "−"; Those control coefficients with indeterminate signs are represented with a letter *G* ($G_{ki}=C_{ki}>0$ *or* $C_{ki}<0$) or a symbol "±". A matrix *M* (a) with the information containing both the stoichiometry and the regulatory properties of the analysed system (elasticities and ratios among fluxes), is inverted to obtain the matrix of control coefficients M^{-1} (b) for independent fluxes and concentrations. (c) An example of estimation of a control coefficient of dependent fluxes from the previously estimated control coefficients of independent fluxes. (d) Table of dependences connecting changes in fluxes and concentrations with changes in enzyme activities for a subset of analyzed control coefficients. Superscripts "f" and "b" refers to net direction of reversible reactions of the non-oxidative branch of PPP (*G,H,I*) following the forward or the backward directions, respectively. The net fluxes for the remaining reversible reactions are set to follow only the forward direction according to Fig. 2. Symbols ("+","−","±") identified with a black circle refer to control coefficients of very low magnitude in comparison with the other ones (see Section 3.2.2).

G6PD and LDH for both K12 and K13 transformed cells, with slight changes also for TKT with both K12 and K13 transformed cells and also for PK with K13 transformed cells. There were no significant changes in the observed HK activities.

3.3.2. Do changes in measured activities satisfy the predictions for concentrations and fluxes?

The table of dependences in Fig. 5b identifies both satisfied and non-satisfied predictions of the sign of control coefficients for those

activities with measured changes (v_B, v_G, v_H, v_K and v_T). Satisfied predictions, which are those where the direction of the changes in a concentration or flux is explained by the direction of the change in an enzyme activity, are marked in green. Otherwise, if the prediction is not satisfied, the sign of the control coefficients is marked in red. For example, the increase in LDH activity (v_T) could help to explain the measured increase in J_A, but not the increase in J_B, which is satisfied by the increased G6PD activity (v_B). Predictions regarding TKT are more complicated because the slight decrease of TKT activity could contribute to a predicted decrease of PenP levels (x_2), but only if the net flux through the non-oxidative branch of PPP is following the backward direction to PenP as is shown in Fig. 5b.

Indeterminate signs (±) identify control coefficients that can be positive or negative, depending on the relative values of the elasticities and ratios between fluxes. For a set of such sign-indeterminate control coefficients, only a limited combination of positive and negative signs is possible. Indeterminate signs (±) marked in green were used in Fig. 5b to highlight that a specific and feasible combination of elasticities and fluxes can result in a combination of signs which satisfy the changes in fluxes and concentrations. For example, the measured decreases in x_2, x_4, and x_7 can be predicted by an increase in v_T activity, which is possible because the negative control coefficients for C_{2T}, C_{4T}, and C_{7T} can be obtained by selecting the appropriate elasticities.

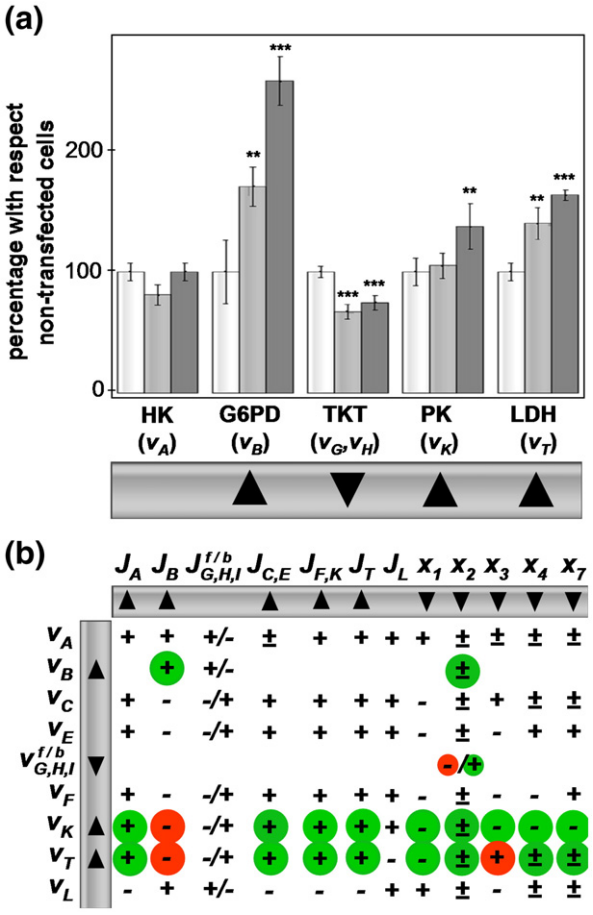

Fig. 5. Specific activities and satisfied predictions. (a) Comparison of specific activities. See legend of Figs. 2 and 3 for meaning of bar height, error bars, colours and triangles. As a reference for specific activities, HK = 130.17 mU mg prot^{-1}, LDH = 2.83 U mg prot^{-1}, G6PD = 215.02 mU mg prot^{-1}, TKT = 35.72 mU mg prot^{-1} and PK = 6.98 U mg prot^{-1} for non-transformed NIH-3T3 cells. P-values using two-tailed Student's t-test: *: $p<0.1$, **: $p<0.05$; ***: $p<0.01$. (b) Satisfied predictions represented in the table of dependences connecting changes in fluxes and concentrations with changes in enzyme activities. See legend of Fig. 4 for meaning of superscripts "f" and "b", and positive-negative symbols ("+","−","±"). Symbols marked in green or red refers to control coefficients that can explain or cannot explain, respectively, the observed directions of a change in a flux or a concentration with respect to the direction of a measured change in an enzyme activity (see Section 3.3.2).

4. Discussion

The existence of control coefficients with fixed or indeterminate signs is dependent on the topology of the metabolic pathway and location of regulatory loops (feedback, feed-forward), branches, etc. [13]. The signs of the control coefficients estimated above (Fig. 4) were obtained by assuming a model adapted to the available data, where the relevant topology and regulation are considered. Analysis of the signs of control coefficients in Fig. 5b provides a complete picture of the potential effect that any change in enzyme activities would have on systemic properties such as fluxes and metabolite concentrations. This picture confirms that the increased fluxes from glucose to lactate (J_A, J_C, J_E, J_F, J_K, J_T) and through the oxidative part of the PPP (J_B) (Fig. 2), and the decreased concentrations of sugar phosphates (x_1, x_2, x_3, x_4, x_7) (Fig. 3), observed in transformed cells, can be explained in part by the increased specific activities for G6PD (v_B), PK (v_K), LDH (v_T), and decreased activity of TKT (v_G,v_H) (Fig. 5a). Interestingly, the differences between the phenotypes of K12 and K13 tranformed cells [22–24] are reflected by the magnitude of the changes in fluxes and not by the sign of these changes. Changes in enzyme activities are also in the same direction (with the same sign of change) for both transformed cells with the exception of PK activity which is only increased significantly in the K13 cell line.

The measured changes in specific enzyme activities accounts for changes in the enzyme concentrations. It should be noted that *in vivo*, changes affecting an enzyme activity can be as a result of the changes on its expression but also due to a variety of events including: changes in cofactors, post-transductional modification or changes in oligomerization state among others. One example of this is the case of PK. Among the different PK isoforms, the M2-PK isoenzyme is expressed in all proliferating cells, including embryonic, tumour and NIH-3T3 cells [41]. The M2-PK isoenzyme occurs in a highly active tetrameric form and in a dimeric form with low affinity for PEP [40]. The tetramer to dimer ratio of M2-PK is not static and depends on F16BP levels in addition to any effects due to other external mechanisms [40].

The measured changes of the specific activities for G6PD (v_B), PK (v_K), and LDH (v_T) satisfy the predictions based on the sign of the control coefficients. Interestingly, Fig. 5b shows that the set of observed changes in fluxes and concentrations accompanying K12- and K13-transformation cannot be attributed to the perturbation of a single enzyme activity. According to results depicted in Fig. 5b, simultaneous activation of G6PD and some of the glycolytic enzymes is required in order to fully explain the observed pattern of changes in fluxes and metabolite concentrations. The experimentally measured increase in G6PD and in some glycolytic enzymes (LDH (v_T) and PK (v_K)) confirms this prediction and helps to explain qualitatively almost all observed increases in fluxes and decreases in concentrations, although it is likely that other glycolytic enzyme activities could also be increased. The predictions of Fig. 5b are also in agreement with the available literature on tumour metabolism that suggests the action of transcription factors, as c-myc and the hypoxia-inducible transcription factor 1 (HIF-1), which are associated with the activation of oncogenes including transforming *ras*. This leads to the reprogramming of different components of the cell metabolism, including higher expression for most of the genes encoding glycolytic enzymes [38,43–48]. Among the enhanced enzymes are mammalian isoforms of HK (HK1 and 2), PK (M2-PK) and LDH (LDH-A). We have also observed changes in LDH for both K12 and K13 cells in addition to changes in PK for K13 cells. However, HK activity is not significantly altered by either of the two transformed cell

lines. Interestingly, in the previous work of Guerrero et al. [22,23] for the same K12- and K13-transformed NIH-3T3 cells used in the present study, they showed an increased expression of GAPDH for both transformed cell lines with respect to the non-transformed ones. From Fig. 5b we can predict that this increase of GAPDH (v_F) can also contribute to the observed metabolic phenotype of transformed cells.

Taking into account that control is distributed among the enzymes of glycolysis, it is not surprising that simultaneously increasing a number of different glycolytic enzymes is required in order to achieve a large increase in glycolytic flux. Thus, in a linear pathway, all the control coefficients are positive and their sum is equal to one [3], which means that, if the control is shared between several enzymes, then the magnitude of each individual control coefficient is expected to be quite low. A very low control coefficient indicates that in order to alter the flux significantly by using modifications of a single enzyme, a very large change in the enzyme concentration is required. However, a simultaneously balanced change in all glycolytic enzyme concentrations should result in both a directly proportional change in the glycolytic flux and also the absence of change in intermediate metabolites [49]. The observed slight decrease in all measured metabolites could be the consequence of increased external demands.

However, it is also interesting to notice that according to Fig. 5b the observed increase in the flux through the oxidative part of PPP is not predicted by an increase in measured glycolytic activities, but is clearly satisfied by an increase in G6PD activity. Comparing K12 and K13 cells, there is a perfect agreement between the higher G6PD activity and the higher flux through the oxidative part of the PPP. Regulation of the expression of G6PD is altered in many tumours, resulting in a significant increase in G6PD activity, and it has been suggested that G6PD may act as a potential oncogene [50]. Increased G6PD activity in NIH-3T3 cells, transfected with human G6PD cDNA, leads to tumorogenic transformations, dividing more quickly and inducing tumors in nude mice [50]. The decreased levels of PenP (x_2) are not compatible with the increased activity of G6PD, but are compatible with an increased demand of ribose (reaction step D). Also, the decreased levels of PenP can be at least in part a consequence of the slight decrease in the TKT activity. The two key enzymes of the PPP, G6PD and TKT, were both previously identified as potential targets in cancer therapy [51–54], and recently, the increased G6PD/TKT ratio was proposed as a tumour metabolome feature [55]. The observed notorious increase of G6PD resulted in a higher G6PD/TKT ratio in both transformed cell lines with respect to non-transformed cells in agreement with the results of Montoya et al. [55]. Here, we have also found that this ratio is higher in K13 than in K12.

Finally, it is interesting to note the fact that metabolic adaptations observed in transformed cells require changes in more than one enzyme, which suggests that a multi-hit strategy would be required to counteract metabolic adaptations in transformed cells. These results support the suggestions of Moreno-Sanchez et al. [56] who proposed that a "multi-targeted MCA advised therapy" would be required to design efficient treatments in cancer based on the fact that control is shared among several steps in metabolic networks.

5. Conclusion

An interesting advantage of control coefficients with fixed signs is that they confer robustness to the system [14]. Consistently, predictions based on fixed signs of control coefficients are also very robust. The structure of the metabolic network and the regulatory dependences affecting most of the metabolic processes, specifically those associated with the carbon metabolism, are available and sufficient to predict the sign of metabolic control coefficients. We have proposed and verified the use of fixed signs of metabolic control coefficients as a useful tool to evaluate the key enzyme activities underlying metabolic adaptations associated with K-*ras* oncogenic transformation in NIH-3T3 cells. The predicted changes of G6PD, TKT, PK, and LDH activities give very good agreement with the observed pattern of changes in fluxes and concentrations. Thus, with a limited knowledge of the metabolic network structure and regulatory circuits, the proposed analysis arises as a tool which can provide a complete picture of predictable effects based on systemic properties—changes in fluxes and metabolite concentrations—with respect to changes in enzyme activities.

Acknowledgments

We thank Michael John Binns for his careful reading, suggestions and corrections. This study was supported by grants SAF2008-00164, from the Ministerio de Ciencia e Innovación, and from Red Temática de Investigación Cooperativa en Cáncer, Instituto de Salud Carlos III, Spanish Ministry of Science and Innovation & European Regional Development Fund (ERDF) "Una manera de hacer Europa"(ISCIII-RTICC grants RD06/0020/0046). It has also received financial support from the AGAUR-Generalitat de Catalunya (grant 2009SGR1308). PA was supported by a Grant from Generalitat de Catalunya (Programa Beatriu de Pinós). AB was supported by a Grant from Consejo Superior de Investigaciones Científicas (Programa JAE Predoc). RM was supported by a Grant ISCIII: PS09/00965.

References

[1] N. Kozer, G. Schreiber, Effect of crowding on protein–protein association rates: fundamental differences between low and high mass crowding agents, J. Mol. Biol. 336 (2004) 763–774.
[2] T. Ureta, Organización del metabolismo: Localización subcelular de enzimas glicolíticas, Arch. Biol. Med. Exp. 18 (1985) 9–32.
[3] D.A. Fell, Understanding the Control of Metabolism, Portland Press, London, 1997.
[4] A. Cornish-Bowden, Fundamentals of Enzyme Kinetics, third ed., Portland Press, London, 2000.
[5] M. Cascante, L.G. Boros, B. Comin-Anduix, P. de Atauri, J.J. Centelles, P.W. Lee, Metabolic control analysis in drug discovery and disease, Nat. Biotechnol. 20 (2002) 243–249.
[6] D.A. Fell, H.M. Sauro, Metabolic control and its analysis. Additional relationships between elasticities and control coefficients, Eur. J. Biochem. 148 (1985) 555–561.
[7] H.V. Westerhoff, D.B. Kell, Matrix method for determining steps most rate-limiting to metabolic fluxes in biotechnological processes, Biotechnol. Bioeng. 30 (1987) 101–107.
[8] C. Reder, Metabolic control theory: a structural approach, J. Theor. Biol. 135 (1988) 175–201.
[9] M. Cascante, R. Franco, E.I. Canela, Use of implicit methods from general sensitivity theory to develop a systemic approach to metabolic control. I. Unbranched pathways, Math. Biosci. 94 (1989) 271–288.
[10] M. Cascante, R. Franco, E.I. Canela, Use of implicit methods from general sensitivity theory to develop a systemic approach to metabolic control. II. Complex systems, Math. Biosci. 94 (1989) 289–309.
[11] A.K. Sen, Metabolic control analysis. An application of signal flow graphs, Biochem. J. 269 (1990) 141–147.
[12] A.K. Sen, A graph-theoretic analysis of metabolic regulation in linear pathways with multiple feedback loops and branched pathways, Biochim. Biophys. Acta 1059 (1991) 293–311.
[13] A.K. Sen, On the sign pattern of metabolic control coefficients, J. Theor. Biol. 182 (1996) 269–275.
[14] V. Baldazzi, D. Ropers, Y. Markowicz, D. Kahn, J. Geiselmann, H. de Jong, The carbon assimilation network in *Escherichia coli* is densely connected and largely sign-determined by directions of metabolic fluxes, PLoS Comput. Biol. 6 (2010) e1000812.
[15] F. Chiaradonna, D. Gaglio, M. Vanoni, L. Alberghina, Expression of transforming K-Ras oncogene affects mitochondrial function and morphology in mouse fibroblasts, Biochim. Biophys. Acta 1757 (2006) 1338–1356.
[16] F. Chiaradonna, E. Sacco, R. Manzoni, M. Giorgio, M. Vanoni, L. Alberghina, Ras-dependent carbon metabolism and transformation in mouse fibroblasts, Oncogene 25 (2006) 5391–5404.
[17] D. Gaglio, C. Soldati, M. Vanoni, L. Alberghina, F. Chiaradonna, Glutamine deprivation induces abortive s-phase rescued by deoxyribonucleotides in k-ras transformed fibroblasts, PLoS ONE 4 (2009) e4715.
[18] X. Liu, X. Wang, J. Zhang, E.K. Lam, V.Y. Shin, A.S. Cheng, J. Yu, F.K. Chan, J.J. Sung, H. C. Jin, Warburg effect revisited: an epigenetic link between glycolysis and gastric carcinogenesis, Oncogene 29 (2010) 442–450.
[19] M. Malumbres, M. Barbacid, RAS oncogenes: the first 30 years, Nat. Rev. Cancer 3 (2003) 459–465.
[20] K. Rajalingam, R. Schreck, U.R. Rapp, S. Albert, Ras oncogenes and their downstream targets, Biochim. Biophys. Acta 1773 (2007) 1177–1195.
[21] A. Young, J. Lyons, A.L. Miller, V.T. Phan, I.R. Alarcón, F. McCormick, Ras signaling and therapies, Adv. Cancer Res. 102 (2009) 1–17.

[22] S. Guerrero, I. Casanova, L. Farré, A. Mazo, G. Capellà, R. Mangues, K-ras codon 12 mutation induces higher level of resistance to apoptosis and predisposition to anchorage-independent growth than codon 13 mutation or proto-oncogene overexpression, Cancer Res. 60 (2000) 6750–6756.
[23] S. Guerrero, A. Figueras, I. Casanova, L. Farré, B. Lloveras, G. Capellà, M. Trias, R. Mangues, Codon 12 and codon 13 mutations at the K-ras gene induce different soft tissue sarcoma types in nude mice, FASEB J. 16 (2002) 1642–1644.
[24] P. Vizán, L.G. Boros, A. Figueras, G. Capella, R. Mangues, S. Bassilian, S. Lim, W.N. Lee, M. Cascante, K-ras codon-specific mutations produce distinctive metabolic phenotypes in NIH3T3 mice fibroblasts, Cancer Res. 65 (2005) 5512–5515.
[25] S. Wolfram, The Mathematica book, fifth ed., Wolfram Media, Inc, 2003.
[26] A. Kunst, B. Draeger, J. Ziegenhorn, D-Glucose; UV-methods with hexokinase and glucose-6-phosphate dehydrogenase, in: methods of enzymatic analysis, Verlag Chemie, Weinheim, Germany, 1984.
[27] J.V. Passonneau, O.H. Lowry, Enzymatic Analysis: A Practical Guide, The Humana Press Inc., Totowa, New Jersey, USA, 1993.
[28] P. Lund, L-glutamine and L-glutamate; UV-method with glutaminase and glutamate dehydrogenase, in: methods of enzymatic analysis, Verlag Chemie, Weinheim, Germany, 1985.
[29] P. Vizán, G. Alcarraz-Vizán, S. Diaz-Moralli, J.C. Rodríguez-Prados, M. Zanuy, J.J. Centelles, O. Jáuregui, M. Cascante, Quantification of intracellular phosphorylated carbohydrates in HT29 human colon adenocarcinoma cell line using liquid chromatography-electrospray ionization tandem mass spectrometry, Anal. Chem. 79 (2007) 5000–5005.
[30] A. Baracca, F. Chiaradonna, G. Sgarbi, G. Solaini, L. Alberghina, G. Lenaz, Mitochondrial complex I decrease is responsible for bioenergetic dysfunction in K-ras transformed cells, Biochim. Biophys. Acta 1797 (2010) 314–323.
[31] W.N. Tian, L.D. Braunstein, J. Pang, K.M. Stuhlmeier, Q.C. Xi, X. Tian, R.C. Stanton, Importance of glucose-6-phosphate dehydrogenase activity for cell growth, J. Biol. Chem. 273 (1998) 10609–10617.
[32] E.H. Smeets, H. Muller, J. de Wael, A NADH-dependent transketolase assay in erythrocyte hemolysates, Clin. Chim. Acta 33 (1971) 379–386.
[33] W.N. Lee, L.G. Boros, J. Puigjaner, S. Bassilian, S. Lim, M. Cascante, Mass isotopomer study of the nonoxidative pathways of the pentose cycle with [1, 2–^{13}C2]glucose, Am. J. Physiol. 274 (1998) E843–E851.
[34] C.H. Schilling, S. Schuster, B.O. Palsson, R. Heinrich, Metabolic pathway analysis: basic concepts and scientific applications in the post-genomic era, Biotechnol. Prog. 15 (1999) 296–303.
[35] K.J. Kauffman, P. Prakash, J.S. Edwards, Advances in flux balance analysis, Curr. Opin. Biotechnol. 14 (2003) 491–496.
[36] F. Llaneras, J. Picó, Stoichiometric modelling of cell metabolism, J. Biosci. Bioeng. 105 (2008) 1–11.
[37] F. Llaneras, J. Picó, An interval approach for dealing with flux distributions and elementary modes activity patterns, J. Theor. Biol. 246 (2007) 290–308.
[38] H. Pelicano, D.S. Martin, R.H. Xu, P. Huang, Glycolysis inhibition for anticancer treatment, Oncogene 25 (2006) 4633–4646.
[39] H. Nakajima, N. Raben, T. Hamaguchi, T. Yamasaki, Phosphofructokinase deficiency; past, present and future, Curr. Mol. Med. 2 (2002) 197–212.
[40] S. Mazurek, Pyruvate kinase type M2: a key regulator of the metabolic budget system in tumor cells, Int. J. Biochem. Cell Biol. (2010), (doi: 10.1016).
[41] S. Mazurek, H.C. Drexler, J. Troppmair, E. Eigenbrodt, U.R. Rapp, Regulation of pyruvate kinase type M2 by A-Raf: a possible glycolytic stop or go mechanism, Anticancer Res. 27 (2007) 3963–3971.
[42] L. Wang, I. Birol, V. Hatzimanikatis, Metabolic control analysis under uncertainty: framework development and case studies, Biophys. J. 87 (2004) 3750–3763.
[43] G. Kroemer, J. Pouyssegur, Tumor cell metabolism: cancer's Achilles' heel, Cancer Cell 13 (2008) 472–482.
[44] P. Vizán, S. Mazurek, M. Cascante, Robust metabolic adaptation underlying tumor progression, Metabolomics 4 (2008) 1–12.
[45] J.W. Kim, K.I. Zeller, Y. Wang, A.G. Jegga, B.J. Aronow, K.A. O'Donnell, C.V. Dang, Evaluation of myc E-box phylogenetic footprints in glycolytic genes by chromatin immunoprecipitation assays, Mol. Cell. Biol. 24 (2004) 5923–5936.
[46] J.D. Gordan, C.B. Thompson, M.C. Simon, HIF and c-Myc: sibling rivals for control of cancer cell metabolism and proliferation, Cancer Cell 12 (2007) 108–113.
[47] G.L. Semenza, Defining the role of hypoxia-inducible factor 1 in cancer biology and therapeutics, Oncogene 29 (2010) 625–634.
[48] G.L. Semenza, HIF-1: upstream and downstream of cancer metabolism, Curr. Opin. Genet. Dev. 20 (2010) 51–56.
[49] H. Kacser, L. Acerenza, A universal method for achieving increases in metabolite production, Eur. J. Biochem. 216 (1993) 361–367.
[50] W. Kuo, J. Lin, T.K. Tang, Human glucose-6-phosphate dehydrogenase (G6PD) gene transforms NIH 3T3 cells and induces tumors in nude mice, Int. J. Cancer 85 (2000) 857–864.
[51] L.G. Boros, J. Puigjaner, M. Cascante, W.N. Lee, J.L. Brandes, S. Bassilian, F.I. Yusuf, R.D. Williams, P. Muscarella, W.S. Melvin, W.J. Schirmer, Oxythiamine and dehydroepiandrosterone inhibit the nonoxidative synthesis of ribose and tumor cell proliferation, Cancer Res. 57 (1997) 4242–4248.
[52] J. Boren, A.R. Montoya, P. de Atauri, B. Comin-Anduix, A. Cortes, J.J. Centelles, W.M. Frederiks, C.J. Van Noorden, M. Cascante, Metabolic control analysis aimed at the ribose synthesis pathways of tumor cells: a new strategy for antitumor drug development, Mol. Biol. Rep. 29 (2002) 7–12.
[53] B. Comin-Anduix, J. Boren, S. Martinez, C. Moro, J.J. Centelles, R. Trebukhina, N. Petushok, W.N. Lee, L.G. Boros, M. Cascante, The effect of thiamine supplementation on tumour proliferation. A metabolic control analysis study, Eur. J. Biochem. 268 (2001) 4177–4182.
[54] B. Raïs, B. Comin, J. Puigjaner, J.L. Brandes, E. Creppy, D. Saboureau, R. Ennamany, W.-N. Paul Lee, L.G. Boros, M. Cascante, Oxythiamine and dehydroepiandrosterone induce a G1 phase cycle arrest in Ehrlich's tumor cells through inhibition of the pentose cycle, FEBS Lett. 456 (1999) 113–118.
[55] A. Ramos-Montoya, W.N. Lee, S. Bassilian, S. Lim, R.V. Trebukhina, M.V. Kazhyna, C.J. Ciudad, V. Noe, J.J. Centelles, M. Cascante, Pentose phosphate cycle oxidative and nonoxidative balance: a new vulnerable target for overcoming drug resistance in cancer, Int. J. Cancer 119 (2006) 2733–2741.
[56] R. Moreno-Sánchez, E. Saavedra, S. Rodríguez-Enríquez, J.C. Gallardo-Pérez, H. Quezada, H.V. Westerhoff, Metabolic control analysis indicates a change of strategy in the treatment of cancer, Mitochondrion 10 (2010) 626–639, (doi:10.1016).

APPENDIX IV

PAGES 235-241

Metabolic network adaptations in cancer as targets for novel therapies

Marta Cascante[1], Adrian Benito, Miriam Zanuy, Pedro Vizán[2], Silvia Marín and Pedro de Atauri

Departament de Bioquimica i Biologia Molecular, Facultat de Biologia, Institut de Biomedicina at Universitat de Barcelona IBUB and IDIBAPS-Hospital Clinic, Av/ Diagonal 645, 08028 Barcelona, Spain

Abstract

Metabolite concentrations and fluxes are the system variables that characterize metabolism. The systematic study of metabolite profiles is known as metabolomics; however, knowledge of the complete set of metabolites may not be enough to predict distinct phenotypes. A complete understanding of metabolic processes requires detailed knowledge of enzyme-controlled intracellular fluxes. These can be estimated through quantitative measurements of metabolites at different times or by analysing the stable isotope patterns obtained after incubation with labelled substrates. We have identified distinct intracellular fluxes associated with metabolic adaptations accompanying cancer. The maintenance of an imbalance between fluxes for the oxidative and non-oxidative PPP (pentose phosphate pathway) has been shown to be critical for angiogenesis and cancer cell survival. Mouse NIH 3T3 cells transformed by different mutated *K-ras* oncogenes have differential routing of glucose to anaerobic glycolysis, the PPP and the Krebs cycle. These results indicate that knowledge of metabolic fingerprints associated with an altered genetic profile could be exploited in the rational design of new therapies. We conclude that the understanding of the multifactorial nature of metabolic adaptations in cancer may open new ways to develop novel multi-hit antitumoral therapies.

The systematic study of the metabolism

Current high-throughput technologies are applied to examine the whole components of a cell. However, understanding the crucial cellular events such as differentiation, cell-cycle progression or apoptosis requires detailed knowledge not only of the components, but also of how they interact in systems [1]. Moreover, high-throughput technologies cannot be designed for the analysis of all cellular components. In the case of the genome, the physicochemical homogeneity of its components has facilitated its analysis, resulting in the spectacular advance of genomics. This homogeneity contrasts with the high heterogeneity that characterizes metabolism. The systematic study of the metabolic compounds is known as metabolomics, where the metabolome is defined as the set of all low-molecular-mass compounds present in a biological system [2]. The large number of different metabolites, differences in their relative concentrations and variability in their physicochemical properties (polarity, hydrophobicity, molecular mass or chemical stability) require the application of different technologies and a huge range of experimental conditions. Thus specific methodologies are being developed for the various groups of metabolites, such as lipids (lipidomics) or sugars (glycomics). Interestingly, such methods could be applied to the study of the metabolome and its importance in the development and progression of tumours [3].

Differential flux distribution

Metabolite concentrations and fluxes are the interdependent system variables that characterize metabolism. A comprehensive characterization of metabolic operation can be obtained from quantitative knowledge of intracellular fluxes, which are intimately associated with the corresponding enzyme activities. Moreover, the metabolic profile of a specific cell represents the integrated end point of many growth-signalling events, and it consists of the simultaneous assessment of fluxes in major metabolic pathways under various physiological conditions, growth phases and substrate environments [4]. Quantitative measurements of metabolites at different times are applied for the measurement of metabolic fluxes. In particular, tracer-based metabolomics is a useful approach for the analysis of the propagation of labelled molecules to metabolic products by NMR or chromatography coupled to MS [GC–MS and LC (liquid chromatography)–MS]. Thus the analysis of the stable isotope patterns obtained after incubation with labelled substrates is applied for the measurement of the fluxes throughout the steps of the metabolic pathways. For example, labelling with [1,2–$^{13}C_2$]glucose and the subsequent

Key words: antitumoral therapy, cancer, flux analysis, metabolomics, systems biology, tumour metabolism.

Abbreviations used: G6PDH, glucose-6-phosphate dehydrogenase; HIF-1, hypoxia-inducible transcription factor-1; LDH, lactacte dehydrogenase; PDH, pyruvate dehydrogenase; PK, pyruvate kinase; PPP, pentose phosphate pathway; ROS, reactive oxygen species; TKT, transketolase; TKTL1, TKT-like-1.

[1]**To whom correspondence should be addressed (email martacascante@ub.edu).**

[2]**Present address:** Laboratory of Developmental Signalling, Cancer Research UK London Research Institute, London WC2A 3PX, U.K.

analyses of its propagation to ribose (RNA), lactate and glutamate has been widely used to simultaneously determine carbon flow towards the PPP (pentose phosphate pathway), glycolysis, direct glucose oxidation, tricarboxylic acid cycle and fatty acid synthesis [4–7]. The use of these analytical methods has demonstrated that there are specific metabolic adaptations in response to cell-transforming agents or cancer-growth-controlling factors [8,9]. In recent years, several computational tools have been developed for the quantitative estimation of fluxes in metabolic networks from isotopomeric distributions (see [10,11] and references therein).

Tumour metabolism and the design of new antitumoral strategies

The first energy metabolism alteration described in cancer cells was the increase in the conversion of glucose into lactate even in the presence of oxygen [12]. The energetic inefficiency of this process, compared with mitochondrial respiration, increases glucose consumption in tumour cells, a difference that has been exploited in the clinical detection of neoplasies by PET (positron emission tomography) imaging [13]. The molecular mechanism underlying this high glycolytic capacity has been extensively analysed and some of the key factors have been identified [14–21]. Since many solid tumours provoke hypoxic conditions, the transcription factor HIF-1 (hypoxia-inducible factor-1) has emerged as a key player in this process. Thus HIF-1, which is modulated by oncogenes such as *Ras* or *Her-2*, increases the expression of several glycolytic enzymes [22–24]. Other molecular mechanisms have been proposed to link tumour progression and glycolytic phenotype, e.g. the oncogenic transcription factor Myc has been related to the expression of several glycolytic enzymes such as LDH (lactate dehydrogenase) [25]. The regulation of glucose metabolism has also been reported to be mediated by the PI3K (phosphoinositide 3-kinase)/Akt/mTOR (mammalian target of rapamycin) pathway [20,26], which is commonly activated in tumour cells. Taken together, these observations reveal that distinct molecular mechanisms cause alterations in the tumour metabolic network. Great efforts to elucidate these mechanisms are expected to be made in the near future.

There is evidence that the up-regulation of genes expressing glycolytic enzymes is associated with the metabolic reprogramming of tumour cells, but the role of mitochondria is less clear. A reduction in the mitochondrial content and differences in its activity has been reported in tumours [26]. Certainly, mitochondrial metabolism is closely related to tumour progression, not only at the energetic level, but also through the generation of ROS (reactive oxygen species). The role of ROS in tumour progression is controversial. On the one hand, mitochondrial malfunction and subsequent production of ROS have been reported in cancer cells [27]. This increase in ROS production could increase the rate of mutagenesis, thus exacerbating malignancy [27,28]. On the other hand, the generation of ROS has been proposed for treatment of cancer [29], following the observation that the generation of oxidative stress leads to apoptosis [30].

Proliferating cells strongly rely on the availability of glycolytic intermediates as precursors of a large number of essential biomolecules. In this way, several anabolic routes are also regulated differentially in tumour cells, for example lipid synthesis [31]. Another example is the synthesis through the PPP of the sugar component of nucleic acids: ribose 5-phosphate. Nucleotide reservoirs are not sufficient to support cell duplication and, therefore, biosynthetic pathways are up-regulated during the cell cycle. Previously, we have shown that the PPP is enhanced in several tumour-derived cell lines [32,33], and we have identified the two key enzymes of this pathway, G6PDH (glucose-6-phosphate dehydrogenase) and TKT (transketolase), as potential targets in cancer therapy [34–38]. These two enzymes belong to the oxidative and non-oxidative branches respectively, of the PPP (see Figure 1). We hypothesized that the balance between oxidative and non-oxidative branches is a requirement to maintain the metabolic efficiency of cancer cells for growth and proliferation. We validated this hypothesis by showing that the perturbation of this balance using a multiple-hit drug strategy results in metabolic inefficiency and cell death [38]. Recently, we have correlated enhanced enzyme activities of G6PDH and TKT with an increased pentose monophosphate/hexose monophosphate ratio in late G_1- and S-phases of cell cycle, suggesting a regulation of these key enzymes during cell-cycle progression [39]. This distinctive modulation of these enzymes may represent a new strategy to inhibit proliferation in anticancer treatments. Moreover, we have shown that growth factor induction of endothelial cells (a common step during angiogenesis) can be reduced by direct inhibition of key enzymes of glycogen metabolism and PPPs [9].

An additional feature of tumour metabolism is the differential expression of isoenzymes, which have been postulated as interesting targets for cancer treatment. The glycolytic isoenzyme M2-PK (pyruvate kinase) is one of the most interesting examples. This isoenzyme can shift between a dimeric and a tetrameric form, depending on the energetic or biosynthetic requirements of the cells [40,41]. Likewise, Coy et al. [42] have described a new isoenzyme of TKT called TKTL-1 (TKT-like-1). The mRNA levels of this isoenzyme are overexpressed in urothelial, ovarian, colon and gastric cancers [43–45]. It has been suggested that TKTL-1 could have distinct kinetic properties and that its overexpression could raise the concentration of G3P (glyceraldehyde 3-phosphate) available for glycolysis, thus contributing to the Warburg effect [42,44].

Most of the research on tumour cell metabolism has focused on glucose utilization, and consistent evidence supports the finding that cancer cells have enhanced glucose consumption. However, an important controversy surrounds the dependence of cancer cells on anaerobic glycolysis. On the one hand, when glucose is no longer available, as is expected in solid tumours, tumour cells are forced to catabolize alternative substrates such as glutamine. Glutamine catabolism represents a valuable energy source and provides

Figure 1 | Schematic representation of the central carbon metabolism

The potential antitumoral targets of the PPP are marked in red. A hypothetical distinct reaction mode of action proposed for TKTL1 is shown with a broken line. Abbreviations: HK, hexokinase; PGI, phosphoglucose isomerase; PFK1, phosphofructokinase 1; F1,6Bpase, fructose-1,6-bisphosphatase; ALD, aldolase; GAPDH, glyceraldehyde-3-phosphate dehydrogenase; TPI, triose-phosphate isomerase; PC, pyruvate carboxylase; CS, citrate synthase, AC, aconitase; IDH, isocitrate dehydrogenase; α-KGDH, α-ketoglutarate dehydrogenase; SCS, succinyl-CoA synthetase; SDH, succinate dehydrogenase; FH, fumarate hydratase; MDH, malate dehydrogenase; GDH, glutamate dehydrogenase; GS, glutaminase; GLS, glutamine synthase; LAC, lactonase; 6-PGDH, 6-phosphogluconate dehydrogenase; TALD, transaldolase; P, phosphate.

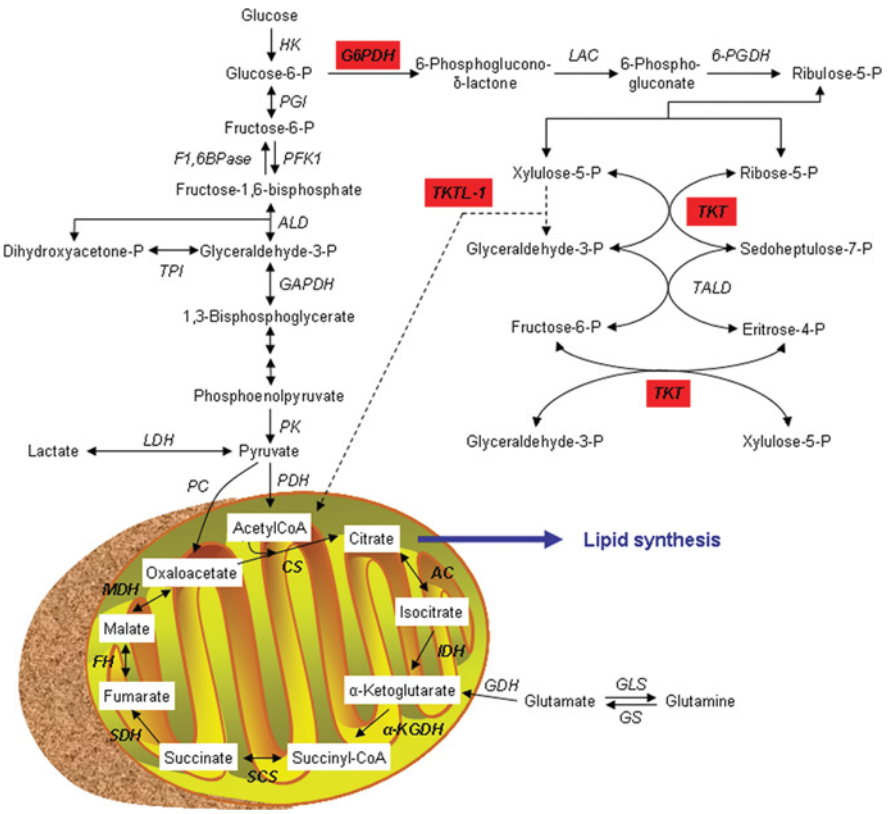

cells with glutamate and aspartate, which are precursors of nucleic acid and serine synthesis. Enhanced glutaminolysis has been associated with neoplastic transformation and its inhibition has been shown to decrease tumour cell proliferation and to correlate with the phenotypic and functional differentiation of these cells [46,47]. On the other hand, it is unclear whether there is a unique suitable phenotype for energetic metabolism in cancer cells [48]. Our results showed that different codon-specific mutations in *K-ras* lead to different metabolic phenotypes in NIH 3T3 mouse fibroblasts [8]. Significant changes in fluxes were observed, taking advantage of [1,2–$^{13}C_2$]glucose tracer labelling, when non-transfected NIH 3T3 cells were stably transfected with a mutated *K-ras* minigene, either at codon 12 (K12) or at codon 13 (K13). These differences support the evidence that the re-routing of glucose carbons towards either anaerobic glycolysis (K12) or PDH (pyruvate dehydrogenase) and the oxidative branch of the PPP (K13) is associated with distinct strategies of proliferation: higher resistance to apoptosis (K12) compared with enhanced mitotic capacity (K13).

The fact that cancer cells have distinctive metabolic profiles compared with normal counterparts offers the exciting possibility of designing new complementary strategies based on the specific reversal of these metabolic adaptations. Moreover, the overexpression of specific isoenzymes in cancer cells is an emerging opportunity to develop novel therapies. It is expected that this specific inhibition will result in the disruption of the necessary metabolic adaptation of cancer cells without affecting the metabolism of non-tumoral cells. In this way, tools such as metabolic control analysis provide the opportunity to systematically analyse the distribution of flux control among the different enzymes of the metabolic network [49,50] and permit researchers to identify those enzymes whose inhibition or overexpression will affect tumour tissue more than normal tissues. These enzymes and tumour-overexpressed isoenzymes are potential

targets for chemotherapy, since their inhibition is expected to have a strong effect on tumour cell metabolism.

In summary, a better comprehension of metabolic adaptations underlying hypoxia, oncogene transformation, cell differentiation, apoptosis and cell-cycle progression can reveal clues to identify complementary targets in the design of rational combinational treatments in chemotherapy. Thus a better understanding of tumour metabolism may open new avenues in drug discovery as well as the possibility to combine drugs that inhibit well-established antitumoral targets, such as proteins controlling cell-cycle progression, with specific inhibitors of cancer cell metabolic adaptations.

Funding

This work was supported by the Spanish Government and the European Union Fondo Europeo de Desarrollo Regional (FEDER) funds [grant numbers SAF2008–00164, ISCIII-RTICC (RD06/0020/0046)], and Generalitat de Catalunya, [grant numbers 2009SGR1308, 2006ITT-10007].

References

1 Kitano, H. (2001) Foundations of Systems Biology, MIT Press, Cambridge, MA
2 Oliver, S.G., Winson, M.K., Kell, D.B. and Baganz, F. (1998) Systematic functional analysis of the yeast genome. Trends Biotechnol. **16**, 373–378
3 Vizán, P., Mazurek, S. and Cascante, M. (2008) Robust metabolic adaptation underlying tumor progression. Metabolomics **4**, 1–12
4 Boros, L.G., Cascante, M. and Lee, W.N. (2002) Metabolic profiling of cell growth and death in cancer: applications in drug discovery. Drug Discovery Today **7**, 364–372
5 Lee, W.N., Boros, L.G., Puigjaner, J., Bassilian, S., Lim, S. and Cascante, M. (1998) Mass isotopomer study of the nonoxidative pathways of the pentose cycle with [1,2–$^{13}C_2$]glucose. Am. J. Physiol. **274**, E843–E851
6 Lee, W.N., Edmond, J., Bassilian, S. and Morrow, J.W. (1996) Mass isotopomer study of glutamine oxidation and synthesis in primary culture of astrocytes. Dev. Neurosci. **18**, 469–477
7 Marin, S., Chiang, K., Bassilian, S., Lee, W.N., Boros, L.G., Fernandez-Novell, J.M., Centelles, J.J., Medrano, A., Rodriguez-Gil, J.E. and Cascante, M. (2003) Metabolic strategy of boar spermatozoa revealed by a metabolomic characterization. FEBS Lett. **554**, 342–346
8 Vizan, P., Boros, L.G., Figueras, A., Capella, G., Mangues, R., Bassilian, S., Lim, S., Lee, W.N. and Cascante, M. (2005) K-ras codon-specific mutations produce distinctive metabolic phenotypes in NIH3T3 mice fibroblasts. Cancer Res. **65**, 5512–5515
9 Vizan, P., Sanchez-Tena, S., Alcarraz-Vizan, G., Soler, M., Messeguer, R., Pujol, M.D., Lee, W.N. and Cascante, M. (2009) Characterization of the metabolic changes underlying growth factor angiogenic activation: identification of new potential therapeutic targets. Carcinogenesis **30**, 946–952
10 Sauer, U. (2006) Metabolic networks in motion: ^{13}C-based flux analysis. Mol. Syst. Biol. **2**, 62
11 Selivanov, V.A., Marin, S., Lee, P.W. and Cascante, M. (2006) Software for dynamic analysis of tracer-based metabolomic data: estimation of metabolic fluxes and their statistical analysis. Bioinformatics **22**, 2806–2812
12 Warburg, O., Posener, K. and Negelein, E. (1924) Über den Stoffwechsel der Karzinomzellen. Biochemische Zeitschrift. **152**, 309–344
13 Gambhir, S.S. (2002) Molecular imaging of cancer with positron emission tomography. Nat. Rev. Cancer **2**, 683–693
14 Elstrom, R.L., Bauer, D.E., Buzzai, M., Karnauskas, R., Harris, M.H., Plas, D.R., Zhuang, H., Cinalli, R.M., Alavi, A., Rudin, C.M. and Thompson, C.B. (2004) Akt stimulates aerobic glycolysis in cancer cells. Cancer Res. **64**, 3892–3899
15 Gatenby, R.A. and Gillies, R.J. (2008) A microenvironmental model of carcinogenesis. Nat. Rev. Cancer. **8**, 56–61
16 Kim, J.-w., Tchernyshyov, I., Semenza, G.L. and Dang, C.V. (2006) HIF-1-mediated expression of pyruvate dehydrogenase kinase: a metabolic switch required for cellular adaptation to hypoxia. Cell Metab. **3**, 177–185
17 Kondoh, H., Lleonart, M.E., Gil, J., Wang, J., Degan, P., Peters, G., Martinez, D., Carnero, A. and Beach, D. (2005) Glycolytic enzymes can modulate cellular life span. Cancer Res. **65**, 177–185
18 Lu, H., Forbes, R.A. and Verma, A. (2002) Hypoxia-inducible factor 1 activation by aerobic glycolysis implicates the Warburg effect in carcinogenesis. J. Biol. Chem. **277**, 23111–23115
19 Matoba, S., Kang, J.G., Patino, W.D., Wragg, A., Boehm, M., Gavrilova, O., Hurley, P.J., Bunz, F. and Hwang, P.M. (2006) p53 regulates mitochondrial respiration. Science **312**, 1650–1653
20 Plas, D.R. and Thompson, C.B. (2005) Akt-dependent transformation: there is more to growth than just surviving. Oncogene **24**, 7435–7442
21 Vander Heiden, M.G., Cantley, L.C. and Thompson, C.B. (2009) Understanding the Warburg effect: the metabolic requirements of cell proliferation. Science **324**, 1029–1033
22 Gordan, J.D., Thompson, C.B. and Simon, M.C. (2007) HIF and c-Myc: sibling rivals for control of cancer cell metabolism and proliferation. Cancer Cell **12**, 108–113
23 Kikuchi, H., Pino, M.S., Zeng, M., Shirasawa, S. and Chung, D.C. (2009) Oncogenic KRAS and BRAF differentially regulate hypoxia-inducible factor-1α and -2α in colon cancer. Cancer Res. **69**, 8499–8506
24 Laughner, E., Taghavi, P., Chiles, K., Mahon, P.C. and Semenza, G.L. (2001) HER2 (neu) signaling increases the rate of hypoxia-inducible factor 1α (HIF-1α) synthesis: novel mechanism for HIF-1-mediated vascular endothelial growth factor expression. Mol. Cell. Biol. **21**, 3995–4004
25 Rimpi, S. and Nilsson, J.A. (2007) Metabolic enzymes regulated by the Myc oncogene are possible targets for chemotherapy or chemoprevention. Biochem. Soc. Trans. **35**, 305–310
26 Rossignol, R., Gilkerson, R., Aggeler, R., Yamagata, K., Remington, S.J. and Capaldi, R.A. (2004) Energy substrate modulates mitochondrial structure and oxidative capacity in cancer cells. Cancer Res. **64**, 985–993
27 Pelicano, H., Carney, D. and Huang, P. (2004) ROS stress in cancer cells and therapeutic implications. Drug Resist. Update **7**, 97–110
28 Wallace, D.C. (2005) Mitochondria and cancer: Warburg addressed. Cold Spring Harb. Symp. Quant. Biol. **70**, 363–374
29 Engel, R.H. and Evens, A.M. (2006) Oxidative stress and apoptosis: a new treatment paradigm in cancer. Front. Biosci. **11**, 300–312
30 Vrablic, A.S., Albright, C.D., Craciunescu, C.N., Salganik, R.I. and Zeisel, S.H. (2001) Altered mitochondrial function and overgeneration of reactive oxygen species precede the induction of apoptosis by 1-O-octadecyl-2-methyl-rac-glycero-3-phosphocholine in p53-defective hepatocytes. FASEB J. **15**, 1739–1744
31 Swinnen, J.V., Brusselmans, K. and Verhoeven, G. (2006) Increased lipogenesis in cancer cells: new players, novel targets. Curr. Opin. Clin. Nutr. Metab. Care **9**, 358–365
32 Boros, L.G., Brandes, J.L., Yusuf, F.I., Cascante, M., Williams, R.D. and Schirmer, W.J. (1998) Inhibition of the oxidative and nonoxidative pentose phosphate pathways by somatostatin: a possible mechanism of antitumor action. Med. Hypoth. **50**, 501–506
33 Cascante, M., Centelles, J.J., Veech, R.L., Lee, W.N. and Boros, L.G. (2000) Role of thiamin (vitamin B-1) and transketolase in tumor cell proliferation. Nutr. Cancer **36**, 150–154
34 Boren, J., Montoya, A.R., de Atauri, P., Comin-Anduix, B., Cortes, A., Centelles, J.J., Frederiks, W.M., Van Noorden, C.J. and Cascante, M. (2002) Metabolic control analysis aimed at the ribose synthesis pathways of tumor cells: a new strategy for antitumor drug development. Mol. Biol. Rep. **29**, 7–12
35 Boros, L.G., Puigjaner, J., Cascante, M., Lee, W.N., Brandes, J.L., Bassilian, S., Yusuf, F.I., Williams, R.D., Muscarella, P., Melvin, W.S. and Schirmer, W.J. (1997) Oxythiamine and dehydroepiandrosterone inhibit the nonoxidative synthesis of ribose and tumor cell proliferation. Cancer Res. **57**, 4242–4248

36 Comin-Anduix, B., Boren, J., Martinez, S., Moro, C., Centelles, J.J., Trebukhina, R., Petushok, N., Lee, W.N., Boros, L.G. and Cascante, M. (2001) The effect of thiamine supplementation on tumour proliferationA metabolic control analysis study. Eur. J. Biochem. **268**, 4177–4182
37 Rais, B., Comin, B., Puigjaner, J., Brandes, J.L., Creppy, E., Saboureau, D., Ennamany, R., Lee, W.N., Boros, L.G. and Cascante, M. (1999) Oxythiamine and dehydroepiandrosterone induce a G1 phase cycle arrest in Ehrlich's tumor cells through inhibition of the pentose cycle. FEBS Lett. **456**, 113–118
38 Ramos-Montoya, A., Lee, W.N., Bassilian, S., Lim, S., Trebukhina, R.V., Kazhyna, M.V., Ciudad, C.J., Noe, V., Centelles, J.J. and Cascante, M. (2006) Pentose phosphate cycle oxidative and nonoxidative balance: a new vulnerable target for overcoming drug resistance in cancer. Int. J. Cancer **119**, 2733–2741
39 Vizan, P., Alcarraz-Vizan, G., Diaz-Moralli, S., Solovjeva, O.N., Frederiks, W.M. and Cascante, M. (2009) Modulation of pentose phosphate pathway during cell cycle progression in human colon adenocarcinoma cell line HT29. Int. J. Cancer **124**, 2789–2796
40 Mazurek, S., Boschek, C.B., Hugo, F. and Eigenbrodt, E. (2005) Pyruvate kinase type M2 and its role in tumor growth and spreading. Semin. Cancer Biol. **15**, 300–308
41 Mazurek, S. and Eigenbrodt, E. (2003) The tumor metabolome. Anticancer Res. **23**, 1149–1154
42 Coy, J.F., Dressler, D., Wilde, J. and Schubert, P. (2005) Mutations in the transketolase-like gene TKTL1: clinical implications for neurodegenerative diseases, diabetes and cancer. Clin. Lab. **51**, 257–273
43 Krockenberger, M., Honig, A., Rieger, L., Coy, J.F., Sutterlin, M., Kapp, M., Horn, E., Dietl, J. and Kammerer, U. (2007) Transketolase-like 1 expression correlates with subtypes of ovarian cancer and the presence of distant metastases. Int. J. Gynecol. Cancer **17**, 101–106
44 Langbein, S., Zerilli, M., Zur Hausen, A., Staiger, W., Rensch-Boschert, K., Lukan, N., Popa, J., Ternullo, M.P., Steidler, A., Weiss, C. et al. (2006) Expression of transketolase TKTL1 predicts colon and urothelial cancer patient survival: Warburg effect reinterpreted. Br. J. Cancer **94**, 578–585
45 Staiger, W.I., Coy, J.F., Grobholz, R., Hofheinz, R.D., Lukan, N., Post, S., Schwarzbach, M.H. and Willeke, F. (2006) Expression of the mutated transketolase TKTL1, a molecular marker in gastric cancer. Oncol. Rep. **16**, 657–661
46 Lobo, C., Ruiz-Bellido, M.A., Aledo, J.C., Marquez, J., Nunez De Castro, I. and Alonso, F.J. (2000) Inhibition of glutaminase expression by antisense mRNA decreases growth and tumourigenicity of tumour cells. Biochem. J. **348**, 257–261
47 Spittler, A., Oehler, R., Goetzinger, P., Holzer, S., Reissner, C.M., Leutmezer, F., Rath, V., Wrba, F., Fuegger, R., Boltz-Nitulescu, G. and Roth, E. (1997) Low glutamine concentrations induce phenotypical and functional differentiation of U937 myelomonocytic cells. J. Nutr. **127**, 2151–2157
48 Zu, X.L. and Guppy, M. (2004) Cancer metabolism: facts, fantasy, and fiction. Biochem. Biophys. Res. Commun. **313**, 459–465
49 Cascante, M., Boros, L.G., Comin-Anduix, B., de Atauri, P., Centelles, J.J. and Lee, P.W. N. (2002) Metabolic control analysis in drug discovery and disease. Nat. Biotech. **20**, 243–249
50 Fell, D.A. (1997) Understanding the Control of Metabolism, Portland Press Ltd, London

Received 5 March 2010
doi:10.1042/BST0381302